

Department of Physics and Astronomy

University of Heidelberg

Master thesis

in Physics

submitted by

Andreas Robert Weiden

born in Cologne

October 31st 2014

Measurement of direct CP -violation in prompt $D^0 \rightarrow K^- K^+$ and $D^0 \rightarrow \pi^- \pi^+$ decays at LHCb

This master thesis has been carried out by Andreas Robert Weiden

at the

Physikalisches Institut Heidelberg

under the supervision of

Prof. Dr. Ulrich Uwer

and

Prof. Dr. André Schöning

Abstract

This master thesis analyzes data corresponding to an integrated luminosity of 3fb^{-1} collected by LHCb in 2011 and 2012 at center of mass energies of $\sqrt{s} = 7$ TeV and $\sqrt{s} = 8$ TeV, respectively. The CP -asymmetries in the two decays $D^0 \rightarrow K^-K^+$ and $D^0 \rightarrow \pi^-\pi^+$ and its charge conjugates are determined. The flavor of the D^0 mesons at production time is determined using the charge of the slow pion in prompt $D^{*+} \rightarrow D^0\pi_s^+$ decays. After applying a kinematic weighting to ensure cancellation of production and detection asymmetries, the difference between the two CP -asymmetries, $\Delta A_{CP} \equiv A_{CP}(KK) - A_{CP}(\pi\pi)$, is measured.

A value of $\Delta A_{CP} = (-0.10 \pm 0.08(\text{stat.}) \pm 0.05(\text{syst.}))\%$ is determined and compared to the value obtained in D^0 decays, where the flavor at production time is determined semileptonically in $B^+ \rightarrow D^0\bar{\mu}^+\nu_\mu$ decays. Both measurements are compatible with zero on the 1σ level, contrary to earlier evidence for CP -violation at the percent level. This analysis comprises the single best measurement of ΔA_{CP} and therefore of direct CP -violation in singly-Cabibbo-suppressed charm decays.

Diese Masterarbeit untersucht Daten entsprechend einer integrierten Luminosität von 3fb^{-1} , die 2011 und 2012 vom LHCb Experiment bei Schwerpunktsenergien von $\sqrt{s} = 7$ TeV und $\sqrt{s} = 8$ TeV am LHC aufgezeichnet wurden. Die CP -Asymmetrien in den beiden Zerfällen $D^0 \rightarrow K^-K^+$ und $D^0 \rightarrow \pi^-\pi^+$ werden gemessen, wobei der ursprüngliche Flavor der D^0 -Mesonen durch die Ladung des Pions in prompten $D^{*+} \rightarrow D^0\pi_s^+$ Zerfällen bestimmt wird. Die Differenz der beiden Asymmetrien, $\Delta A_{CP} \equiv A_{CP}(KK) - A_{CP}(\pi\pi)$, wird gemessen. Zuvor stellt eine kinematische Gewichtung sicher, dass Produktions- und Detektionsasymmetrien sich in dieser Differenz aufheben.

Als Ergebnis wird ein Wert von $\Delta A_{CP} = (-0.10 \pm 0.08(\text{stat.}) \pm 0.05(\text{syst.}))\%$ gefunden. Dieser wird mit dem Wert aus D^0 -Zerfällen, in denen der ursprüngliche Flavor durch den Zerfall $B^+ \rightarrow D^0\bar{\mu}^+\nu_\mu$ bestimmt wird, verglichen. Beide Messungen sind innerhalb von 1σ kompatibel mit Null, im Gegensatz zu zuvor bestehenden Hinweisen auf CP -Verletzung von bis zu einem Prozent. Diese Messung ist die weltweit beste Einzelmessung von ΔA_{CP} und damit auch von direkter CP -Verletzung in einfach Cabibbo-unterdrückten D -Meson Zerfällen.

Contents

1. Introduction	1
2. Theoretical Description	5
2.1. Standard model of particle physics	5
2.2. Neutral meson decays and CP -violation	10
2.3. Analysis strategy	16
2.4. Sensitivity to new physics	17
3. The LHCb experiment at the LHC	19
3.1. The Large Hadron Collider	19
3.2. The LHCb detector	19
3.2.1. Vertex detector (VELO)	20
3.2.2. Tracking system	21
3.2.3. Ring Imaging Cherenkov detector (RICH)	22
3.2.4. Calorimeter	23
4. Data selection	25
4.1. Reconstruction	26
4.2. Trigger	26
4.2.1. Level-0 trigger	27
4.2.2. High Level Trigger	29
4.3. Stripping	31
4.4. Decay Tree Fitter (DTF)	32
4.5. Selection requirements	32
4.5.1. Fiducial Cuts	35
4.6. Data sets	36
4.7. Treatment of multiple candidates	37
5. Description of mass distributions	41
5.1. Mass difference	41
5.2. D^0 mass	42
5.3. Two-dimensional fit	44
5.4. Final model	45
6. Determination of CP-asymmetries	46

7. Kinematic weighting	52
8. Systematic uncertainties	59
8.1. Significance of deviations	59
8.2. Influence of setting the model parameters constant	61
8.3. Binning	63
8.4. Signal model	66
8.5. Background model	67
8.6. Two-dimensional determination of the asymmetries and peaking background	68
8.7. Multiple candidates	72
8.8. Fiducial cuts	74
8.9. Stability checks	75
8.9.1. Run number	75
8.9.2. Number of primary vertices	75
8.9.3. The quality of the $\pi_s D^0$ vertex	75
8.9.4. The quality of the slow pion impact parameter	80
8.9.5. Slow pion transverse momentum	83
8.9.6. Separation in phase space	83
8.9.7. D^0 flight distance	83
8.9.8. D^0 transverse momentum	87
8.9.9. The quality of the D^0 impact parameter	87
8.9.10. The azimuthal angle of D^0	87
8.9.11. The D^0 mass	91
8.9.12. Particle identification	91
8.10. Total systematic uncertainty	94
9. Conclusion	95
A. Appendix	99
A.1. Peaking background	99
A.2. Run number	108
A.3. Number of primary vertices	115
A.4. The quality of the fitted $\pi_s D^0$ vertex	121
A.5. The quality of the slow pion impact parameter	127
A.6. Slow pion transverse momentum	133
A.7. Separation in phase space	140
A.8. D^0 flight distance	146
A.9. D^0 transverse momentum	153
A.10. The quality of the D^0 impact parameter	160
A.11. The azimuthal angle of D^0	167
A.12. The D^0 mass	174
A.13. Particle identification	180
References	186

1. Introduction

In the early 20th century Einstein derived his famous equation $E = mc^2$, which proposed the equivalence of energy and mass [1]. As a consequence, matter can be created out of pure energy. Conservation laws require the production of the same amount of matter and anti-matter. Assuming that the Big Bang initially just produced energy, and everything after the Big Bang follows above physical laws, the same amount of matter and anti-matter were present at the beginning of our universe. However, the visible universe today is made up almost exclusively from matter. Therefore, at some point an asymmetry in interactions of matter and anti-matter must have been prevalent. More precisely, three necessary conditions are required to produce matter and anti-matter at different rates, as proposed in 1967 by Andrei Sakharov [2]:

- Baryon number (B) violation,
- Charge-symmetry (C) and charge-parity-symmetry (CP) violation,
- Interactions out of thermal equilibrium.

Baryon number is the number of particles consisting of three quarks or anti-quarks minus the number of their anti-particles (see Sec. 2.1 for the definition of quarks). Charge- and charge-parity-symmetry are two out of a handful of possible global symmetries in physics. Charge-symmetry (C) is realized if a physics process proceeds in the same way if every particle is replaced by its anti-particle. Parity-symmetry (P) is physics staying invariant under inversion through the origin. The third fundamental symmetry is time-symmetry, *i.e.* the physical laws proceed in the same way when reversing time (and consequently also all momenta). CP-symmetry is the symmetry after applying both transformations, C and P, subsequently. While CP-symmetry is violated, CPT-symmetry is believed to be realized in nature.

Of Sakharov's three conditions, the first one can be realized in the current Standard Model of particle physics (SM) (see Sec. 2.1), the third condition is satisfied, as long as the expansion of the universe is faster than the rate of the interaction generating the baryon-asymmetry. Lastly, the second condition is partly included in the SM, because the quark mixing matrix, the Cabibbo-Kobayashi-Maskawa matrix (CKM matrix), which will be described later, allows CP-symmetry-violation (*CP*-violation). However, the magnitude of this CP violation is too small to account for the observed asymmetry (see Sec. 2.1). Therefore only two other explanations are possible. Either the CP violation arises in the lepton sector (from the neutrino mixing matrix), which will be testable

in the near future (with the *NOVA* experiment [3]) or there are physics processes beyond the SM (new physics).

To search for such new physics, it is paramount to study processes where CP violation might occur and where the SM contribution is small. Examples of such processes are the decays of the charmed meson D^0 , $D^0 \rightarrow K^-K^+$ and $D^0 \rightarrow \pi^-\pi^+$ and the corresponding decays of its anti-particle, the \bar{D}^0 . An interesting probe is the measurement of the observed CP asymmetry in the two decay channels $A_{CP}(KK)$ and $A_{CP}(\pi\pi)$ (see Sec. 2.2 & 2.3). To minimize nuisance asymmetries (production and detector asymmetries), the difference between these two asymmetries is measured, as described in detail in Sec. 2. This difference is called $\Delta A_{CP} \equiv A_{CP}(KK) - A_{CP}(\pi\pi)$.

The measurement of ΔA_{CP} , which has been performed multiple times at different detectors with ever increasing data samples, has triggered a lot of interest. So far, three previous measurements using prompt charm decays have been performed at LHCb: one using the early 2010 data [4], one using 0.6fb^{-1} of data [5], and one using 1.0fb^{-1} of data collected in 2011 [6]. The latter measurement is preliminary and has not been published. Two complementary analyses using secondary charm decays (semileptonic) were also conducted by LHCb, resulting in a measurements with a different sign [7, 8]. Additionally, this measurement has also been conducted at CDF [9], Belle [10] and BaBar [11].

The prompt-tagged (presented here) and the semileptonic-tagged analyses are fully independent, without overlap of data samples. Therefore the results are statistically independent. Also the tagging and associated systematic uncertainties are completely disentangled and the fitters and the analysis methods are different. The analysis of 0.6fb^{-1} of data taken in 2011 lead to a 3.5σ discrepancy between the average of the prompt-tagged results and the SM prediction of zero. The analysis of the full 3fb^{-1} available to LHCb carried out in this master thesis aims to resolve whether this evidence holds up to scrutiny. A confirmation of a *CP*-asymmetry of this magnitude would very likely signal new, yet to be understood, physics (see Sec. 2.4). The second goal of this master thesis is to ascertain whether the discrepancy between the prompt results and the two semileptonic results can be resolved. An overview of these results is summarized in Tab. 1.1 and a graphical overview is shown in Fig. 1.1.

In this thesis the full analysis of the 2011 and 2012 data is presented, as carried out in Heidelberg. Most of the material presented here can also be found in the analysis note [13]. With the exception of the figures shown in Sec. 7, which were provided by Evelina Gersabeck, all plots were produced by me. Not shown here are the differences between the two reconstructions, which are documented in the analysis note.

The aforementioned analysis note is the basis for the LHCb publication currently in preparation.

Originally the individual asymmetries and their difference were blinded by a random offset. This offset was removed for the final results of this master thesis. Any results in

Experiment	ΔA_{CP}	Ref.
LHCb (prompt, 38pb ⁻¹)	$(-0.28 \pm 0.70 \pm 0.25)\%$	[4]
LHCb (prompt, 0.6fb ⁻¹)	$(-0.82 \pm 0.21 \pm 0.11)\%$	[12],[5]
LHCb (prompt, 1fb ⁻¹ , prelim.)	$(-0.34 \pm 0.15 \pm 0.10)\%$	[6]
LHCb (semileptonic, 1fb ⁻¹)	$(+0.49 \pm 0.30 \pm 0.14)\%$	[7]
LHCb (semileptonic, 3fb ⁻¹)	$(+0.14 \pm 0.16 \pm 0.08)\%$	[8]
CDF (prompt, 9.7fb ⁻¹)	$(-0.62 \pm 0.21 \pm 0.10)\%$	[9]
Belle (prompt, 976fb ⁻¹)	$(-0.87 \pm 0.41 \pm 0.06)\%$	[10]
BaBar (prompt, 385.8 fb ⁻¹)	$(+0.24 \pm 0.62 \pm 0.26)\%$	[11]
Naïve average	$(-0.25 \pm 0.11)\%$	

Table 1.1.: Previous ΔA_{CP} results, with the naïve average (statistical and systematical uncertainties are added in quadrature and assumed to be fully uncorrelated between analyses, indirect CP violation not taken into account) of the results with the most statistics from all experiments, excluding the semileptonic result from LHCb.

this work do not compromise official LHCb results and are to be regarded as *preliminary*.

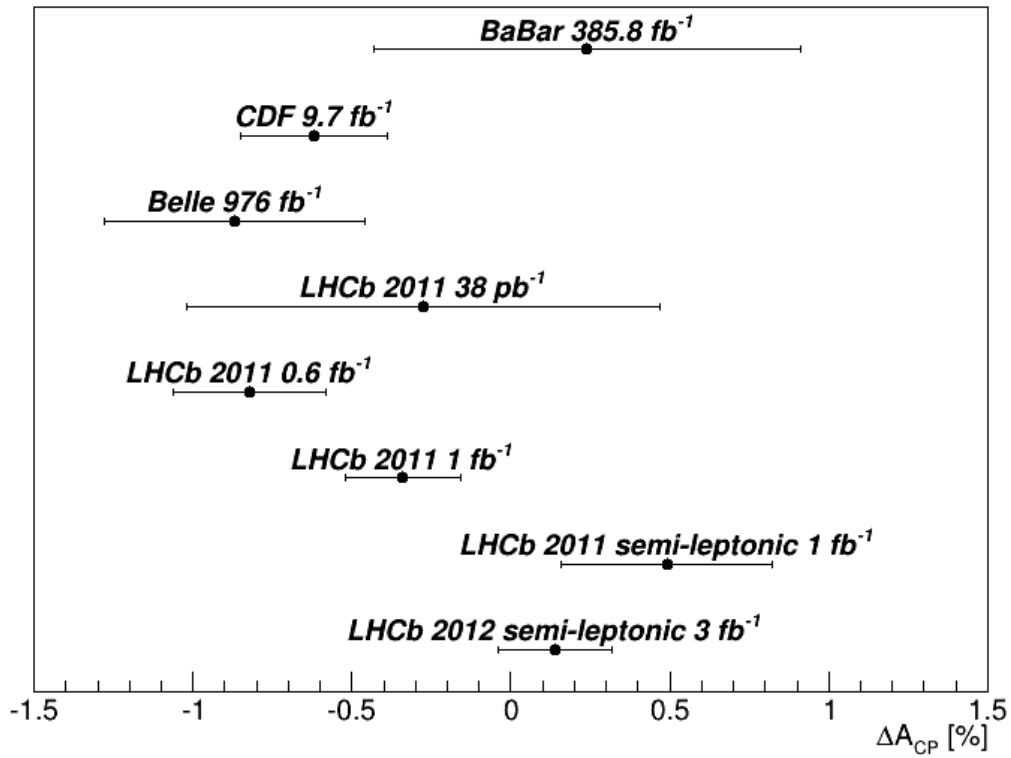


Figure 1.1.: Comparison of the different ΔA_{CP} results. Statistical and systematical errors are added in quadrature for error bars.

2. Theoretical Description

2.1. Standard model of particle physics

So far, four fundamental forces of nature have been discovered:

- **Gravity**, which manifests itself in the attraction between two massive bodies.
- **The electro-magnetic force**, describing the attraction or repulsion of particles with charge and their interaction with magnetic fields.
- **The strong nuclear force**, responsible for binding the constituents of the proton and neutron through the interaction of particles with color-charge.
- **The weak nuclear force**, the interaction of particles with a weak charge, responsible for some types of radioactive decays.

Of these four fundamental forces, three have been successfully described by a quantum field theory (QFT). The only fundamental force not described on a quantum level is gravity. Gravity, however, is the weakest of the four forces (it is 10^{25} times weaker than the next weakest force, the weak nuclear force, and 10^{38} times weaker than the strongest force, the strong nuclear force) and can in general be neglected in particle physics since the relevant masses are very small (e.g. the mass of a proton, $m_p \approx 1.67 \cdot 10^{-27}$ kg).

The current understanding about the other three fundamental forces is united in what is known as the *Standard Model of particle physics* (SM). It describes these forces as symmetry groups, under which the Lagrangian of a particle stays invariant. The electro-magnetic and the weak force (unified in the electro-weak force) are described by the symmetry group $SU_L(2) \times U(1)$ and the strong force by the symmetry group $SU(3)$.

The SM is divided into matter particles with half-integer spins (called fermions) and force carriers with integer spins (called bosons).

Each of the three forces is mediated by at least one of the bosons. Namely, there is the photon (γ) for the electro-magnetic force, the W^\pm and Z bosons for the weak force and eight different gluons (g) for the strong force. In addition, there is a scalar field permeating the whole universe, whose symmetry is spontaneously broken, giving mass to the elementary particles. Excitations of this field are called Higgs-boson (H). The

description of this scalar field and its spontaneous symmetry-breaking was awarded with the Nobel prize in physics in 2013 [14].

The fermions are divided into two parts, depending on their interaction with the strong force. Those that do interact strongly are called quarks, those that do not, are called leptons. The leptons have integer (electro-magnetic) charge, while the quarks have charges which are all multiples of $1/3$. For the leptons there are the charged ones (like the electron, with a charge -1) and the uncharged ones, the light (and in the SM even massless) neutrinos. For the quarks there are the up-type quarks (with a charge of $+2/3$) and the down-type quarks (with a charge of $-1/3$).

Both leptons and quarks are separated into generations. Each particle has two heavier cousins who share almost all characteristics, like charge (electro-magnetic, color and weak) and spin. The only thing differentiating them is their mass.

An overview over this plethora of particles can be seen in Fig. 2.1. In addition to these

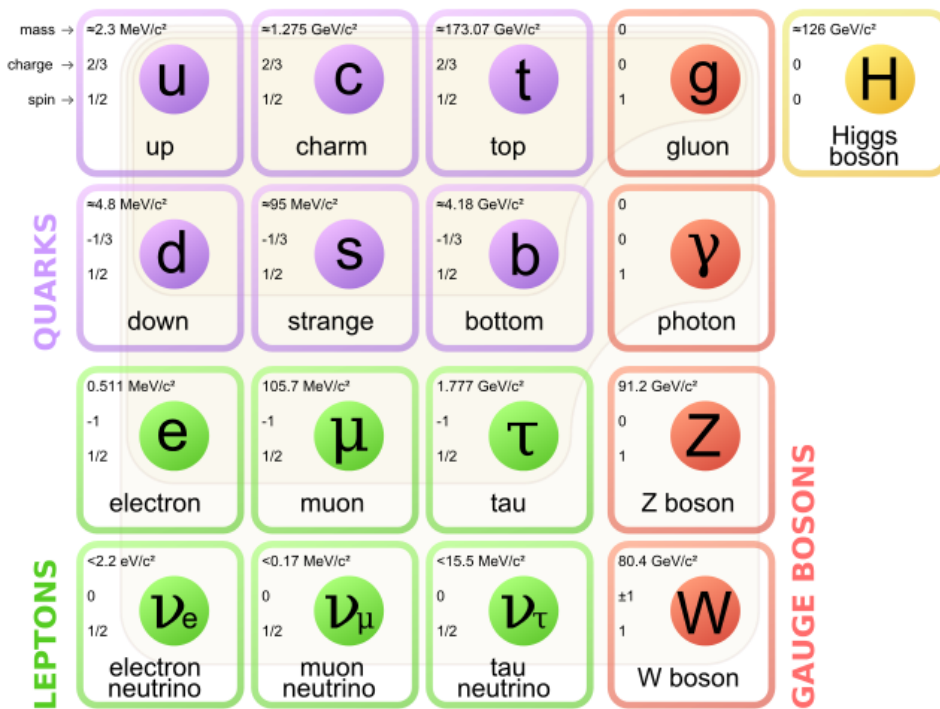


Figure 2.1.: The Standard Model of Particle Physics with the 6 quarks and 6 leptons and the gauge bosons [15].

24 particles, every particle has an anti-particle. If the two meet they can annihilate to energy (taking the form of a photon, a Z^0 or a gluon). Equivalently, a particle - anti-particle pair can be created from the vacuum if at least twice the rest mass of the particle is available as energy. Particles and anti-particles share the same mass and lifetime but many quantum numbers are opposite (first and foremost the charge, but also quantum numbers like charmness, which describes the number of charm-quarks present). Neutral

particles can be their own anti-particles, like the photon. However, this is not necessary. For the neutrinos it is not yet clear whether they are their own anti-particle.

All particles except the lightest ones are unstable, since they can decay into lighter particles. Therefore the world around us is almost exclusively made up of these particles. Two *up*-quarks combined with one *down*-quark form the stable proton, while two *down*-quarks combined with one *up*-quark form the neutron (which is already unstable, if not in a potential). Together they form the nuclei of atoms, which are orbited by electrons, forming atoms.

Particles that consist of three quarks (like the proton and neutron) are called baryons. The number of baryons is usually conserved in SM interactions. The only exception to this are non-perturbative sphaleron processes in the early universe, allowing Sakharov's first condition (baryon number violation) to be satisfied.

Composite particles consisting of a quark and an anti-quark are called mesons. All mesons are unstable. Examples for mesons are pions (quark content of $|u\bar{d}\rangle$ for the π^+), kaons (quark content of $|u\bar{s}\rangle$ for the K^+) and D-mesons (quark content of $|u\bar{c}\rangle$ for the D^0), which are all three relevant for this analysis.

Decays of the elementary particles which let one particle decay into another particle of a different generation are called flavor changing. These are usually governed by the weak interaction, which is intimately connected to the Englert-Higgs-mechanism [16, 17]. Besides charge and spin, chirality is another quantum number relevant in particle physics. For massless particles, like the photon, it is equivalent to the helicity of a particle, defined as the projection of the spin of the particle onto the direction of momentum. Particles can be either left-handed (spin and momentum anti-parallel) or right-handed (spin and momentum parallel). In general, chirality is defined through the transformation with the Poincaré group. A theory where particles of different chirality couple differently is called a chiral theory. It automatically violates parity-symmetry, since it is not invariant under mirroring all spatial coordinates. The weak interaction is such a chiral theory, left-handed quarks only couple to left-handed quarks and right-handed anti-quarks, but not to right-handed quarks or left-handed anti-quarks via the weak interaction. This is why its symmetry group $SU_L(2)$ has an index L to denote its left-handedness. The weak interaction violates P-symmetry maximally, since it exclusively couples left-handed quarks.

However, the spontaneous symmetry-breaking of the electro-weak symmetry, through the Englert-Higgs-mechanism, changes the Lagrangian and introduces terms of the form $\overline{Q}_L d_r$, coupling left-handed quarks to right-handed quarks, which was forbidden before. These interactions are called Yukawa interactions and are described by

$$\mathcal{L}_Y = -Y_{ij}^d \overline{Q}_{Li}^I \phi d_{Rj}^I - Y_{ij}^u \overline{Q}_{Li}^I \epsilon \phi^* u_{Rj}^I + \text{h.c.} [18], \quad (2.1)$$

where $Y^{u,d}$ are 3×3 complex matrices, ϕ is the Higgs field, i, j are generation labels, and ϵ is the 2×2 anti-symmetric tensor. Q_L^I are left-handed quark doublets and d_R^I and u_r^I

are right-handed down- and up-type quark singlets, respectively, in the weak-eigenstate basis. *h.c.* symbolizes that the hermitian conjugate of the given equation is implicitly added. When ϕ acquires a vacuum expectation value, $\langle\phi\rangle = (0, v/\sqrt{2})$, Eq. 2.1 yields mass terms for the quarks. The physical states are obtained by diagonalizing $Y^{u,d}$ by four unitary matrices, $V_{L,R}^{u,d}$, as $M_{diag}^f = V_L^f Y^f V_R^{\dagger}(v/\sqrt{2})$, $f = u, d$. As a result, the charged-current W^\pm interactions couple to the physical u_{Lj} and d_{Lk} quarks with couplings given by

$$\frac{-g}{\sqrt{2}}(\overline{u}_L, \overline{c}_L, \overline{t}_L)\gamma^\mu W_\mu^+ V_{CKM} \begin{pmatrix} d_L \\ s_L \\ b_L \end{pmatrix} + \text{h.c.}, \quad V_{CKM} \equiv V_L^u V_L^{d\dagger} = \begin{pmatrix} V_{ud} & V_{us} & V_{ub} \\ V_{cd} & V_{cs} & V_{cb} \\ V_{td} & V_{ts} & V_{tb} \end{pmatrix}, \quad (2.2)$$

where g is the coupling constant of the weak interaction and γ^μ are the four Dirac matrices. This matrix is called the Cabibbo-Kobayashi-Maskawa (CKM) matrix [19]. It relates the weak eigenstates to the (physical) mass eigenstates.

The CKM matrix is a complex 3×3 matrix. Because of unitarity only four of the 18 degrees of freedom remain, namely three angles and one complex phase. Historically, the CKM matrix was introduced because of this reason. Namely, a unitary matrix with rank less than three has only real parameters and no complex phase. However, a complex phase is paramount, if CP -violation is necessary (see Eq. 2.54 and Eq. 2.55). The CKM matrix successfully predicted the existence of a third generation of quarks, which was honored with the Nobel prize in 2008.

The standard parametrization of the CKM matrix consists of three Euler angles, $\theta_{12}, \theta_{23}, \theta_{13}$, which denote the transition from e.g generation two to one (θ_{12}), with $c_{ij} \equiv \cos(\theta_{ij})$ and $s_{ij} \equiv \sin(\theta_{ij})$. Moreover it consists of a complex, CP violating, phase δ_{13} . It is represented by the matrix

$$V_{CKM} = \begin{pmatrix} c_{12}c_{13} & s_{12}c_{13} & s_{12}e^{-i\delta_{13}} \\ -s_{12}c_{23} - c_{12}s_{23}s_{13}e^{i\delta_{13}} & c_{12}s_{23} - s_{12}s_{23}s_{13}e^{i\delta_{13}} & s_{23}c_{13} \\ s_{12}s_{23} - c_{12}c_{23}s_{13}e^{i\delta_{13}} & c_{12}s_{23} - s_{12}c_{23}s_{13}e^{i\delta_{13}} & c_{23}c_{13} \end{pmatrix}. \quad (2.3)$$

Experimentally, it is known that $s_{13} \ll s_{23} \ll s_{12} \ll 1$. However, with the standard parametrization it is not easy to recognize this hierarchy of the CKM matrix. For this purpose the Wolfenstein parametrization [20] was introduced. With this parametrization it is also straightforward to identify in which processes CP -violation can occur and roughly with which strength. The three real parameters λ, A, ρ , and the complex phase η are related to the standard parametrization by

$$\lambda = s_{12}, \quad (2.4)$$

$$A\lambda^2 = s_{23} \quad \text{and} \quad (2.5)$$

$$A\lambda^3(\rho - i\eta) = s_{13}e^{-i\delta_{13}}. \quad (2.6)$$

It is represented by the matrix

$$V_{CKM}^{wf} \begin{pmatrix} 1 - \lambda^2/2 & \lambda & A\lambda^3(\rho - i\eta) \\ -\lambda & 1 - \lambda^2/2 & A\lambda^2 \\ A\lambda^3(1 - \rho - i\eta) & -A\lambda^2 & 1 \end{pmatrix} + \mathcal{O}(\lambda^4), \quad (2.7)$$

which is unitary to all orders of λ . The parameter λ is also called Cabibbo angle, $\sin(\theta_C)$, and governs the decay of second to first generation quarks. It was introduced by Cabibbo to preserve the universality of the weak interaction [21], defining a CKM-matrix with only two generations (which does not allow CP -violation).

One feature of the CKM matrix is the Jarlskog invariant [22]. It is invariant under multiplying the CKM matrix with a global phase and is defined as

$$J = \pm \Im(V_{ij}V_{kl}V_{il}^*V_{kj}^*), \quad i \neq k, j \neq l. \quad (2.8)$$

Using the Wolfenstein parametrization, this becomes

$$J \approx A^2 \lambda^6 \eta \approx 2.97 \cdot 10^{-5}. \quad (2.9)$$

All CP -violation in the SM can be parametrized by the Jarlskog invariant. When appropriately normalized, it is of order 10^{-20} . In the universe the CP -asymmetry can be measured and expressed via

$$\eta = \frac{n_B - n_{\bar{B}}}{n_\gamma} = (6.21 \pm 0.16) \times 10^{-10} [23], \quad (2.10)$$

where $n_B, n_{\bar{B}}$ and n_γ are the number densities of baryons, anti-baryons and photons, respectively, and η is the matter-anti-matter asymmetry.. The numerical value is obtained from a combination of the measurement of the cosmic microwave background and large scale structure data (WMAP 5 year data, Baryon Acoustic Oscillations and Type Ia Supernovae) [24].

It becomes apparent that the the Jarlskog invariant, and therefore the SM, cannot explain the full CP -asymmetry observed in nature by many orders of magnitude. Therefore one of the most important searches for new physics is searching for CP violation not described in the SM. As has been mentioned in Sec. 1, there are only two possible explanations for this. Either a new source of CP violation arises in the lepton sector (from the neutrino mixing matrix) or there are physics processes beyond the SM (new physics). One area where such new physics is discoverable is in neutral meson decays, where CP -asymmetries can be measured in a multitude of decay channels. The theoretical background needed to understand these decays and how CP -violation is observable is described in the next section.

2.2. Neutral meson decays and CP -violation

Generally, any flavored meson, here represented by the neutral D^0 meson with the quark content $|\bar{u}c\rangle$, is described by:

$$F|D^0\rangle = +|D^0\rangle \quad \text{and} \quad F|\bar{D}^0\rangle = -|\bar{D}^0\rangle, \quad (2.11)$$

where F is an operator yielding the flavor number, in this case *charmness* (the number of charm quarks in a composite particle). This means that the meson and its anti-particle are two eigenstates of the corresponding flavor operator with the eigenvalues ± 1 .

The time evolution of a physical state, described by these two flavor eigenstates, can be written as:

$$\Psi(t) = a(t)|D^0\rangle + b(t)|\bar{D}^0\rangle, \quad (2.12)$$

with a priori any two time-dependent functions $a(t)$ and $b(t)$. However, $\Psi(t)$ should satisfy the Schrödinger equation with a non-hermitian effective Hamiltonian

$$i\hbar\frac{d}{dt}\Psi(t) = \mathcal{H}\Psi(t). \quad (2.13)$$

This effective Hamiltonian is non-hermitian because decays into states not described by the two flavor states can occur (for example the two decays studied in this analysis, $D^0 \rightarrow K^-K^+$ and $D^0 \rightarrow \pi^-\pi^+$). The effective Hamiltonian \mathcal{H} can be separated into a hermitian and an anti-hermitian part:

$$\mathcal{H} = \mathbf{M} - \frac{i}{2}\mathbf{\Gamma}, \quad (2.14)$$

where both \mathbf{M} and $\mathbf{\Gamma}$ are hermitian matrices. These are called *mass matrix* and *decay matrix*, respectively, because of their physical roles, which will become apparent later.

For the physical two-state system at hand, $|\psi\rangle = \begin{pmatrix} D^0 \\ \bar{D}^0 \end{pmatrix}$, these can be represented by 2×2 matrices and \mathcal{H} can be written as:

$$\mathcal{H} = \begin{pmatrix} M_{11} - \frac{i}{2}\Gamma_{11} & M_{12} - \frac{i}{2}\Gamma_{12} \\ M_{21} - \frac{i}{2}\Gamma_{21} & M_{22} - \frac{i}{2}\Gamma_{22} \end{pmatrix}. \quad (2.15)$$

The hermiticity of \mathbf{M} and $\mathbf{\Gamma}$ guarantee that $M_{12} = M_{21}^*$ and $\Gamma_{12} = \Gamma_{21}^*$, while CPT invariance ensures $M_{11} = M_{22}$ and $\Gamma_{11} = \Gamma_{22}$.

Here, elements on the diagonal describe either a state remaining unchanged (via the elements M_{11} and M_{22}) or decaying outside of the $\begin{pmatrix} D^0 \\ \bar{D}^0 \end{pmatrix}$ subspace (via the elements Γ_{11} and Γ_{22}). The off-diagonal elements describe transitions between the two states, *i.e.* flavor oscillations ($D^0 \rightarrow \bar{D}^0$ or $\bar{D}^0 \rightarrow D^0$). These oscillations can occur via virtual intermediate states (described by M_{12} and M_{21}) or via real intermediate states, such as decays to final states shared by both states (described via Γ_{12} and Γ_{21}). Thus the names *mass matrix* and *decay matrix*.

One can obtain the physical states $|D_{1,2}\rangle$ of this two-flavor-state system by diagonalizing the Hamiltonian, such that:

$$\mathcal{H} |D_{1,2}\rangle = \lambda_{1,2} |D_{1,2}\rangle, \quad (2.16)$$

with $\lambda_{1,2} = m_{1,2} - \frac{i}{2}\Gamma_{1,2}$ the eigenvalues of the Hamiltonian and where $m_{1,2}$ are the masses and $\Gamma_{1,2}$ are the decay widths of the physical particles.

The time-evolution of the physical states is then defined as:

$$|D_{1,2}(t)\rangle = e^{-i\mathcal{H}t} |D_{1,2}(t=0)\rangle \quad (2.17)$$

$$= e^{-im_{1,2}t} e^{-\Gamma_{1,2}\frac{t}{2}} |D_{1,2}(t=0)\rangle. \quad (2.18)$$

The physical states $|D_{1,2}\rangle$ are only linear combinations of the original flavor-states and can therefore be written as:

$$|D_1\rangle = p|D^0\rangle + q|\bar{D}^0\rangle \quad (2.19)$$

$$|D_2\rangle = p|D^0\rangle - q|\bar{D}^0\rangle, \quad (2.20)$$

with the two complex numbers p and q satisfying $|p|^2 + |q|^2 = 1$.

Correspondingly, this means for the flavor-states:

$$|D^0\rangle = \frac{1}{2p} (|D_1\rangle + |D_2\rangle) \quad (2.21)$$

$$|\bar{D}^0\rangle = \frac{1}{2q} (|D_1\rangle - |D_2\rangle). \quad (2.22)$$

Using this, the time-evolution of the flavor-states can be found by substituting the time-evolutions of the physical states:

$$|D^0(t)\rangle = \frac{1}{2p} \left(e^{-im_1t - \Gamma_1\frac{t}{2}} |D_1(t=0)\rangle + e^{-im_2t - \Gamma_2\frac{t}{2}} |D_2(t=0)\rangle \right), \quad (2.23)$$

with $|D_1(t=0)\rangle = p|D^0\rangle + q|\bar{D}^0\rangle$ and $|D_2(t=0)\rangle = p|D^0\rangle - q|\bar{D}^0\rangle$, which can be written as

$$|D^0(t)\rangle = g_+(t) |D^0\rangle + \left(\frac{q}{p}\right) g_-(t) |\bar{D}^0\rangle. \quad (2.24)$$

Likewise, for the anti-particle

$$|\bar{D}^0(t)\rangle = g_+(t) |\bar{D}^0\rangle + \left(\frac{p}{q}\right) g_-(t) |D^0\rangle, \quad (2.25)$$

with the functions $g_{\pm}(t)$ defined as:

$$g_{\pm}(t) = \frac{1}{2} \left(e^{-im_1 t - \Gamma_1 \frac{t}{2}} \pm e^{-im_2 t - \Gamma_2 \frac{t}{2}} \right), \quad (2.26)$$

$$= \frac{1}{2} e^{-imt} \left(e^{-\frac{i}{2}\Delta m t - \Gamma_1 \frac{t}{2}} \pm e^{+\frac{i}{2}\Delta m t - \Gamma_2 \frac{t}{2}} \right), \quad (2.27)$$

with the useful definitions:

$$\Delta m = m_2 - m_1, \quad m = \frac{1}{2} (m_1 + m_2), \quad (2.28)$$

$$\Delta \Gamma = \Gamma_2 - \Gamma_1, \quad \Gamma = \frac{1}{2} (\Gamma_1 + \Gamma_2). \quad (2.29)$$

Also needed further on are:

$$|g_{\pm}(t)|^2 = \frac{e^{-\Gamma t}}{2} \left(\cosh\left(\frac{1}{2}\Delta\Gamma t\right) \pm \cos(\Delta m t) \right), \quad (2.30)$$

$$g_{\pm}^*(t)g_{\mp}(t) = \frac{e^{-\Gamma t}}{2} \left(-\sinh\left(\frac{1}{2}\Delta\Gamma t\right) \pm i \sin(\Delta m t) \right). \quad (2.31)$$

To study flavor-oscillations, one would now only need to evaluate the following expression:

$$P(D^0 \rightarrow \bar{D}^0) = |\langle \bar{D}^0 | D^0(t) \rangle|^2 = |g_-(t)|^2 \left| \frac{q}{p} \right|^2, \quad (2.32)$$

$$P(\bar{D}^0 \rightarrow D^0) = |\langle D^0 | \bar{D}^0(t) \rangle|^2 = |g_-(t)|^2 \left| \frac{p}{q} \right|^2. \quad (2.33)$$

For the further discussion, however, not the probabilities, but only the amplitudes are needed.

For a more in-depth description of neutral meson mixing see [25, 26].

As discussed above, both in the diagonal and in the off-diagonal of the effective Hamiltonian, there are parts which influence the decay. To study CP -violation in neutral meson decay, the following four decay amplitudes can be considered:

$$\mathcal{A}_f = \mathcal{A}(D^0 \rightarrow f), \quad \bar{\mathcal{A}}_f = \mathcal{A}(\bar{D}^0 \rightarrow f), \quad (2.34)$$

$$\mathcal{A}_{\bar{f}} = \mathcal{A}(D^0 \rightarrow \bar{f}), \quad \bar{\mathcal{A}}_{\bar{f}} = \mathcal{A}(\bar{D}^0 \rightarrow \bar{f}). \quad (2.35)$$

Also relevant is the following combination of these amplitudes:

$$\lambda_f = \frac{q}{p} \frac{\bar{\mathcal{A}}_f}{\mathcal{A}_f} = -\eta_{CP} \left| \frac{q}{p} \right| \left| \frac{\bar{\mathcal{A}}_f}{\mathcal{A}_f} \right| e^{i\phi}, \quad (2.36)$$

where q and p are the coefficients in Eq. 2.19, η_{CP} is the CP -eigenvalue of the final state f ($\eta_{CP} = 1$ for $f \in KK, \pi\pi$), and ϕ is the CP violating relative phase between q/p and $\bar{\mathcal{A}}_f/\mathcal{A}_f$. The decay rate of a D^0 decaying into some final state f is then given by:

$$\Gamma(D^0 \rightarrow f) = |\mathcal{A}^{tot}(D^0 \rightarrow f)|^2 = |\mathcal{A}(D^0 \rightarrow f) + \mathcal{A}(D^0 \rightarrow \bar{D}^0 \rightarrow f)|^2. \quad (2.37)$$

The amplitude \mathcal{A}^{tot} also includes the amplitude of the D^0 first oscillating into its own anti-particle, which then also decays into the same final-state.

The individual time-dependent amplitudes in above formula are given by:

$$\mathcal{A}(D^0 \rightarrow f)(t) = \mathcal{A}_f \langle D^0 | D^0(t) \rangle = \mathcal{A}_f g_+(t), \quad (2.38)$$

$$\mathcal{A}(D^0 \rightarrow \bar{D}^0 \rightarrow f)(t) = \bar{\mathcal{A}}_f \langle \bar{D}^0 | D^0(t) \rangle = \bar{\mathcal{A}}_f \frac{q}{p} g_-(t). \quad (2.39)$$

This leads to:

$$\Gamma(D^0 \rightarrow f) = |\mathcal{A}_f|^2 [|g_+(t)|^2 + |\lambda_f|^2 |g_-(t)|^2 + 2\Re(\lambda_f g_+^*(t) g_-(t))]. \quad (2.40)$$

Using equations 2.30 and 2.31, this expands to:

$$\begin{aligned} \Gamma(D^0 \rightarrow f) &= |\mathcal{A}_f|^2 \frac{e^{-\Gamma t}}{2} \left[(1 + |\lambda_f|^2) \cosh\left(\frac{\Delta\Gamma}{2}t\right) + 2\Re(\lambda_f) \sinh\left(\frac{\Delta\Gamma}{2}t\right) \right. \\ &\quad \left. + (1 - |\lambda_f|^2) \cos(\Delta mt) - 2\Im(\lambda_f) \sin(\Delta mt) \right] \end{aligned} \quad (2.41)$$

$$= |\mathcal{A}_f|^2 (1 + |\lambda_f|^2) \frac{e^{-\Gamma t}}{2} \left(\cosh\left(\frac{\Delta\Gamma}{2}t\right) + D_f \sinh\left(\frac{\Delta\Gamma}{2}t\right) + C_f \cos(\Delta mt) - S_f \sin(\Delta mt) \right), \quad (2.42)$$

with

$$D_f = \frac{2\Re(\lambda_f)}{1 + |\lambda_f|^2}, \quad C_f = \frac{1 - |\lambda_f|^2}{1 + |\lambda_f|^2}, \quad S_f = \frac{2\Im(\lambda_f)}{1 + |\lambda_f|^2}. \quad (2.43)$$

These coefficients satisfy $|D_f|^2 + |C_f|^2 + |S_f|^2 = 1$.

Similarly, for the time dependent decay rate of the \bar{D}^0

$$\begin{aligned} \Gamma(\bar{D}^0 \rightarrow f)(t) &= |\mathcal{A}_f|^2 (1 + |\lambda_f|^2) \frac{e^{-\Gamma t}}{2} \\ &\quad \cdot \left(\cosh\left(\frac{\Delta\Gamma}{2}t\right) + D_f \sinh\left(\frac{\Delta\Gamma}{2}t\right) - C_f \cos(\Delta mt) + S_f \sin(\Delta mt) \right). \end{aligned} \quad (2.44)$$

Note that only the signs in front of C_f and S_f changed.

Defining the CP -asymmetry A_{CP} as follows:

$$A_{CP}(t) = \frac{\Gamma(D^0 \rightarrow f)(t) - \Gamma(\bar{D}^0 \rightarrow f)(t)}{\Gamma(D^0 \rightarrow f)(t) + \Gamma(\bar{D}^0 \rightarrow f)(t)} \quad (2.45)$$

$$= \frac{2C_f \cos(\Delta mt) - 2S_f \sin(\Delta mt)}{2 \cosh\left(\frac{\Delta\Gamma}{2}t\right) + 2D_f \sinh\left(\frac{\Delta\Gamma}{2}t\right)}, \quad (2.46)$$

it can be seen that the CP -asymmetry vanishes if $\lambda_f = \frac{q\bar{A}_f}{pA_f} = 1$. In this case, both C_f and S_f become zero and therefore the numerator becomes zero as well. Also, D_f just becomes one, ensuring that the asymmetry does not diverge. It does not vanish if either $\frac{\bar{A}_f}{A_f} \neq 1$, $\frac{q}{p} \neq 1$ or if one of these ratios introduces a complex phase, such that $\Im(\lambda_f) \neq 0$ and therefore $S_F \neq 0$. These three cases lead to a classification of CP -violation:

- **CP -violation in decay** (direct CP -violation)
if $\Gamma(D^0 \rightarrow f) \neq \Gamma(\bar{D}^0 \rightarrow \bar{f})$, which implies $\left| \frac{\bar{A}_f}{A_f} \right| \neq 1$. In case of a CP -eigenstate $\bar{f} = \eta_{CP}f$ with $\eta_{CP}=1$, as is the case for $D^0 \rightarrow K^-K^+$ and $D^0 \rightarrow \pi^-\pi^+$, also $\left| \frac{\bar{A}_f}{A_f} \right| \neq 1$.
- **CP -violation in mixing** (indirect CP -violation)
 $\mathcal{P}(D^0 \rightarrow \bar{D}^0) \neq \mathcal{P}(\bar{D}^0 \rightarrow D^0)$, implying $\left| \frac{q}{p} \right| \neq 1$.
- **CP -violation in interference between mixing and decay** (indirect CP -violation)
 $\Im(\lambda_f) = \Im\left(\frac{q\bar{A}_f}{pA_f}\right) \neq 0$. Either $\frac{q}{p}$ or $\frac{\bar{A}_f}{A_f}$ has a non-trivial phase.

Both direct and indirect CP -violation contribute to A_{CP} . These two contributions can be separated in the following way to first order:

$$A_{CP}(f; t) = a_{CP}^{dir}(f) + \frac{t}{\tau} a_{CP}^{ind}, \quad (2.47)$$

where a_{CP}^{dir} is the direct CP -asymmetry, τ is the D^0 lifetime and a_{CP}^{ind} is the indirect CP -asymmetry. After time-integration, where the time-acceptance of the experiment needs to be taken into account, this becomes:

$$A_{CP} \approx a_{CP}^{dir}(f) - A_\Gamma(1 - (a_{CP}^{dir}(f))^2) \frac{\langle t \rangle}{\tau} \approx a_{CP}^{dir}(f) + A_\Gamma \frac{\langle t \rangle}{\tau}, \quad (2.48)$$

where $\langle t \rangle$ denotes the average decay time in the reconstructed sample. A_Γ is the asymmetry of the lifetimes of the D^0 and \bar{D}^0 . It is approximately given by

$$A_\Gamma \approx \eta_{CP} \left[\frac{1}{2}(A_m + A_d)y \cos \phi - x \sin \phi \right], \quad (2.49)$$

with $x^2 = (0.06 \pm 0.25)\%$, $y = (4.2 \pm 2.2)\%$ the mixing parameters for D^0 - \bar{D}^0 mixing [27], $\eta_{CP} = 1$, and A_m and A_d representing a CP -violation contribution from mixing and direct CP -violation, respectively. A_m and A_d are related to λ_f via $|q/p|^{\pm 2} \approx 1 \pm A_m$ and $|\bar{A}_f/A_f|^{\pm 2} \approx 1 \pm A_d$ and $|\lambda^\pm|^2 \approx (1 \pm A_m)(1 \pm A_d)$. Furthermore, $a_{CP}^{dir} \approx -1/2A_d$ [28, 29].

Taking the difference between the two final states K^-K^+ and $\pi^-\pi^+$ yields

$$\begin{aligned} \Delta A_{CP} &\equiv A_{CP}(K^-K^+) - A_{CP}(\pi^-\pi^+) \\ &= a_{CP}^{dir}(K^-K^+) - a_{CP}^{dir}(\pi^-\pi^+) \\ &\quad - A_\Gamma(K^-K^+) \frac{\Delta \langle t(K^-K^+) \rangle}{\tau} - A_\Gamma(\pi^-\pi^+) \frac{\Delta \langle t(\pi^-\pi^+) \rangle}{\tau}. \end{aligned} \quad (2.50)$$

Here $\Delta\langle t \rangle$ denotes the difference in the average decay times of the two decays $D^0 \rightarrow K^-K^+$ and $D^0 \rightarrow \pi^-\pi^+$. The fraction $\Delta\langle t \rangle/\tau$ multiplying the indirect CP -violation was (0.098 ± 0.003) for LHCb in 2011 [5].

Assuming the CP violating phase ϕ to be universal, as was shown for example in [30] and [31], this can be rewritten as

$$\Delta A_{CP} \approx \Delta a_{CP}^{dir} \left(1 + y \cos \phi \frac{\overline{\langle t \rangle}}{\tau} \right) + \left(a_{CP}^{ind} + \overline{a_{CP}^{dir}} y \cos \phi \right) \frac{\Delta\langle t \rangle}{\tau} [28], \quad (2.51)$$

where $\Delta X \equiv X(K^-K^+) - X(\pi^-\pi^+)$ and $\overline{X} \equiv (X(K^-K^+) + X(\pi^-\pi^+))/2$. $\overline{\langle t \rangle}/\tau$ was equal to (2.083 ± 0.001) for LHCb in 2011 [5]. ΔA_{CP} is mostly a measure of direct CP -violation, since both a_{CP}^{ind} and $\frac{\Delta\langle t \rangle}{\tau}$ are small.

As an alternative to using the mixing parameters directly, the direct and indirect CP -violation can also be included as:

$$\Delta A_{CP} \approx \Delta a_{CP}^{dir} \left(1 + y_{CP} \frac{\overline{\langle t \rangle}}{\tau} \right) - \frac{\Delta\langle t \rangle}{\tau} a_{CP}^{ind} \quad (2.52)$$

and

$$A_{\Gamma} = -a_{CP}^{ind} - a_{CP}^{dir} y_{CP}, \quad (2.53)$$

where $y_{CP} = y$ if and only if no CP -violation is present. The current world-average is $y_{CP} = (0.866 \pm 0.155)\%$ [32].

To better understand why CP -violation is observable in the decays $D^0 \rightarrow K^-K^+$ and $D^0 \rightarrow \pi^-\pi^+$ in the first place, the relevant amplitudes are considered here again. As stated *e.g.* in [33], in the SM the CP -conjugate decay amplitudes for CP even final states can also be written as:

$$\begin{aligned} \mathcal{A}_f &\equiv \mathcal{A}(D^0 \rightarrow f) = \mathcal{A}_f^T [1 + r_f e^{i(\delta_f - \gamma)}], \\ \overline{\mathcal{A}}_f &\equiv \mathcal{A}(\overline{D}^0 \rightarrow f) = \mathcal{A}_f^T [1 + r_f e^{i(\delta_f + \gamma)}], \end{aligned} \quad (2.54)$$

where \mathcal{A}_f^T is the leading amplitude, here proportional to $(V_{cs}V_{us}^* - V_{cd}V_{us}^*)$ and r_f is the relative magnitude of the sub-leading amplitude, here proportional to $V_{cb}V_{ub}^*$. Both amplitudes carry a weak CKM phase (in this case $\gamma = (66.4_{-3.3}^{+1.2})^\circ$ [34],[35]) and a difference between the strong phases of the two amplitudes δ_f .

Then the direct CP -violation is given by:

$$a_{CP}^{dir}(f) \equiv \frac{|\mathcal{A}_f|^2 - |\overline{\mathcal{A}}_f|^2}{|\mathcal{A}_f|^2 + |\overline{\mathcal{A}}_f|^2} = 2r_f \sin(\gamma) \sin(\delta_f). \quad (2.55)$$

In order for direct CP -violation to occur in a decay such as $D^0 \rightarrow K^-K^+$ or $D^0 \rightarrow \pi^-\pi^+$, we need therefore two amplitudes, one leading, one sub-leading, with different strong and

weak phases. The different weak phases are given by contributions involving different CKM elements and the difference in the strong phase by different strong interaction processes.

The Feynman diagrams of these two processes are shown in Fig. 2.2. The tree level process is the leading amplitude, while the penguin diagram is the sub-leading amplitude. The penguin diagram includes a gluon exchange and has thus a different strong phase. γ is non-zero, as quoted above. Both diagrams are singly-Cabibbo suppressed (SCS) decays, since in both cases there is only one W -boson exchanged (the *gluon* in the penguin diagram does not count) and each vertex is multiplied by the corresponding CKM matrix element.

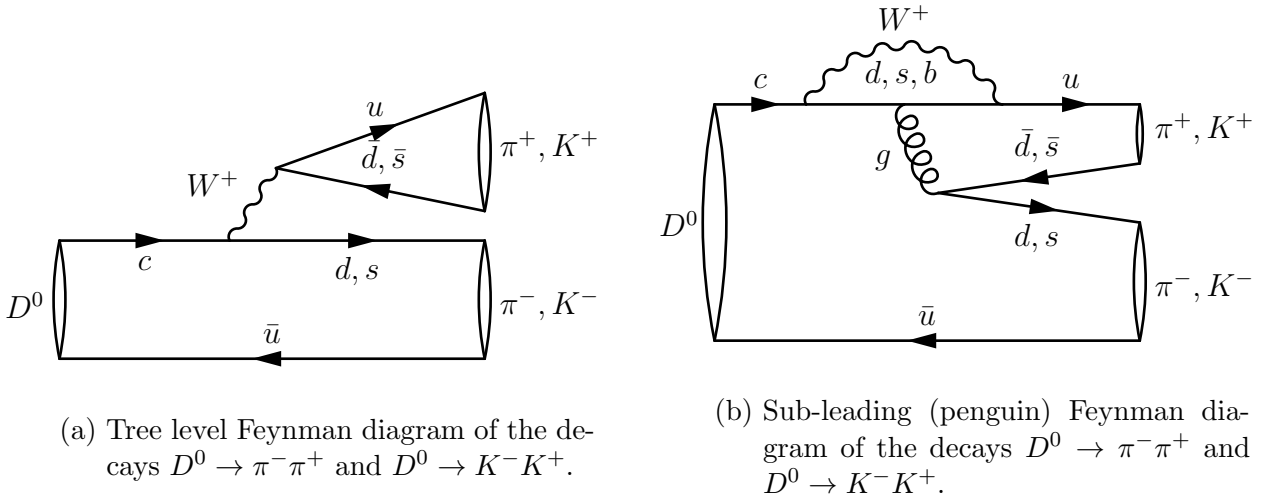


Figure 2.2.: Leading and sub-leading Feynman diagrams of the decays.

2.3. Analysis strategy

The measured asymmetries, $A_{raw}(f) = \frac{N(D^0 \rightarrow f) - N(\bar{D}^0 \rightarrow f)}{N(D^0 \rightarrow f) + N(\bar{D}^0 \rightarrow f)}$, with $N(X)$ the measured number yields in that decay channel, are not equivalent to $A_{CP}(f)$, but contain asymmetries introduced by the detector and the production process. The production process analyzed here are D^0 mesons produced from prompt $D^{*+} \rightarrow \bar{D}^0 \pi_s^+$ decays. The measured asymmetries can be described, neglecting second or higher orders due to the fact that all relevant asymmetries should be small, by the following:

$$A_{raw}(f) \approx A_{CP}(f) + A_D(f) + A_D(\pi_s^+) + A_P(D^{*+}), \quad (2.56)$$

where $A_D(f)$ is the detection asymmetry in the final state f , $A_D(\pi_s^+)$ is the detection asymmetry of the slow pion and $A_P(D^{*+})$ is the production asymmetry of the D^* -mesons. Since both relevant final states of the D^0 ($D^0 \rightarrow K^- K^+$, $D^0 \rightarrow \pi^- \pi^+$) are

self-conjugate CP -even eigenstates, there can be no detection asymmetry, leading to $A_D(K^-K^+) = A_D(\pi^-\pi^+) = 0$. The other two nuisance asymmetries, $A_D(\pi_s^+)$ and $A_P(D^{*+})$, are completely independent of f . They are therefore the same for $f = K^-K^+$ and $f = \pi^-\pi^+$ and cancel to first order in the difference between the two final states,

$$\Delta A_{CP} \equiv A_{CP}(K^-K^+) - A_{CP}(\pi^-\pi^+) = A_{raw}(K^-K^+) - A_{raw}(\pi^-\pi^+). \quad (2.57)$$

The observable ΔA_{CP} is robust against detector systematics and production asymmetries, and is sensitive to any direct CP -violation in SCS charm decays.

The $A_{raw}(K^-K^+)$ and $A_{raw}(\pi^-\pi^+)$ are not expected to be the same but to be of the same order of magnitude with opposite signs, and thus the sensitivity to CP -violation is enhanced in ΔA_{CP} .

However, the nuisance asymmetries $A_D(\pi_s^+)$ and $A_P(D^{*+})$ can vary as a function of some variables, e.g. the production asymmetries can vary as function of the D^{*+} transverse momentum and the pseudorapidity. If these distributions are very different for both modes, the nuisance asymmetries will not fully cancel. To minimize any second order effects, a weighting technique is used to equalize the relevant kinematic distributions.

2.4. Sensitivity to new physics

As is explained e.g. in [30], D -meson decays are a unique probe to study CP -violation and search for possible new physics contributions. First, the SM predicts very small CP -violation effects, $\mathcal{O}(10^{-3})$, which can be reached with the current experimental sensitivity. Therefore any sizable signal observed in this analysis would directly become a limit for new physics. The basic argument why the SM expectation is so small is that both D^0 - \bar{D}^0 mixing (responsible for indirect CP -violation) and SCS D decays (which are studied here) involve to a very good approximation only the first two quark generations. The b quark in the penguin loop in Fig. 2.2b is heavily CKM suppressed. This is what makes this analysis interesting, especially in light of the previous evidence for CP -violation at the percent level found by LHCb [5]. Further theoretical effort has been made after this evidence for CP -violation, which yielded the non-result that the SM might or might not be able to explain also $\Delta A_{CP} \sim \mathcal{O}(10^{-2})$. An exhaustive list of these efforts, as well as a list of potential effects of physics beyond the SM can be found in [36].

Second, the neutral D^0 system is the only system involving up -type quarks in mixing and decay. This makes it a unique probe into models which couple to the up -type sector (for example in supersymmetric models with alignment, [37, 38]).

Third, SCS decays are sensitive to new physics contributions to penguin and dipole operators. Among all hadronic D decays, the SCS decays are uniquely sensitive to CP -violation in $c \rightarrow u\bar{q}q$ quark transitions and, consequently, to new contributions to the

$\Delta C = 1$ QCD penguin and chromomagnetic dipole operators (with C being *charmness*). In particular, such contributions can affect neither the Cabibbo favored ($c \rightarrow s\bar{d}u$) nor the doubly Cabibbo suppressed ($c \rightarrow d\bar{s}u$) decays.

3. The LHCb experiment at the LHC

3.1. The Large Hadron Collider

The Large Hadron Collider (LHC) of the European Organization for Nuclear Research (french: Conseil Européen pour la Recherche Nucléaire, CERN) is a proton-proton collider located near Geneva, Switzerland. It has been running since 2010, with 2011 being the first full year of data taking. It ran at a center of mass energy of $\sqrt{s} = 7\text{TeV}$ in 2011 and $\sqrt{s} = 8\text{TeV}$ in 2012. The setup of the LHC is discussed in detail in the technical design report [39]. Four major experiments are collecting data of mainly pp -collisions. One of them is the LHCb-experiment.

3.2. The LHCb detector

A full technical description of the detector and its performance can be found in [40]. Here only an overview over the components which played a crucial role in this analysis is given. A view of the detector with its components can be seen in Fig. 3.1.

The LHCb detector is a particle detector at the LHC. It is a forward-spectrometer, similar to the design of fixed-target experiments, covering the pseudo-rapidity range from two to five, where the pseudorapidity η is defined as:

$$\eta = -\ln \left[\tan \left(\frac{\theta}{2} \right) \right], \quad (3.1)$$

with θ the opening angle between the particle track and the z -axis, which goes along the beampipe. The y -axis goes along the vertical, up being positive, therefore forming a right-handed coordinate system. The upper pseudo-rapidity limit is due to the edges of the detector. The lower acceptance bound is due to the beampipe, in which the proton bunches are accelerated in an ultrahigh vacuum. The part of the detector in front of the magnet (to the left in Fig. 3.1) is called upstream and the part of the detector behind the magnet (to the right) is called downstream.

The design of the LHCb detector was heavily influenced by the main production mechanism of heavy quark pairs (b or c), boson gluon fusion. Both quark pairs are emitted in the same direction. The cross section increases rapidly for small or large scattering

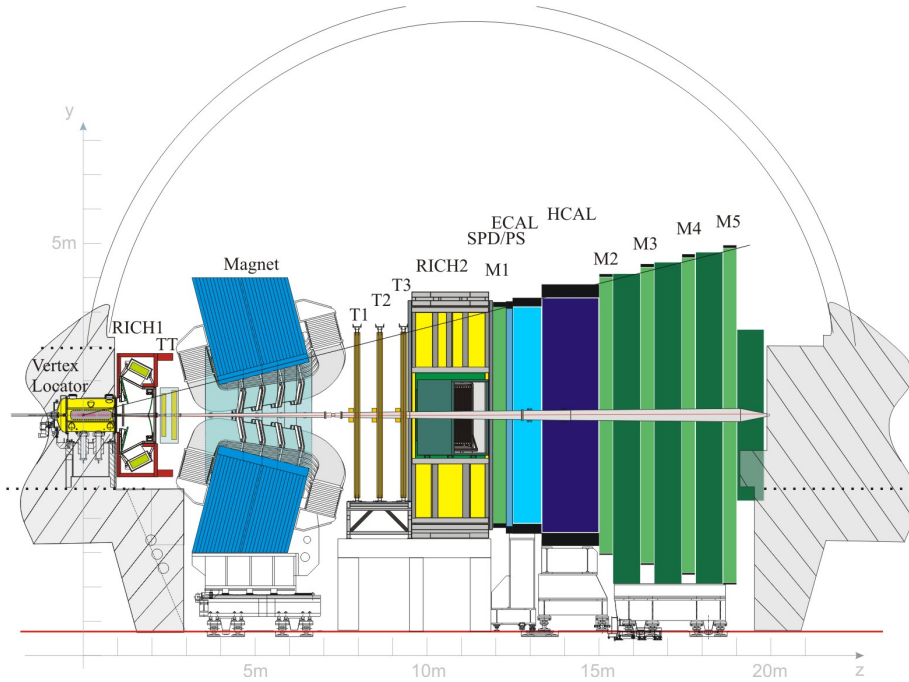


Figure 3.1.: View of the LHCb detector [40].

angles, as shown in Fig. 3.2 for $b - \bar{b}$ -production. Despite the design being optimized for B physics, LHCb is also well suited for charm physics. The production cross section of $pp \rightarrow c\bar{c}X$ at $\sqrt{s} = 7\text{TeV}$ is approximately 1.2 mb within the LHCb acceptance [41], which is roughly ten times the cross-section for $pp \rightarrow b\bar{b}X$ ($74\mu\text{b}$) [42]. This amounts to 10^{12} $c\bar{c}$ events per 1fb^{-1} of data, giving LHCb the largest sample of charm decays in the world.

In order to identify the final states correctly one of the main challenges of the detector is to track individual charged particles and measure their momenta. The other big challenge is the particle identification of the charged tracks. To achieve these goals, the LHCb detector is equipped with an excellent tracking system and a sophisticated particle identification system described in the following.

3.2.1. Vertex detector (VELO)

The *VELO* is a tracking detector constructed around the collision point to determine the position of the event vertices. It needs exceptionally good spatial resolution to be able to distinguish multiple primary vertices and flight distances down to a few μm . It consists of a series of layers of silicon pixel detectors with a primary vertex resolution in the x-y-plane of $11\mu\text{m}$ and of $60\mu\text{m}$ in the z-plane (for $N_{\text{track}} \approx 30$). The silicon modules provide a measure of the r and ϕ coordinates.

The detector modules can be retracted from the beam line, because the innermost sensors

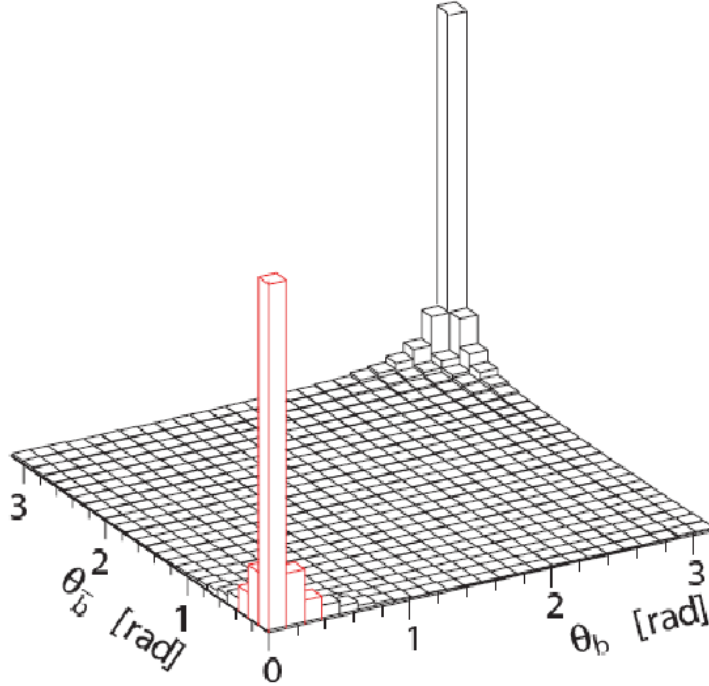


Figure 3.2.: Angular distribution of a $b\bar{b}$ -pair in the detector.

are closer to the beam than the safe distance during beam injection. A schematic view of the VELO detector layout is shown in Fig. 3.3.

3.2.2. Tracking system

The tracking system is used to measure the momentum of charged particles by measuring the curvature of their tracks in a magnetic field. For this purpose, LHCb has a magnet with an integrated magnetic field of 4 Tm. The magnet is not super-conducting due to economic reasons. The magnetic field is parallel to the y -axis and its orientation can be reversed. Roughly 50% of the data taken is with the magnetic field pointing in positive y direction, the other half with it pointing in the negative y direction. These two magnetic field configurations are called *up* and *down* during the rest of this thesis.

In addition to the VELO, which reconstructs tracks around the primary collision point, there are three more tracking systems. The first part is the Trigger Tracker (TT), a single tracking station upstream of the magnet covering the full LHCb acceptance. The second and third part are the Inner Tracker (IT) and the Outer Tracker (OT), which are placed downstream of the magnet (T1-T3 in Fig. 3.1). The IT covers the inner, high occupancy, region around the beampipe, while the OT covers the outer parts of the acceptance.

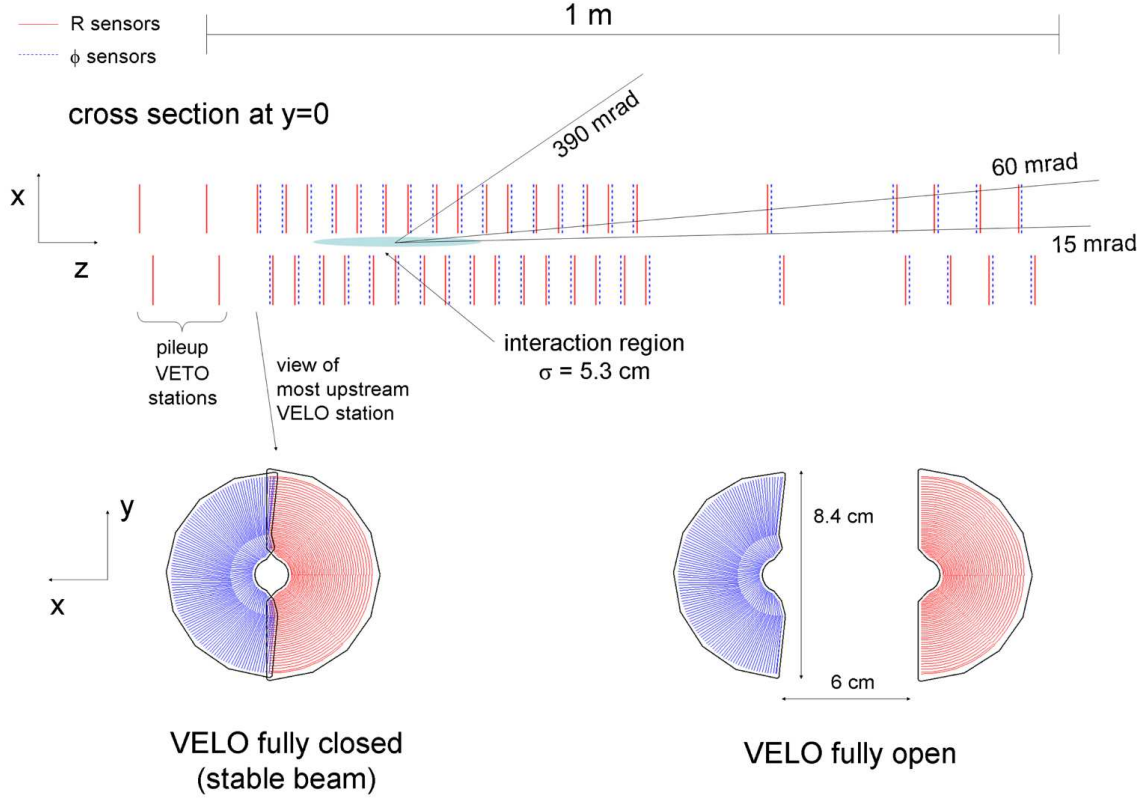


Figure 3.3.: Cross section in the (x, z) plane of the VELO silicon sensors, at $y = 0$, with the detector in the fully closed position. The front face of the first modules is also illustrated in both the closed and open positions. The two pile-up veto stations are located upstream of the VELO sensors [40].

The TT and the IT are silicone detectors designed for a spatial resolution of about $50\mu\text{m}$ and a high hit occupancy. The other major design constraint was a low material budget, to reduce multiple scattering both before and after the magnet.

The OT is a drift-time detector to measure the tracks of charged particles. It consists of individual, gas-filled straw-tubes with an inner diameter of about 4.9mm . The momentum resolution required to reconstruct the invariant mass of B - and D -mesons with sufficient accuracy is $\delta p/p \approx 0.4\%$. This translates into a spatial resolution of about $200\mu\text{m}$, which the OT is available to deliver.

3.2.3. Ring Imaging Cherenkov detector (RICH)

To be able to select the final states $D^0 \rightarrow K^- K^+$ and $D^0 \rightarrow \pi^- \pi^+$ which are used in this analysis, it is paramount to be able to distinguish between kaons and pions. The

particle identification is done by using the Cherenkov radiation of the charged particles. Cherenkov radiation is emitted by charged particles at an angle to their flight path if they are traversing a medium with a velocity greater than the speed of light in that medium. The opening angle of this light cone is given by

$$\cos(\theta_C) = \frac{1}{n\beta}, \quad (3.2)$$

where $\beta = \frac{v}{c}$ is the fraction of the speed of light of the particle and n is the refractive index in the medium. As can be seen in Fig. 3.4, this angle is different for different particles at the same momentum, since their masses are different. It also changes as a function of the refractive index of the medium (radiator) used.

The LHCb detector features two Ring Imaging Cherenkov (RICH) detectors, where the photons produced when crossing the radiators are reflected onto photomultipliers (PMTs). The hits in the PMTs are then used to reconstruct rings (the projections of the light cones on the detectors). The detector upstream of the magnet, RICH 1, covers the low momentum charged particle range $P \approx 1 - 60\text{GeV}/c$ using an aerogel and a C_4F_{10} radiator. The detector downstream of the magnet, RICH 2, covers the high momentum range from $P \approx 15\text{GeV}/c$ up to and beyond $100\text{ GeV}/c$ using a CF_4 radiator.

The RICH system provides good particle identification over the entire momentum range, as can be seen in Fig. 3.4. The average efficiency to identify a kaon with a momentum between 2 and $100\text{ GeV}/c$ correctly as a kaon is $\varepsilon(K \rightarrow K) \approx 95\%$. The corresponding average pion misidentification rate is $\varepsilon(\pi \rightarrow K) \approx 5\%$. Around $30\text{ GeV}/c$ the identification probability is $\varepsilon(K \rightarrow K) \approx 97\%$ and the misidentification probability $\varepsilon(\pi \rightarrow K) \approx 5\%$.

3.2.4. Calorimeter

The LHCb experiment is equipped with three calorimeters. An electromagnetic calorimeter (ECAL) stops electromagnetically interacting particles which are not hadrons, like electrons and photons. They produce electromagnetic showers, which are contained in the ECAL and allow an energy and position measurement. In front of the ECAL a pre-shower detector is located. The ECAL is followed by a hadronic calorimeter (HCAL). The HCAL stops strongly interacting particles, such as pions and kaons (which can also be electrically neutral, such as neutral pions). The calorimeter system is required for two reasons. It allows a measurement of the transverse energy E_T (the component of the energy perpendicular to the beam-axis), including the neutral component. This is needed in the Level-0-trigger (see Sec. 4.2). It also provides the identification of electrons, photons and hadrons and measures their energies and positions.

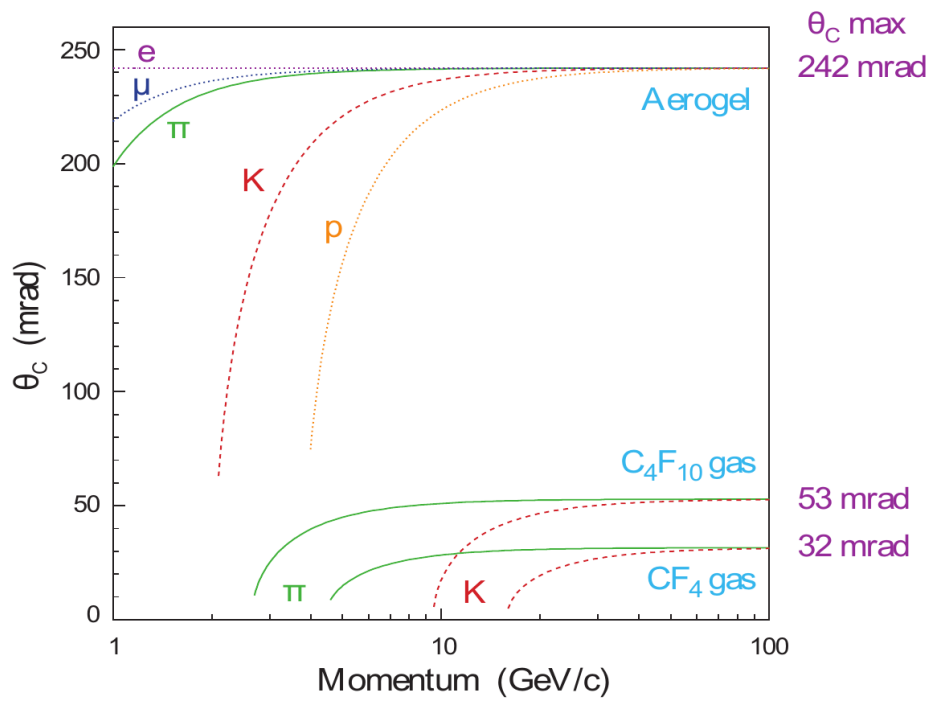


Figure 3.4.: Cherenkov angle versus particle momentum for the different RICH radiators [40].

4. Data selection

To measure ΔA_{CP} , the two decays $D^0 \rightarrow K^- K^+$ and $D^0 \rightarrow \pi^- \pi^+$ need to be selected. The process of achieving this is described in this section. To measure the individual CP -asymmetries, it is important to distinguish the decays of a D^0 and a \bar{D}^0 . However, since they produce the same final state, a method to identify the original flavor of the decaying particle is required. Choosing D^* decays, the flavor of the D^0 at production time can be determined by the charge of the D^* . This method is called prompt-tagging, if the D^* was produced at a primary vertex. The full decays studied here are then $D^{*+} \rightarrow D^0(\rightarrow K^- K^+) \pi_s^+$ and $D^{*+} \rightarrow D^0(\rightarrow \pi^- \pi^+) \pi_s^+$ and its charge conjugates¹ $D^{*-} \rightarrow \bar{D}^0(\rightarrow K^- K^+) \pi_s^-$ and $D^{*-} \rightarrow \bar{D}^0(\rightarrow \pi^- \pi^+) \pi_s^-$. The pion from the first decay is denoted with a subscript s for slow. This results from the fact that the difference between the mass of the $D^{*\pm}$ and the D^0 is only slightly larger than the rest mass of the pion, leaving only little energy for its momentum. The charge of the slow pion, π_s , uniquely determines whether the kaon or pion pair comes from the decay of a D^0 or \bar{D}^0 , a positive charge denoting a D^0 .

The data samples used in this analysis correspond to an integrated luminosity of approximately 1.0 fb^{-1} and 2.0 fb^{-1} for 2011 and 2012, respectively, collected by LHCb. During the 2011 and 2012 data taking periods, the LHC was operating at a center-of-mass energy of $\sqrt{s} = 7 \text{ TeV}$ and 8 TeV , respectively.

The recorded data is split into samples according to the two data taking periods, since the data collected in 2011 has already been unblinded, while this is not in general the case for 2012, yet.

The LHCb trigger is used to separate the possibly interesting events from the majority of events, which are just elastic pp -scattering. It is described in Sec. 4.2. Afterwards, the events are classified and further selection requirements are applied. This process, called stripping, is described in Sec. 4.3. In the end, selection criteria specific to an analysis are applied. The selection criteria used in this analysis are described in Sect 4.5.

¹The inclusion of charge-conjugate processes is from now on implied, unless explicitly stated otherwise.

4.1. Reconstruction

First, the way particle decays relevant for this analysis are reconstructed is sketched. First, information from the tracking system is combined to form parts of particle tracks (track segments). These track segments, together with calorimeter and muon information, are used by the trigger to decide whether the event was interesting. Then particle hypotheses are assigned from the information of other sub-detectors. Information from the two RICH detectors is used to separate the particles from each other. If a particle produced Cherenkov-light in the two RICH detectors it was charged and the opening angle is used to determine its velocity. The RICH detectors deliver a likelihood for a particle to belong to a certain particle species, *i.e.* for every charged track there exists a likelihood that it was a pion, a kaon, a proton, an electron and so on. The difference between two such likelihoods can be used to evaluate whether a particle was more likely to have been e.g. a pion rather than a kaon. This specific difference is called *Difference in Log Likelihood of being a kaon or a pion* ($DLL_{K\pi}$) and is used in the selection (see Sec. 4.5).

The tracks, with particle hypotheses assigned, are then used to construct mother particles, either from the primary vertex or a secondary decay vertex. In this way, e.g. two tracks with the most likely particle hypothesis being a kaon (hereafter referred to as *kaon*) are combined to form a D^0 meson. This D^0 candidate can then be further combined with a pion track if they point somewhere close to a primary vertex to form a D^* candidate.

4.2. Trigger

The LHCb experiment is designed to operate at an average instantaneous luminosity of $2 \times 10^{32} \text{cm}^{-2} \text{s}^{-1}$. This luminosity is much lower than the maximum LHC design luminosity. In order to maintain this lower (but almost constant) instantaneous luminosity, the beams are displaced with respect to each other, lowering the overlapping area. This offset is continuously reduced, while the bunches deteriorate, ensuring a constant instantaneous luminosity for an extended period of time (see Fig. 4.1). This reduction in data rate is a compromise to reduce the radiation damage to the detector components and electronics. Furthermore, the average number of visible interactions per bunch crossing at LHCb is about $\mu = 1.8$. This way the reconstruction becomes easier to handle, since only one or two primary vertices need to be identified. Even with a reduced instantaneous luminosity, the interaction rate is much higher than the rate, at which events can be written to offline storage. In addition, not every event is interesting, many are just elastic pp -collisions. To reduce this rate to a manageable rate, and enhance the data written to storage with interesting physics processes, the online trigger is used. The LHCb trigger is a two (three) level trigger system, described in the following sub-sections. A sketch of the different trigger levels is shown in Fig. 4.2.

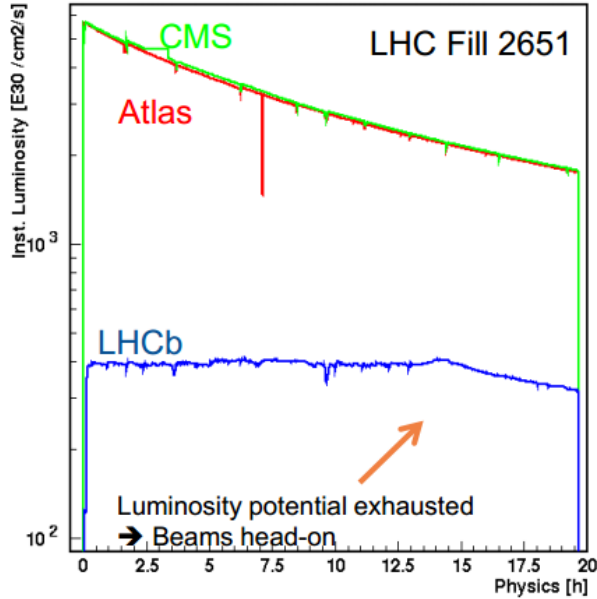


Figure 4.1.: Comparison of the instantaneous luminosity as delivered to the LHCb experiment and the other LHC experiments [43]. The latter receive a higher instantaneous (and integrated) luminosity, while LHCb is able to maintain an almost constant instantaneous luminosity at (or rather by a factor of two above) the design luminosity of the detector.

4.2.1. Level-0 trigger

The first trigger level is the Level-0 trigger (L0). This trigger is implemented in custom hardware and reduces the rate at which events are processed from 40 MHz (the bunch crossing rate of the LHC), of which about 10 MHz are visible in the detector², to about 1 MHz (the rate at which the full detector can be read out).

The L0 trigger searches for events which have particles with high energies, since especially B mesons have a high mass. This is also true for charmed mesons. It therefore attempts to reconstruct

- the clusters in the calorimeters with the highest E_T (hadrons, electrons and photon clusters),
- the two highest p_T muons in the muon chambers.

The second criterion is not relevant for the decays studied here. However, it is paramount for the many semileptonic B decays studied at LHCb. It is also important for the complementary measurement of ΔA_{CP} with a semileptonic tagging of the initial D^0 flavor. Additionally, the number of primary pp interactions in each bunch crossing is

²An interaction is only visible in the detector if at least two charged particles have sufficient hits in the VELO and subsequent tracker stations to be reconstructible.

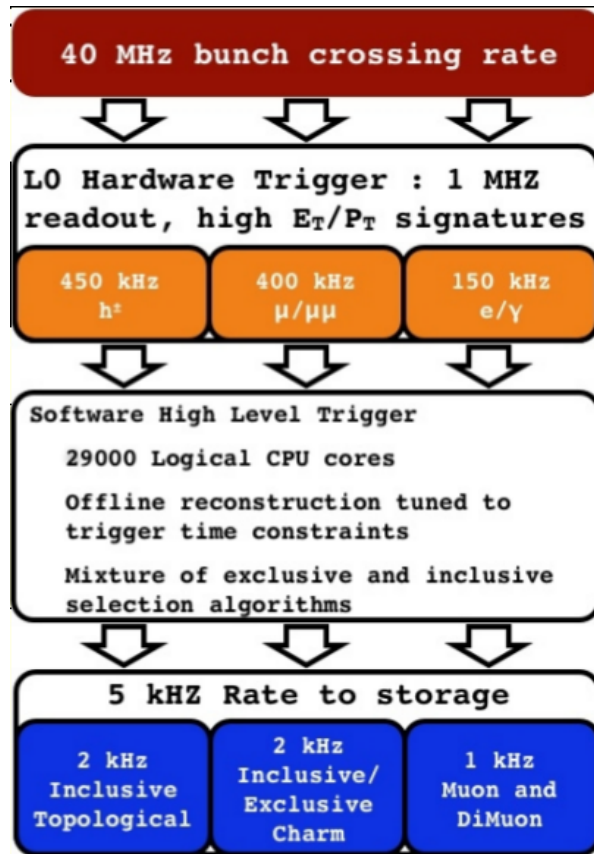


Figure 4.2.: Sketch of the trigger layout of LHCb. The different stages, as well as the different lines are visible.

estimated in the VELO and the total observed energy and an estimate for the number of tracks is determined.

In this thesis two different L0 triggers were used. One requires that at least one of the D^0 daughters is a hadron with TriggerOnSignal (TOS) on `Hlt1TrackAllL0`. This means, that one of the D^0 daughters triggered this event with its energy deposition in the calorimeters and it can be identified as a hadron by its energy deposition in the hadronic calorimeter. Furthermore, there is the possibility that something else triggered the event, therefore both daughters are TriggerIndependent(of)Signal (TIS).

This distinction is important, since in TOS events the triggering particle tends to have a higher p_T , since having a high E_T is one of the trigger requirements and the two are correlated. For the TIS events, this condition does not exist and therefore the kinematics for the two triggers are different. This can be seen in Fig. 4.3, where the transverse momentum of the D^0 is shown for the $D^0 \rightarrow K^- K^+$ magnetic field up TIS and TOS samples. Having these two trigger lines tests whether the trigger requirements bias the final measurement.

The data samples used in this analysis are therefore split into the two disjoint sub-samples

1. L0Hadron TOS on D^0 ,
2. (NOT L0Hadron TOS on D^0) AND (L0Global TIS on D^{*+}),

which are per construction statistically independent. These two subsets of the data are referred to as *TOS* and *TIS* in the rest of this thesis.

4.2.2. High Level Trigger

The second level of the LHCb trigger is the High Level Trigger (HLT) implemented in software, which is further separated into HLT1 and HLT2. This second level reduces the event rate from 1 MHz down to 5 kHz (the rate at which events can be written to storage for further offline analysis). In order to do so, the HLT makes use of the full event data. Candidates found by the L0 trigger are refined by the full information available.

4.2.2.1. HLT1

The first part of the HLT, HLT1 reconstructs the particles in the VELO, the position of primary vertices and it determines the impact parameters³ of the particles. Only tracks satisfying the minimum track quality, impact parameter, momentum, and transverse

³see Sec. 8.9.4 for the definition of the impact parameter

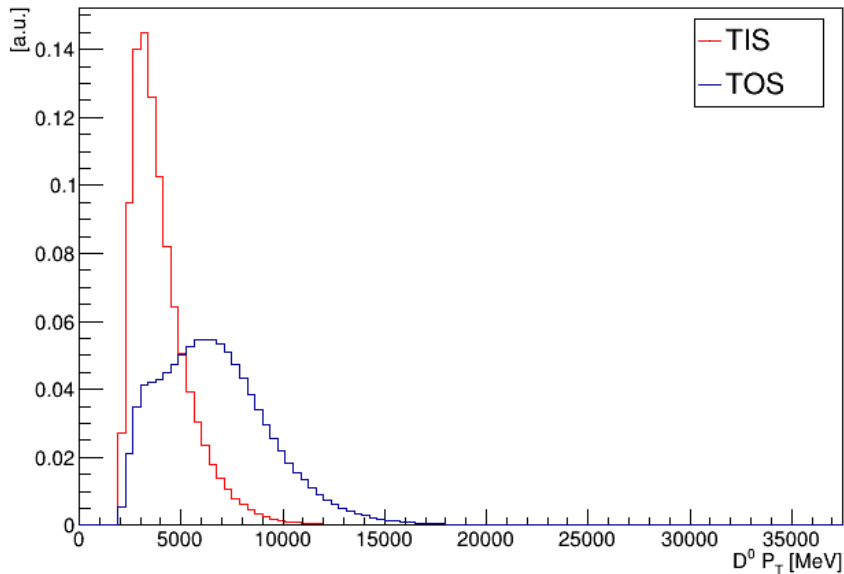


Figure 4.3.: Distribution of the reconstructed transverse momentum of the D^0 in the sample KK down for both trigger settings (TIS and TOS). Both distributions are normalized such that their integral is unity. The influence of the L0 trigger for the TOS sample (requiring some transverse energy for one of the daughters) becomes apparent.

momentum are processed further. This reduces the event rate sufficiently, such that the rest of the track reconstruction can be run for the selected events.

4.2.2.2. HLT2

In the second part of the HLT, the HLT2, sets of tracks with very loose selection criteria on their momentum and impact parameter are combined to form composite particles. These include particles such as $K^* \rightarrow K^+\pi^-$, $D^0 \rightarrow hh$ or $J/\psi \rightarrow \mu^+\mu^-$. Afterwards criteria on the invariant mass or on momenta of the composite particles pointing back to the primary vertex are applied.

The two HLT2 trigger lines used for the measurement of ΔA_{CP} are called

KK : `Hlt2CharmHadD02KK` OR `Hlt2CharmHadD02HH_D02KK`

and

$\pi\pi$: `Hlt2CharmHadD02PiPi` OR `Hlt2CharmHadD02HH_D02PiPi`,

which select $D^0 \rightarrow hh$ decays with $h \in K, \pi$.

For each final state there are two trigger lines listed, because the trigger names changed after the early 2011 data taking.

4.3. Stripping

Even after the trigger requirements, the data sets produced are still large. To ease physics analysis, events are classified according to selection criteria characteristic for certain physics classes and written to disk in so-called streams. The different streams have different selection criteria to enhance specific physics processes. This procedure is called *stripping*. In this analysis, the `DstarForPromptCharm` line from the CHARM micro-DST stream [12] is used, selecting decays of D^* produced at a primary vertex (where they decay almost instantly through the strong interaction). The data has been reconstructed with reconstruction version 14 and stripping version 20. The two final states $K^-K^+\pi_s^+$ and $\pi^-\pi^+\pi_s^+$ (and its charge conjugates) are selected by the same stripping line with coherent selection requirements to ensure no differences due to different selection criteria.

DstarForPromptCharm stripping line

The `DstarForPromptCharm` stripping line begins with global event selection criteria and a D^0 selection including the final states $K^-\pi^+$, K^-K^+ , $K^+\pi^-$ and $\pi^+\pi^-$. The D^0 candidates are then combined with pions to form $D^{*+} \rightarrow D^0\pi_s$ candidates. The following criteria are applied to achieve this:

- Global event selection:
 - Number of primary vertices: 1–3
 - Number of tracks in `Rec/Track/Best` < 400
 - Number of hits in `Raw/Spd/Digits` < 500
 - Number of clusters in `Raw/IT/Clusters` < 1000
 - Number of VELO tracks in `Rec/Track/Best` < 200
- soft pion criteria:
 - Base list: `Phys/StdNoPIDsPions`
 - Track $\chi^2/\text{NDF} < 5$
- D^0 selection:
 - For the $D^0 \rightarrow \pi^+\pi^-$ final state, the mass window is tightened to: $-50 < [m(D^0) - m_{\text{nominal}}] < +75 \text{ MeV}/c^2$

- Pre-fit (combination) selection:
 - $m(D^0\pi^+) < 2500 \text{ MeV}/c^2$
 - $\Delta m = m(D^0\pi^+) - m(D^0) < 165 \text{ MeV}/c^2$
- Post-fit (mother) selection:
 - Vertex fit $\chi^2 < 64$
 - $\Delta m = m(D^0\pi^+) - m(D^0) < 155 \text{ MeV}/c^2$

4.4. Decay Tree Fitter (DTF)

The data set used for this analysis has been processed using the DecayTreeFitter (DTF) package [44]. The DTF refines the reconstructed masses by imposing additional criteria at the decay vertices. Here, it is used with the constraint that the D^* decay chain has to point back to a reconstructed primary vertex in the event and that the difference between the D^* mass and the D^0 mass is at least the pion mass. Other possible constraints could be e.g. that the reconstructed D^* mass is the PDG value. The masses of all other particles are then refitted with these additional constraints. The constraints applied here improve the D^* mass resolution and consequently give a gain in the precision of the raw asymmetries.

However, some additional quality controls need to be applied to ensure that the fit output is sensible. First, it is required that the DTF converged (implemented as $\text{NDF} > 0$). Second, it is required that the DTF fit quality is reasonable (see Sec. 4.5): $\chi^2 < 750$ (for $\text{NDF}=5$).

In Fig. 4.4 the $\Delta m = m(D^*) - m(D^0) = m(D^0\pi_s) - m(D^0)$ distribution with and without the DTF is shown. The gain in resolution in Δm is roughly a factor of 2, as measured with the width of a simple Gaussian distribution. Without the DTF, this width is $\sigma = 0.73 \text{ MeV}$, where after application of the DTF, this width becomes $\sigma = 0.34 \text{ MeV}$. Also in Fig. 4.4 is the correlation between non-DTF and DTF Δm . It is visible, that the application of the DTF does cause some migrations of events, with the overall effect of an improvement of resolution. The constraint on Δm^{DTF} to be bigger than the charged pion mass ($139.57 \text{ MeV}/c^2$ [18]) is also visible.

4.5. Selection requirements

In order to improve the signal over background ratio and reduce the number of and wrongly combined D^* candidates, further selection criteria are applied. These are almost

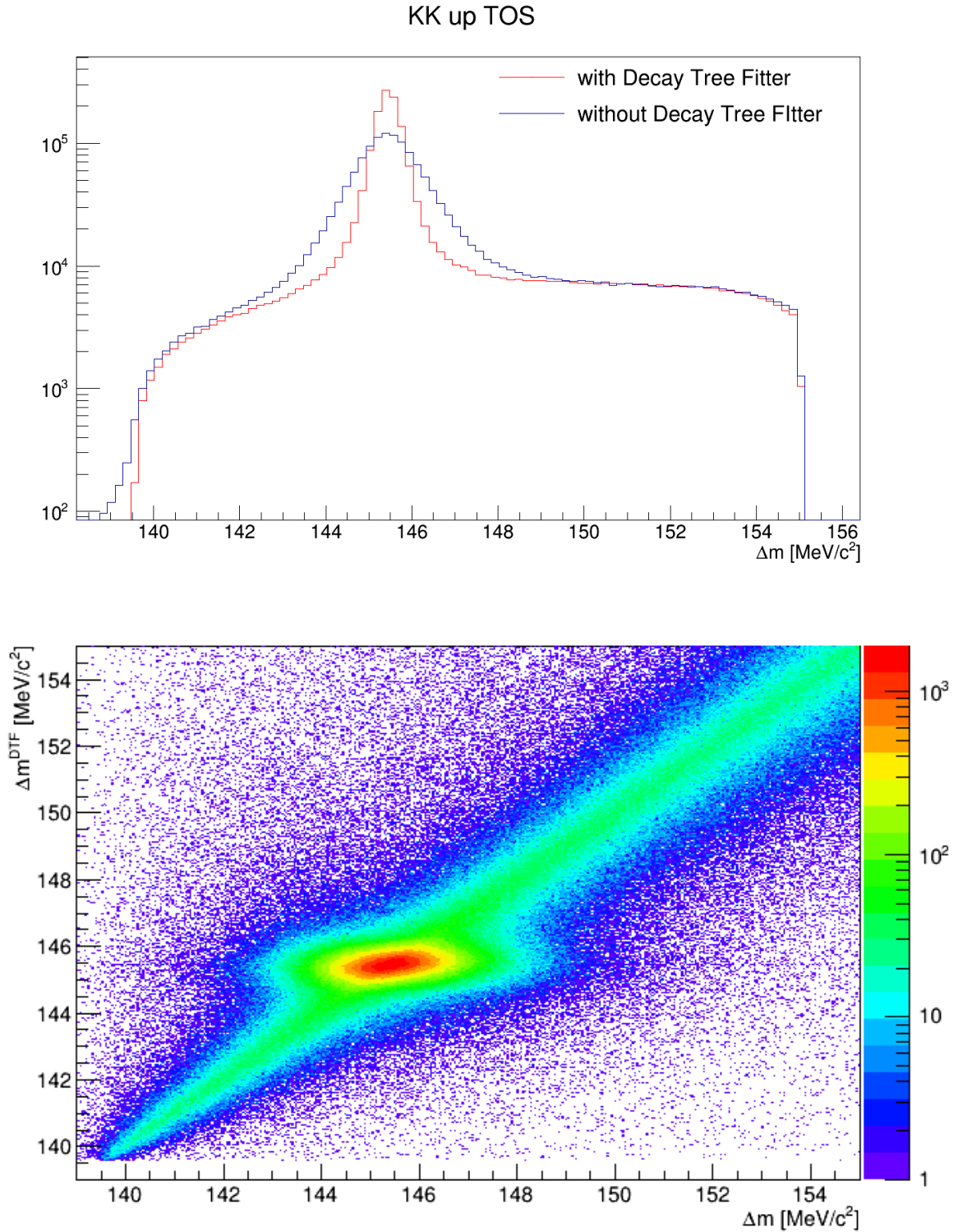


Figure 4.4.: Comparison of the Δm distribution with and without the Decay Tree Fitter (top) and correlation between non-DTF Δm and DTF Δm (bottom) on the example of the 2012 KK up TOS sample.

equivalent to the ones already used in the preliminary 2011 analysis [6]. The selection criteria are summarized in Tab. 4.1.

Table 4.1.: Selection criteria used in this analysis.

Particle	Variable	Selection criterion
D^*	χ_{DTF}^2 ⁴	$\in (0, 750)$
	Δm^{DTF}	$\in (139.77, 151.57) \text{ MeV}/c^2$
D^0	$m(D^0)$	$\in (1760, 1940) \text{ MeV}/c^2$
$D^0 \rightarrow K^- K^+$	$DLL_{K\pi}$	> 5 for both K
$D^0 \rightarrow \pi^- \pi^+$	$DLL_{K\pi}$	< -5 for both π

The two most important requirements are on the mass of the reconstructed D^0 , $m(D^0)$, and on the reconstructed D^* mass. For the latter not the D^* mass directly, but a different measure defined as $\Delta m = m(D^*) - m(D^0) = m(D^0\pi_s) - m(D^0)$ is used. This measure has the advantage of a much much better resolution and in addition cancels systematic uncertainties due to the difference measurement. The shape of the backgrounds is also different and easier to describe. In total, this allows an easier separation into signal and background. The reconstructed D^0 mass is required to lie within a window around the nominal D^0 mass. This window is chosen slightly different for the two final states, because the mass resolution for kaons and pions in the final state is slightly different. The values used are reported in Tab. 4.2. This requirement is the only major criterion

Table 4.2.: D^0 mass windows for the determination of ΔA_{CP} in Δm .

Particle	Variable	Cut
$D^0 \rightarrow K^- K^+$	$m(D^0)$	$\in (1850, 1884) \text{ MeV}/c^2$
$D^0 \rightarrow \pi^- \pi^+$	$m(D^0)$	$\in (1845, 1889) \text{ MeV}/c^2$

different compared to the preliminary 2011 analysis. In addition, this criterion is not applied on the data sample level, but on-the-fly when performing the determination of the asymmetries. Thus, the asymmetries can also be determined with a two-dimensional model (in Δm and $m(D^0)$), which allows the determination of the influence of possible backgrounds peaking in Δm (see Sec. 8.6). In Fig. 4.5, the two-dimensional distribution with the selection criteria for the Δm fit as red lines are shown.

Furthermore, the DecayTreeFitter (see Sec. 4.4) has to have converged properly. This ensures that the reconstructed D^* candidate points in the direction of a primary vertex and is a reasonable D^* candidate (and not just random combinations of kaons and pions). This criterion is not able to reduce the background from random combinations to zero, but is able to constrain it. The second additional criterion concerns the particle

⁴The definition of χ_{DTF}^2 used here differs from the one used in the preliminary 2011 analysis. There $\chi_{DTF}^2 = \chi_{DTF}^2/ndf$, where ndf is the number of degrees of freedom, was used. The number of degrees of freedom is five for all events. Therefore in the 2011 analysis $0 < \chi_{DTF}^2 < 150$ is used.

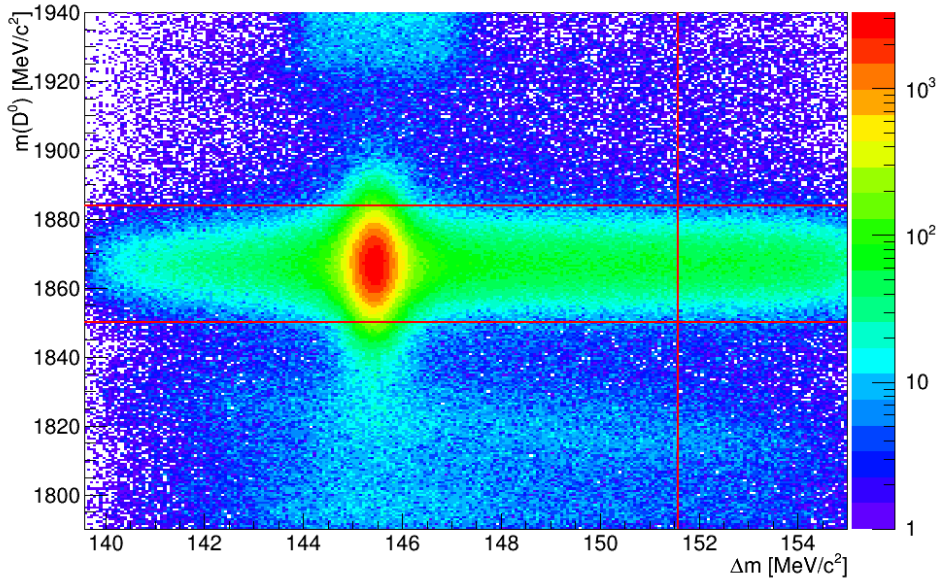


Figure 4.5.: Distribution of the events in the KK up TOS sample in the plane of Δm and $m(D^0)$. The red lines represent the selection requirements for the determination of the asymmetries using the Δm distribution.

identification. Since in the end it is the goal to measure the difference of the CP -asymmetries in the two decays $D^0 \rightarrow K^-K^+$ and $D^0 \rightarrow \pi^-\pi^+$, it is important to be able to cleanly distinguish between the two. In addition to the two signal decays, also the decays $D^0 \rightarrow K^-\pi^+$ and $D^0 \rightarrow K^+\pi^-$ are possible (the latter is doubly-Cabibbo suppressed and plays no role here, though). Therefore, a single misidentification of one of the two particles in a $D^0 \rightarrow K^-\pi^+$ decay would result in it being counted as either of the two signal decays. Additionally, a double misidentification in one of the signal decay channels would contaminate the other channel. To avoid this, the $DLL_{K\pi}$ (see Sec. 4.1) is used. For the decay $D^0 \rightarrow K^-K^+$, the $DLL_{K\pi}$ is required to be greater than five for both kaons. This requirement is a slightly tighter requirement than usual to ensure a clean separation between $D^0 \rightarrow K^-K^+$ and $D^0 \rightarrow \pi^-\pi^+$ decays. Similarly, for the decay $D^0 \rightarrow \pi^-\pi^+$, the $DLL_{K\pi}$ is required to be less than minus five. These requirements ensure that the two hadrons in the final state are much more likely to have been either two kaons or two pions than a misidentified different decay.

4.5.1. Fiducial Cuts

One possible reason for asymmetries induced by the detector are given by the combination of the limits of the detector acceptance and the magnet. Tracks which are close to the edges of the detector acceptance before the magnet will be swept out of the acceptance by the magnet, depending on their charge. In addition, tracks close to the

beampipe will be swept into the beampipe, again depending on their charge. Swapping the magnetic polarity inverses this effect, sweeping out particles of the opposite charge. This effect should cancel when taking the average of the magnetic field polarities *up* and *down*. Still, since the approximations made e.g. in Eq. 2.51 and 2.56 are only valid to first order, it is important that all asymmetries are small. The regions right at the edge of the detector can have a charge-asymmetry of up to 100%, which can definitely not be considered small. Therefore, these regions of high charge-asymmetry are excluded using the fiducial cuts described in Appendix N of [12]. For convenience, these criteria are outlined here. The momentum components of the soft pion are called p_x, p_y, p_z . Then, if $|p_y/p_z| > 0.2$ and:

$$|p_x| \leq \alpha(p_z - p_0), \quad (4.1)$$

with

$$\begin{aligned} \alpha &= 0.317, \\ p_0 &= 2400\text{MeV}/c, \end{aligned}$$

the event is being rejected, because it is at the edge of the detector acceptance. Alternatively, if $|p_y/p_z| < 0.2$ and

$$p_1 - \beta p_z < |p_x| < p_2 + \beta_2 p_z, \quad (4.2)$$

with

$$\begin{aligned} p_1 &= 418\text{MeV}/c, \\ p_2 &= 497\text{MeV}/c, \\ \beta_1 &= 0.01397, \\ \beta_2 &= 0.01605, \end{aligned}$$

the event is being rejected because it is too close to the beampipe. The effect of the specific values of the chosen parameters is studied as a source of systematic uncertainty (see Sec. 8.8).

4.6. Data sets

As already discussed in Sec. 4.2.1, the data are split according to the L0 trigger, which can be either *TIS* or *TOS* and according to the magnetic field polarity. This can be either *up* or *down*. The yields after all stripping and selection requirements obtained in the four different possible classes, separated by the decay and year recorded, are presented in Tab. 4.3. Since the 2011 data was previously unblinded, while the 2012 data was not, 2011 and 2012 data are analyzed separately. In total this yields eight sub-samples for each year. In total, roughly 18 million events are analyzed in this analysis.

Table 4.3.: Yields of the different data sets used in this analysis, after the selection. The data is split according to final state, year, magnetic polarity, and trigger.

Sample	Entries
KK-2012-up-TIS	3,363,368
KK-2012-up-TOS	1,581,564
KK-2012-down-TIS	3,401,069
KK-2012-down-TOS	1,592,377
PiPi-2012-up-TIS	1,053,064
PiPi-2012-up-TOS	483,221
PiPi-2012-down-TIS	1,094,394
PiPi-2012-down-TOS	502,278
KK-2011-up-TIS	1,053,294
KK-2011-up-TOS	542,533
KK-2011-down-TIS	1,507,126
KK-2011-down-TOS	791,765
PiPi-2011-up-TIS	337,338
PiPi-2011-up-TOS	171,801
PiPi-2011-down-TIS	482,644
PiPi-2011-down-TOS	248,011
Total	18,205,847

4.7. Treatment of multiple candidates

The combination of kaon or pion candidates into D^0 candidates and then further into D^* candidates does not always yield exactly one combination. Rather it happens that two or more different π_s can be combined with the same D^0 to form different D^* candidates and that more than one candidate survives the selection criteria. These additional entries are called multiple candidates. Other possibilities, such as different D^0 candidates are negligible, since the number of slow pions in an event far exceeds the number of pion or kaon pairs with sufficient momenta to form a D^0 whose mass lies within the required mass window. To measure the number of events with more than one D^* candidate, the following percentage is evaluated for all sub-samples.

$$multiple\ candidates = 1 - \frac{Number\ of\ events}{Number\ of\ candidates}, \quad (4.3)$$

where the same event can have more than one candidate, as described above. In Tab. 4.4 these ratios can be seen for all eight 2012 sub-samples, both before the selection, and after the selection.

These multiple candidates should in general not influence the measurement of ΔA_{CP} , since they do not peak in Δm , but contribute to the background of random pions

combined with a D^0 candidate, starting at the rest mass of the pion. Nevertheless, the effect of multiple candidates needs to be studied. At the very least, these events may bias the analysis towards events with higher multiplicities, since events with a higher multiplicity have a higher chance of having more than one D^* candidate survive the selection.

Table 4.4.: Fraction of multiple candidates, as defined in Eq. 4.3 for all eight sub-samples, before and after the selection.

Sample	multiple candidates before selection	multiple candidates after selection
$\pi\pi$ up TOS	7.95%	4.36%
$\pi\pi$ down TOS	7.89%	4.26%
$\pi\pi$ up TIS	13.95%	7.92%
$\pi\pi$ down TIS	13.94%	7.86%
KK up TOS	7.52%	4.06%
KK down TOS	7.48%	4.08%
KK up TIS	13.23%	7.48%
KK down TIS	13.14%	7.47%

In previous analyses, there have been different approaches used to deal with multiple candidates. In the preliminary 2011 analysis [6], all multiple candidates were retained. As a cross-check, one candidate was chosen randomly. The difference of these two approaches in ΔA_{CP} was taken as systematic uncertainty. This approach neglects the fact that there is information available on which π_s is the most likely candidate and also the knowledge that only one (if any) of the candidates can be an actual signal event. At BELLE, $\chi^2 = \chi^2_{production} + \chi^2_{decay}$, the sum of the production and decay vertex χ^2 was taken to choose the best candidate [45].

Here, a different qualifier is evaluated, a combination of the χ^2 from the DTF and the probability of the π_s being classified as a ghost track (P_{ghost}), converted to a χ^2 term. The former gives a measure of how well the D^* candidate points back to a primary vertex and matches the decay chain. Reconstructed tracks may in reality consist of measurements from several different particles, noise and spillover (leftovers from the previous bunch-crossing) measurements, which happen to look like a track to the pattern recognition [46]. The latter gives a probability of this for the track of the π_s . The qualifier is then:

$$\chi^2 = \chi^2_{DTF} + \left(\frac{P_{ghost} - \mu_{ghost}}{\sigma_{ghost}} \right)^2, \quad (4.4)$$

where μ_{ghost} and σ_{ghost} are the theoretical value and the square root of the variance of the ghost probability, respectively. The theoretical value of the ghost probability is taken as zero, whereas the variance is taken from data (with $\sigma^2 = rms^2 - \mu^2$). This value varies slightly between the final states and magnetic field polarity, as can be seen in Tab. 4.5. The average of these values is used. Thus, Eq. 4.4 becomes:

Data set	<i>rms</i>	μ	$\frac{1}{\sigma_{ghost}}$
KK down	0.1866	0.1069	6.538
KK up	0.1879	0.1076	6.492
$\pi\pi$ down	0.1953	0.1164	6.377
$\pi\pi$ up	0.1968	0.1174	6.331
Average			6.4 ± 0.1

Table 4.5.: Width of the ghost probability of the π_s for the two final states and the different magnetic field polarities.

$$\chi^2 = \chi_{DTF}^2 + (P_{ghost} \cdot 6.4)^2 \quad (4.5)$$

The ghost probability is considered alongside the χ_{DTF}^2 , because there are events, which have a low χ_{DTF}^2 but also have a ghost probability close to one. This can be seen in Fig. 4.6, where the plane of χ_{DTF}^2 vs. the ghost probability is shown for $\chi_{DTF}^2 < 100$. Multiple candidates of the same event are sorted by this qualifier and only the candidate

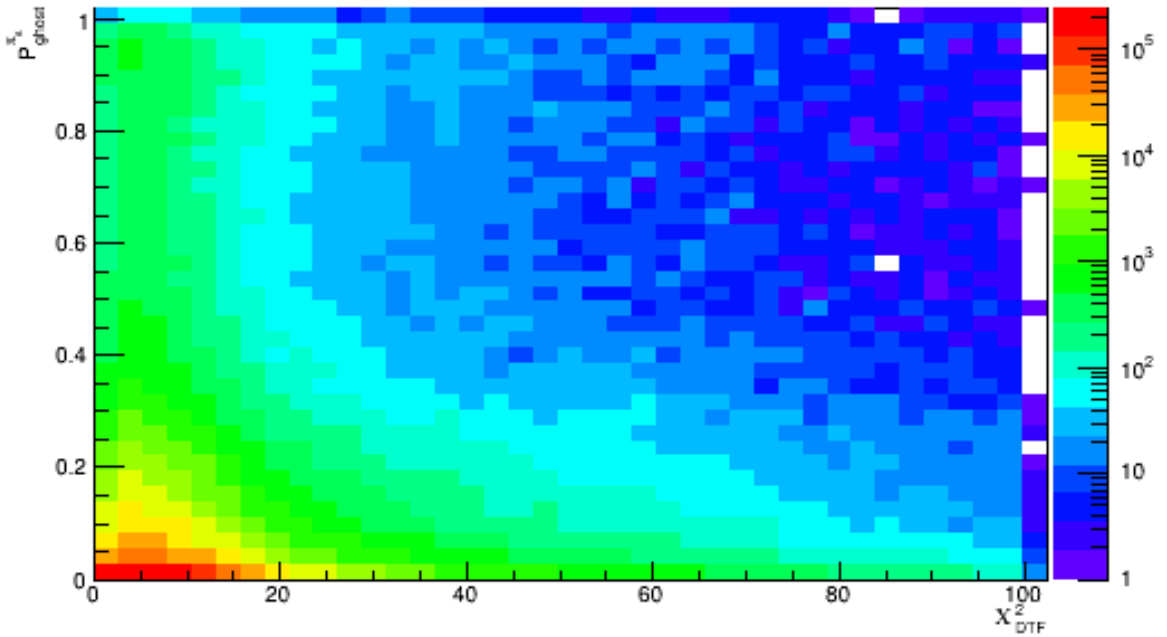


Figure 4.6.: χ_{DTF}^2 versus π_s ghost probability in the $D^0 \rightarrow K^- K^+$ 2012, magnetic field up, sample after the nominal selection. The rise towards higher ghost rates is visible, especially at low χ_{DTF}^2 .

with the lowest qualifier is retained. In events with only one candidate surviving the selection, this candidate is kept. The effect of this measure can be seen in Fig. 4.7. Here the Δm spectra of the chosen candidate, the not selected candidates, all candidates surviving this selection (*i.e.* also events with one candidate), as well as the Δm spectrum

of retaining all candidates are shown. It can be seen that the qualifier chooses the signal candidate more often than it rejects it, the peak height of the chosen candidate is roughly twice the height of the rejected candidates. The signal to background ratios (S/B) (defined here as the peak height divided by the background height at 152 MeV) for the three spectra are 6.0, 11.6, 48.2 and 42.5, respectively. From this it also becomes clear, that using this qualifier rejects mostly background candidates.

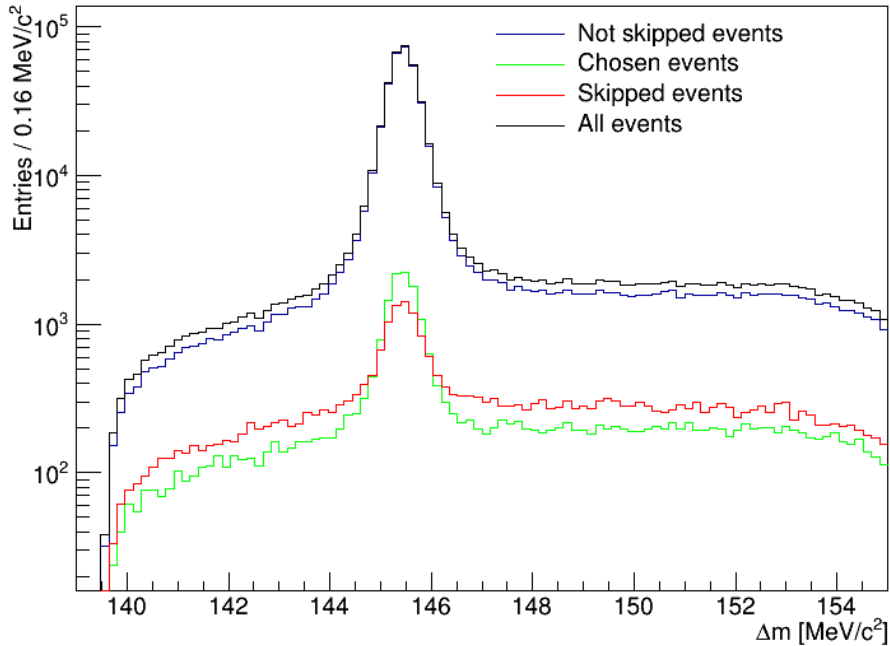


Figure 4.7.: Δm spectrum for the PiPi 2012, magnetic field up, sample after the selection. Included is the spectrum for the candidates chosen with the qualifiers (green), the ones skipped with it (red), all not skipped events (blue) (=chosen events + events with only one candidate, which are chosen automatically) and the spectrum without any selection of a candidate.

All approaches (retaining all candidates, choosing one candidate according to some selection criterion, choosing a random candidate, using only events for which only one candidate exists) were considered. In the end it was decided to stay with the approach of the preliminary 2011 analysis and keep all candidates surviving the selection to avoid any possible bias introduced through a selection. As a cross-check all of the different treatments of multiple candidates are studied. This is presented in Sec. 8.7.

5. Description of mass distributions

In contrast to the preliminary analysis performed on the 1fb^{-1} of data recorded in 2011, where a binned χ^2 fit was employed, here binned and unbinned maximum-likelihood fits are used. For the final result only the distribution in the mass-difference Δm is fitted. In order to determine a possible peaking background in Δm , originating from misreconstructed or misidentified events, the correlation of Δm and $m(D^0)$ can be exploited. For this a fit in the plane of Δm and $m(D^0)$ is performed.

The models described in this section were implemented with the *RooFit* [47] package available in *ROOT* [48]. They are implemented as Probability Density Functions (PDFs), where the PDF gives for all values of x a probability that an event is being described by that PDF ($x \in \Delta m, m(D^0)$).

In general, the models to describe the data defined here are only phenomenologically motivated. The models for the signal part should be Gaussian-like, since the mass resolution is dominated by the detector resolution and not the natural line-width of the particles. The exact combination of Gaussian functions or similar PDFs is purely motivated by its ability to describe the data reasonably well. The same is true for the description of the background. Variations of the parametrizations defined here are studied as sources of systematic uncertainty (see Sec. 8.4 and 8.5 for signal and background model, respectively).

5.1. Mass difference

The signal model in Δm is described by the sum of two Gaussian functions

$$G_i^\pm(\mu^\pm, \sigma_i^\pm; \Delta m) = \frac{1}{\sigma_i^\pm \sqrt{2\pi}} \exp \left[-\frac{1}{2} \left(\frac{\Delta m - \mu^\pm}{\sigma_i^\pm} \right)^2 \right], \quad (5.1)$$

and one Johnson function:

$$J^\pm(\mu^\pm, \sigma^\pm, \gamma, \delta; \Delta m) = \frac{\delta}{\sigma^\pm \sqrt{2\pi} \sqrt{1. + \left(\frac{\Delta m - \mu^\pm}{\sigma^\pm} \right)^2}} \exp \left[-\frac{1}{2} \left(\gamma + \delta \cdot \text{asinh} \left(\frac{\Delta m - \mu^\pm}{\sigma^\pm} \right) \right)^2 \right], \quad (5.2)$$

where μ^\pm is the location parameter, σ^\pm the scale parameter and γ and δ are shape parameters. In addition, $\sigma^- = w \cdot \sigma^+$, with the factor w describing the possibly different widths between D^{*+} and D^{*-} decays. The Johnson function can be asymmetric around its peak and can rise much faster than a Gaussian function. All three functions share the same mean (or location parameter) μ^\pm , which is allowed to be different for D^{*+} and D^{*-} decays. The full signal PDF is given by

$$\begin{aligned} \mathcal{P}_{sig}^\pm(\Delta m) = & f_1 \cdot G_1^\pm(\mu^\pm, \sigma_1^\pm; \Delta m) \\ & + (1 - f_1) \cdot f_2 \cdot G_2^\pm(\mu^\pm, \sigma_2^\pm; \Delta m) \\ & + (1 - f_1)(1 - f_2) \cdot J^\pm(\mu^\pm, \sigma^\pm, \gamma, \Delta; \Delta m), \end{aligned} \quad (5.3)$$

where the fractions $f_{1,2,3}$ between the three functions are defined recursively to ensure that their sum is unity.

The background is described using a parametrization stemming from the *BaBar* experiment, which is implemented in *Roofit* as follows (up to the normalization):

$$\mathcal{P}_{bg}(A, B, C, \Delta m_0; \Delta m) = \left(1 - e^{-\frac{(\Delta m - \Delta m_0)}{C}}\right) \cdot \left(\frac{\Delta m}{\Delta m_0}\right)^A + B \cdot \left(\frac{\Delta m}{\Delta m_0} - 1\right), \quad (5.4)$$

where Δm_0 is the turn-on point of the function and A, B, C are shape parameters. Since both A and B describe the tail of the distribution (C describes the behavior directly after the turn-on), B is fixed to 0, to reduce the number of free parameters. This leads to:

$$\mathcal{P}_{bg}(A, C, \Delta m_0; \Delta m) = \left(1 - e^{-\frac{(\Delta m - \Delta m_0)}{C}}\right) \cdot \left(\frac{\Delta m}{\Delta m_0}\right)^A. \quad (5.5)$$

Alternatively, A can be fixed to 0, which is studied to evaluate the systematic effect of a different background shape (see Sec. 8.5). This leads to:

$$\mathcal{P}_{bg}(B, C, \Delta m_0; \Delta m) = \left(1 - e^{-\frac{(\Delta m - \Delta m_0)}{C}}\right) + B \cdot \left(\frac{\Delta m}{\Delta m_0} - 1\right). \quad (5.6)$$

The background shape is not allowed to vary between D^{*+} and D^{*-} decays. However, the shape parameters are allowed to differ between $D^0 \rightarrow K^- K^+$ and $D^0 \rightarrow \pi^- \pi^+$ decays, magnetic field polarity *up* and *down*, and trigger *TIS* and *TOS*. They are in general not the same.

5.2. D^0 mass

For simplicity the same names for some of the parameters are used here, however, they are not the same as in Δm , *i.e.* an additional index of $m(D^0)$ is implicit.

The signal model in $m(D^0)$ is also described by a sum of two Gaussian functions

$$G_i(\mu_i, \sigma_i; m) = \frac{1}{\sigma_i \sqrt{2\pi}} \exp \left[-\frac{1}{2} \left(\frac{m - \mu_i}{\sigma_i} \right)^2 \right], \quad (5.7)$$

and an added bifurcated Gaussian function

$$G_{bifur}(\mu_2, \sigma_L, \sigma_R; m) = N \cdot \begin{cases} \exp \left[-\frac{1}{2} \left(\frac{m - \mu_2}{\sigma_L} \right)^2 \right], & \text{if } m < \mu_2 \\ \exp \left[-\frac{1}{2} \left(\frac{m - \mu_2}{\sigma_R} \right)^2 \right], & \text{else,} \end{cases} \quad (5.8)$$

with some normalization N , which is not expressed here for simplicity. A bifurcated Gaussian function is a Gaussian, where both sides of the peak are allowed to have a different width. The bifurcated Gaussian function and the second Gaussian function share the same mean, μ_2 . In total the signal part in $m(D^0)$ is described by

$$\begin{aligned} \mathcal{P}_{sig}(m) &= f_1 \cdot G_{bifur}(\mu_2, \sigma_L, \sigma_R; m) \\ &+ (1 - f_1) f_2 \cdot G_1(\mu_1, \sigma_1; m) \\ &+ (1 - f_1)(1 - f_2) \cdot G_2(\mu_2, \sigma_2; m), \end{aligned} \quad (5.9)$$

where $m = m(D^0)$.

For the one-dimensional fit the background in $m(D^0)$ is described by a 2nd order Chebychev-polynomial function. This is equivalent to a regular 2nd order polynomial, but without correlation between the parameters, since the Chebychev-polynomials are all orthogonal to each other.

$$\begin{aligned} \mathcal{P}_{bg}(c_1, c_2; m) &= T_0 + c_1 T_1(x) + c_2 T_2(x) \\ &= 1 + c_1 x + c_2 (2x^2 + 1) \end{aligned} \quad (5.10)$$

with

$$T_0(x) = 1, \quad (5.11)$$

$$T_1(x) = x, \quad (5.12)$$

$$T_2(x) = 2x^2 + 1, \quad (5.13)$$

and

$$x = 2 \frac{m - m_{min}}{m_{max} - m_{min}} - 1, \quad (5.14)$$

where the definition of x ensures the correct normalization in the interval where the PDF is evaluated.

5.3. Two-dimensional fit

The signal model for the two-dimensional determination of the asymmetries in the plane $(\Delta m, m(D^0))$ is just the product PDF of the two previously defined signal PDFs:

$$\mathcal{P}_{sig}(\Delta m, m) = \mathcal{P}_{sig}(\Delta m) \cdot \mathcal{P}_{sig}(m). \quad (5.15)$$

For the two-dimensional fit, an additional background is added. The first part of the two-dimensional background is the background from the random slow pions. Since this background is the combination of a slow pion with a real D^0 , in m the signal PDF is used:

$$\mathcal{P}_{bg}^{rand}(\Delta m, m) = \mathcal{P}_{bg}(\Delta m) \cdot \mathcal{P}_{sig}(m). \quad (5.16)$$

The second background considered in the two-dimensional fit is a background that possibly peaks in Δm . It could bias the analysis, when performing only a one-dimensional fit in Δm . It is assumed to be described by a peaking distribution in Δm and by the combinatorial background in $m(D^0)$, since they are not real D^0 candidates:

$$\mathcal{P}_{bg}^{peak}(\Delta m, m) = \mathcal{P}_{bg}^{peak}(\Delta m) \cdot \mathcal{P}_{bg}(m), \quad (5.17)$$

with

$$\mathcal{P}_{bg}^{peak}(\Delta m) = \mathcal{P}_{bg}(\Delta m) + (1 - f_1) \cdot G_{bifur}(\Delta m), \quad (5.18)$$

where $G_{bifur}(\Delta m)$ is another bifurcated Gaussian, which is just a simplified signal shape. This simplified shape, instead of the full Δm signal model, is used due to the expected limited statistics of the peaking background component. This leads to the two-dimensional description of the peaking background

$$calP_{bg}^{peak}(\Delta m, m) = \mathcal{P}_{bg}(\Delta m) \cdot \mathcal{P}_{bg}^{peak}(m) + (1 - f_1) \cdot G_{bifur}(\Delta m) \cdot \mathcal{P}_{bg}(m). \quad (5.19)$$

From this the full background PDF is constructed:

$$\mathcal{P}_{bg}(\Delta m, m) = \mathcal{P}_{bg}^{peak}(\Delta m, m) + (1 - f_2) \cdot \mathcal{P}_{bg}^{rand}(\Delta m, m) \quad (5.20)$$

Therefore all possible combinations of signal and background PDFs in the two dimensions Δm and $m(D^0)$ are considered (*sig, sig*; *sig, bg*; *bg, sig*; *bg, bg*). The exception is the combination of the signal-shape in Δm and the background-shape in $m(D^0)$. For this combination a simplified model was chosen for the Δm signal part.

5.4. Final model

Independent of the variable (and in how many dimensions) the fit is performed, the final PDF is always composed as follows:

$$\begin{aligned}\mathcal{P}^+ &= \frac{N_{sig}}{2}(1 + A_{raw}) \cdot \mathcal{P}_{sig}^+ + N_{bg}^+ \cdot \mathcal{P}_{bg}, \\ \mathcal{P}^- &= \frac{N_{sig}}{2}(1 - A_{raw}) \cdot \mathcal{P}_{sig}^- + N_{bg}^- \cdot \mathcal{P}_{bg},\end{aligned}\tag{5.21}$$

where \mathcal{P}_{sig} and \mathcal{P}_{bg} are the corresponding signal and background models as discussed above, depending on the variable in which the fit is performed. \mathcal{P}^+ and \mathcal{P}^- are the PDFs for the two decays $D^{*+} \rightarrow D^0 \pi_s^+$ and $D^{*-} \rightarrow \bar{D}^0 \pi_s^-$, respectively. N_{bg}^+ and N_{bg}^- are the number of background events of the two decays and N_{sig} is the total number of signal events, defined as $N_{sig} = N - N_{bg}^+ - N_{bg}^-$, with the total number of events in the sample, N . A_{raw} is the raw CP -asymmetry (see Sec. 2.3), which is measured for the two decays $D^0 \rightarrow K^- K^+$ and $D^0 \rightarrow \pi^- \pi^+$ to determine ΔA_{CP} . This value is determined, along with the various shape-parameters, fractions and the two numbers of background events by performing a (binned) maximum-likelihood fit.

6. Determination of CP -asymmetries

In this section the results of the CP -asymmetry measurements are presented. The model for the mass difference described in Sec. 5.1 is used to describe the data in Δm . Unbinned maximum-likelihood fits are performed to obtain the raw asymmetries in the different sub-samples. The result is the weighted average of the two triggers TIS and TOS , and both magnetic field polarities. Originally the individual asymmetries for the 2012 data samples were shifted by a random offset, blinding the analysis. Since this blinding has been removed for this thesis, all results are unblinded (yet still preliminary).

The 2011 data results are presented in Table 6.1 and the corresponding Δm plots are shown in Fig. 6.2 and Fig. 6.3. The results for the 2012 data are given in Tab. 6.2 with the corresponding Δm plots shown in Fig. 6.4 and Fig. 6.5. For both years of data taking, the model is able to describe the Δm distributions with a good agreement, as is visible from the residual distributions underneath the spectra. The residual distribution is defined as $\frac{data(\Delta m) - pdf(\Delta m)}{\sigma_{data}(\Delta m)}$. A good overview of the agreement of the results for the different sub-samples can be seen in Fig. 6.1. In the following, whenever no year is specified, the results are determined on the 2fb^{-1} collected in 2012.

Table 6.1.: Results of the raw asymmetries and ΔA_{CP} for 2011 data.

Sample	$A_{raw}(KK)[\%]$	$A_{raw}(\pi\pi)[\%]$	$\Delta A_{CP}[\%]$
up TOS 2011	-1.437 ± 0.169	-1.059 ± 0.302	-0.378 ± 0.346
up TIS 2011	-1.985 ± 0.139	-1.729 ± 0.251	-0.256 ± 0.287
down TOS 2011	-0.694 ± 0.137	-0.356 ± 0.251	-0.338 ± 0.286
down TIS 2011	-0.150 ± 0.117	-0.095 ± 0.211	-0.055 ± 0.241
weighted average	-0.942 ± 0.068	-0.719 ± 0.124	-0.228 ± 0.142

Table 6.2.: Results of the raw asymmetries and ΔA_{CP} for 2012 data.

Sample	$A_{raw}(KK)[\%]$	$A_{raw}(\pi\pi)[\%]$	$\Delta A_{CP}[\%]$
up TOS	-1.297 ± 0.103	-1.154 ± 0.185	-0.143 ± 0.212
up TIS	-1.799 ± 0.082	-1.512 ± 0.149	-0.287 ± 0.170
down TOS	-0.455 ± 0.103	-0.184 ± 0.181	-0.272 ± 0.208
down TIS	-0.227 ± 0.081	-0.456 ± 0.146	0.229 ± 0.167
weighted average	-0.953 ± 0.045	-0.850 ± 0.081	-0.096 ± 0.093

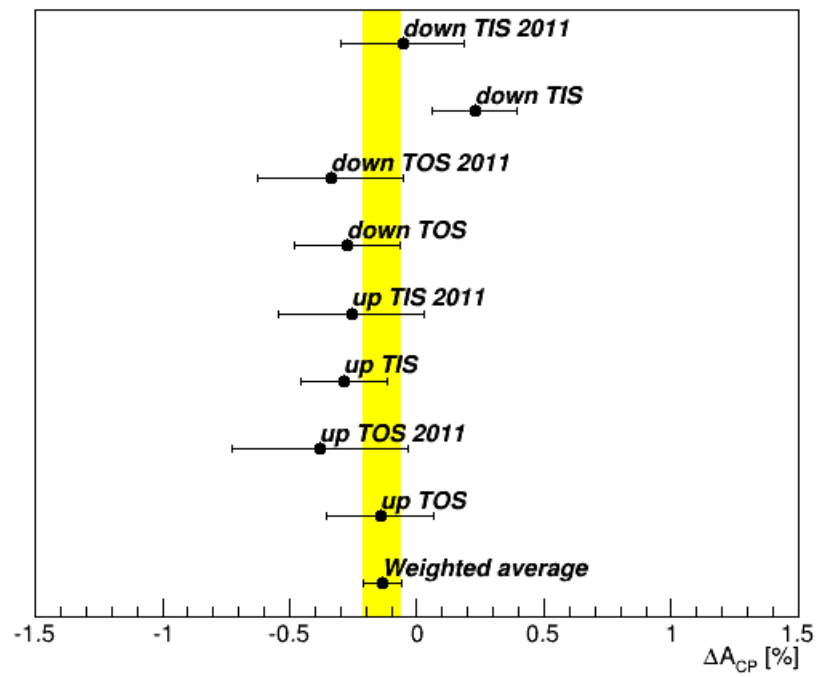


Figure 6.1.: Overview over the unblinded results from the 2011 and 2012 fits.

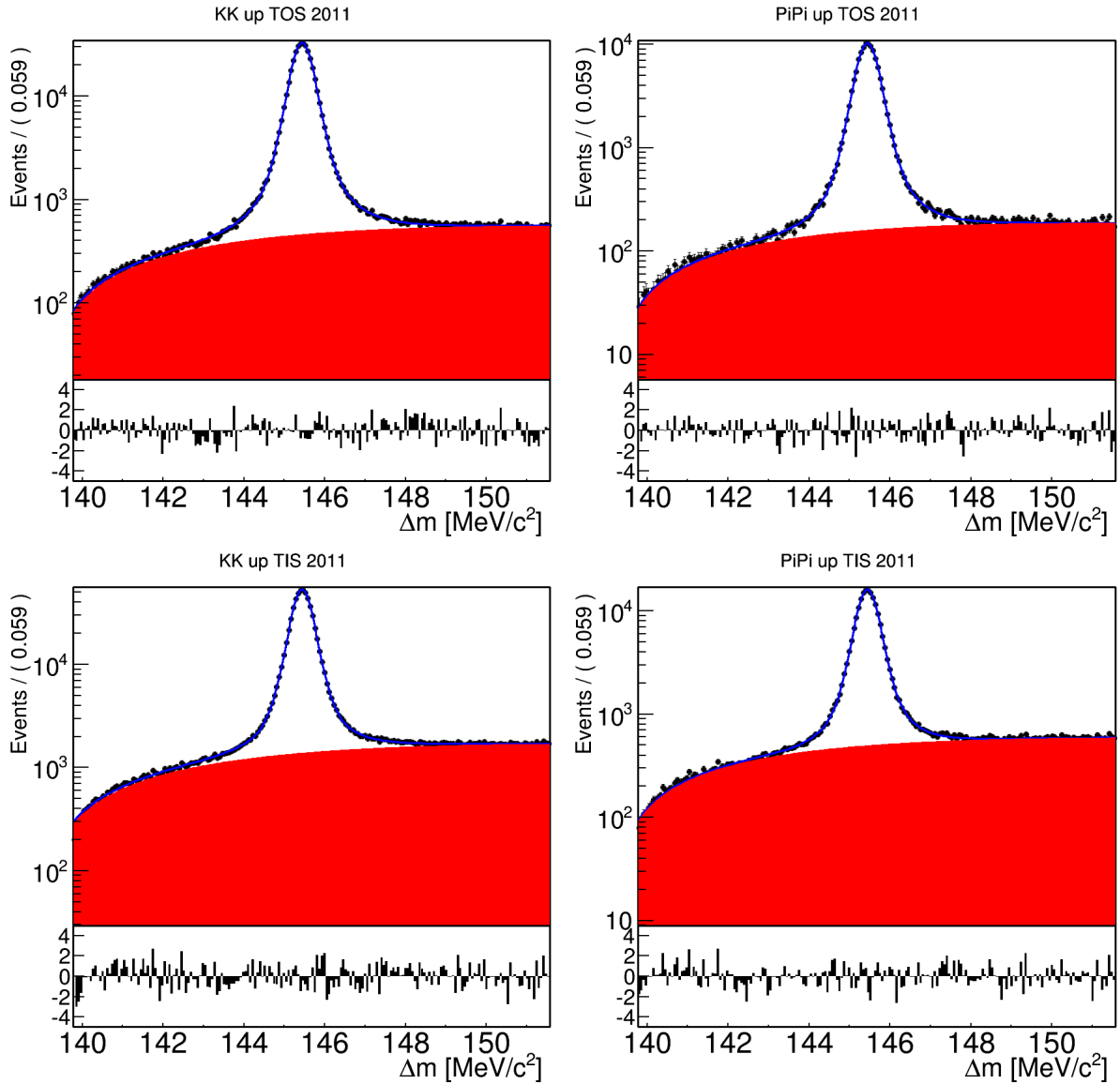


Figure 6.2.: Δm spectra of $D^0 \rightarrow K^- K^+$ (left) and $D^0 \rightarrow \pi^- \pi^+$ decays (right) for the two different triggers TOS (top) and TIS (bottom) for magnetic field polarity *up* for 2011 data. The red region is the random slow pion background, while the signal model is the remaining white region. The total model used to describe the data is the blue line, with the data points in black. The errors of the data points are absorbed in the size of the points.

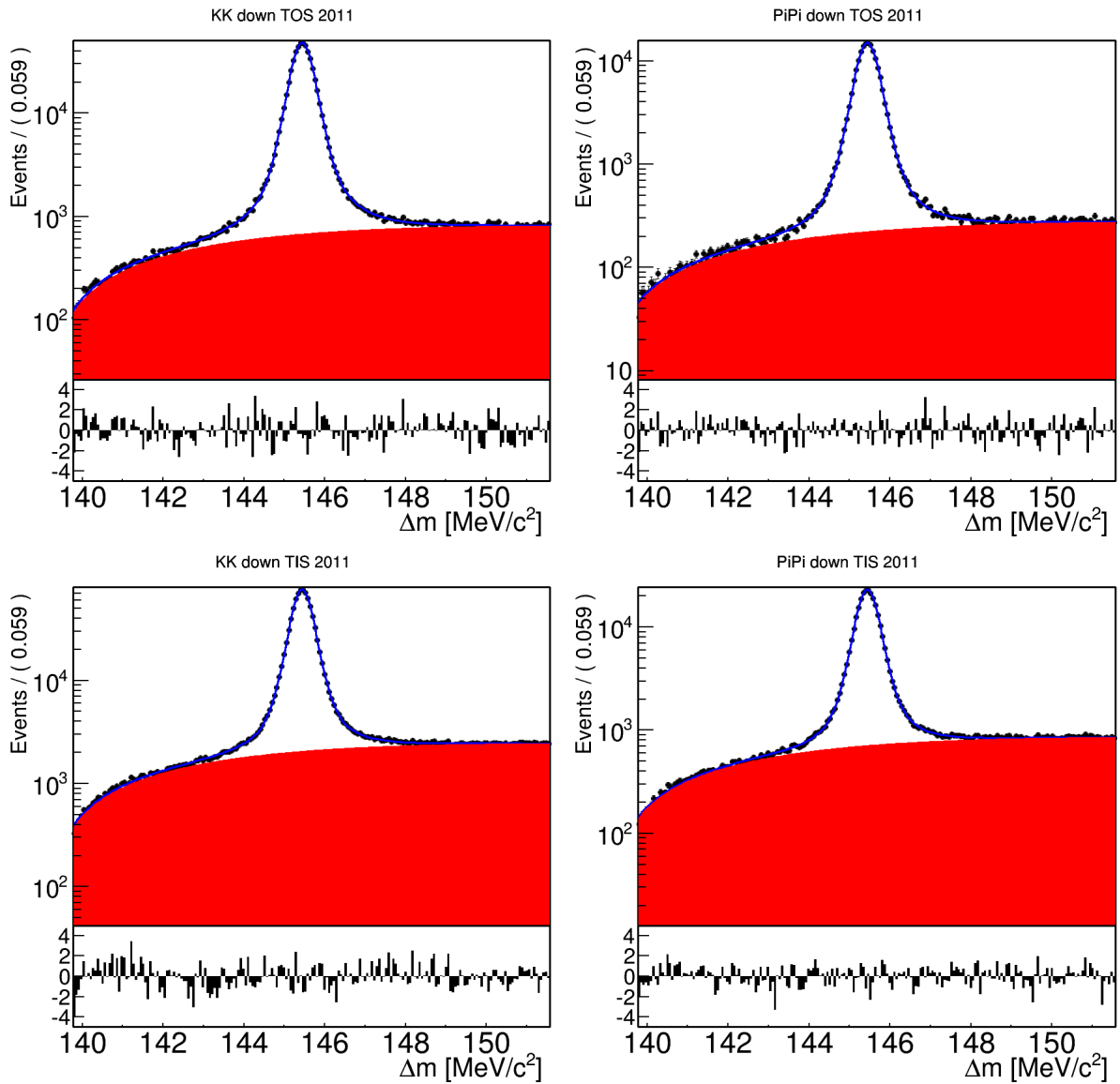


Figure 6.3.: Δm spectra of $D^0 \rightarrow K^- K^+$ (left) and $D^0 \rightarrow \pi^- \pi^+$ decays (right) for the two different triggers TOS (top) and TIS (bottom) for magnetic field polarity *down* for 2011 data. The red region is the random slow pion background, while the signal model is the remaining white region. The total model used to describe the data is the blue line, with the data points in black. The errors of the data points are absorbed in the size of the points.

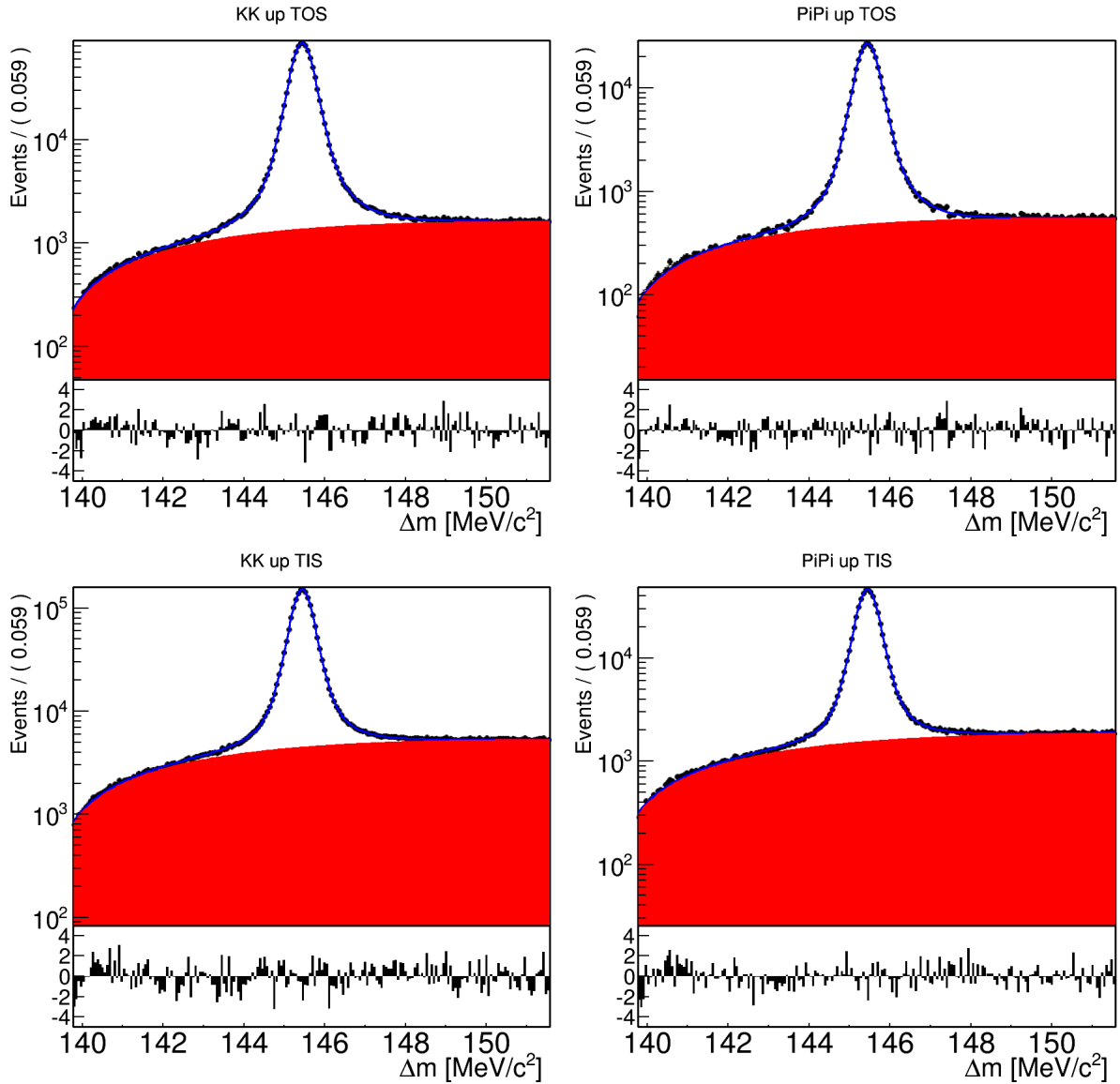


Figure 6.4.: Δm spectra of $D^0 \rightarrow K^- K^+$ (left) and $D^0 \rightarrow \pi^- \pi^+$ decays (right) for the two different triggers TOS (top) and TIS (bottom) for magnetic field polarity *up* for 2012 data. The red region is the random slow pion background, while the signal model is the remaining white region. The total model used to describe the data is the blue line, with the data points in black. The errors of the data points are absorbed in the size of the points.

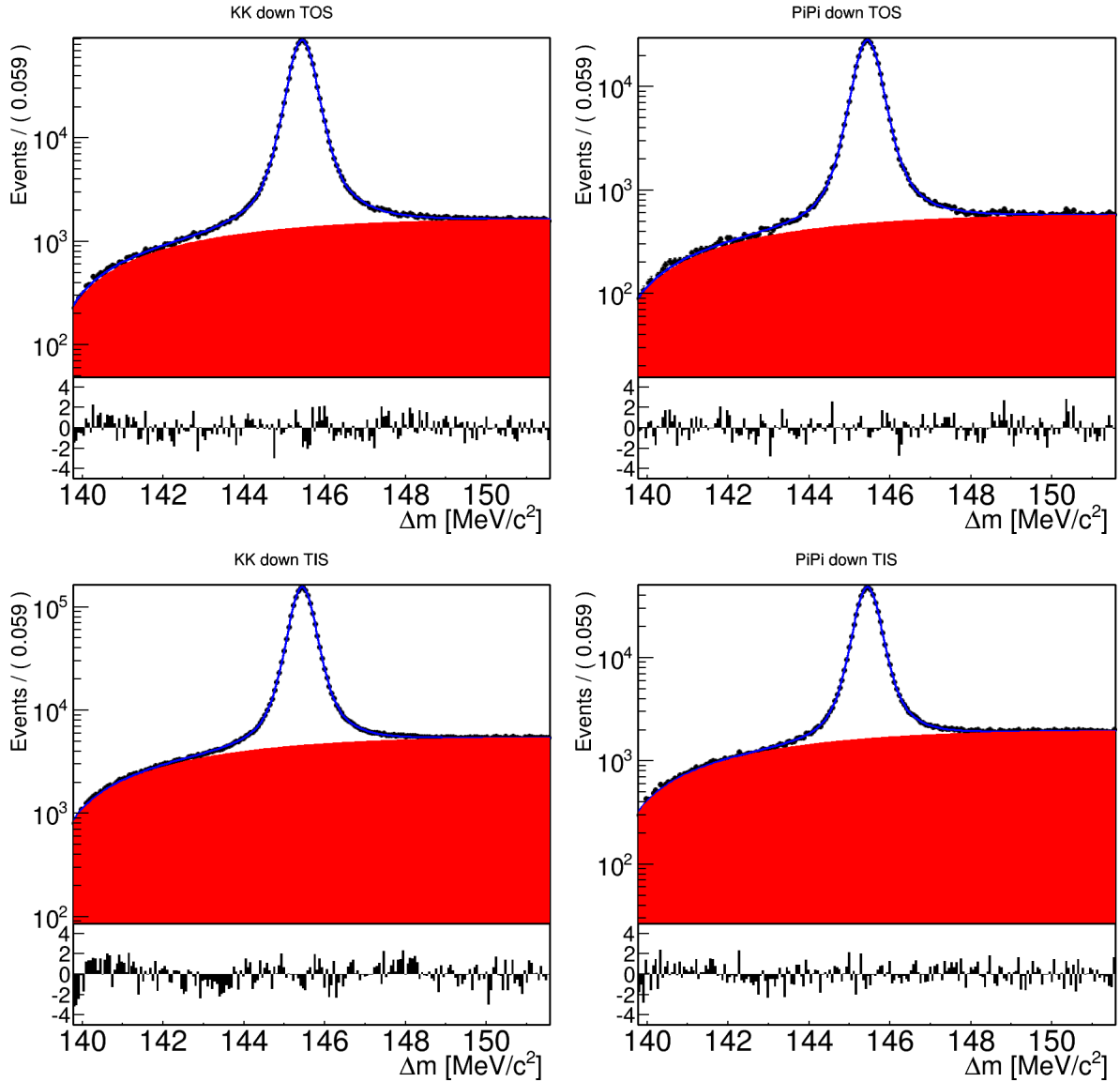


Figure 6.5.: Δm spectra of $D^0 \rightarrow K^- K^+$ (left) and $D^0 \rightarrow \pi^- \pi^+$ decays (right) for the two different triggers TOS (top) and TIS (bottom) for magnetic field polarity *down* for 2012 data. The red region is the random slow pion background, while the signal model is the remaining white region. The total model used to describe the data is the blue line, with the data points in black. The errors of the data points are absorbed in the size of the points.

7. Kinematic weighting

One possible difference between the two decays $D^0 \rightarrow K^+K^-$ and $D^0 \rightarrow \pi^+\pi^-$ can arise due to the kinematic dependency of the individual asymmetries. The physical CP -asymmetries do not depend on the kinematics but the production and detection asymmetries do. Therefore, a non-perfect cancellation of the production and detection asymmetries can lead to larger values of ΔA_{CP} . This is especially the case if the asymmetries become large, invalidating the first order approximation made in Eq. 2.56. Since the two samples are kinematically different after reconstruction and selection (the D^* with $D^0 \rightarrow \pi^-\pi^+$ events tend to have slightly lower momentum) this dependency would result in different individual asymmetries and therefore an artificially enhanced ΔA_{CP} . To remove this difference in kinematics, a three dimensional weighting of the KK sample to the $\pi\pi$ sample is performed. As weighting variables the D^* p_T , P and ϕ are used.

As a first step, the sPlot technique [49] is employed to separate signal from background. This is necessary to only consider kinematic differences between the signals and not a possible difference of the background. The sPlot technique provides signal weights (sWeights) for each value of Δm . The distribution of the sWeights versus Δm can be seen in Fig. 7.1. As is visible, this technique very effectively distinguishes between the background and the signal part of the Δm distribution. Regions which are dominated by background have sWeights below zero, while the region with the signal is boosted by sweights above one.

The kinematic weighting is first done in the two dimensions of $D^* P$ (in 25 bins in the range 30000-180000 MeV/c) and $D^* p_T$ (in 25 bins in the range 2100-18000 MeV/c).

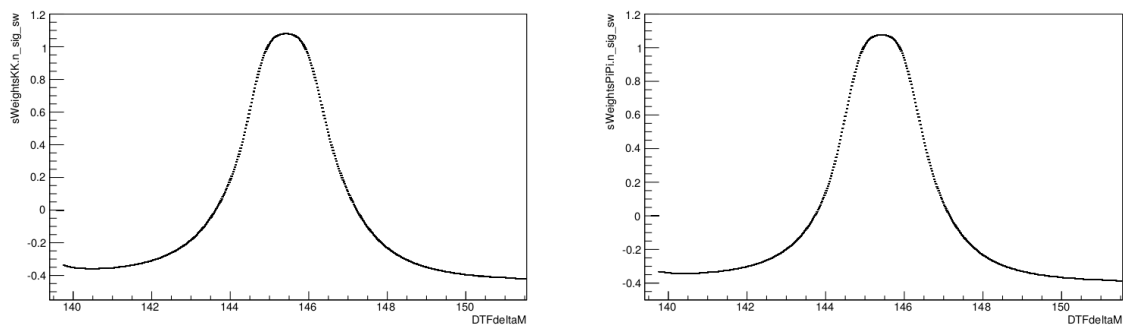


Figure 7.1.: Distribution of the sWeights versus Δm for $D^0 \rightarrow K^-K^+$ (left) and $D^0 \rightarrow \pi^-\pi^+$ (right) decays for 2012 data, TOS, magnetic field polarity down.

Afterwards a one dimensional weighting in $D^* \phi$ (in 25 bins) is carried out. This was historically done, because a true three dimensional weighting might create too many empty bins, resulting in unreasonable kinematic weights.

In the limit of infinite statistics the weights would be calculated for each $D^0 \rightarrow K^- K^+$ or $D^0 \rightarrow \pi^- \pi^+$ event with the formula:

$$w_{KK} = \frac{g^{\pi\pi}(p_T, P)}{g^{KK}(p_T, P)} \times \frac{h^{\pi\pi}(\phi)}{h^{KK}(\phi)} \quad \text{or} \quad (7.1)$$

$$w_{\pi\pi} = 1, \quad (7.2)$$

where $g^f(p_T, P)$ is a continuous two-dimensional function describing the distribution in p_T and P for the final state f and $h^f(\phi)$ the one-dimensional equivalent for the azimuthal angle of the D^* . In reality these are not continuous functions, but histograms filled from data, where each event is weighted with the sWeight depending on its Δm value.

The distributions of the D^* kinematics (p_T , P , η and ϕ) for both decays, before and after the weighting, can be seen in Fig. 7.2. Shown are 2012 data, TOS, magnetic field polarity down. The distributions for all the data samples are presented in the Appendix of the analysis note [13]. They do not differ significantly from the distributions shown here. By construction the distributions agree after the weighting. The p_T , P , η and ϕ distributions of D^0 and the π_s are shown in Fig. 7.3 and 7.4, respectively. The distributions agree very well after the weighting up to a point where not enough statistics is available.

The distribution of the calculated kinematic weights can be seen in Fig. 7.5. Most of the weights are smaller than two and larger than zero. A few hundred events regularly lie outside this range and are not shown in this plot. It has been checked that these events with much larger or much smaller weight do not affect the result by omitting them (see analysis note [13]).

An alternative true three dimensional weighting of the D^* η , ϕ and p_T is done to study the systematic effect of the choice of weighting procedure. The three dimensional weighting has the advantage of taking into account possible correlations of the $D^* \phi$ with the η and p_T . However, in some bins, due to the lack of statistics, some events (typically a few hundred) will get very large weights. To avoid this, the number of bins in $D^* \phi$ is reduced to 10. As the distribution of the transverse momentum $D^* p_T$ has a core with a large number of events and a large tail with very few events, it is transformed via the function $f(p_T) = 2./\pi * \tan^{-1}((p_T - A)/B)$, where A is the minimum p_T of the D^* , and B is the value of $D^* p_T$ at the peak of the distribution. The momentum distributions are different for TIS and TOS and therefore the parameters differ: $A_{TOS} = 2060\text{MeV}/c$, $B_{TOS} = 6745\text{MeV}/c$ and $A_{TIS} = A_{TOS}$, $B_{TIS} = 3300\text{MeV}/c$. This transformation maps p_T to the range $[0; 1]$ and allows for an equidistant binning in p_T .

Finally, in Tab. 7.1 and Tab. 7.2 the results for the different data sets are reported, both without and with the weighting applied for 2011 and 2012 data, respectively. $p - dacp$ refers to the nominal weighting, and eta to the alternative one. These are the final

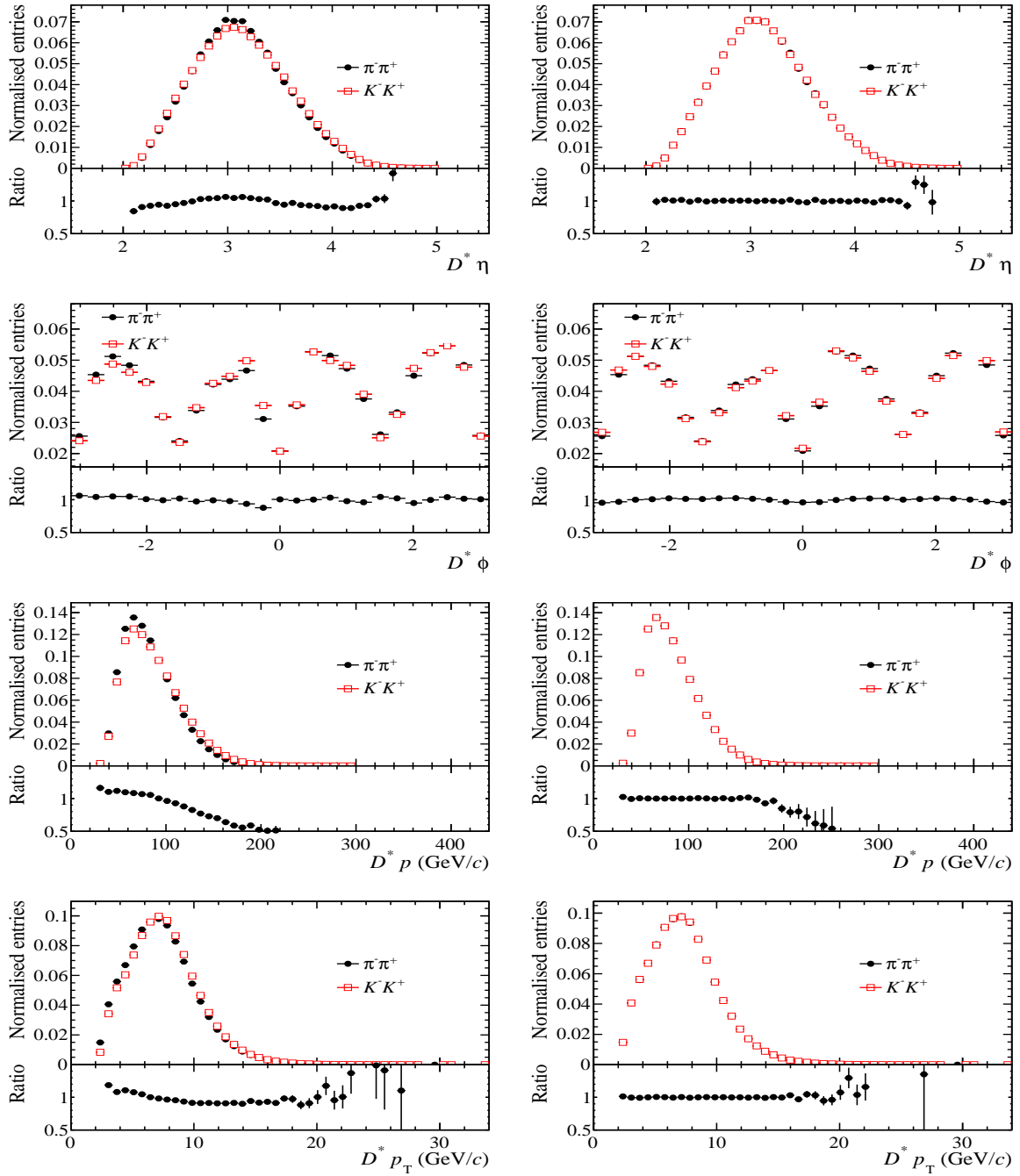


Figure 7.2.: Kinematic distributions of the D^* before (left) and after (right) the weighting. Shown are 2012 data, TOS, magnetic field polarity down.

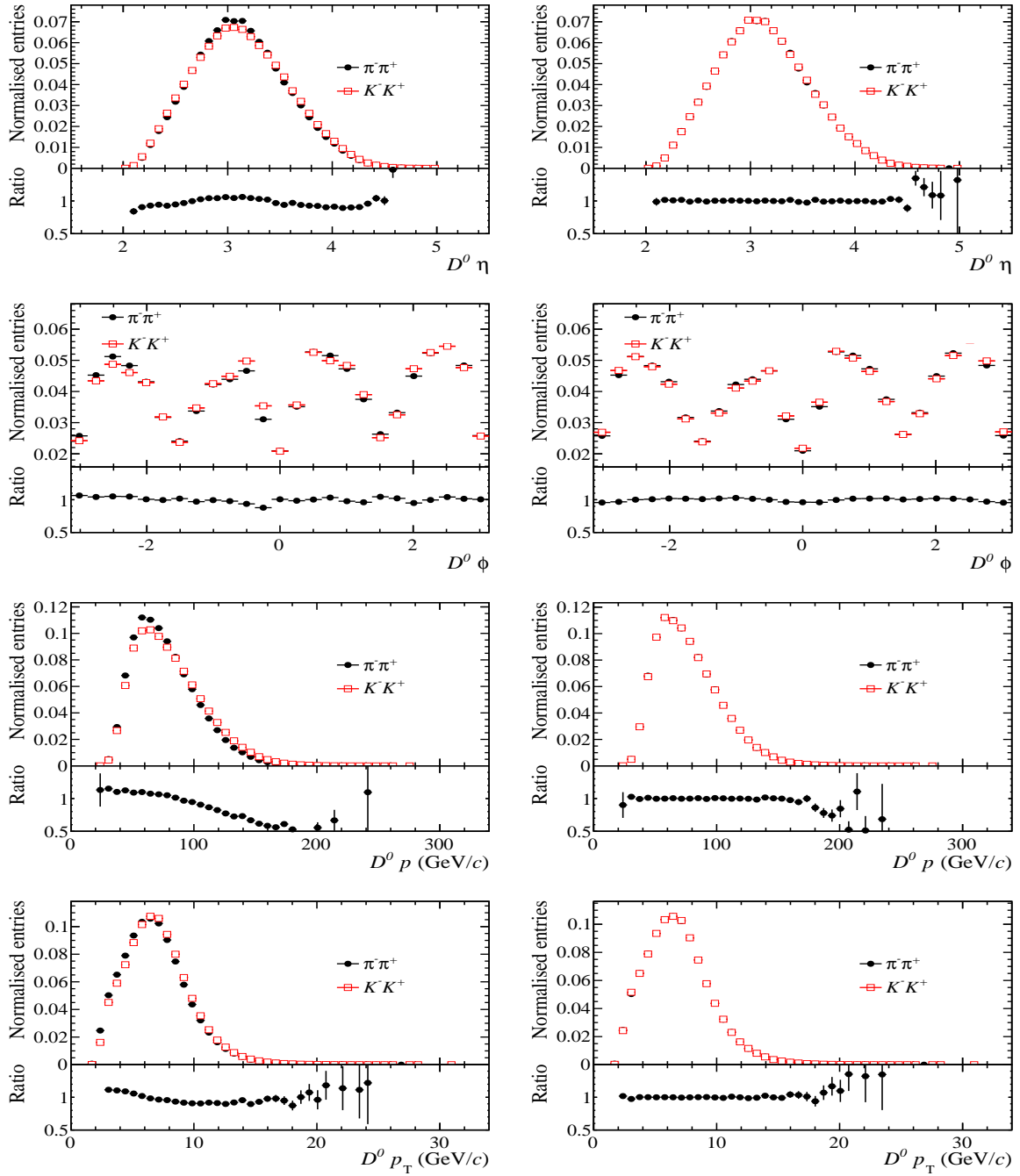


Figure 7.3.: Kinematic distributions of the D^0 before (left) and after (right) the weighting. Shown are 2012 data, TOS, magnetic field polarity down.

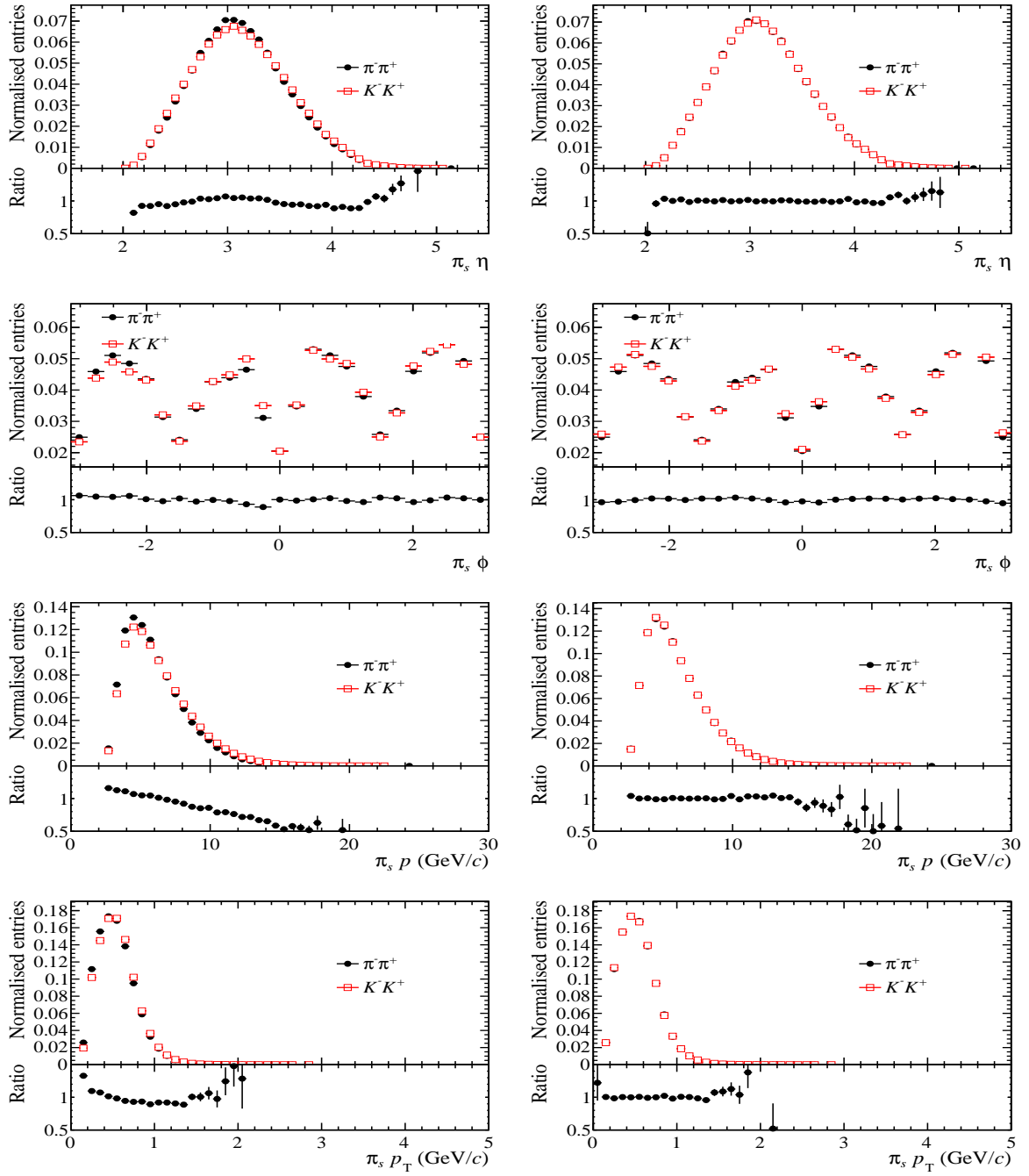


Figure 7.4.: Kinematic distributions of the π_s before (left) and after (right) the weighting. Shown are 2012 data, TOS, magnetic field polarity down.

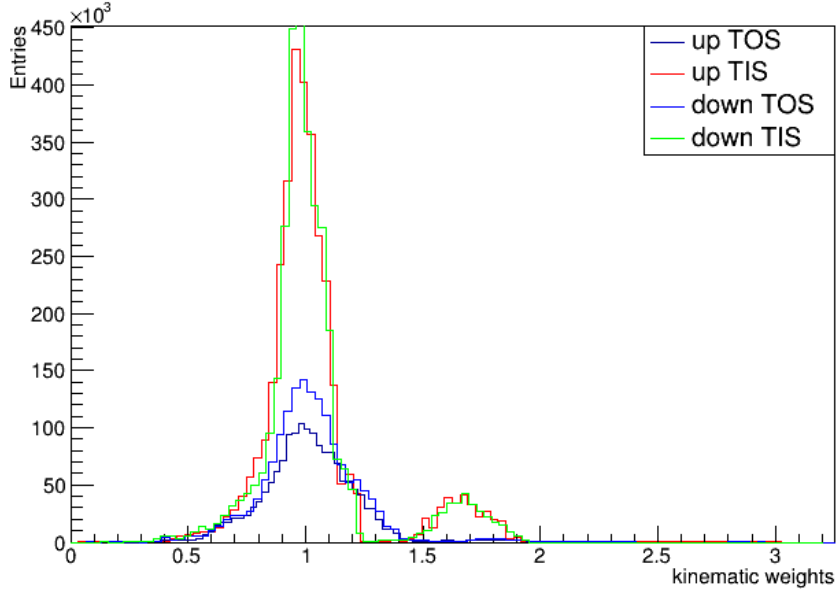


Figure 7.5.: Distribution of the kinematic weights for 2012 $D^0 \rightarrow K^- K^+$ decays. The distribution of the weights is different for TIS and TOS events, but does not depend on the magnetic field polarity.

central values for this analysis. The asymmetries were obtained by fixing the shape parameters to the values obtained in Sec. 6. The systematic effect of this is studied in Sec. 8.2. Overall, the kinematic weighting shifts the asymmetries to values closer to zero.

The full difference between the averaged result with the 2 dimensional weighting in P and p_t factorized with the 1 dimensional weighting in ϕ and the averaged result with the three dimensional weighting in η , p_t and ϕ is taken as a systematic uncertainty. This difference is 0.01% and 0.016% for 2011 and 2012 data, respectively. The other sources of systematic uncertainty, as well as several cross-checks, are studied in Sec. 8.

Table 7.1.: Unblinded results of the two different weighting schemes for 2011 data. Difference between the two weighting schemes: 0.009%.

Sample	$A_{raw}(KK)[\%]$	$A_{raw}(\pi\pi)[\%]$	$\Delta A_{CP}[\%]$
up TOS 2011*	-1.437 ± 0.169	-1.059 ± 0.302	-0.378 ± 0.346
up TOS 2011 reweight p dacp	-1.448 ± 0.167	-1.061 ± 0.301	-0.387 ± 0.344
up TOS 2011 reweight eta	-1.429 ± 0.166	-1.061 ± 0.301	-0.368 ± 0.344
up TIS 2011	-1.985 ± 0.139	-1.729 ± 0.251	-0.256 ± 0.287
up TIS 2011 reweight p dacp	-1.930 ± 0.137	-1.729 ± 0.251	-0.200 ± 0.285
up TIS 2011 reweight eta	-1.886 ± 0.139	-1.729 ± 0.251	-0.157 ± 0.287
down TOS 2011*	-0.694 ± 0.137	-0.356 ± 0.251	-0.338 ± 0.286
down TOS 2011 reweight p dacp	-0.618 ± 0.138	-0.359 ± 0.251	-0.259 ± 0.286
down TOS 2011 reweight eta	-0.614 ± 0.138	-0.359 ± 0.251	-0.256 ± 0.286
down TIS 2011*	-0.150 ± 0.117	-0.095 ± 0.211	-0.055 ± 0.241
down TIS 2011 reweight p dacp	-0.116 ± 0.115	-0.102 ± 0.211	-0.014 ± 0.240
down TIS 2011 reweight eta	-0.184 ± 0.117	-0.102 ± 0.211	-0.082 ± 0.241
weighted average	-0.942 ± 0.068	-0.719 ± 0.124	-0.228 ± 0.142
weighted average reweight p dacp	-0.905 ± 0.068	-0.722 ± 0.124	-0.182 ± 0.141
weighted average reweight eta	-0.912 ± 0.068	-0.722 ± 0.124	-0.191 ± 0.141

Table 7.2.: Results of the two different weighting schemes for 2012 data. Difference between the two weighting schemes: 0.016%.

Sample	$A_{raw}(KK)[\%]$	$A_{raw}(\pi\pi)[\%]$	$\Delta A_{CP}[\%]$
up TOS	-1.297 ± 0.103	-1.154 ± 0.185	-0.143 ± 0.212
up TOS reweight p dacp	-1.266 ± 0.102	-1.156 ± 0.185	-0.110 ± 0.211
up TOS reweight eta	-1.273 ± 0.102	-1.156 ± 0.185	-0.118 ± 0.211
up TIS	-1.799 ± 0.082	-1.512 ± 0.149	-0.287 ± 0.170
up TIS reweight p dacp	-1.776 ± 0.081	-1.516 ± 0.148	-0.260 ± 0.169
up TIS reweight eta	-1.725 ± 0.082	-1.516 ± 0.148	-0.209 ± 0.169
down TOS	-0.455 ± 0.103	-0.184 ± 0.181	-0.272 ± 0.208
down TOS reweight p dacp	-0.404 ± 0.101	-0.184 ± 0.181	-0.220 ± 0.207
down TOS reweight eta	-0.400 ± 0.101	-0.184 ± 0.181	-0.216 ± 0.207
down TIS	-0.227 ± 0.081	-0.456 ± 0.146	0.229 ± 0.167
down TIS reweight p dacp	-0.219 ± 0.080	-0.459 ± 0.145	0.240 ± 0.166
down TIS reweight eta	-0.213 ± 0.081	-0.459 ± 0.145	0.246 ± 0.166
weighted average	-0.953 ± 0.045	-0.850 ± 0.081	-0.096 ± 0.093
weighted average reweight p dacp	-0.928 ± 0.044	-0.853 ± 0.081	-0.068 ± 0.092
weighted average reweight eta	-0.909 ± 0.045	-0.853 ± 0.081	-0.052 ± 0.093

8. Systematic uncertainties

In this section various crosschecks are performed to test the asymmetry and the ΔA_{CP} dependence on different variables. The measurements are done in different bins of an observable. Usually, bins with roughly the same number of candidates are chosen.

The behavior of the raw asymmetries and ΔA_{CP} is expected to be different: while the raw asymmetries can exhibit some dependence on a kinematic variable, ΔA_{CP} should not depend on the kinematics and its distribution in bins of some variable is expected to be flat, ideally. The measurements for TIS and TOS are separated, as well as the year of data taking. The different results are shown averaged (weighted by their respective statistical error). For some results the individual asymmetries and ΔA_{CP} separated by magnetic polarity and trigger are provided in the appendix both graphically and tabulated. The significance of the deviations in each bin is also provided there.

All fits were a binned maximum-likelihood fit with 400 bins to reduce the run time (the exception to this is the cross-check, whether a different binning changes the result). The baseline selection was used throughout, with no multiple candidate rejection. The shape parameters of the model are usually fixed to the values obtained in the nominal fit. For some of the cross-checks a weighted fits was employed. This is denoted where applicable.

The results marked with *ref* in the figures are the reference results as obtained in Sec. 7 and include the kinematic weighting if the fit also included the weighting. It is especially necessary to include the kinematic weighting when studying the dependence of ΔA_{CP} of the kinematics of the D^0 and π_s .

8.1. Significance of deviations

Generally, the significance s of deviations between two results $a_1 \pm \sigma_1$ and $a_2 \pm \sigma_2$, with the correlation coefficient ρ between the two results is defined as

$$s = \frac{\Delta}{\sigma_\Delta} = \frac{|a_1 - a_2|}{\sqrt{\sigma_1^2 + \sigma_2^2 - 2\rho\sigma_1\sigma_2}}, \quad (8.1)$$

One limiting case for this formula is a vanishing correlation, $\rho = 0$. This leads to:

$$s = \frac{|a_1 - a_2|}{\sqrt{\sigma_1^2 + \sigma_2^2}}. \quad (8.2)$$

This is the simplest case and gives a lower bound on the significance. It can be used for example when comparing the results from the two magnetic polarities and trigger settings, which are statistically independent.

Another limiting case is assuming full correlation between the two methods, $\rho = 1$. This gives an upper limit on the significance and simplifies equation 8.1 to:

$$s = \frac{|a_1 - a_2|}{\sigma_1 - \sigma_2}, \quad (8.3)$$

This approach can be used for example for the comparisons between different binnings. It assumes that exactly the same data is analyzed in two different ways.

When one result is obtained in a sub sample of the other result, a slightly different approach is needed. Let $a_1 = \frac{1}{N}\sum_N x_i$ be the result obtained in the full sample with N events, with the uncertainty $\sigma_1 = \frac{\sigma}{\sqrt{N}}$, where σ is the uncertainty due to one event. Let analogously $a_2 = \frac{1}{n}\sum_n x_i$ be the result obtained in a sub-sample containing only n events, with the uncertainty $\sigma_2 = \frac{\sigma}{\sqrt{n}}$.

Then the correlation between the two samples is given by the size of the sub-sample, compared to the full sample:

$$\rho = \sqrt{\frac{n}{N}} = \frac{\sigma_1}{\sigma_2}. \quad (8.4)$$

Inserting this correlation into equation 8.1 leads to:

$$s = \frac{|a_1 - a_2|}{\sqrt{|\sigma_1^2 - \sigma_2^2|}}. \quad (8.5)$$

This approach determines the significance to confirm that the results obtained in the binning of one variable do not significantly deviate from the result obtained in the full sample.

8.2. Influence of setting the model parameters constant

For most of the systematic uncertainty checks, the shape parameters of the model are set constant. This includes the widths of the signal shape, as well as the relative fractions between the different components of the signal shape. Also, all parameters of the background shape are kept constant. Not set constant are the means of the signal model and the relative change in their width between D^{*+} and D^{*-} decays. The values are extracted from a full fit to the corresponding data sample (up/down TIS/TOS 2011/2012) to account for any differences in the parameters.

The fit results with the shape parameters set constant, compared to the nominal fit results are shown in Tab. 8.1 and 8.2 for 2011 and 2012, respectively. It is visible that fixing the shape parameters does not lead to different results. The same holds for fixing only the signal part of the model or only the shape parameters of the background. Nevertheless, systematic uncertainties corresponding to the differences between the weighted averages of the nominal fits and the fits with setting all parameters constant (0.002% and 0.001% for 2011 and 2012, respectively) are assigned. It is especially noteworthy that the estimation of the errors is not affected by this.

However, the shape parameters may change with some kinematic variable. This is not checked here and would affect measuring ΔA_{CP} as a function of that kinematic variable. We have to rely on the fact that any such effect will likely be small and not affect the outcome (the number of signal events) differently for D^{*+} and D^{*-} decays and thus introduce an asymmetry. If the shape parameters varied largely, this would result in the fit not converging properly. It was checked that this is not the case for the results presented.

Table 8.1.: Effect of setting part of the fit model constant with the parameter values obtained in a previous fit to the 2011 data. The first weighted average is the average of the nominal fit results, whereas the following weighted average is the average of the results with the model fixed.

Sample	$A_{raw}(KK)[\%]$	$A_{raw}(\pi\pi)[\%]$	$\Delta A_{CP}[\%]$
up TOS 2011	-1.437 ± 0.169	-1.059 ± 0.302	-0.378 ± 0.346
up TOS 2011 fixed	-1.439 ± 0.169	-1.061 ± 0.301	-0.378 ± 0.346
up TIS 2011	-1.985 ± 0.139	-1.729 ± 0.251	-0.256 ± 0.287
up TIS 2011 fixed	-1.991 ± 0.139	-1.729 ± 0.251	-0.262 ± 0.286
down TOS 2011	-0.694 ± 0.137	-0.356 ± 0.251	-0.338 ± 0.286
down TOS 2011 fixed	-0.696 ± 0.140	-0.359 ± 0.251	-0.337 ± 0.287
down TIS 2011	-0.150 ± 0.117	-0.095 ± 0.211	-0.055 ± 0.241
down TIS 2011 fixed	-0.152 ± 0.117	-0.102 ± 0.211	-0.051 ± 0.241
weighted average	-0.942 ± 0.068	-0.719 ± 0.124	-0.228 ± 0.142
weighted average fixed	-0.949 ± 0.069	-0.722 ± 0.124	-0.226 ± 0.142

Table 8.2.: Effect of setting part of the fit model constant with the parameter values obtained in a previous fit to the 2012 data. The first weighted average is the average of the nominal fit results, whereas the following weighted averages are the averages of the results with some part of the model fixed.

Sample	$A_{raw}(KK)[\%]$	$A_{raw}(\pi\pi)[\%]$	$\Delta A_{CP}[\%]$
up TOS	-1.297 ± 0.103	-1.154 ± 0.185	-0.143 ± 0.212
up TOS fixed	-1.299 ± 0.104	-1.156 ± 0.185	-0.143 ± 0.212
up TOS fixed sig	-1.299 ± 0.104	-1.156 ± 0.185	-0.143 ± 0.212
up TOS fixed bkg	-1.297 ± 0.104	-1.156 ± 0.185	-0.142 ± 0.212
up TIS	-1.799 ± 0.082	-1.512 ± 0.149	-0.287 ± 0.170
up TIS fixed	-1.802 ± 0.082	-1.516 ± 0.148	-0.286 ± 0.170
up TIS fixed sig	-1.802 ± 0.082	-1.514 ± 0.148	-0.288 ± 0.170
up TIS fixed bkg	-1.800 ± 0.082	-1.513 ± 0.149	-0.287 ± 0.170
down TOS	-0.455 ± 0.103	-0.184 ± 0.181	-0.272 ± 0.208
down TOS fixed	-0.458 ± 0.103	-0.184 ± 0.181	-0.273 ± 0.208
down TOS fixed sig	-0.458 ± 0.103	-0.184 ± 0.181	-0.273 ± 0.208
down TOS fixed bkg	-0.456 ± 0.103	-0.183 ± 0.181	-0.273 ± 0.208
down TIS	-0.227 ± 0.081	-0.456 ± 0.146	0.229 ± 0.167
down TIS fixed	-0.230 ± 0.081	-0.459 ± 0.145	0.229 ± 0.166
down TIS fixed sig	-0.230 ± 0.081	-0.459 ± 0.145	0.228 ± 0.166
down TIS fixed bkg	-0.227 ± 0.081	-0.457 ± 0.146	0.230 ± 0.167
weighted average	-0.953 ± 0.045	-0.850 ± 0.081	-0.096 ± 0.093
weighted average fixed	-0.955 ± 0.045	-0.853 ± 0.081	-0.096 ± 0.093
weighted average fixed sig	-0.955 ± 0.045	-0.852 ± 0.081	-0.097 ± 0.093
weighted average fixed bkg	-0.953 ± 0.045	-0.851 ± 0.081	-0.096 ± 0.093

8.3. Binning

Initially, the fit performed was an unbinned maximum-likelihood fit for both years of data taking. The default binning chosen for the kinematic weighting, the cross-checks and the systematic studies is 400 bins in Δm to reduce processing time. This value is varied here to study whether the choice of the binning affects the result. This is particularly important, because one strategy to deal with fits with a not positive-definite error-matrix¹ is rerunning them with a reduced number of bins and the parameters from the previous fit as start parameters (the other strategies include rerunning the fit with the parameters from the previous fit as start parameters and lowering the estimate of background events). The rerunning with a reduced number of bins is turned off for this check.

The results are reported in Tab. 8.4 and Tab. 8.3 for 2012 and 2011, respectively. No deviation is visible, except effect due to setting the model parameters constant. Therefore, no systematic uncertainty is assigned.

¹Which occurs *e.g.* if parameters are strongly correlated, which is the case for some of the shape parameters.

Table 8.3.: Results of the fit performed with different number of bins and unbinned for 2011 data.

Sample	$A_{raw}(KK)[\%]$	$A_{raw}(\pi\pi)[\%]$	$\Delta A_{CP}[\%]$
up TIS 2011	-1.985 ± 0.139	-1.729 ± 0.251	-0.256 ± 0.287
up TIS 2011 200 bins	-1.999 ± 0.139	-1.737 ± 0.251	-0.263 ± 0.286
up TIS 2011 400 bins	-1.991 ± 0.139	-1.729 ± 0.251	-0.262 ± 0.286
up TIS 2011 500 bins	-1.990 ± 0.139	-1.728 ± 0.251	-0.262 ± 0.286
up TIS 2011 1000 bins	-1.989 ± 0.139	-1.728 ± 0.251	-0.261 ± 0.286
up TOS 2011	-1.437 ± 0.169	-1.059 ± 0.302	-0.378 ± 0.346
up TOS 2011 200 bins	-1.444 ± 0.169	-1.067 ± 0.301	-0.377 ± 0.346
up TOS 2011 400 bins	-1.439 ± 0.169	-1.061 ± 0.301	-0.378 ± 0.346
up TOS 2011 500 bins	-1.438 ± 0.169	-1.060 ± 0.301	-0.378 ± 0.346
up TOS 2011 1000 bins	-1.438 ± 0.169	-1.060 ± 0.301	-0.378 ± 0.346
down TIS 2011	-0.150 ± 0.117	-0.095 ± 0.211	-0.055 ± 0.241
down TIS 2011 200 bins	-0.161 ± 0.117	-0.112 ± 0.211	-0.049 ± 0.241
down TIS 2011 400 bins	-0.152 ± 0.117	-0.102 ± 0.211	-0.051 ± 0.241
down TIS 2011 500 bins	-0.152 ± 0.117	-0.100 ± 0.211	-0.052 ± 0.241
down TIS 2011 1000 bins	-0.151 ± 0.117	-0.099 ± 0.211	-0.052 ± 0.241
down TOS 2011	-0.694 ± 0.137	-0.356 ± 0.251	-0.338 ± 0.286
down TOS 2011 200 bins	-0.700 ± 0.140	-0.363 ± 0.251	-0.337 ± 0.287
down TOS 2011 400 bins	-0.696 ± 0.140	-0.359 ± 0.251	-0.337 ± 0.287
down TOS 2011 500 bins	-0.695 ± 0.140	-0.358 ± 0.251	-0.338 ± 0.287
down TOS 2011 1000 bins	-0.694 ± 0.140	-0.357 ± 0.251	-0.338 ± 0.287
weighted average	-0.942 ± 0.068	-0.719 ± 0.124	-0.228 ± 0.142
weighted average 200 bins	-0.956 ± 0.069	-0.729 ± 0.124	-0.226 ± 0.142
weighted average 400 bins	-0.949 ± 0.069	-0.722 ± 0.124	-0.226 ± 0.142
weighted average 500 bins	-0.948 ± 0.069	-0.721 ± 0.124	-0.227 ± 0.142
weighted average 1000 bins	-0.947 ± 0.069	-0.720 ± 0.124	-0.227 ± 0.142

Table 8.4.: Results of the fit performed with different number of bins and unbinned for 2012 data.

Sample	$A_{raw}(KK)[\%]$	$A_{raw}(\pi\pi)[\%]$	$\Delta A_{CP}[\%]$
up TIS	-1.799 ± 0.082	-1.512 ± 0.149	-0.287 ± 0.170
up TIS 200 bins	-1.811 ± 0.082	-1.525 ± 0.148	-0.286 ± 0.170
up TIS 400 bins	-1.802 ± 0.082	-1.516 ± 0.148	-0.286 ± 0.170
up TIS 500 bins	-1.802 ± 0.082	-1.515 ± 0.148	-0.287 ± 0.170
up TIS 1000 bins	-1.800 ± 0.082	-1.512 ± 0.148	-0.288 ± 0.170
up TOS	-1.297 ± 0.103	-1.154 ± 0.185	-0.143 ± 0.212
up TOS 200 bins	-1.303 ± 0.104	-1.160 ± 0.185	-0.143 ± 0.212
up TOS 400 bins	-1.299 ± 0.104	-1.156 ± 0.185	-0.143 ± 0.212
up TOS 500 bins	-1.298 ± 0.104	-1.153 ± 0.185	-0.144 ± 0.212
up TOS 1000 bins	-1.297 ± 0.104	-1.153 ± 0.185	-0.144 ± 0.212
down TIS	-0.227 ± 0.081	-0.456 ± 0.146	0.229 ± 0.167
down TIS 200 bins	-0.238 ± 0.081	-0.467 ± 0.145	0.229 ± 0.166
down TIS 400 bins	-0.230 ± 0.081	-0.459 ± 0.145	0.229 ± 0.166
down TIS 500 bins	-0.229 ± 0.081	-0.457 ± 0.145	0.229 ± 0.166
down TIS 1000 bins	-0.227 ± 0.081	-0.456 ± 0.145	0.229 ± 0.166
down TOS	-0.455 ± 0.103	-0.184 ± 0.181	-0.272 ± 0.208
down TOS 200 bins	-0.463 ± 0.103	-0.191 ± 0.181	-0.272 ± 0.208
down TOS 400 bins	-0.458 ± 0.103	-0.184 ± 0.181	-0.273 ± 0.208
down TOS 500 bins	-0.457 ± 0.103	-0.185 ± 0.181	-0.272 ± 0.208
down TOS 1000 bins	-0.456 ± 0.103	-0.183 ± 0.181	-0.272 ± 0.208
weighted average	-0.953 ± 0.045	-0.850 ± 0.081	-0.096 ± 0.093
weighted average 200 bins	-0.963 ± 0.045	-0.860 ± 0.081	-0.096 ± 0.093
weighted average 400 bins	-0.955 ± 0.045	-0.853 ± 0.081	-0.096 ± 0.093
weighted average 500 bins	-0.955 ± 0.045	-0.852 ± 0.081	-0.097 ± 0.093
weighted average 1000 bins	-0.953 ± 0.045	-0.850 ± 0.081	-0.097 ± 0.093

8.4. Signal model

The choice of the signal description is only phenomenologically motivated. The only physics motivation is that the width of the reconstructed invariant mass is dominated by the momentum resolution of the detector and not by the width of the particle. Therefore, a model describing the signal must be a combination of Gaussian or Gaussian-like PDFs. To test whether ΔA_{CP} changes with a different description, the Johnson function is replaced by a third Gaussian to describe the signal. The results of this change are reported in Tab. 8.5 and Tab. 8.6 for 2011 and 2012, respectively. The full difference between the weighted averages is assigned as systematic uncertainty. These differences are 0.007% and 0.010% for 2011 and 2012, respectively.

Table 8.5.: Comparison of fit results using three Gaussian functions to describe the signal and the nominal signal description for 2011 data.

Sample	$A_{raw}(KK)[\%]$	$A_{raw}(\pi\pi)[\%]$	$\Delta A_{CP}[\%]$
up TIS 2011	-1.985 ± 0.139	-1.729 ± 0.251	-0.256 ± 0.287
up TIS 2011 triple gauss	-1.982 ± 0.140	-1.731 ± 0.252	-0.251 ± 0.288
up TOS 2011	-1.437 ± 0.169	-1.059 ± 0.302	-0.378 ± 0.346
up TOS 2011 triple gauss	-1.415 ± 0.170	-1.037 ± 0.303	-0.378 ± 0.348
down TIS 2011	-0.150 ± 0.117	-0.095 ± 0.211	-0.055 ± 0.241
down TIS 2011 triple gauss	-0.152 ± 0.118	-0.103 ± 0.213	-0.050 ± 0.243
down TOS 2011	-0.694 ± 0.137	-0.356 ± 0.251	-0.338 ± 0.286
down TOS 2011 triple gauss	-0.692 ± 0.141	-0.366 ± 0.252	-0.326 ± 0.289
weighted average	-0.942 ± 0.068	-0.719 ± 0.124	-0.228 ± 0.142
weighted average triple gauss	-0.942 ± 0.069	-0.723 ± 0.125	-0.221 ± 0.143

Table 8.6.: Comparison of fit results using three Gaussian functions to describe the signal and the nominal signal description for 2012 data.

Sample	$A_{raw}(KK)[\%]$	$A_{raw}(\pi\pi)[\%]$	$\Delta A_{CP}[\%]$
up TIS	-1.799 ± 0.082	-1.512 ± 0.149	-0.287 ± 0.170
up TIS triple gauss	-1.758 ± 0.086	-1.573 ± 0.154	-0.185 ± 0.176
up TOS	-1.297 ± 0.103	-1.154 ± 0.185	-0.143 ± 0.212
up TOS triple gauss	-1.249 ± 0.105	-1.107 ± 0.188	-0.142 ± 0.215
down TIS	-0.227 ± 0.081	-0.456 ± 0.146	0.229 ± 0.167
down TIS triple gauss	-0.237 ± 0.084	-0.425 ± 0.151	0.188 ± 0.173
down TOS	-0.455 ± 0.103	-0.184 ± 0.181	-0.272 ± 0.208
down TOS triple gauss	-0.453 ± 0.105	-0.176 ± 0.170	-0.278 ± 0.200
weighted average	-0.953 ± 0.045	-0.850 ± 0.081	-0.096 ± 0.093
weighted average triple gauss	-0.933 ± 0.047	-0.821 ± 0.082	-0.086 ± 0.094

8.5. Background model

Instead of setting the shape parameter B to zero in Eq. 5.4, and using the shape described by Eq. 5.5, the parameter A is set to zero, obtaining Eq. 5.6. This gives a slightly different behavior in the right tail of the function, since the influence of B on the curvature after the turn-on of the function is less than the influence of A in the former approach. The determination of the asymmetries is repeated with this different background description. The results can be found in Tab. 8.7 and Tab. 8.8 for 2011 and 2012, respectively. For 2011 the small variation of 0.001% is assigned as systematic uncertainty, while for 2012 no variation is discernible.

Table 8.7.: Effect of fixing A to zero and freeing B , thus choosing a different background model for 2011 data. †: Fit with error matrix not positive-definite.

Sample	$A_{raw}(KK)[\%]$	$A_{raw}(\pi\pi)[\%]$	$\Delta A_{CP}[\%]$
up TIS 2011	-1.985 ± 0.139	-1.729 ± 0.251	-0.256 ± 0.287
up TIS 2011 fix a [†]	-1.985 ± 0.139	-1.728 ± 0.218	-0.257 ± 0.258
up TOS 2011	-1.437 ± 0.169	-1.059 ± 0.302	-0.378 ± 0.346
up TOS 2011 fix a	-1.436 ± 0.169	-1.060 ± 0.301	-0.376 ± 0.345
down TIS 2011	-0.150 ± 0.117	-0.095 ± 0.211	-0.055 ± 0.241
down TIS 2011 fix a	-0.149 ± 0.117	-0.097 ± 0.211	-0.053 ± 0.241
down TOS 2011	-0.694 ± 0.137	-0.356 ± 0.251	-0.338 ± 0.286
down TOS 2011 fix a	-0.693 ± 0.140	-0.357 ± 0.251	-0.336 ± 0.288
weighted average	-0.942 ± 0.068	-0.719 ± 0.124	-0.228 ± 0.142
weighted average fix a	-0.944 ± 0.069	-0.794 ± 0.119	-0.227 ± 0.138

Table 8.8.: Effect of fixing A to zero and freeing B , thus choosing a different background model for 2012 data.

Sample	$A_{raw}(KK)[\%]$	$A_{raw}(\pi\pi)[\%]$	$\Delta A_{CP}[\%]$
up TIS	-1.799 ± 0.082	-1.512 ± 0.149	-0.287 ± 0.170
up TIS fix a	-1.802 ± 0.082	-1.516 ± 0.148	-0.286 ± 0.170
up TOS	-1.297 ± 0.103	-1.154 ± 0.185	-0.143 ± 0.212
up TOS fix a	-1.299 ± 0.104	-1.156 ± 0.185	-0.143 ± 0.212
down TIS	-0.227 ± 0.081	-0.456 ± 0.146	0.229 ± 0.167
down TIS fix a	-0.230 ± 0.081	-0.459 ± 0.145	0.229 ± 0.166
down TOS	-0.455 ± 0.103	-0.184 ± 0.181	-0.272 ± 0.208
down TOS fix a	-0.458 ± 0.103	-0.184 ± 0.181	-0.273 ± 0.208
weighted average	-0.953 ± 0.045	-0.850 ± 0.081	-0.096 ± 0.093
weighted average fix a	-0.955 ± 0.045	-0.853 ± 0.081	-0.096 ± 0.093

8.6. Two-dimensional determination of the asymmetries and peaking background

As described in Sec. 5, there is also a model available to describe the distribution of the data sample in $m(D^0)$. This allows the asymmetries to be determined in the plane of Δm and $m(D^0)$, respecting possible correlations. It also allows an estimation of the peaking background, *i.e.* background that peaks under the signal in Δm , but not in $m(D^0)$. In Tab. 8.9 and Tab. 8.10, the comparison between the results from the one-dimensional determination (in Δm) and the two-dimensional determination are shown for 2011 and 2012, respectively. In Fig. 8.1 and Fig. 8.2 the projections in Δm and $m(D^0)$ are shown for 2011 and 2012 up TOS data, respectively. For the $D^0 \rightarrow K^- K^+$ decays, the background model is not perfectly describing the data, but reasonably well. The full difference between the weighted averages of the one-dimensional and the two-dimensional determination are taken as systematic uncertainties for the peaking background. They are 0.027% and 0.012% for 2011 and 2012, respectively. This is a conservative approach, since part of the difference might also be due to the different procedure, which can not easily be disentangled.

In Tab. 8.11 and Tab. 8.12 the yields for the peaking background part of the model are shown for 2011 and 2012, respectively. The number of events are reported only in the signal region ($m(D^0) \in [1848, 1885]\text{MeV}/c^2$ and $\Delta m \in [144.7, 146.2]\text{MeV}/c^2$). It can be seen that there is more peaking background for the $D^0 \rightarrow \pi^- \pi^+$ decays than for the $D^0 \rightarrow K^- K^+$ decays. This might be due to the fact that the wrong two of the three pions in this final state could be combined to form the D^0 . These events would not peak in $m(D^0)$, but would peak in Δm . For $D^0 \rightarrow K^- K^+$ events this is only possible when misidentifying at least one particle as a kaon and therefore the fraction of peaking background is less for these decays.

Table 8.9.: Results of the two-dimensional determination of the asymmetries for 2011 data, compared with the one-dimensional result.

Sample	$A_{raw}(KK)[\%]$	$A_{raw}(\pi\pi)[\%]$	$\Delta A_{CP}[\%]$
up TIS 2011	-1.985 ± 0.139	-1.729 ± 0.251	-0.256 ± 0.287
up TIS 2011 2d	-1.982 ± 0.138	-1.684 ± 0.250	-0.298 ± 0.286
up TOS 2011	-1.437 ± 0.169	-1.059 ± 0.302	-0.378 ± 0.346
up TOS 2011 2d	-1.426 ± 0.166	-1.056 ± 0.303	-0.370 ± 0.345
down TIS 2011	-0.150 ± 0.117	-0.095 ± 0.211	-0.055 ± 0.241
down TIS 2011 2d	-0.183 ± 0.116	-0.079 ± 0.212	-0.103 ± 0.242
down TOS 2011	-0.694 ± 0.137	-0.356 ± 0.251	-0.338 ± 0.286
down TOS 2011 2d	-0.700 ± 0.139	-0.356 ± 0.251	-0.344 ± 0.287
weighted average	-0.942 ± 0.068	-0.719 ± 0.124	-0.228 ± 0.142
weighted average 2d	-0.957 ± 0.068	-0.705 ± 0.124	-0.255 ± 0.142

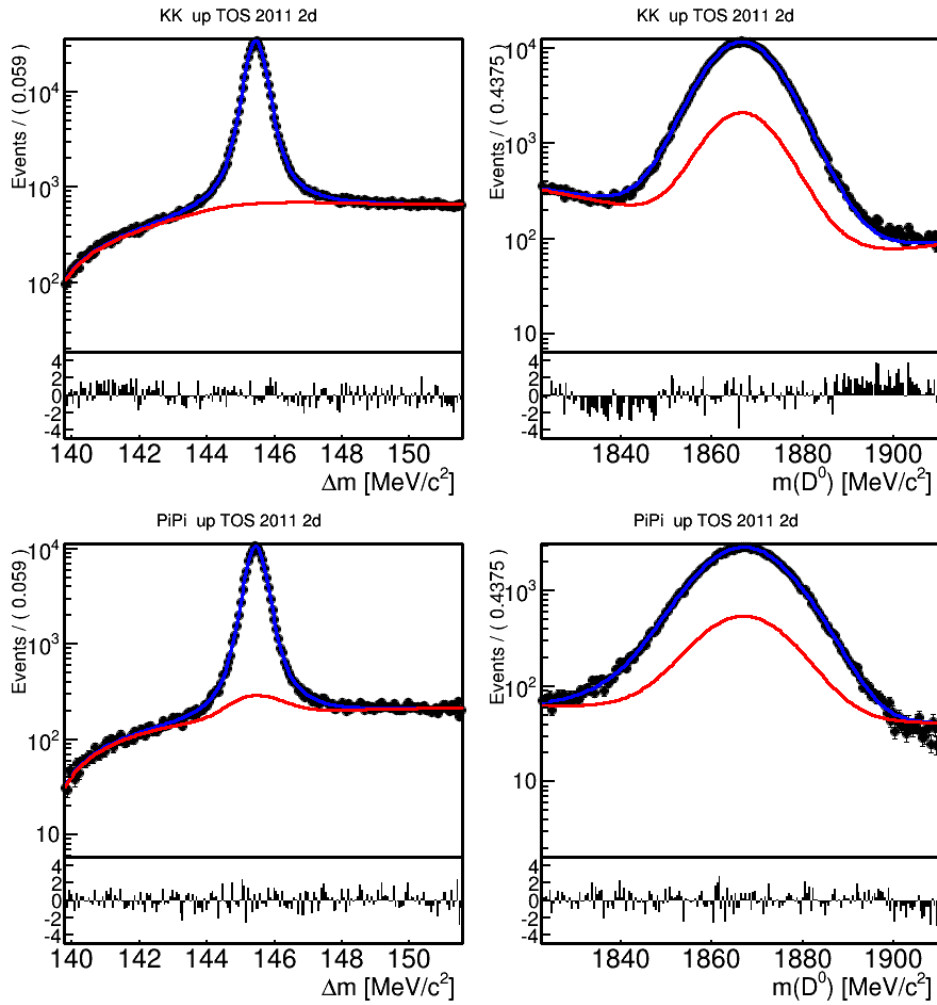


Figure 8.1.: Two dimensional determination (Δm left, $m(D^0)$ right) of the asymmetries on the example of 2011 up TOS data for $D^0 \rightarrow K^- K^+$ (top) and $D^0 \rightarrow \pi^- \pi^+$ (bottom) decays. The black points are the binned data, the blue line is the whole model and in red is the total background (including peaking background).

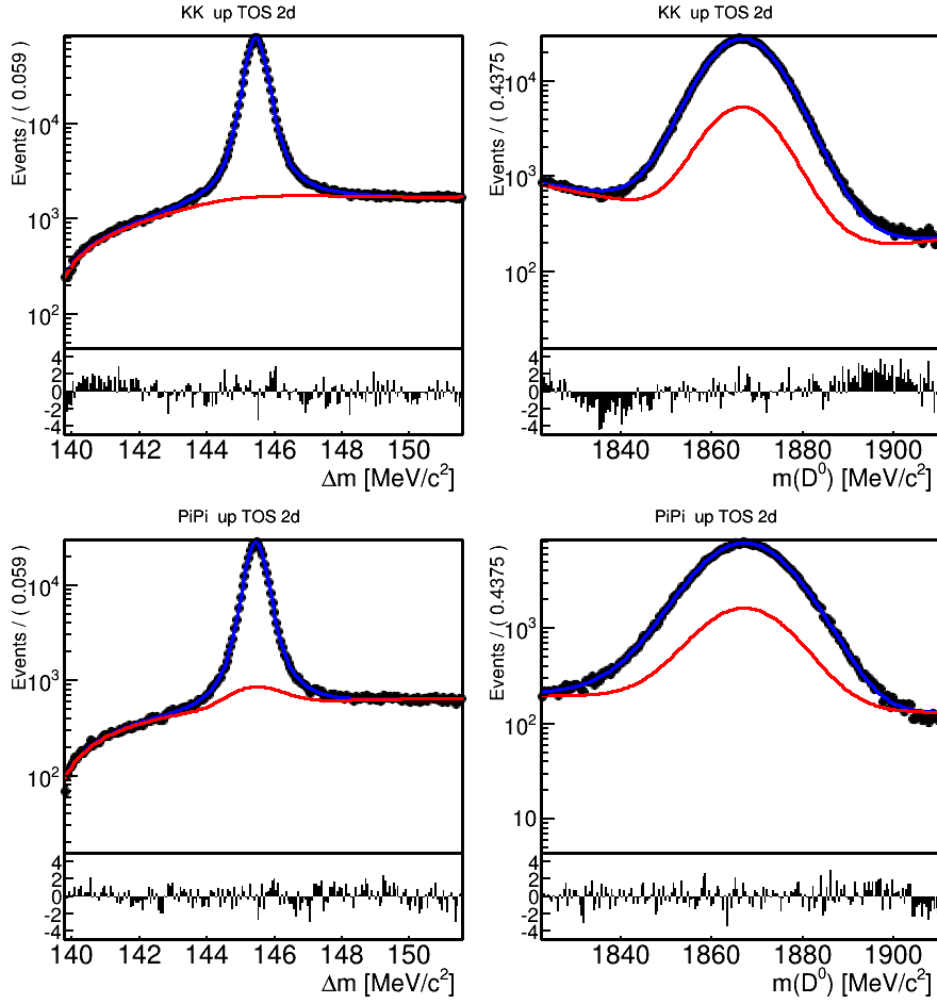


Figure 8.2.: Two dimensional determination of the asymmetries on the example of 2012 up TOS data for $D^0 \rightarrow K^-K^+$ (top) and $D^0 \rightarrow \pi^-\pi^+$ (bottom) decays. The black points are the binned data, the blue line is the whole model and in red is the total background (including peaking background).

Table 8.10.: Results of the two-dimensional determination of the asymmetries for 2012 data, compared with the one-dimensional result. †: Fits with error matrix not positive-definite.

Sample	$A_{raw}(KK)[\%]$	$A_{raw}(\pi\pi)[\%]$	$\Delta A_{CP}[\%]$
up TIS	-1.799 ± 0.082	-1.512 ± 0.149	-0.287 ± 0.170
up TIS 2d	-1.790 ± 0.085	-1.504 ± 0.150	-0.286 ± 0.172
up TOS	-1.297 ± 0.103	-1.154 ± 0.185	-0.143 ± 0.212
up TOS 2d†	-1.288 ± 0.109	-1.142 ± 0.184	-0.146 ± 0.214
down TIS	-0.227 ± 0.081	-0.456 ± 0.146	0.229 ± 0.167
down TIS 2d †	-0.282 ± 0.084	-0.494 ± 0.147	0.212 ± 0.169
down TOS	-0.455 ± 0.103	-0.184 ± 0.181	-0.272 ± 0.208
down TOS 2d	-0.480 ± 0.108	-0.178 ± 0.182	-0.302 ± 0.212
weighted average	-0.953 ± 0.045	-0.850 ± 0.081	-0.096 ± 0.093
weighted average 2d	-0.970 ± 0.047	-0.856 ± 0.081	-0.108 ± 0.094

Table 8.11.: Signal and background yields in the signal region for 2011 data.

Sample	Signal	Background	Peaking background	Peaking fraction [%]
up TIS 2011 2d KK	555928 ± 1522	39413 ± 144	4381 ± 16	0.79
up TIS 2011 2d PiPi	164542 ± 2664	13275 ± 264	3096 ± 61	1.88
up TOS 2011 2d KK	358336 ± 727	13104 ± 59	1946 ± 8	0.54
up TOS 2011 2d PiPi	108198 ± 552	4838 ± 56	1369 ± 15	1.27
down TIS 2011 2d KK	789849 ± 1822	56280 ± 172	6468 ± 19	0.82
down TIS 2011 2d PiPi	233337 ± 924	19599 ± 94	4475 ± 21	1.92
down TOS 2011 2d KK	522014 ± 1259	19332 ± 109	2799 ± 15	0.54
down TOS 2011 2d PiPi	156116 ± 618	6873 ± 62	2026 ± 18	1.30

Table 8.12.: Signal and background yields in the signal region for 2012 data.

Sample	Signal	Background	Peaking background	Peaking fraction [%]
up TIS 2d KK	1417410 ± 7926	101004 ± 752	11951 ± 89	0.84
up TIS 2d PiPi	474339 ± 1722	42970 ± 173	10238 ± 41	2.16
up TOS 2d KK	853168 ± 1680	33388 ± 148	4765 ± 21	0.56
up TOS 2d PiPi	289536 ± 893	14393 ± 90	4041 ± 25	1.40
down TIS 2d KK	1476780 ± 7566	81763 ± 722	11458 ± 101	0.78
down TIS 2d PiPi	493508 ± 1066	45135 ± 113	10656 ± 26	2.16
down TOS 2d KK	868847 ± 1757	33952 ± 158	4505 ± 20	0.52
down TOS 2d PiPi	301210 ± 1253	14337 ± 128	4188 ± 37	1.39

8.7. Multiple candidates

The treatment of multiple candidates in the nominal selection is described in Sec. 4.7. As a cross-check, the other possibilities to treat multiple candidates are explored here. The fit is repeated with events for which exactly one candidate survives the selection, where one event was chosen according to the qualifier described in Sec. 4.7 and where one random candidate was chosen (only for 2012 data). The results of these different fits are shown in Tab. 8.13 and Tab. 8.14 for 2011 and 2012, respectively. The biggest effect is visible for the samples where a random candidate is chosen for 2012 and where the candidate is chosen by the qualifier for 2011. The largest differences between the weighted averages, (0.028% and 0.025% for 2011 and 2012, respectively), are taken as systematic uncertainties.

Table 8.13.: Results for different treatments of multiple candidates for 2011 data. Largest difference: 0.028%. †: Fit with error matrix not positive-definite.

Sample	$A_{raw}(KK)[\%]$	$A_{raw}(\pi\pi)[\%]$	$\Delta A_{CP}[\%]$
up TIS 2011	-1.985 ± 0.139	-1.729 ± 0.251	-0.256 ± 0.287
up TIS only one candidate 2011	-1.932 ± 0.144	-1.710 ± 0.260	-0.222 ± 0.297
up TIS 2011 chosen candidate	-1.995 ± 0.141	-1.665 ± 0.254	-0.330 ± 0.290
up TOS 2011	-1.437 ± 0.169	-1.059 ± 0.302	-0.378 ± 0.346
up TOS only one candidate 2011	-1.315 ± 0.172	-1.066 ± 0.306	-0.249 ± 0.351
up TOS 2011 chosen candidate	-1.415 ± 0.170	-1.135 ± 0.303	-0.280 ± 0.348
down TIS 2011	-0.150 ± 0.117	-0.095 ± 0.211	-0.055 ± 0.241
down TIS only one candidate 2011	-0.056 ± 0.121	0.014 ± 0.218	-0.070 ± 0.249
down TIS 2011 chosen candidate [†]	-0.183 ± 0.117	-0.075 ± 0.213	-0.108 ± 0.243
down TOS 2011	-0.694 ± 0.137	-0.356 ± 0.251	-0.338 ± 0.286
down TOS only one candidate 2011	-0.668 ± 0.143	-0.208 ± 0.255	-0.461 ± 0.292
down TOS 2011 chosen candidate	-0.707 ± 0.141	-0.334 ± 0.252	-0.373 ± 0.289
weighted average	-0.942 ± 0.068	-0.719 ± 0.124	-0.228 ± 0.142
weighted average only one candidate	-0.873 ± 0.071	-0.640 ± 0.127	-0.234 ± 0.145
weighted average chosen candidate	-0.954 ± 0.069	-0.703 ± 0.125	-0.256 ± 0.143

Table 8.14.: Results for different treatments of multiple candidates for 2012 data.
Largest difference: 0.025%.

Sample	$A_{raw}(KK)[\%]$	$A_{raw}(\pi\pi)[\%]$	$\Delta A_{CP}[\%]$
up TIS	-1.799 ± 0.082	-1.512 ± 0.149	-0.287 ± 0.170
up TIS only one candidate	-1.743 ± 0.085	-1.460 ± 0.154	-0.283 ± 0.176
up TIS chosen candidate	-1.764 ± 0.083	-1.517 ± 0.150	-0.247 ± 0.171
up TIS random candidate	-1.753 ± 0.084	-1.446 ± 0.151	-0.307 ± 0.173
up TOS	-1.297 ± 0.103	-1.154 ± 0.185	-0.143 ± 0.212
up TOS only one candidate	-1.257 ± 0.105	-1.090 ± 0.188	-0.167 ± 0.215
up TOS chosen candidate	-1.287 ± 0.104	-1.091 ± 0.185	-0.196 ± 0.213
up TOS random candidate	-1.289 ± 0.104	-1.100 ± 0.186	-0.189 ± 0.213
down TIS	-0.227 ± 0.081	-0.456 ± 0.146	0.229 ± 0.167
down TIS only one candidate	-0.069 ± 0.084	-0.314 ± 0.151	0.245 ± 0.173
down TIS chosen candidate	-0.181 ± 0.082	-0.429 ± 0.147	0.248 ± 0.168
down TIS random candidate	-0.127 ± 0.083	-0.359 ± 0.148	0.232 ± 0.170
down TOS	-0.455 ± 0.103	-0.184 ± 0.181	-0.272 ± 0.208
down TOS only one candidate	-0.418 ± 0.104	-0.043 ± 0.184	-0.376 ± 0.212
down TOS chosen candidate	-0.451 ± 0.103	-0.120 ± 0.182	-0.331 ± 0.209
down TOS random candidate	-0.420 ± 0.104	-0.101 ± 0.183	-0.319 ± 0.210
weighted average	-0.953 ± 0.045	-0.850 ± 0.081	-0.096 ± 0.093
weighted average only one candidate	-0.871 ± 0.047	-0.747 ± 0.083	-0.118 ± 0.095
weighted average chosen candidate	-0.925 ± 0.046	-0.818 ± 0.082	-0.101 ± 0.093
weighted average random candidate	-0.899 ± 0.046	-0.772 ± 0.082	-0.121 ± 0.094

8.8. Fiducial cuts

To study the effect of the specific implementation of the fiducial cuts (see Sec. 4.5.1), the parameters are varied, changing the requirements. Specifically the following three cases were studied:

- Applying the baseline fiducial cut to exclude the beampipe, but a reduced fiducial volume criterion to exclude the edge regions with large asymmetry (*i.e.* $\alpha = 0.34$).
- Applying a reduced fiducial volume criterion to exclude the beampipe ($p_1 = 468\text{MeV}/c$ and $p_2 = 447\text{MeV}/c$) and the baseline fiducial cut to exclude the edge regions.
- Loosen both fiducial cuts (*i.e.* $\alpha = 0.34$, $p_1 = 468\text{MeV}/c$ and $p_2 = 447\text{MeV}/c$).

The results of these three variations can be found in Tab. 8.15. A systematic uncertainty of 0.025% is assigned, corresponding to the maximum variation observed. This variation is compatible with the variation found in the preliminary 2011 analysis (0.02%). Therefore this value is used for both data samples.

Table 8.15.: Results for the three sets of fiducial volume selection criteria and the nominal setting.

Sample	$A_{raw}(KK)[\%]$	$A_{raw}(\pi\pi)[\%]$	$\Delta A_{CP}[\%]$
up TIS	-1.799 ± 0.082	-1.512 ± 0.149	-0.287 ± 0.170
up TIS fid looser edge	-1.776 ± 0.082	-1.494 ± 0.147	-0.282 ± 0.168
up TIS fid looser beampipe	-1.776 ± 0.081	-1.445 ± 0.146	-0.331 ± 0.167
up TIS fid looser both	-1.749 ± 0.080	-1.423 ± 0.145	-0.326 ± 0.166
up TOS	-1.297 ± 0.103	-1.154 ± 0.185	-0.143 ± 0.212
up TOS fid looser edge	-1.283 ± 0.102	-1.197 ± 0.182	-0.086 ± 0.209
up TOS fid looser beampipe	-1.262 ± 0.102	-1.072 ± 0.182	-0.190 ± 0.208
up TOS fid looser both	-1.252 ± 0.101	-1.114 ± 0.180	-0.138 ± 0.206
down TIS	-0.227 ± 0.081	-0.456 ± 0.146	0.229 ± 0.167
down TIS fid looser edge	-0.231 ± 0.080	-0.449 ± 0.144	0.217 ± 0.165
down TIS fid looser beampipe	-0.269 ± 0.080	-0.482 ± 0.144	0.214 ± 0.164
down TIS fid looser both	-0.273 ± 0.079	-0.477 ± 0.142	0.204 ± 0.163
down TOS	-0.455 ± 0.103	-0.184 ± 0.181	-0.272 ± 0.208
down TOS fid looser edge	-0.473 ± 0.102	-0.180 ± 0.179	-0.293 ± 0.206
down TOS fid looser beampipe	-0.527 ± 0.101	-0.270 ± 0.178	-0.257 ± 0.205
down TOS fid looser both	-0.538 ± 0.100	-0.267 ± 0.176	-0.271 ± 0.202
weighted average	-0.953 ± 0.045	-0.850 ± 0.081	-0.096 ± 0.093
weighted average fid looser edge	-0.948 ± 0.045	-0.850 ± 0.080	-0.092 ± 0.092
weighted average fid looser beampipe	-0.966 ± 0.045	-0.839 ± 0.080	-0.121 ± 0.091
weighted average fid looser both	-0.959 ± 0.044	-0.838 ± 0.079	-0.115 ± 0.091

8.9. Stability checks

In this part, ΔA_{CP} is determined binned in a number of variables. It is expected to not vary greatly with any of the variables studied here.

8.9.1. Run number

The results of the fit should not vary with the data taking periods used in the analysis. Therefore, the run number dependency of the fit results is studied. The weighted average of the two triggers can be found in Fig. 8.3 for both 2011 and 2012 data. While ΔA_{CP} does vary to some degree around the baseline result (bold line with hatched error region), no dependency is visible. In both data taking periods the results are compatible with a polynomial of order zero (with $\chi^2/ndf = 0.94$ and 1.15 for 2011 and 2012, respectively). The largest deviation from the baseline result is less than 3σ . See App. A.2 for the plots of the individual asymmetries as well as tables with the results in all bins.

8.9.2. Number of primary vertices

To check, whether pile-up² or events with multiple pp -interactions are influencing the asymmetry measurement, the fit is performed in bins of the number of reconstructed primary vertices, $nPVs$. In case of more than one PV in an event, the PV might be misidentified, leading to the mis-calculation of impact parameters, flight-distances and so on. The number of D^0 from not-prompt D^* decays might also be larger. The results of the asymmetries determination as a function of $nPVs$ are shown in Fig. 8.4. The corresponding graphs of the individual asymmetries can be found in App. A.3. The results are compatible with a polynomial of order zero, as indicated by the resulting χ^2/ndf of 1.14 and 0.62 for 2011 and 2012, respectively. The deviations at higher number of primary vertices is purely statistical, the largest significance being 2.51σ (down TOS, $nPVs = 5$).

8.9.3. The quality of the $\pi_s D^0$ vertex

The full decay chain is fitted with the *DecayTreeFitter* and the χ_{DTF}^2/ndf obtained is the quality criterion of the reconstructed vertex. The higher the value, the larger the probability that the slow pion and the D^0 did not originate from the same D^* decay. The presence of a background might compromise the ΔA_{CP} measurement. The dependence of ΔA_{CP} versus the DTF vertex χ_{DTF}^2 is shown in Fig. 8.5, while the plots of the individual asymmetries and the table of all fit results can be found in App. A.4. The scale of the

²Residual signal remaining in detector from parts of the previous event.

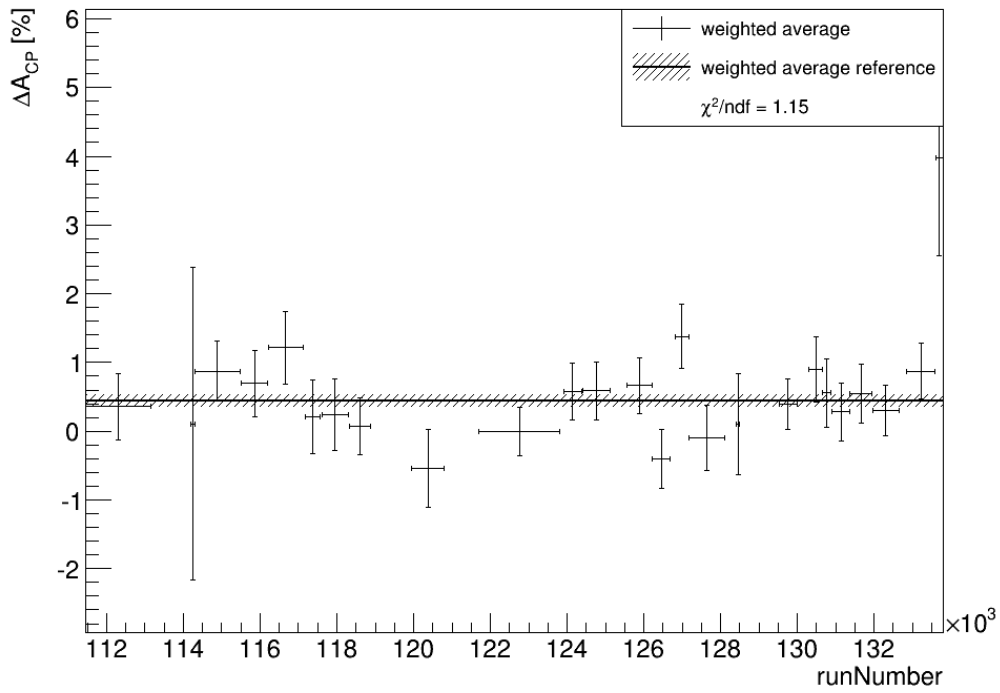
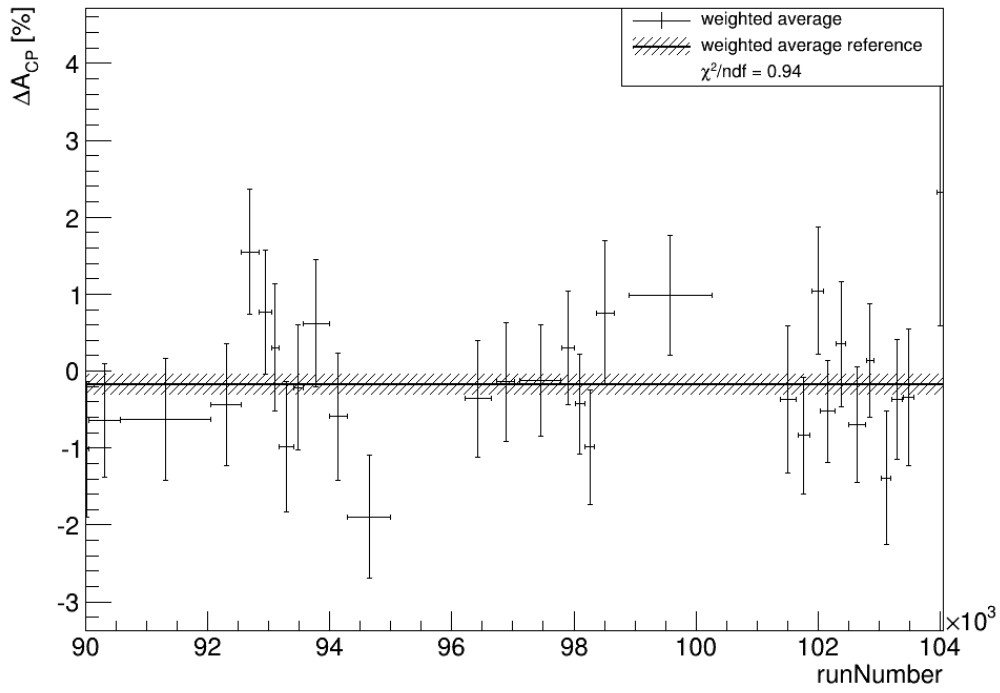


Figure 8.3.: ΔA_{CP} vs. $runNumber$, averaged over magnet polarity and trigger for 2011 (top) and 2012 (bottom). The solid line with the hatched region as error band indicates the fit result when not distinguishing between the run numbers.

x-axis is logarithmic to be able to see the whole range of the χ^2_{DTF}/ndf . A binning with roughly equal statistics in each bin is chosen and the weighting was applied to cancel any effect of the different kinematics. No dependency is visible, as is confirmed by the χ^2/ndf 's of a polynomial of order zero, 0.48 and 1.08 for 2011 and 2012, respectively.

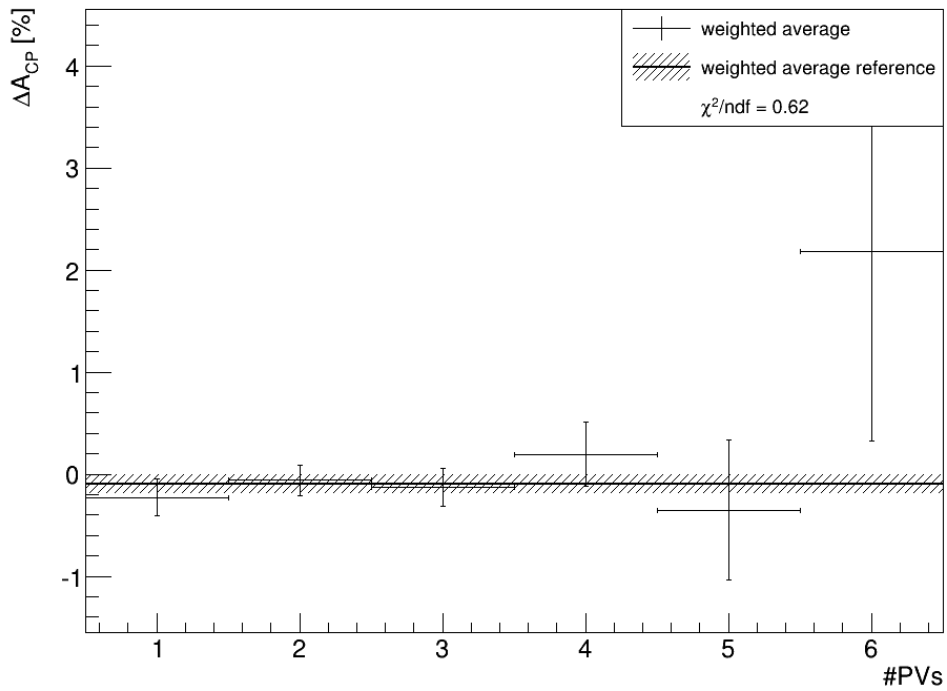
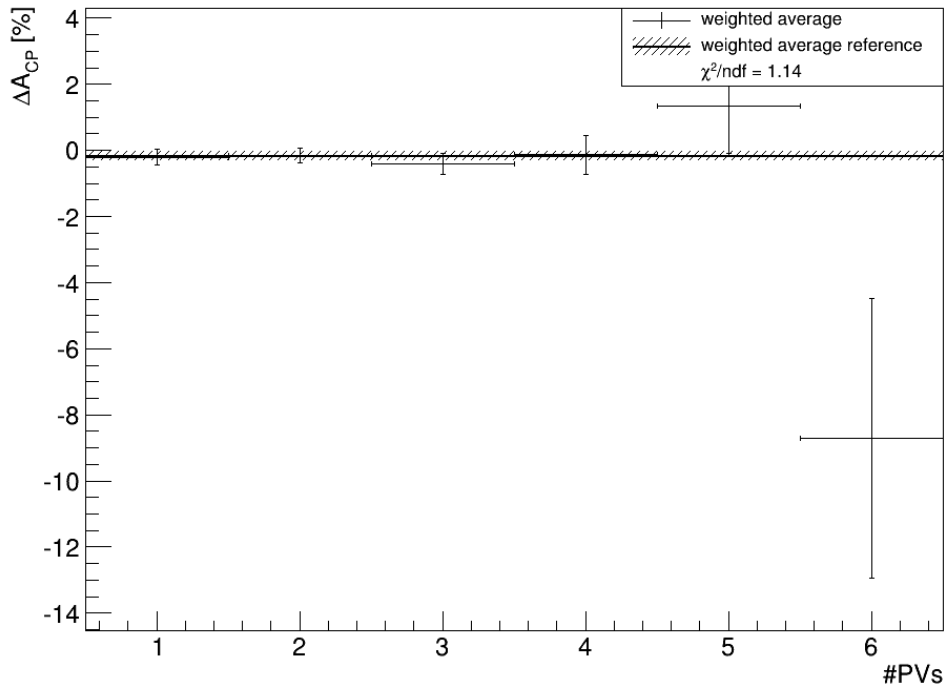


Figure 8.4.: ΔA_{CP} vs. number of primary vertices, $\#PVs$, averaged over magnetic polarities and trigger for 2011 (top) and 2012 (bottom). The solid line with the hatched region as error band indicates the fit result when not distinguishing between the number of primary vertices.

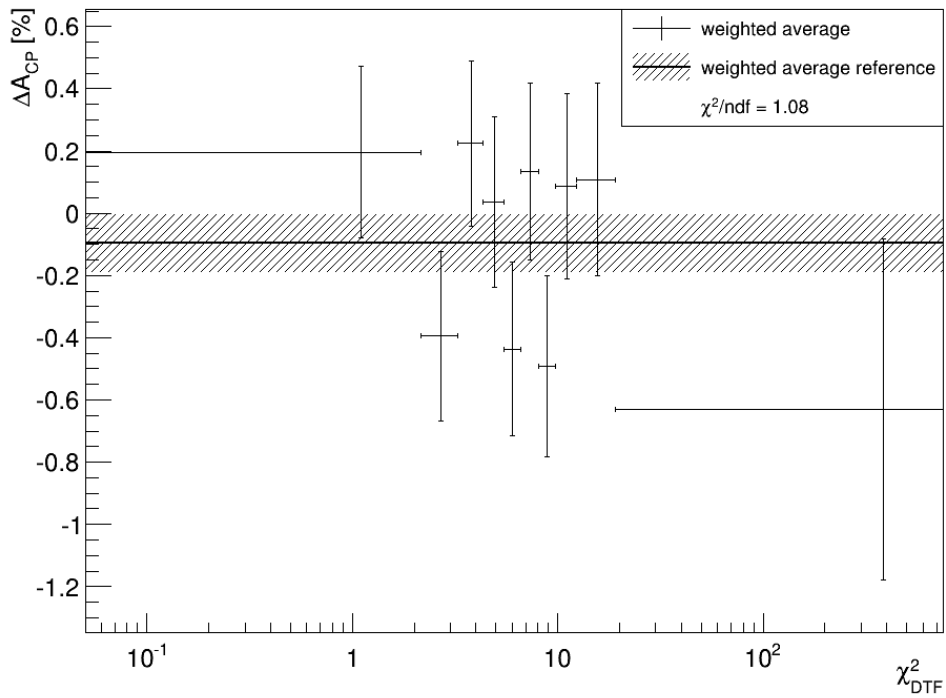
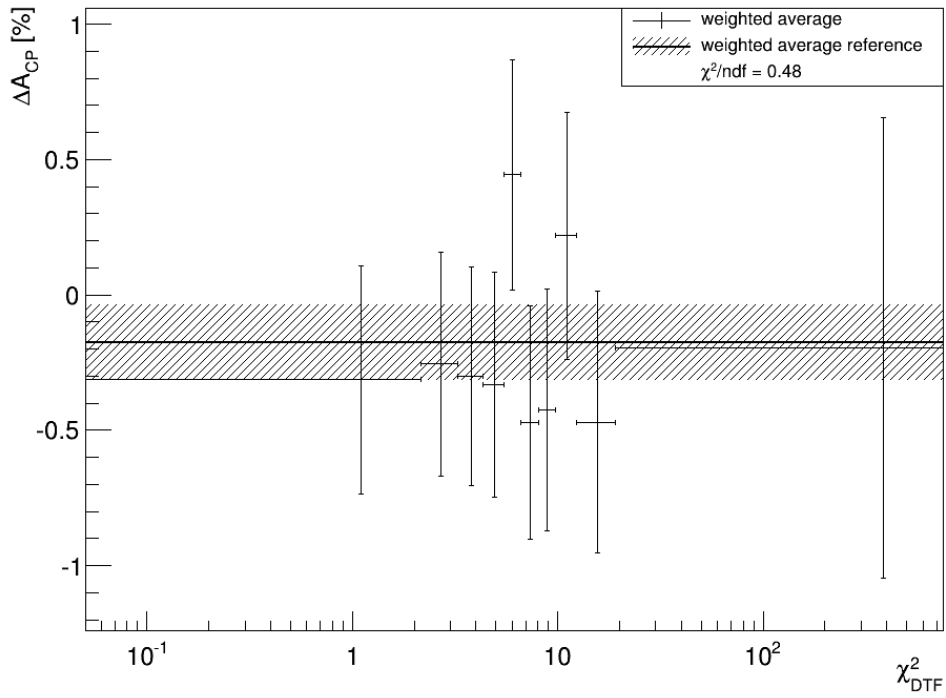


Figure 8.5.: ΔA_{CP} vs. χ^2_{DTF} , averaged over magnetic polarities and trigger for 2011 (top) and 2012 (bottom). The line with the hatched region as error band indicates the fit result when not binning in χ^2_{DTF} .

8.9.4. The quality of the slow pion impact parameter

The impact parameter is a quantity used for separation of prompt and secondary decays. It is defined as the closest distance between the track of a particle and the primary vertex. If necessary, the track is extended until it reaches the vicinity of the primary vertex. In Fig. 8.6 a graphic demonstration of the impact parameter for a semileptonically produced D^0 is shown. The definition is equivalent for the slow pion.

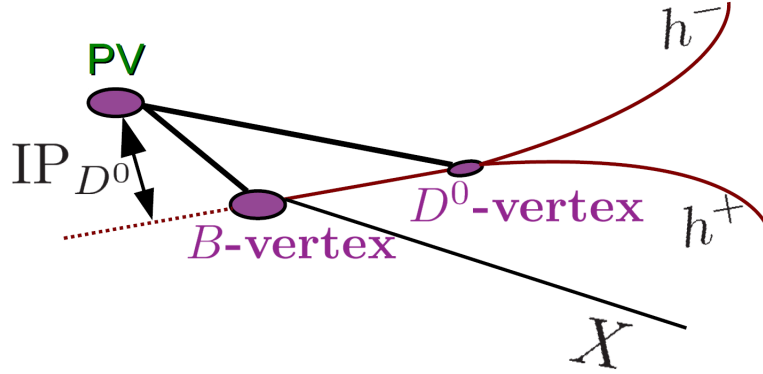


Figure 8.6.: Definition of the impact parameter (IP) of a semileptonically produced D^0 decaying into two hadrons (h^-h^+).

In the preliminary 2011 analysis [6], the quality of the slow pion impact parameter with respect to the primary vertex, $\pi_s IP \chi^2$, was identified as the major source of systematic uncertainty, because of a possible trend in ΔA_{CP} for high $\pi_s IP \chi^2$. Therefore this contribution is checked here again. A binning with roughly equal statistics in each bin is chosen and the weighting is applied to cancel any effect due to the different kinematic distributions.

In Fig. 8.7, it can be seen that the individual asymmetries show a strong dependency on this variable, namely for high $\pi_s IP \chi^2$, the individual asymmetries become very big ($\mathcal{O}(10\%)$). Since this is similar for both raw asymmetries, no net effect on ΔA_{CP} for 2012 data is observed, as shown in Fig. 8.8. For 2011 the last bin was interpreted as a hint for a dependency of ΔA_{CP} on $\pi_s IP \chi^2$. As a conservative precaution this was taken as systematic uncertainty for the preliminary 2011 result. However, with the distribution of ΔA_{CP} versus $\pi_s IP \chi^2$ in the 2012 data sample below the 2011 distribution, it becomes clear that this effect is statistical only.

Any remaining differences are due to the break-down of the assumption that the asymmetries should all be small. This leads to a non-perfect cancellation in these bins. Figures of the individual asymmetries and tables of all fit results can be found in App. A.5.

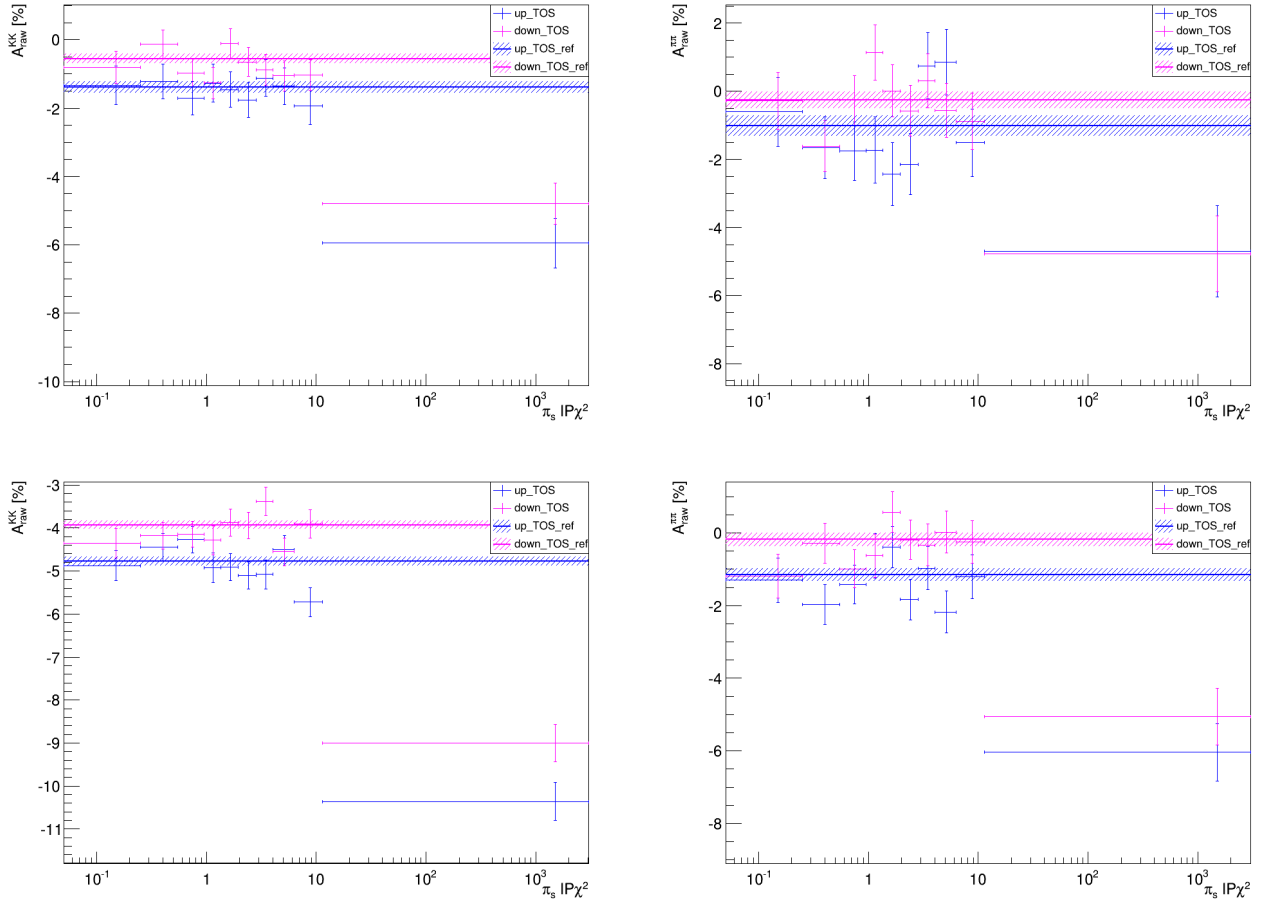


Figure 8.7.: $A_{raw}(D^0 \rightarrow K^- K^+)$ (left) and $A_{raw}(D^0 \rightarrow \pi^- \pi^+)$ (right) vs. χ^2_{DTF} , 2011 (top) and 2012 (bottom) for the TOS trigger line. The lines with the hatched regions as error band indicate the fit results when not binning in $\pi_s IP\chi^2$.

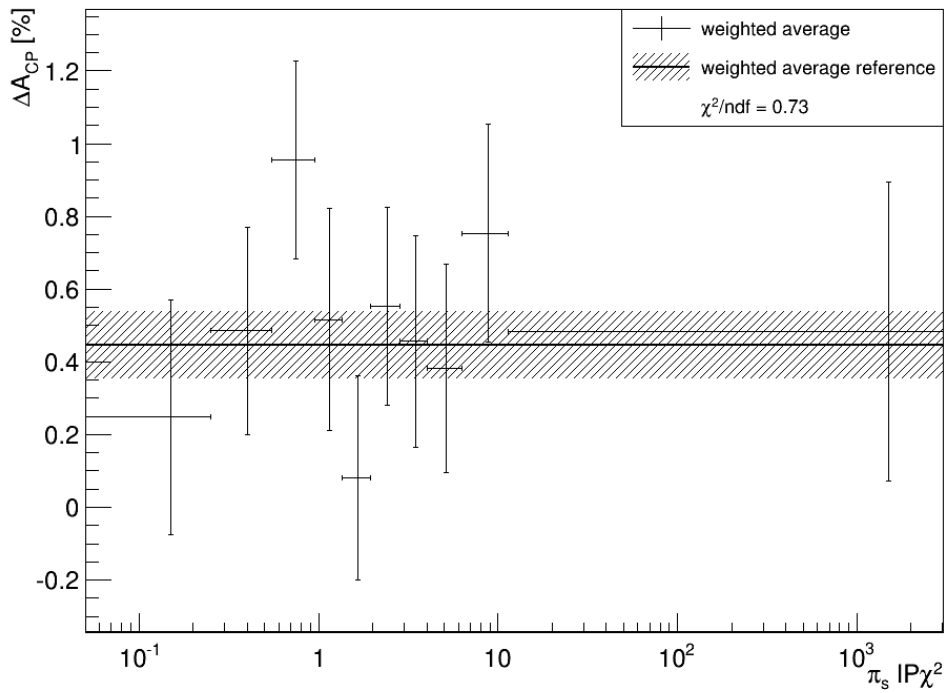
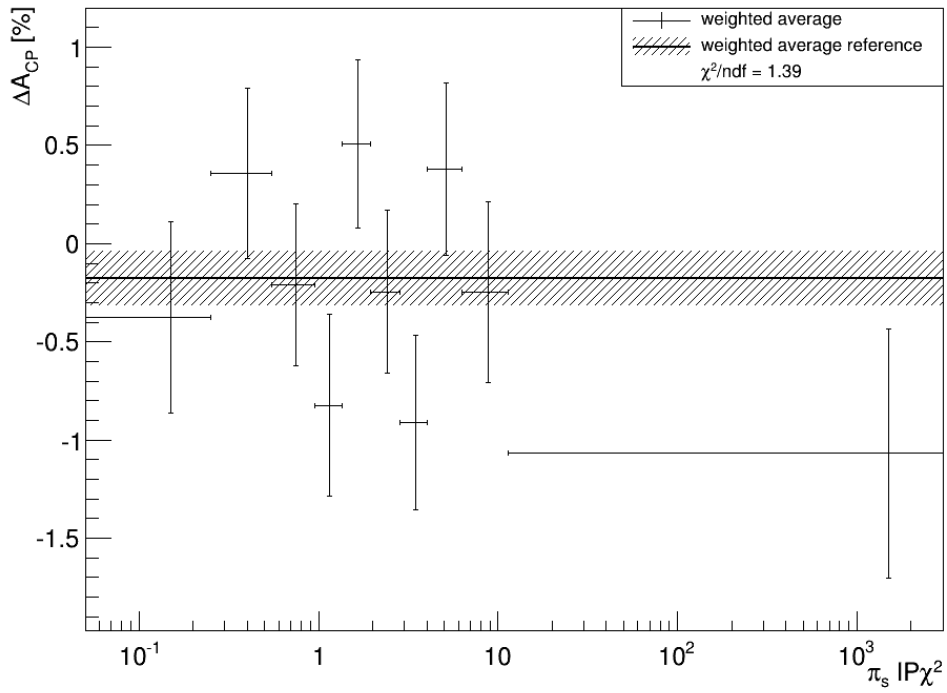


Figure 8.8.: ΔA_{CP} vs. $\pi_s IP\chi^2$, averaged over magnetic polarities and trigger for 2011 (top) and 2012 (bottom). The line with the hatched region as error band indicates the fit result when not binning in $\pi_s IP\chi^2$.

8.9.5. Slow pion transverse momentum

Since the slow pion is not very energetic, it is particularly sensitive to detector effects. Therefore ΔA_{CP} as a function of the slow pion kinematics is studied. A binning with roughly equal statistics in each bin is chosen and the weighting is applied to cancel any effect due to the different kinematic distributions. The dependence of ΔA_{CP} versus the slow pion transverse momentum, $\pi_s p_T$, is shown in Fig 8.9. ΔA_{CP} is mostly independent of $\pi_s p_T$, a polynomial of order zero is able to sufficiently describe the different results (with a χ^2/ndf of 0.74 and 0.42 for 2011 and 2012, respectively).

8.9.6. Separation in phase space

The separation in phase space between the D^0 and the π_s is given by

$$\Delta R = \sqrt{\Delta\eta^2 + \Delta\phi^2}, \quad (8.6)$$

with $\Delta\eta = \eta(D^0) - \eta(\pi_s)$ and $\Delta\phi = \phi(D^0) - \phi(\pi_s)$. An effect on ΔA_{CP} observed at small separation in phase space would hint at clustering effects, especially in the electromagnetic calorimeter. A binning with roughly equal statistics in each bin is chosen and the weighting is applied to cancel any effect due to the different kinematic distributions.

The results averaged over magnetic polarity and trigger are shown in Fig. 8.10, while the individual asymmetries and a table of all fit results can be found in App. A.7. No dependency is observable, only slight trends are visible. However, the results are reasonably described by a polynomial of order zero (with a χ^2/ndf of 0.78 and 0.63 for 2011 and 2012, respectively).

8.9.7. D^0 flight distance

The longer the D^0 was flying through the detector, the higher the chance that it was not produced from a D^* produced at a primary vertex but rather from decaying B -mesons which fly a certain distance themselves, before they decay. Therefore it has to be checked, that the ΔA_{CP} distribution does not depend on the flight distance of the D^0 . A binning with roughly equal statistics in each bin is chosen and the weighting is applied to cancel any effect due to the different kinematic distributions.

The results averaged over magnetic polarity and trigger are shown in Fig. 8.11, while the individual asymmetries and a table of all fit results can be found in App. A.8. Here, as well, no dependency of ΔA_{CP} on this variable is visible.

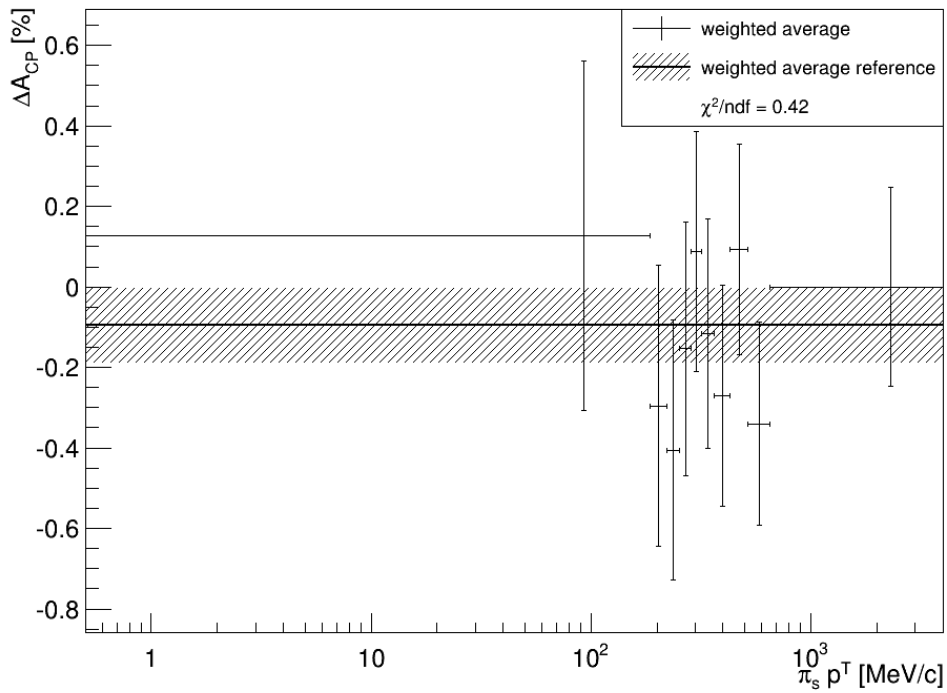
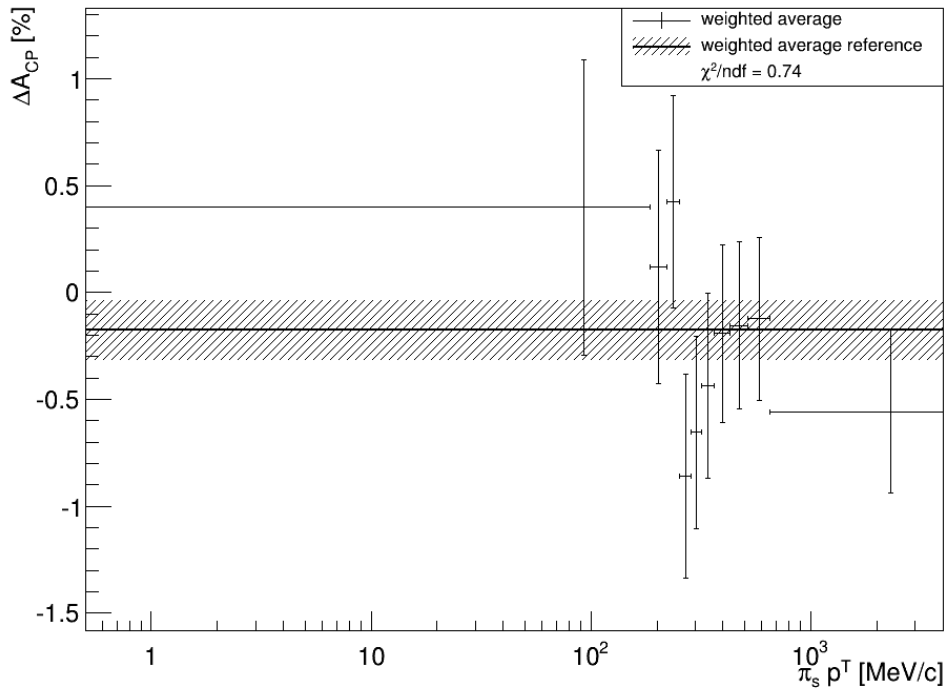


Figure 8.9.: ΔA_{CP} vs. $\pi_s p_T$, averaged over magnetic polarities and trigger for 2011 (top) and 2012 (bottom). The line with the hatched region as error band indicates the fit result when not binning in $\pi_s p_T$.

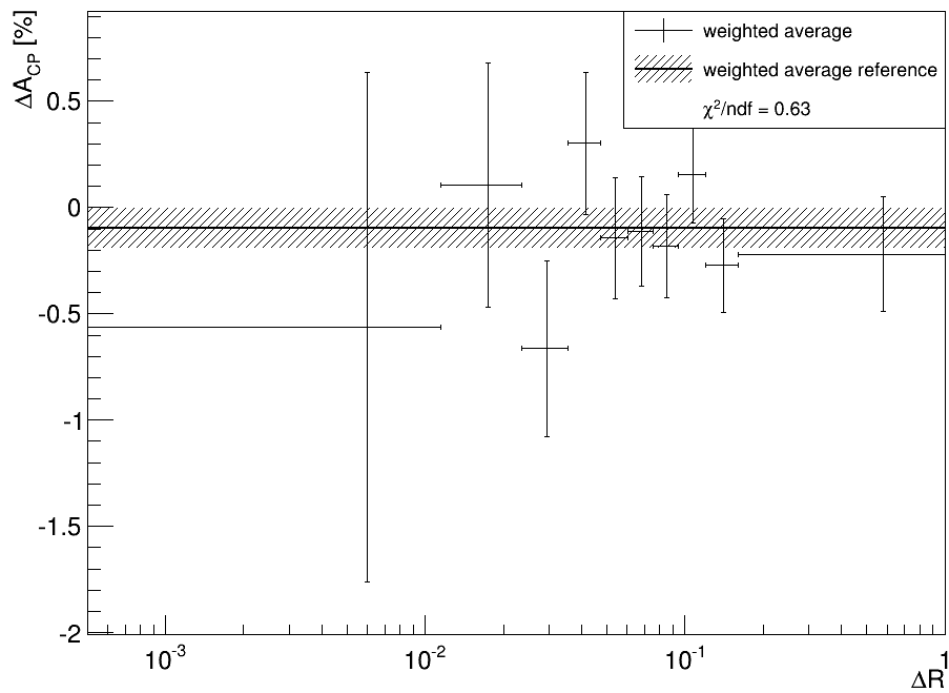
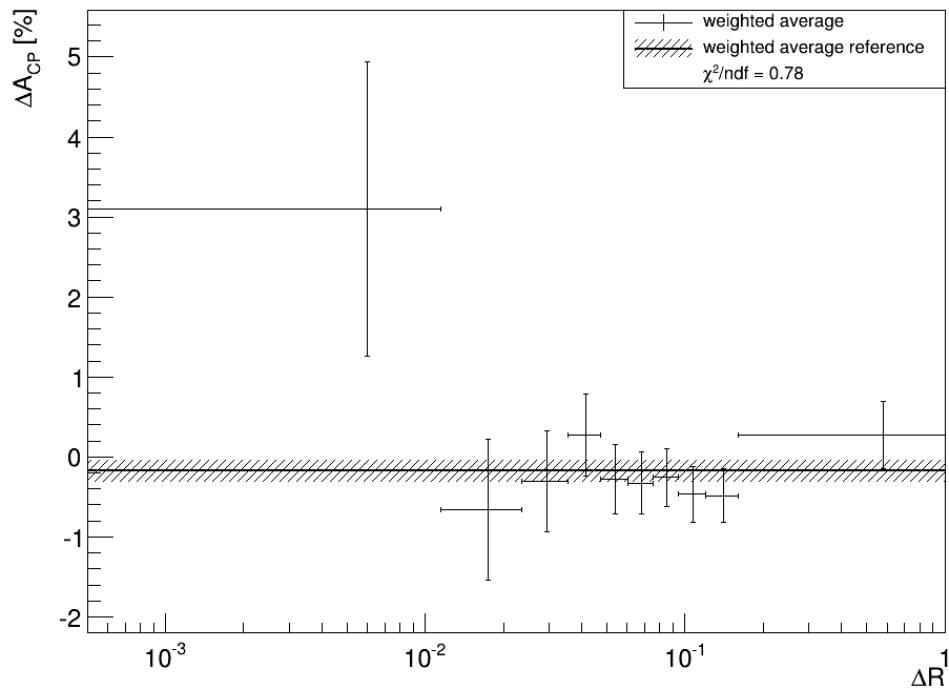


Figure 8.10.: ΔA_{CP} vs. ΔR , averaged over magnetic polarities and trigger for 2011 (top) and 2012 (bottom). The line with the hatched region as error band indicates the fit result when not binning in ΔR .

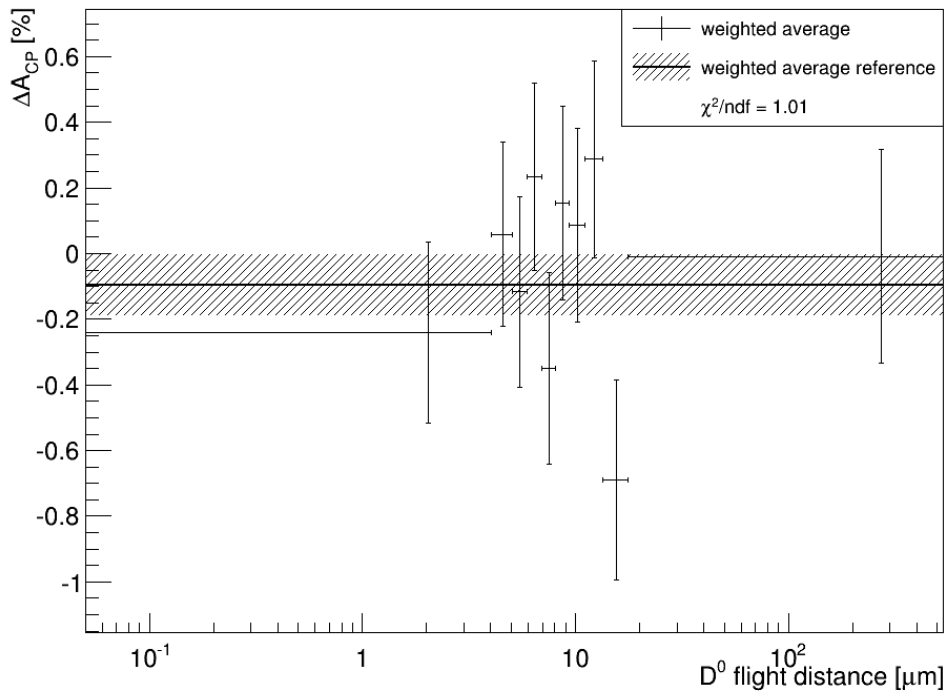
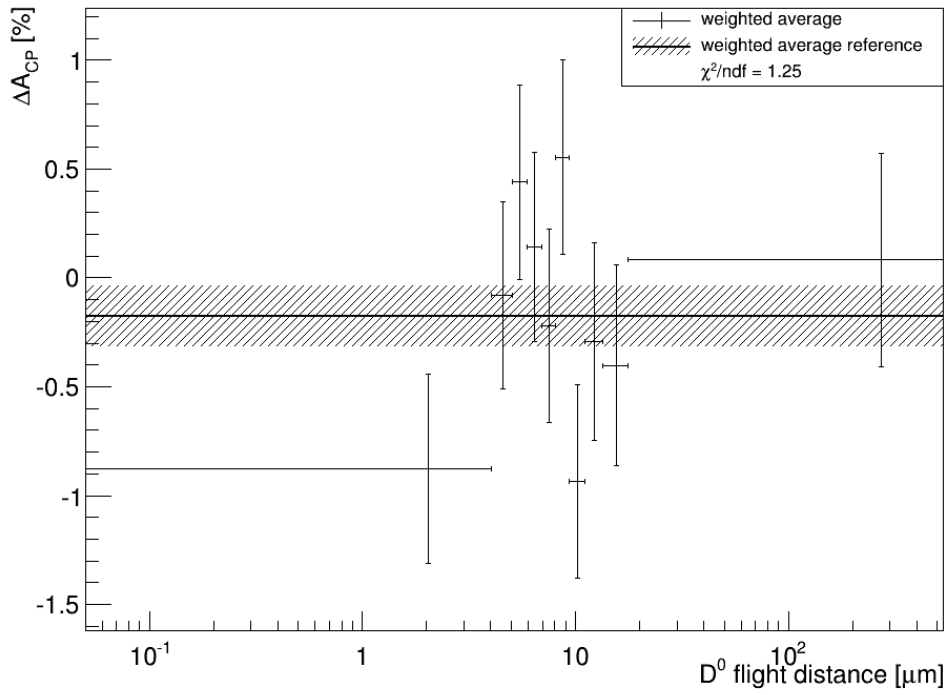


Figure 8.11.: ΔA_{CP} vs. D^0 flight distance, averaged over magnetic polarities and trigger for 2011 (top) and 2012 (bottom). The line with the hatched region as error band indicates the fit result when not binning in D^0 flight distance.

8.9.8. D^0 transverse momentum

Similarly to the $\pi_s p_T$ study, the raw asymmetries versus the $D^0 p_T$ are sensitive to detector effects. While the raw asymmetries show a dependency with the D^0 transverse momentum (see App. A.9), ΔA_{CP} should be independent of $D^0 p_T$. A binning with roughly equal statistics in each bin is chosen and the weighting is applied to cancel any effect due to the different kinematic distributions.

The results averaged over magnetic polarity and trigger are shown in Fig. 8.12, while the individual asymmetries and a table of all fit results can be found in App. A.9. Again, no effect is visible.

8.9.9. The quality of the D^0 impact parameter

As an alternative measure of the contamination of secondary decays, the $D^0 IP \chi^2$ can be used. If the particle decaying into the D^0 first flies some distance in the detector and decays then, the chances are quite high that the D^0 does not point back very well to the PV. A binning with roughly equal statistics in each bin is chosen and the weighting is applied to cancel any effect due to the different kinematic distributions.

The results averaged over magnetic polarity and trigger are shown in Fig. 8.13, while the individual asymmetries and a table of all fit results can be found in App. A.10. Again, no dependency of ΔA_{CP} is visible.

8.9.10. The azimuthal angle of D^0

Due to the detector layout, the individual asymmetries and ΔA_{CP} vary as a function of the D^0 azimuthal angle ϕ around the z -axis. However, the effects should average out when combining the two magnetic field polarities. A binning with roughly equal statistics in each bin is chosen and the weighting is applied to cancel any effect due to the different kinematic distributions.

The results averaged over magnetic polarity and trigger are shown in Fig. 8.14, while the individual asymmetries and a table of all fit results can be found in App. A.11. After averaging over the magnetic field polarity, no dependency is observable.

Any remaining deviations are probably due to the break down of the assumption of all asymmetries being small.

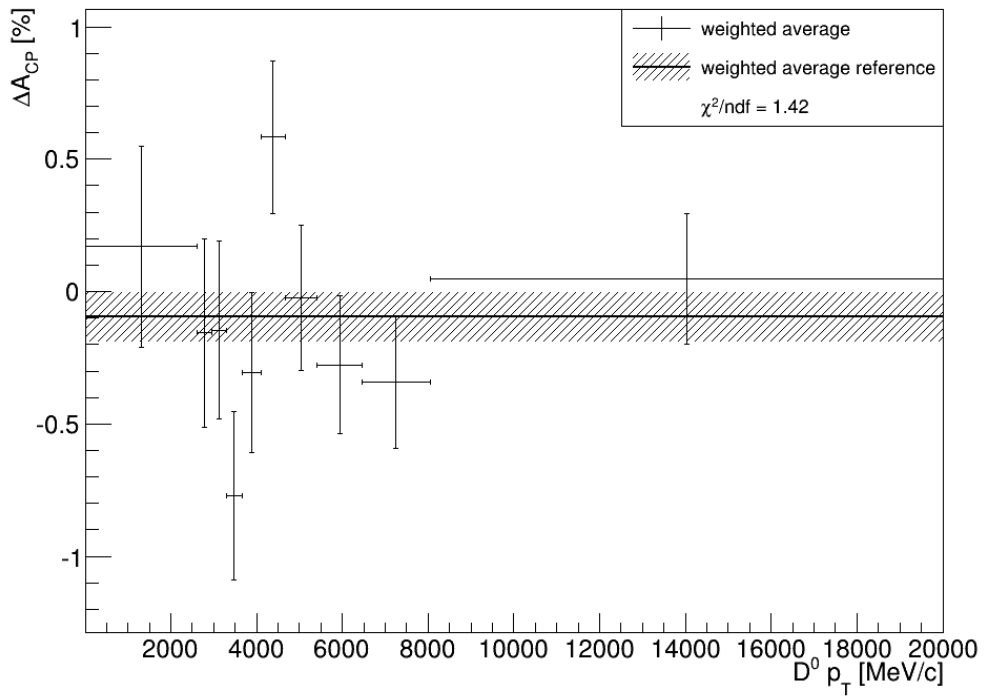
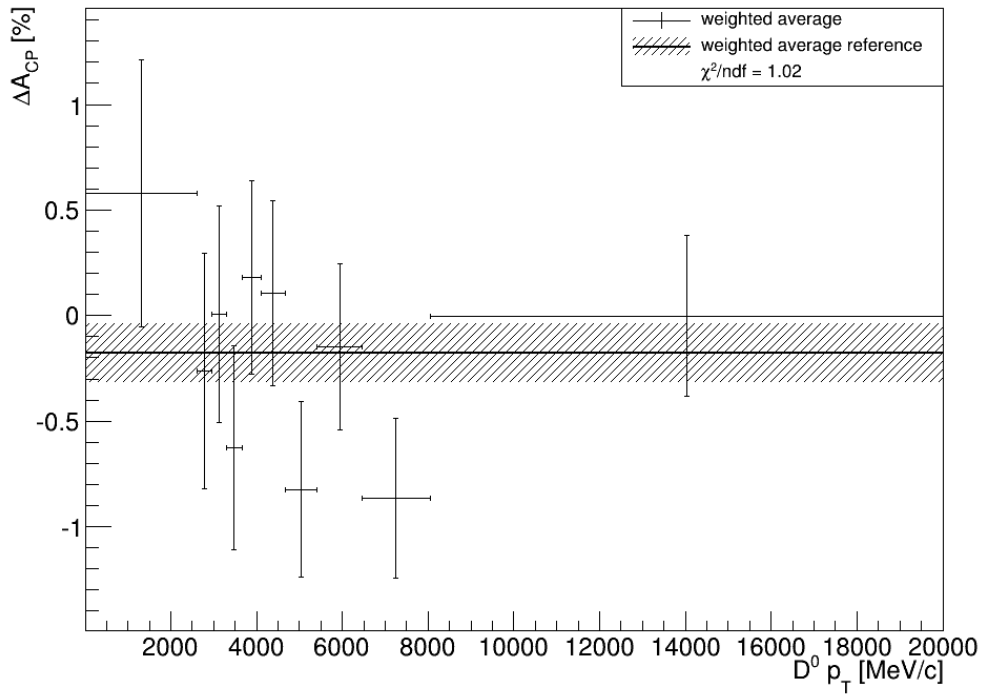


Figure 8.12.: ΔA_{CP} vs. $D^0 p_T$, averaged over magnetic polarities and trigger for 2011 (top) and 2012 (bottom). The line with the hatched region as error band indicates the fit result when not binning in $D^0 p_T$.

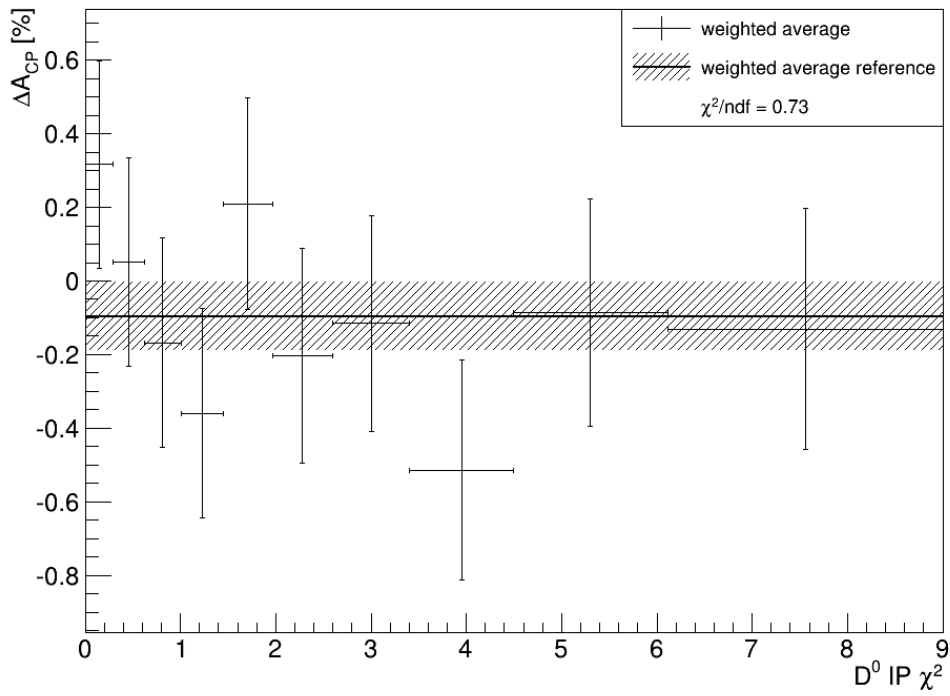
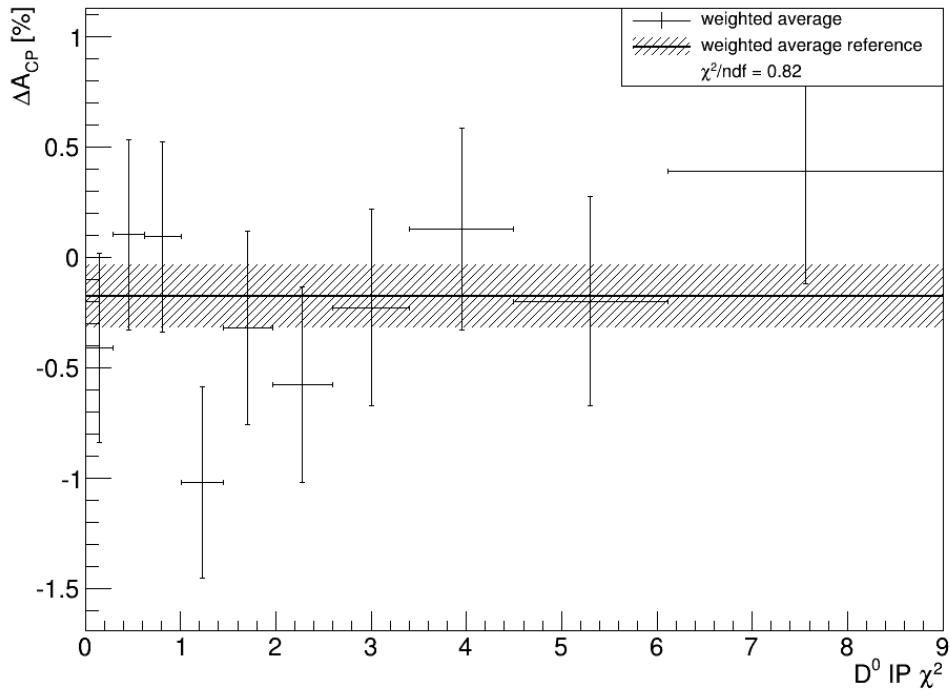


Figure 8.13.: ΔA_{CP} vs. $D^0 IP \chi^2$, averaged over magnetic polarities and trigger for 2011 (top) and 2012 (bottom). The line with the hatched region as error band indicates the fit result when not binning in $D^0 IP \chi^2$.

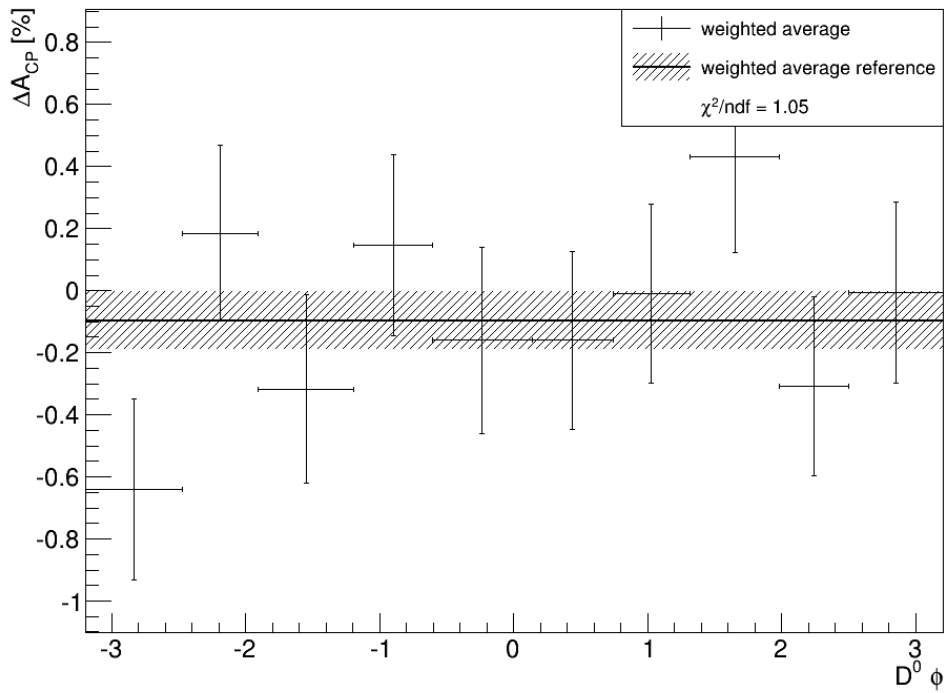
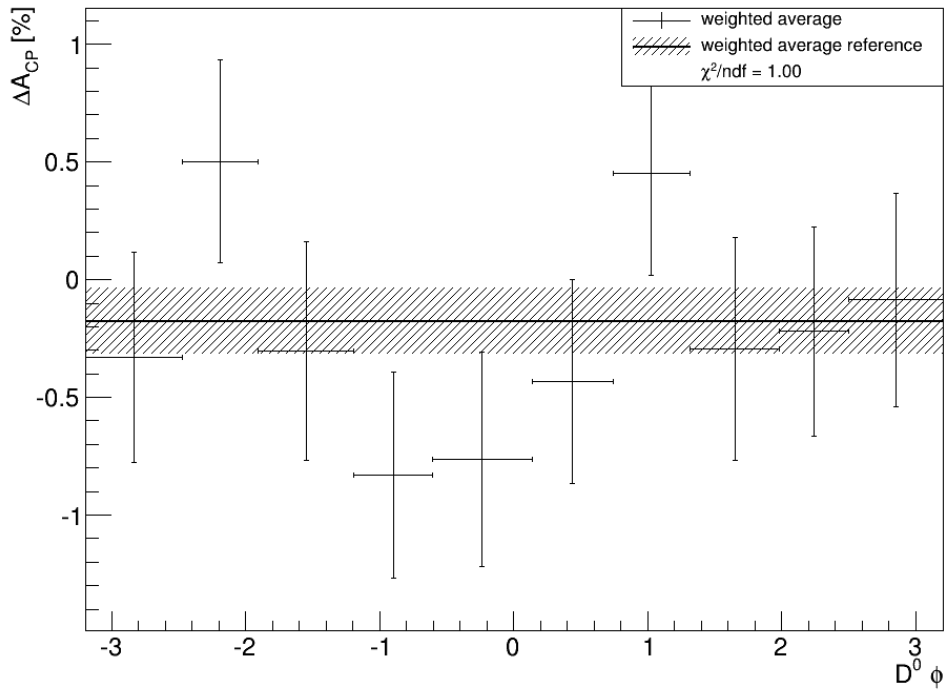


Figure 8.14.: ΔA_{CP} vs. $D^0\phi$, averaged over magnetic polarities and trigger for 2011 (top) and 2012 (bottom). The line with the hatched region as error band indicates the fit result when not binning in $D^0\phi$.

8.9.11. The D^0 mass

A peaking background in $m(D^0)$ might be a source of an asymmetry. Within the signal window in $m(D^0)$, the result should not change significantly. A binning with roughly equal statistics is chosen and the weighting is applied to cancel any effect due to the different kinematic distributions.

The results averaged over magnetic polarity and trigger are shown in Fig. 8.15, while the individual asymmetries and a table of all fit results can be found in App. A.12. Also here, no dependency of ΔA_{CP} is observed.

8.9.12. Particle identification

The selection requirement to only choose events with $DLL_{K\pi} > 5$ and $DLL_{K\pi} < -5$ for $D^0 \rightarrow K^-K^+$ and $D^0 \rightarrow \pi^-\pi^+$ decays, respectively, should not influence the final result. Therefore this requirement is varied from $DLL_{K\pi} > 5$ or $DLL_{K\pi} < -5$ to $DLL_{K\pi} > 50$ or $DLL_{K\pi} < -50$. Unfortunately, no data without the nominal selection requirement is available and a relaxation of this requirement can not be studied here. As can be seen in Fig. 8.16, for reasonable values (in the region below ten) the result does not change. For higher values there is some deviation, but overall ΔA_{CP} is stable versus the specific selection requirement on the particle identification. What is interesting to note is that the small difference between the two magnetic field polarities, especially for the TIS trigger, vanishes at a requirement of roughly 20, without losing much statistics (see App. A.13 for all figures and tables). This might be a hint that the TIS sample is not completely charge symmetric. However, this effect is taken into account by taking the weighted average of the two trigger lines and magnetic field polarities.

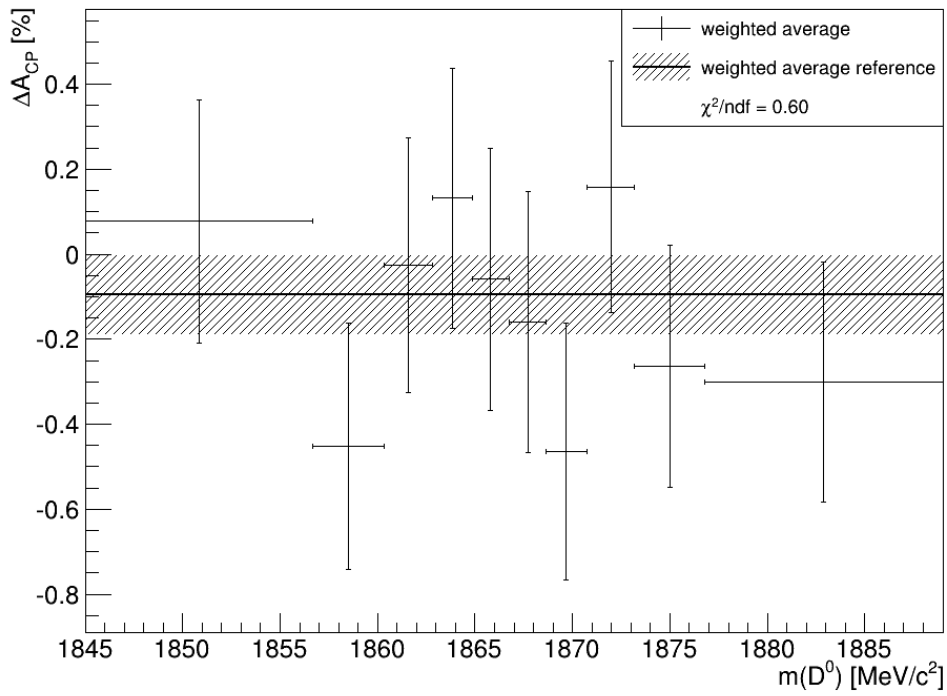
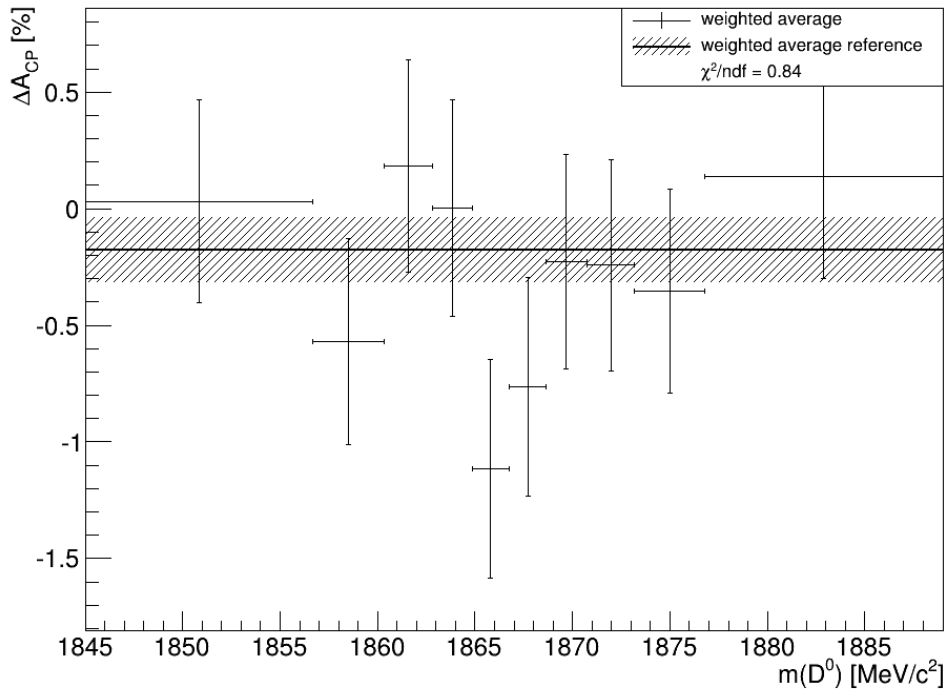


Figure 8.15.: ΔA_{CP} vs. $m(D^0)$, averaged over magnetic polarities and trigger for 2011 (top) and 2012 (bottom). The line with the hatched region as error band indicates the fit result when not binning in $m(D^0)$.

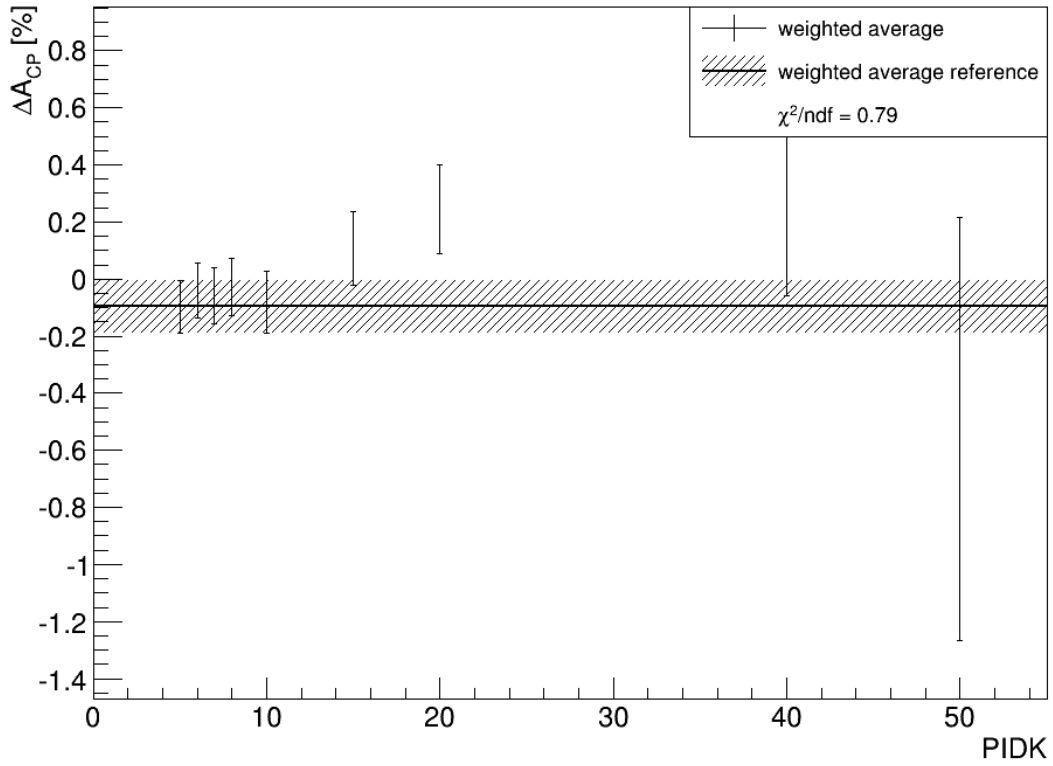


Figure 8.16.: ΔA_{CP} vs. $PIDK$, averaged over magnetic polarities and trigger for 2012 data. The line with the hatched region as error band indicates the fit result when not binning in $PIDK$.

8.10. Total systematic uncertainty

It has been shown that the result for ΔA_{CP} is stable against a multitude of possible systematic dependencies, mostly related to the kinematics of some part of the decay chain. At the same time, multiple sources of systematic uncertainty were studied. In Table 8.16 all these sources of systematic uncertainty are summarized for 2011 and 2012, respectively. Systematic uncertainties of 0.048% and 0.042% are assigned. All uncertainties are assumed to be independent and are therefore summed in quadrature. The two largest systematic uncertainties for both years are the treatment of the multiple candidates and the fiducial cuts. For 2011 also the peaking background is important, while this uncertainty is more constrained by the added statistics in the 2012 data sample. For future analysis of ΔA_{CP} at LHCb the fiducial cuts would need to be revisited and the parameters describing them would need to be determined more precisely. Furthermore, tighter selection requirements might be needed to reduce the number of multiple candidates.

Table 8.16.: Summary table of all the contributions to the the systematic uncertainty for 2011 (top) and 2012 (bottom) data.

Source	Systematic uncertainty [%]
Fixing model	0.002
Binning	< 0.001
Signal model	0.007
Background model	0.001
Peaking background	0.027
Multiple candidates	0.028
Fiducial Cuts	0.025
Kinematic Weighting	0.009
Total	0.048

Source	Systematic uncertainty [%]
Fixing model	0.001
Binning	< 0.001
Signal model	0.010
Background model	< 0.001
Peaking background	0.012
Multiple candidates	0.025
Fiducial Cuts	0.025
Kinematic Weighting	0.016
Total	0.042

9. Conclusion

The results of a search for time-integrated CP -violation in the decays $D^0 \rightarrow K^- K^+$ and $D^0 \rightarrow \pi^- \pi^+$, which has been performed on data corresponding to an integrated luminosity of 3fb^{-1} collected by LHCb in 2011 and 2012 have been presented. The individual raw CP -asymmetries (which are including production and detection asymmetries) have been determined as well as ΔA_{CP} , the difference of the CP -asymmetries of the two final states. To ensure that the different kinematic distributions of the two decay channels do not generate a non-physical asymmetry, a weighting scheme was applied. After this weighting the following two results have been reached, by averaging over the magnetic field polarity and trigger settings:

$$\Delta A_{CP} = (-0.182 \pm 0.141(\text{stat.}) \pm 0.048(\text{syst.}))\%, \quad (9.1)$$

for the 2011 data sample and

$$\Delta A_{CP} = (-0.068 \pm 0.092(\text{stat.}) \pm 0.042(\text{syst.}))\%, \quad (9.2)$$

for the 2012 data sample, where the first uncertainty is statistical and the second is systematic. A weighted average of these two results yields the final result for the full 3fb^{-1} of data available to LHCb:

$$\Delta A_{CP} = (-0.104 \pm 0.077(\text{stat.}) \pm 0.044(\text{syst.}))\%, \quad (9.3)$$

where the systematic uncertainty is the weighted average of the individual systematic uncertainties.

This measurement of ΔA_{CP} is still statistically limited, the systematic uncertainty being smaller than the statistical by a factor of 1.75. As can be seen from the minimal reduction of the systematic uncertainty when doubling the data sample (2012 compared to 2011), the systematic uncertainty will likely not be reduced significantly with more data available after the LHC has started physics collisions again in the middle of 2015, while this is obviously the case for the statistical uncertainty. The result can be compared to the results of previous analyses, as has already been done in the introduction, but now including the full 3fb^{-1} of data available to LHCb, which is shown in Fig. 9.1. The sensitivity of this analysis completely dominates the weighted average of all available analyses. and this analysis compromises therefore the single best measurement of ΔA_{CP} and accordingly of direct CP -violation in SCS charm decays.

Together with the result from the complementary semileptonic analysis, $\Delta A_{CP} = (+0.14 \pm 0.16(stat.) \pm 0.08(syst.))\%$ [8], this results in an average of

$$\Delta A_{CP} = (-0.06 \pm 0.08)\%, \quad (9.4)$$

with statistical and systematic uncertainty added in quadrature. The SM expectation, $\Delta A_{CP} < \mathcal{O}(10^{-3})$ is therefore plausible, $\Delta A_{CP} = 0$ being within the 1σ interval. The significance of the difference between the two results is reduced from 1.9σ between the preliminary 2011 prompt result and the full semileptonic result to 1.2σ , thereby significantly reconciling the two complementary approaches.

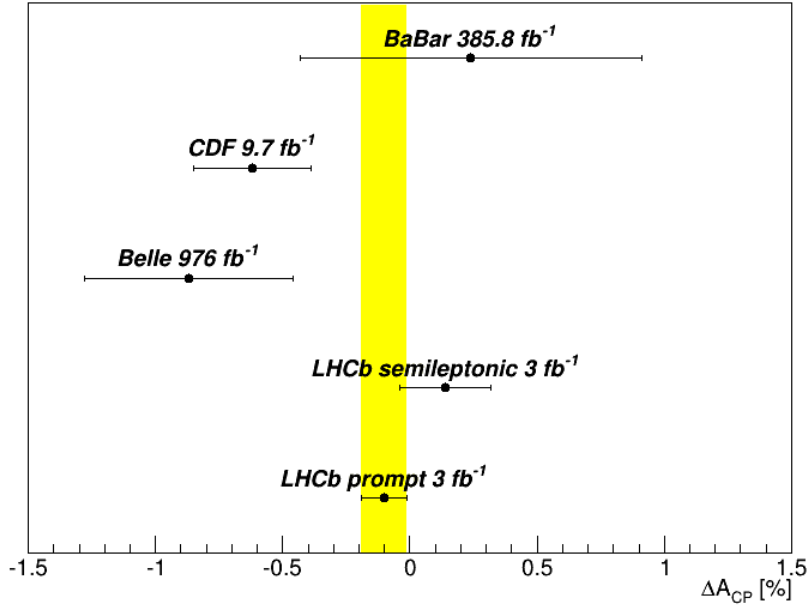


Figure 9.1.: Average ΔA_{CP} of all available data.

As was shown in Sec. 2.3, when measuring both ΔA_{CP} and A_{Γ} , as has been done now at LHCb, direct and indirect CP -violation can be separated using the equations

$$\Delta A_{CP} = \Delta a_{CP}^{dir} \left(1 + y_{CP} \frac{\langle \bar{t} \rangle}{\tau} \right) - \frac{\Delta \langle t \rangle}{\tau} a_{CP}^{ind} \quad (9.5)$$

and

$$A_{\Gamma} = -a_{CP}^{ind} - a_{CP}^{dir} y_{CP}, \quad (9.6)$$

where the contribution of the decay-dependent direct CP -violation to A_{Γ} is negligible. In Fig. 9.2 the amplitude of indirect CP -violation and the difference of the amplitudes of direct CP -violation in the two decay modes $D^0 \rightarrow K^- K^+$ and $D^0 \rightarrow \pi^- \pi^+$ are shown. Both the status before this analysis and just the results of the LHCb analyses

are presented. The LHCb results for ΔA_{CP} and A_Γ alone are enough to surpass the sensitivity of all previous analyses combined. It can be seen that including this result, the SM is favored within the 1σ region. The point of best agreement between the four measurements using LHCb data is

$$\Delta a_{CP}^{dir} = (-0.057 \pm 0.079)\%, \quad a_{CP}^{ind} = (0.016 \pm 0.054)\%. \quad (9.7)$$

This can be compared to the previous world averages from the Heavy Flavor Averaging Group (HFAG) [32], which already included the previous LHCb measurements:

$$\Delta a_{CP}^{dir} = (-0.253 \pm 0.104)\%, \quad a_{CP}^{ind} = (0.013 \pm 0.052)\%. \quad (9.8)$$

While the values are statistically compatible, the evidence for direct CP -violation up to the order of $\mathcal{O}(10^{-2})$ seen in earlier analysis is not observed here. Since the data collected in 2012 by LHCb has not been analyzed with respect to the life-time asymmetry A_Γ yet, also the amplitude of indirect CP -violation will be determined more precisely in the near future.

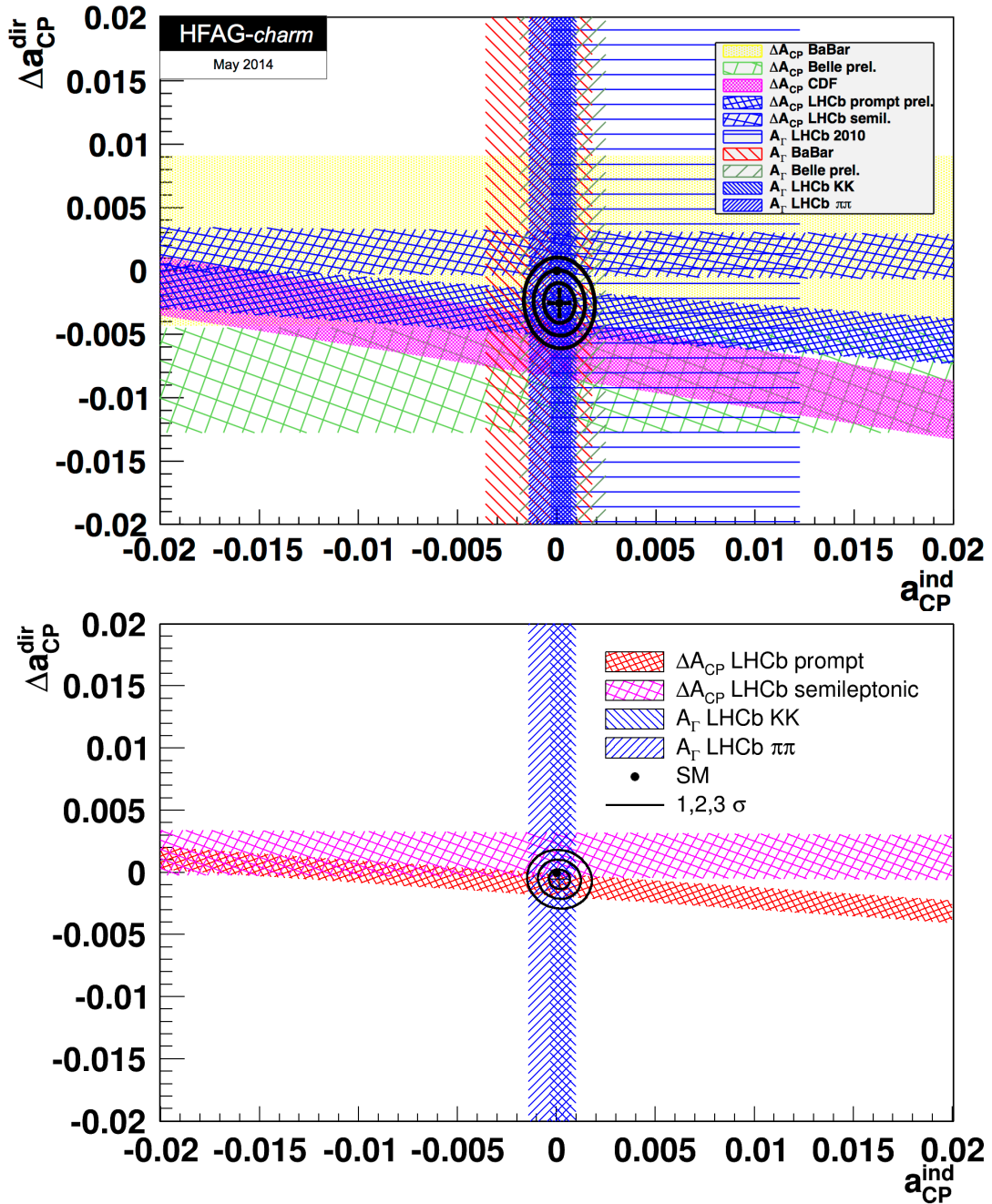


Figure 9.2.: Status of direct and indirect CP -violation before (top) and after (bottom) this analysis. The top figure is taken from HFAG [32]. The bottom figure contains only the most recent LHCb measurements, including this analysis (red).

A. Appendix

This appendix contains tables with the individual asymmetries in all the cases where these were not reported in the text itself. Also included are figures of the individual asymmetries and ΔA_{CP} separated by trigger and magnetic field polarity binned in the several variables studied before.

A.1. Peaking background

Here, the Δm distributions for the two-dimensional determination of the asymmetries for all magnetic field polarities and trigger settings are presented. Magnetic field up TOS and TIS can be found in Fig. A.1 and A.2, respectively, magnetic field down TOS and TIS in Fig. A.1 and A.2, respectively, for 2011. For 2012, magnetic field up TOS and TIS can be found in Fig. A.5 and A.6, respectively, magnetic field down TOS and TIS in Fig. A.5 and A.6, respectively

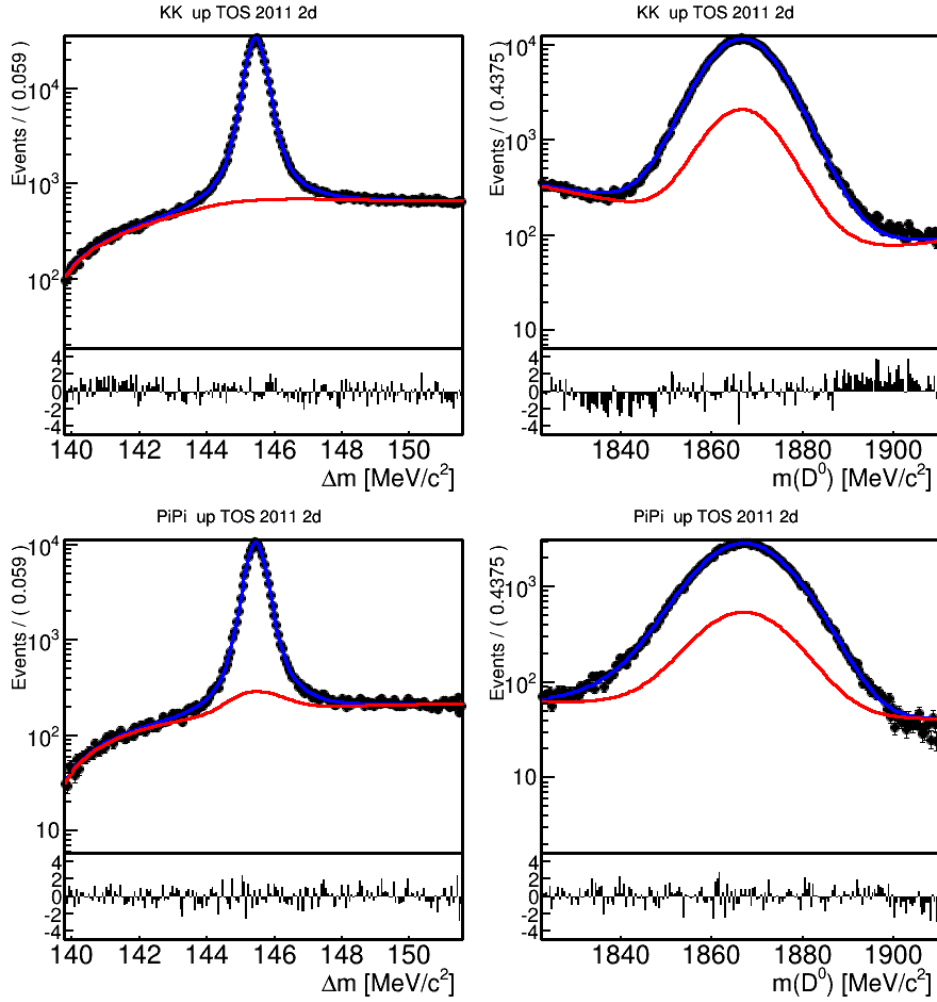


Figure A.1.: Two dimensional determination of the asymmetries on the example of 2011 up TOS data for $D^0 \rightarrow K^- K^+$ (top) and $D^0 \rightarrow \pi^- \pi^+$ (bottom) decays. The black points are the binned data, the blue line the whole model and in red is the total background (including peaking background).

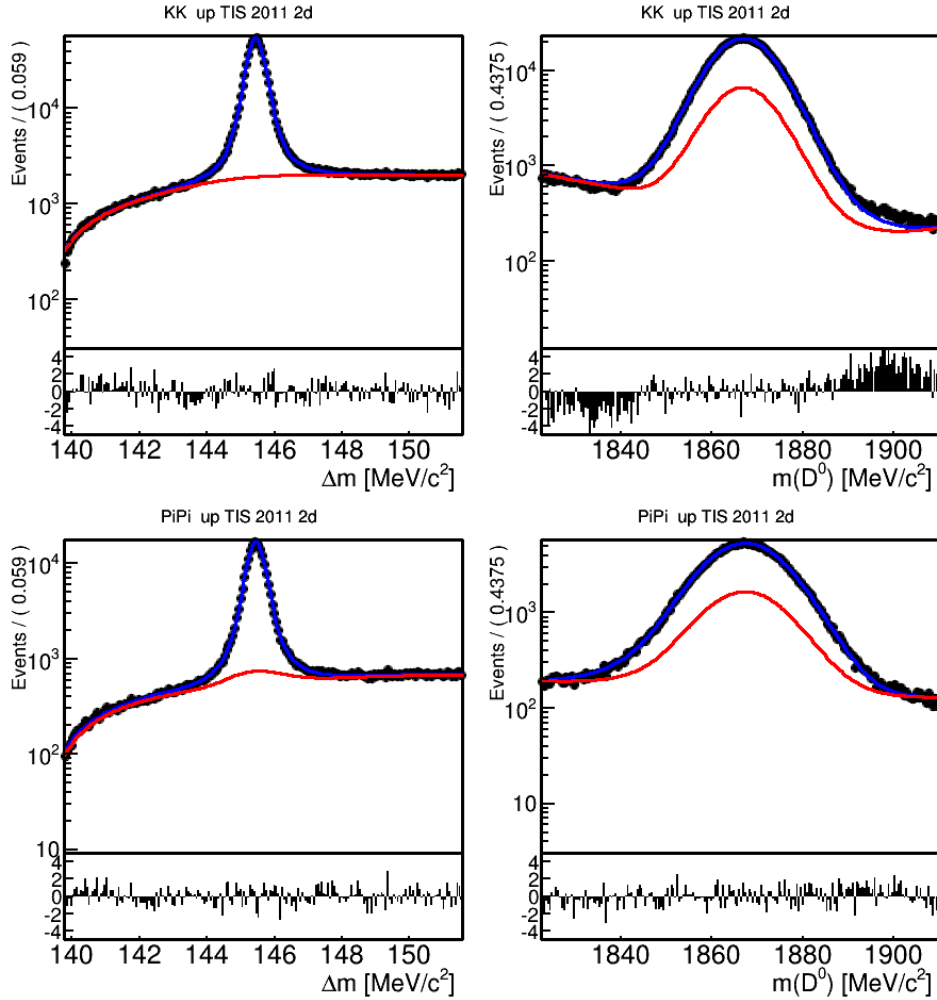


Figure A.2.: Two dimensional determination of the asymmetries on the example of 2011 up TIS data for $D^0 \rightarrow K^- K^+$ (top) and $D^0 \rightarrow \pi^- \pi^+$ (bottom) decays. The black points are the binned data, the blue line the whole model and in red is the total background (including peaking background).

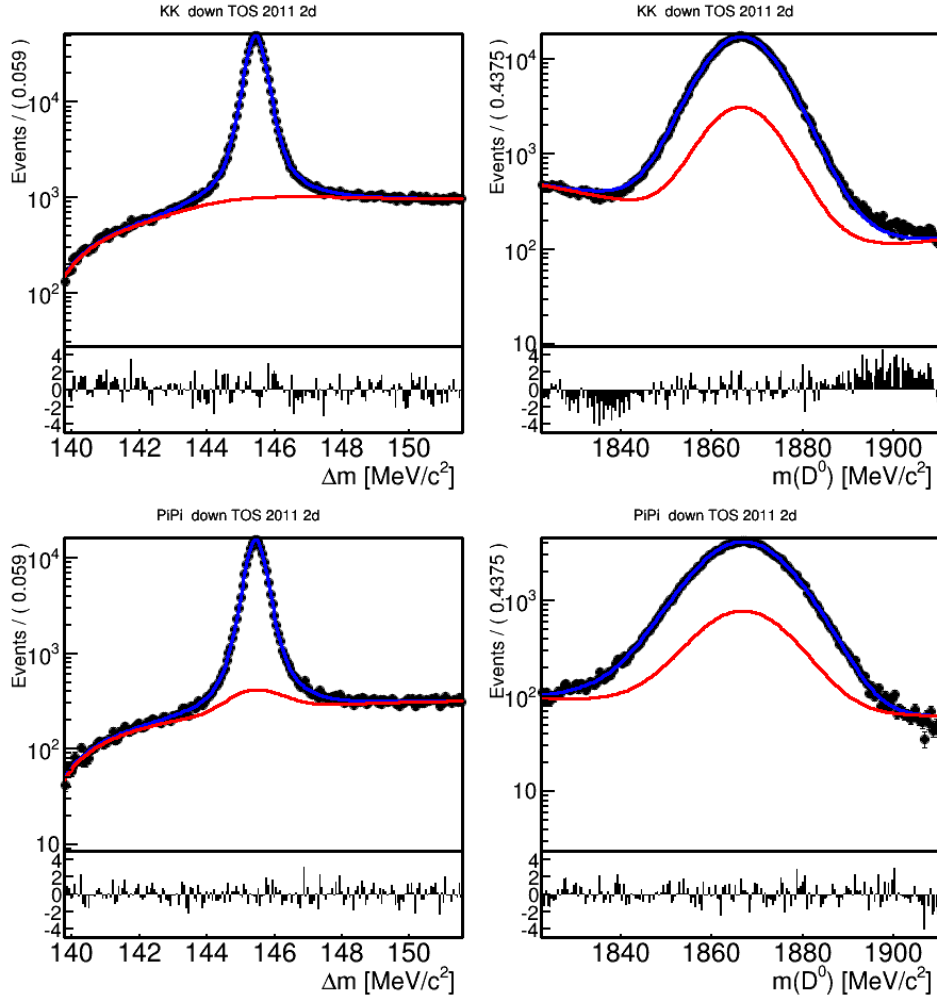


Figure A.3.: Two dimensional determination of the asymmetries on the example of 2011 down TOS data for $D^0 \rightarrow K^-K^+$ (top) and $D^0 \rightarrow \pi^-\pi^+$ (bottom) decays. The black points are the binned data, the blue line the whole model and in red is the total background (including peaking background).

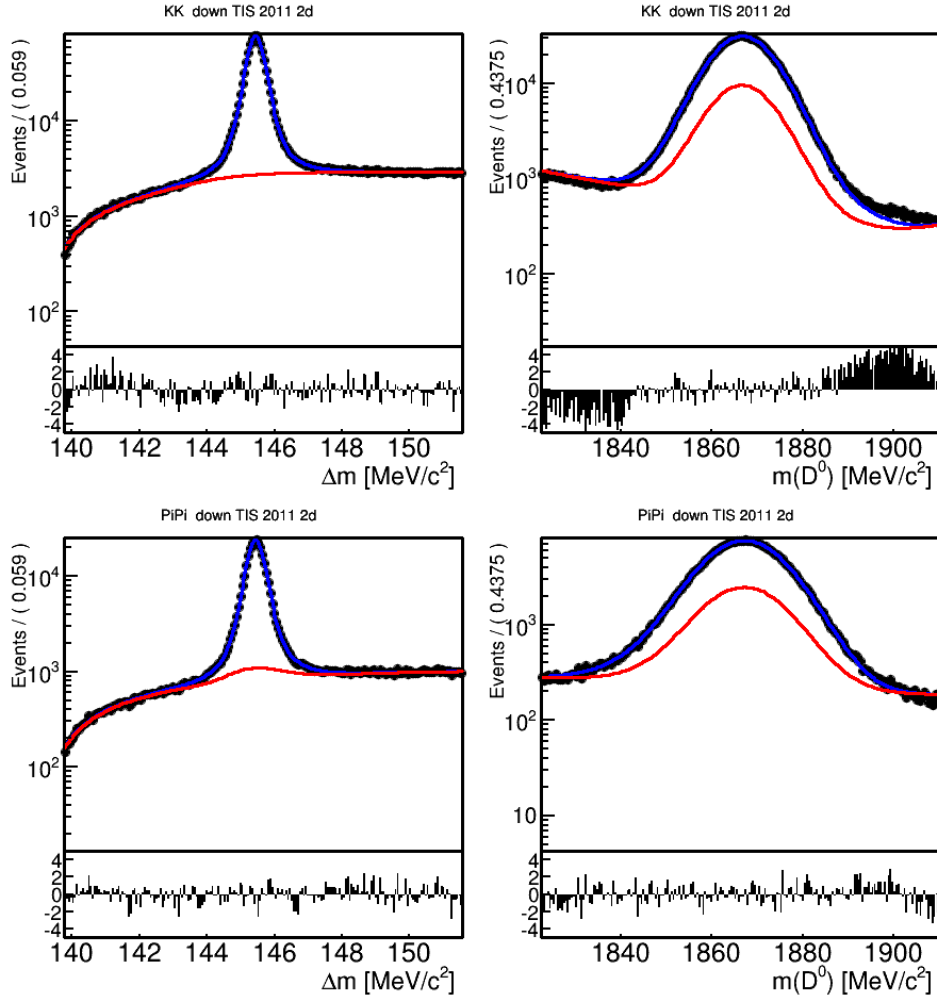


Figure A.4.: Two dimensional determination of the asymmetries on the example of 2011 down TIS data for $D^0 \rightarrow K^-K^+$ (top) and $D^0 \rightarrow \pi^-\pi^+$ (bottom) decays. The black points are the binned data, the blue line the whole model and in red is the total background (including peaking background).

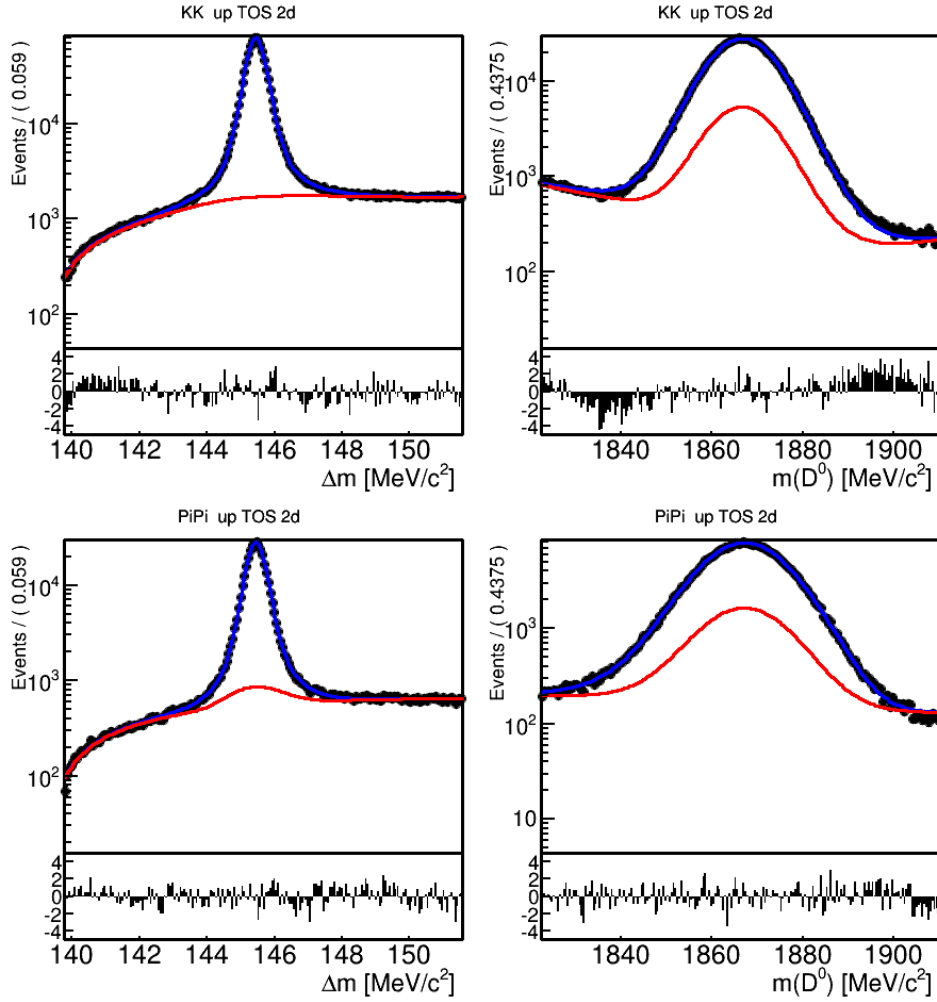


Figure A.5.: Two dimensional determination of the asymmetries on the example of 2012 up TOS data for $D^0 \rightarrow K^- K^+$ (top) and $D^0 \rightarrow \pi^- \pi^+$ (bottom) decays. The black points are the binned data, the blue line the whole model and in red is the total background (including peaking background).

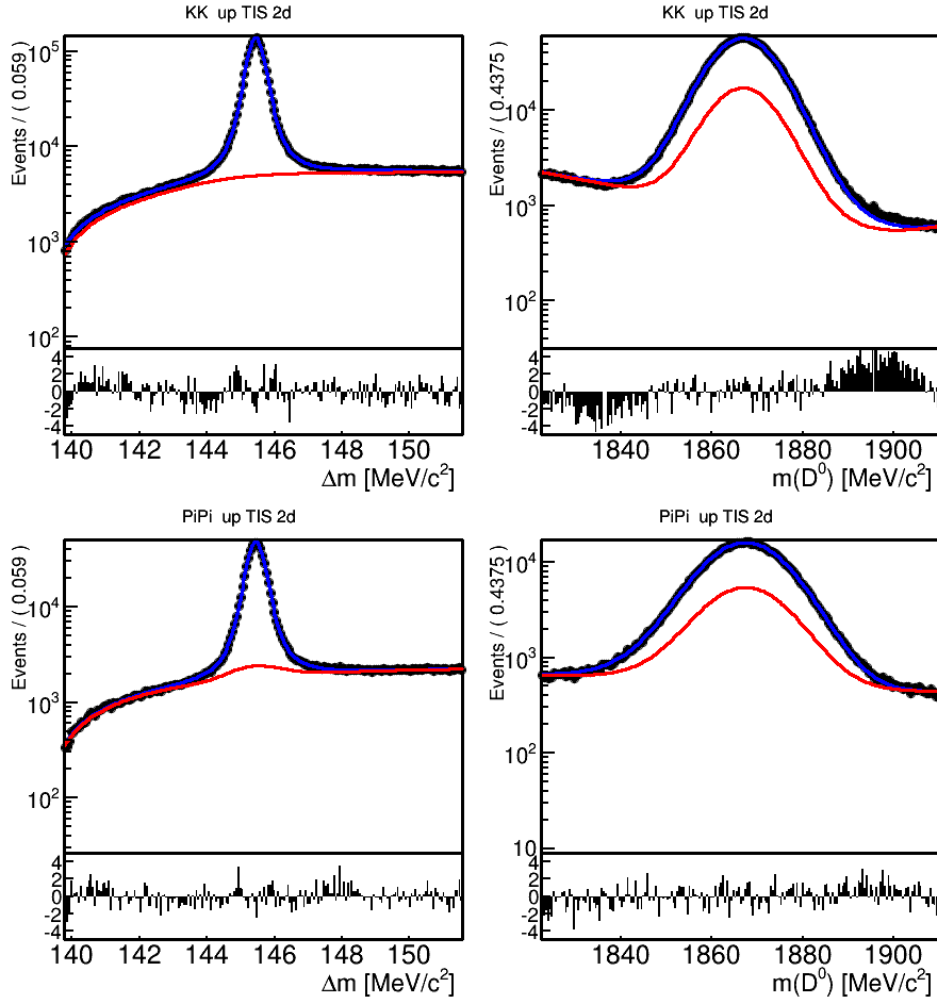


Figure A.6.: Two dimensional determination of the asymmetries on the example of 2012 up TIS data for $D^0 \rightarrow K^- K^+$ (top) and $D^0 \rightarrow \pi^- \pi^+$ (bottom) decays. The black points are the binned data, the blue line the whole model and in red is the total background (including peaking background).

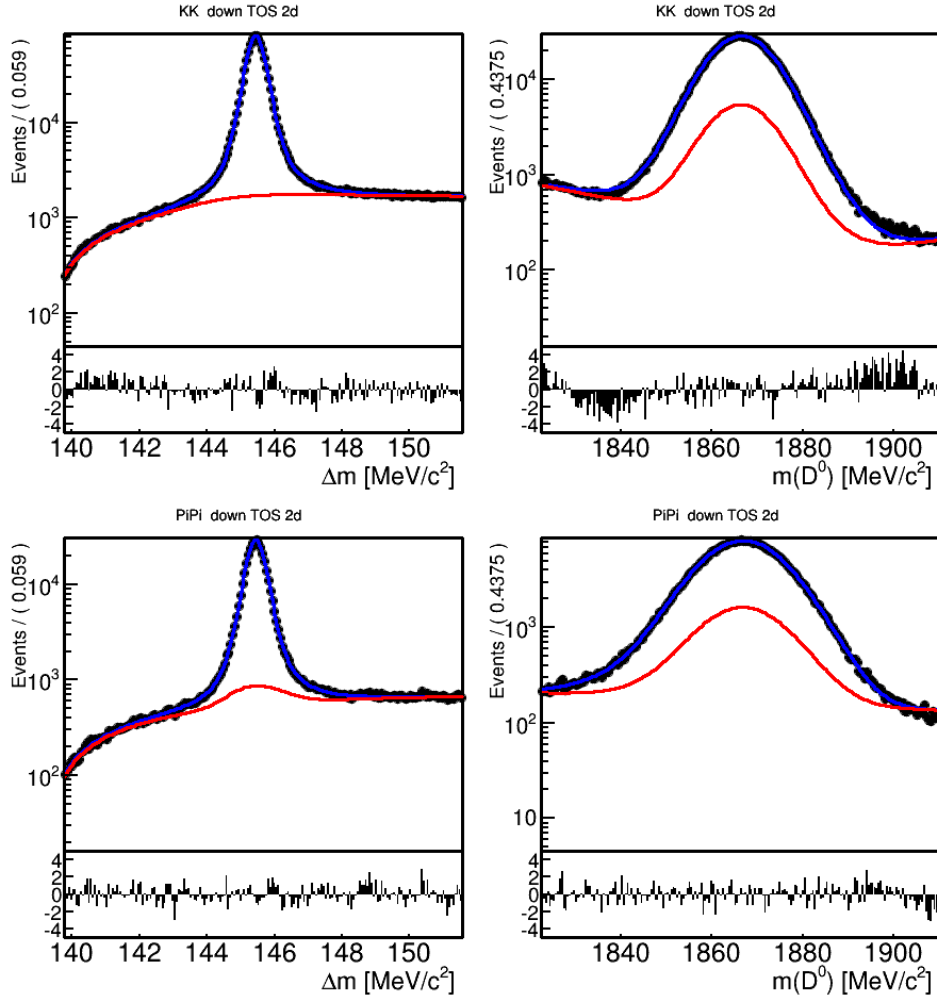


Figure A.7.: Two dimensional determination of the asymmetries on the example of 2012 down TOS data for $D^0 \rightarrow K^-K^+$ (top) and $D^0 \rightarrow \pi^-\pi^+$ (bottom) decays. The black points are the binned data, the blue line the whole model and in red is the total background (including peaking background).

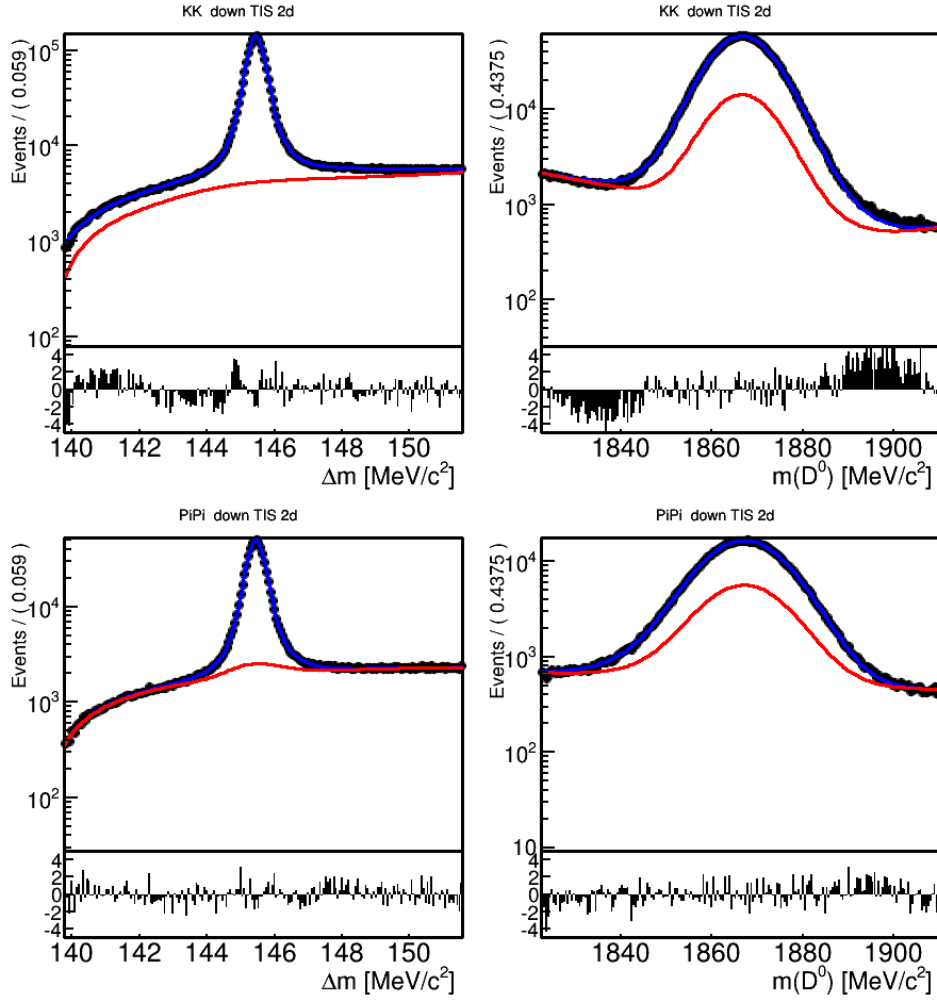


Figure A.8.: Two dimensional determination of the asymmetries on the example of 2012 down TIS data for $D^0 \rightarrow K^- K^+$ (top) and $D^0 \rightarrow \pi^- \pi^+$ (bottom) decays. The black points are the binned data, the blue line the whole model and in red is the total background (including peaking background).

A.2. Run number

In Fig. A.9 and A.11 the individual asymmetries and ΔA_{CP} versus the run number can be found for 2011 and 2012, respectively. The significances of the deviations of results from the baseline result in that class of magnetic polarity and trigger can be found in Fig. A.10 and A.12. In Tab. A.1 and A.2 the results are shown for 2011 and 2012, respectively.

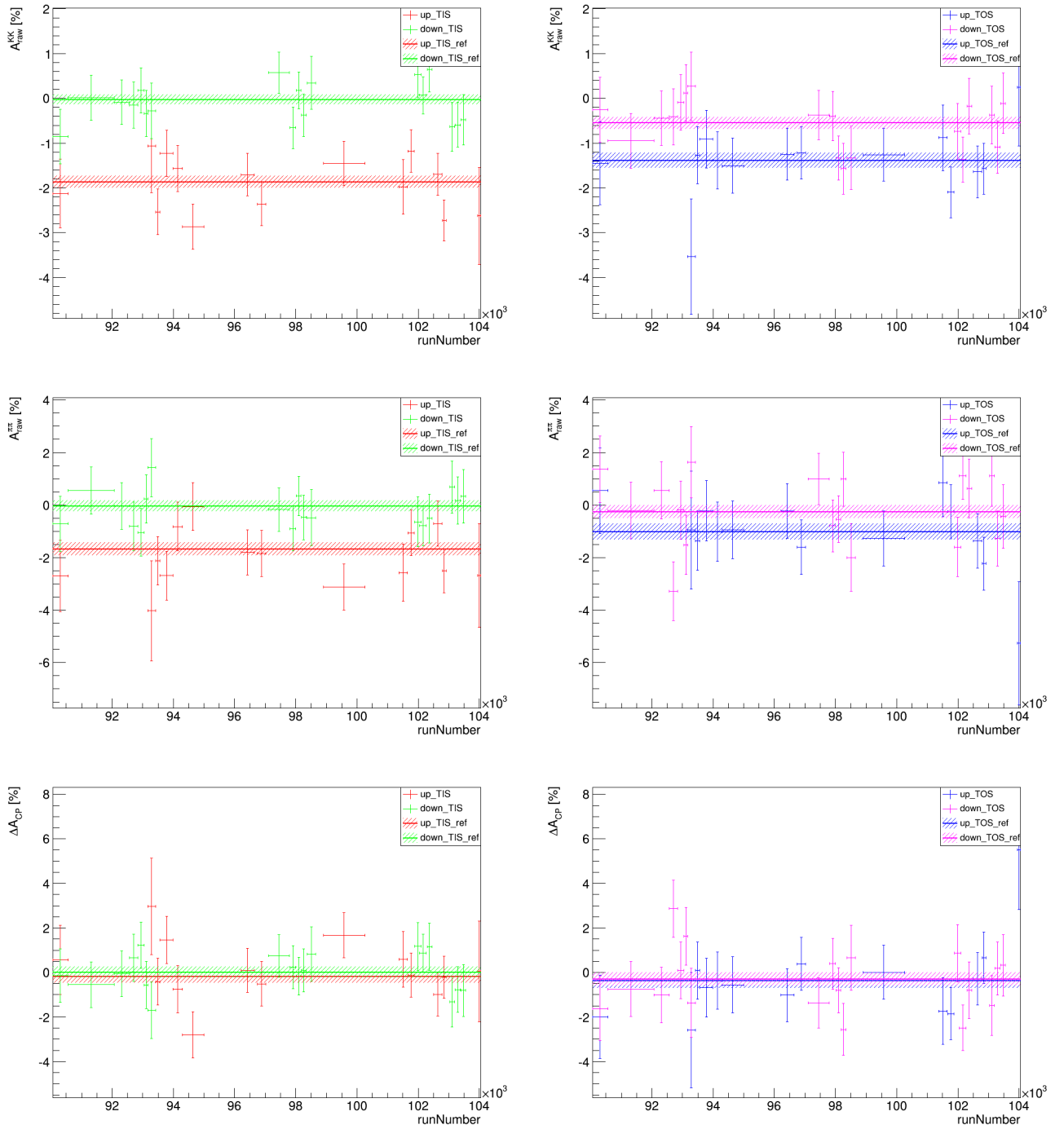


Figure A.9.: A_{raw} vs. $runNumber$, separated by magnetic field polarity and trigger setting for 2011 data.

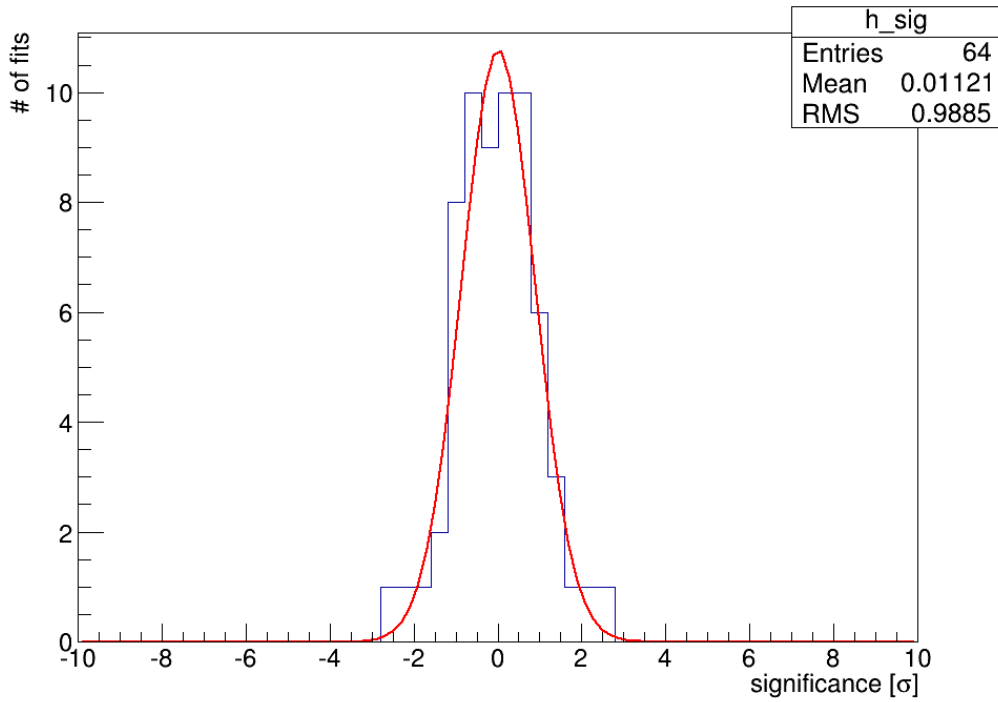
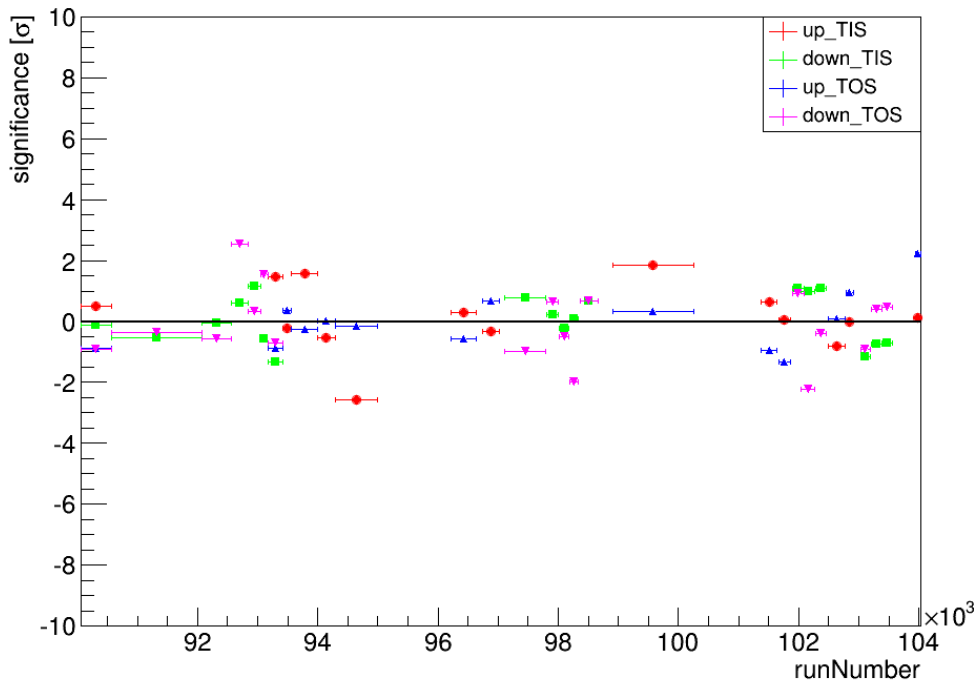


Figure A.10.: Significance vs. *runNumber* (top) and histogram of significances (bottom) for 2011 data.

Table A.1.: Results of the individual asymmetries in the different run number bins, separated by magnetic field polarity and trigger for 2011 data. Highest significance: 2.62.

Sample	$A_{raw}(KK)$ [%]	$A_{raw}(\pi\pi)$ [%]	ΔA_{CP} [%]	significance
up TIS	-1.8660 ± 0.1368	-1.6779 ± 0.2505	-0.1881 ± 0.2854	-
90055.00 < runNumber < 90569.00	-2.1260 ± 0.7679	-2.6965 ± 1.3577	0.5705 ± 1.5598	0.49
93166.00 < runNumber < 93415.00	-1.0665 ± 1.0415	-4.0249 ± 1.9008	2.9584 ± 2.1674	1.46
93415.00 < runNumber < 93564.00	-2.5358 ± 0.5099	-2.1235 ± 0.9220	-0.4123 ± 1.0536	0.22
93564.00 < runNumber < 93993.00	-1.2283 ± 0.5114	-2.6845 ± 0.9250	1.4562 ± 1.0570	1.62
93993.00 < runNumber < 94294.00	-1.5619 ± 0.5159	-0.8160 ± 0.9286	-0.7459 ± 1.0623	0.55
94294.00 < runNumber < 95000.00	-2.8658 ± 0.5006	-0.0633 ± 0.9089	-2.8025 ± 1.0376	2.62
96214.00 < runNumber < 96642.00	-1.7018 ± 0.4780	-1.8006 ± 0.8660	0.0989 ± 0.9891	0.30
96740.00 < runNumber < 97028.00	-2.3610 ± 0.4860	-1.8490 ± 0.8765	-0.5120 ± 1.0023	0.34
98900.00 < runNumber < 100256.00	-1.4527 ± 0.4925	-3.1198 ± 0.8854	1.6671 ± 1.0132	1.91
101373.00 < runNumber < 101643.00	-1.9734 ± 0.6083	-2.5700 ± 1.0899	0.5966 ± 1.2481	0.65
101665.00 < runNumber < 101862.00	-1.1763 ± 0.4721	-1.0552 ± 0.8700	-0.1212 ± 0.9899	0.07
102499.00 < runNumber < 102772.00	-1.6940 ± 0.4722	-0.7127 ± 0.8586	-0.9812 ± 0.9799	0.85
102788.00 < runNumber < 102907.00	-2.7215 ± 0.4583	-2.5091 ± 0.8332	-0.2125 ± 0.9510	0.03
103936.00 < runNumber < 104037.00	-2.6243 ± 1.0790	-2.6795 ± 1.9836	0.0552 ± 2.2580	0.11
down TIS	-0.0274 ± 0.1151	-0.0383 ± 0.2102	0.0109 ± 0.2397	-
90055.00 < runNumber < 90569.00	-0.8520 ± 0.6048	-0.7131 ± 1.0480	-0.1389 ± 1.2100	0.13
90569.00 < runNumber < 92063.00	0.0132 ± 0.5041	0.5593 ± 0.8943	-0.5461 ± 1.0266	0.56
92063.00 < runNumber < 92560.00	-0.0852 ± 0.5029	-0.0285 ± 0.8915	-0.0566 ± 1.0236	0.07
92560.00 < runNumber < 92840.00	-0.1512 ± 0.5140	-0.8101 ± 0.9222	0.6588 ± 1.0558	0.63
92840.00 < runNumber < 93050.00	0.1804 ± 0.5075	-1.0410 ± 0.9097	1.2214 ± 1.0417	1.19
93050.00 < runNumber < 93166.00	-0.3394 ± 0.5144	0.2352 ± 0.9261	-0.5747 ± 1.0594	0.57
93166.00 < runNumber < 93415.00	-0.2732 ± 0.6202	1.4269 ± 1.1126	-1.7002 ± 1.2738	1.37
97114.00 < runNumber < 97789.00	0.5733 ± 0.4601	-0.1706 ± 0.8255	0.7439 ± 0.9451	0.80
97805.00 < runNumber < 98002.00	-0.6579 ± 0.4622	-0.8985 ± 0.8448	0.2405 ± 0.9630	0.25
98019.00 < runNumber < 98174.00	0.1784 ± 0.4079	0.3447 ± 0.7414	-0.1663 ± 0.8462	0.22
98187.00 < runNumber < 98332.00	-0.3766 ± 0.4707	-0.4731 ± 0.8545	0.0965 ± 0.9756	0.09
98369.00 < runNumber < 98656.00	0.3475 ± 0.5905	-0.4753 ± 1.0666	0.8228 ± 1.2191	0.68
101891.00 < runNumber < 102092.00	0.5315 ± 0.5160	-0.6382 ± 0.9442	1.1697 ± 1.0760	1.10
102039.00 < runNumber < 102269.00	0.0686 ± 0.4175	-0.7926 ± 0.7554	0.8612 ± 0.8630	1.03
102291.00 < runNumber < 102452.00	0.6488 ± 0.5106	-0.5088 ± 0.9318	1.1575 ± 1.0625	1.11
103031.00 < runNumber < 103186.00	-0.6302 ± 0.5456	0.6840 ± 0.9950	-1.3142 ± 1.1348	1.19
103203.00 < runNumber < 103379.00	-0.5893 ± 0.4941	0.1759 ± 0.8958	-0.7653 ± 1.0231	0.78
103391.00 < runNumber < 103556.00	-0.4733 ± 0.5642	0.3370 ± 1.0228	-0.8104 ± 1.1681	0.72
up TOS	-1.3870 ± 0.1665	-1.0138 ± 0.3011	-0.3732 ± 0.3440	-
90055.00 < runNumber < 90569.00	-1.4489 ± 0.9293	0.5502 ± 1.6256	-1.9991 ± 1.8725	0.88
93166.00 < runNumber < 93415.00	-3.5348 ± 1.2886	-0.9476 ± 2.2478	-2.5872 ± 2.5910	0.86
93415.00 < runNumber < 93564.00	-1.2677 ± 0.6360	-1.3521 ± 1.1185	0.0845 ± 1.2866	0.37
93564.00 < runNumber < 93993.00	-0.9079 ± 0.6453	-0.2173 ± 1.1516	-0.6906 ± 1.3201	0.25
93993.00 < runNumber < 94294.00	-1.3798 ± 0.6376	-1.0146 ± 1.1241	-0.3653 ± 1.2923	0.01
94294.00 < runNumber < 95000.00	-1.5029 ± 0.6177	-0.9462 ± 1.0945	-0.5566 ± 1.2568	0.15
96214.00 < runNumber < 96642.00	-1.2445 ± 0.5767	-0.2247 ± 1.0393	-1.0197 ± 1.1886	0.57
96740.00 < runNumber < 97028.00	-1.2112 ± 0.5847	-1.5994 ± 1.0445	0.3883 ± 1.1970	0.66
98900.00 < runNumber < 100256.00	-1.2583 ± 0.5933	-1.2676 ± 1.0520	0.0093 ± 1.2077	0.33
101373.00 < runNumber < 101643.00	-0.8785 ± 0.7339	0.8523 ± 1.2981	-1.7308 ± 1.4912	0.94
101665.00 < runNumber < 101862.00	-2.0974 ± 0.5702	-0.2488 ± 1.0290	-1.8486 ± 1.1765	1.31
102499.00 < runNumber < 102772.00	-1.6402 ± 0.5786	-1.3576 ± 1.0359	-0.2826 ± 1.1866	0.08
102788.00 < runNumber < 102907.00	-1.5714 ± 0.5649	-2.2232 ± 1.0096	0.6518 ± 1.1569	0.93
103936.00 < runNumber < 104037.00	0.2488 ± 1.3092	-5.2631 ± 2.3385	5.5119 ± 2.6800	2.21
down TOS	-0.5525 ± 0.1383	-0.2554 ± 0.2507	-0.2971 ± 0.2863	-
90055.00 < runNumber < 90569.00	-0.2525 ± 0.7265	1.3632 ± 1.2629	-1.6158 ± 1.4569	0.92
90569.00 < runNumber < 92063.00	-0.9495 ± 0.6142	-0.2053 ± 1.0817	-0.7442 ± 1.2439	0.37
92063.00 < runNumber < 92560.00	-0.4409 ± 0.6116	0.5617 ± 1.0879	-1.0026 ± 1.2480	0.58
92560.00 < runNumber < 92840.00	-0.4106 ± 0.6283	-3.2753 ± 1.1159	2.8647 ± 1.2806	2.53
92840.00 < runNumber < 93050.00	-0.0928 ± 0.6216	-0.1910 ± 1.1046	0.0982 ± 1.2675	0.32
93050.00 < runNumber < 93166.00	0.1163 ± 0.6329	-1.5147 ± 1.1318	1.6310 ± 1.2967	1.52
93166.00 < runNumber < 93415.00	0.2701 ± 0.7690	1.6411 ± 1.3570	-1.3710 ± 1.5598	0.70
97114.00 < runNumber < 97789.00	-0.3765 ± 0.5503	0.9870 ± 0.9817	-1.3634 ± 1.1254	0.98
97805.00 < runNumber < 98002.00	-0.3956 ± 0.5530	-0.7929 ± 0.9975	0.3973 ± 1.1405	0.63
98019.00 < runNumber < 98174.00	-1.3342 ± 0.4911	-0.5374 ± 0.8828	-0.7968 ± 1.0102	0.52
98187.00 < runNumber < 98332.00	-1.5700 ± 0.5667	0.9873 ± 1.0276	-2.5572 ± 1.1735	1.99
98369.00 < runNumber < 98656.00	-1.3289 ± 0.7075	-1.9920 ± 1.2842	0.6631 ± 1.4662	0.67
101891.00 < runNumber < 102092.00	-0.7307 ± 0.6204	-1.5919 ± 1.1275	0.8612 ± 1.2870	0.92
102039.00 < runNumber < 102269.00	-1.3706 ± 0.5048	1.1183 ± 0.8988	-2.4889 ± 1.0309	2.21
102291.00 < runNumber < 102452.00	-0.1714 ± 0.6194	0.6366 ± 1.1150	-0.8080 ± 1.2755	0.41
103031.00 < runNumber < 103186.00	-0.3689 ± 0.6437	1.1185 ± 1.1701	-1.4874 ± 1.3354	0.91
103203.00 < runNumber < 103379.00	-1.0905 ± 0.5867	-1.2719 ± 1.0412	0.1814 ± 1.1951	0.41
103391.00 < runNumber < 103556.00	-0.1090 ± 0.6764	-0.4275 ± 1.2063	0.3185 ± 1.3830	0.45

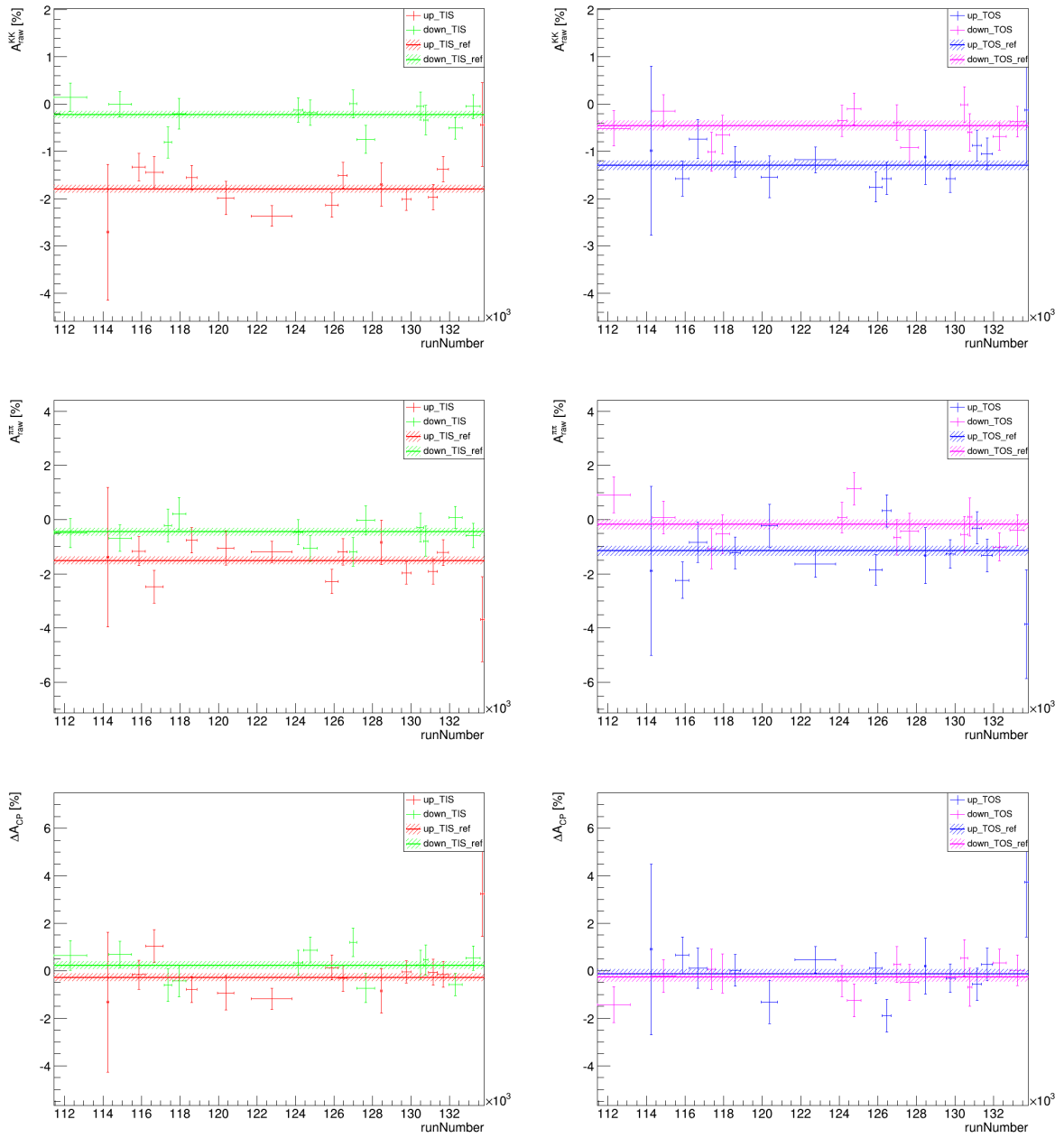


Figure A.11.: A_{raw} vs. $runNumber$, separated by magnetic field polarity and trigger setting for 2012 data.

Table A.2.: Results of the individual asymmetries in the different run number bins, separated by magnetic field polarity and trigger for 2012 data. Highest significance: 2.67

Sample	$A_{raw}(KK)[\%]$	$A_{raw}(\pi\pi)[\%]$	$\Delta A_{CP}[\%]$	significance
up TIS	-1.7988 \pm 0.0825	-1.5120 \pm 0.1487	-0.2868 \pm 0.1700	-
114200.00 < <i>runNumber</i> < 114290.00	-2.7097 \pm 1.4375	-1.3869 \pm 2.5677	-1.3229 \pm 2.9427	0.35
115510.00 < <i>runNumber</i> < 116195.00	-1.3298 \pm 0.2927	-1.1596 \pm 0.5426	-0.1702 \pm 0.6165	0.20
116210.00 < <i>runNumber</i> < 117110.00	-1.4380 \pm 0.3266	-2.4798 \pm 0.6010	1.0419 \pm 0.6840	2.01
118320.00 < <i>runNumber</i> < 118885.00	-1.5507 \pm 0.2561	-0.7613 \pm 0.4753	-0.7894 \pm 0.5399	0.98
119950.00 < <i>runNumber</i> < 120800.00	-1.9860 \pm 0.3515	-1.0505 \pm 0.6324	-0.9355 \pm 0.7235	0.92
121705.00 < <i>runNumber</i> < 123803.00	-2.3677 \pm 0.2202	-1.1834 \pm 0.3930	-1.1843 \pm 0.4505	2.15
125560.00 < <i>runNumber</i> < 126215.00	-2.1390 \pm 0.2556	-2.2764 \pm 0.4540	0.1375 \pm 0.5211	0.86
126230.00 < <i>runNumber</i> < 126685.00	-1.5056 \pm 0.2723	-1.1820 \pm 0.4867	-0.3236 \pm 0.5577	0.07
128405.00 < <i>runNumber</i> < 128500.00	-1.6970 \pm 0.4581	-0.8453 \pm 0.8165	-0.8517 \pm 0.9363	0.61
129530.00 < <i>runNumber</i> < 129985.00	-2.0171 \pm 0.2296	-1.9758 \pm 0.4096	-0.0413 \pm 0.4695	0.56
130905.00 < <i>runNumber</i> < 131374.00	-1.9705 \pm 0.2648	-1.9082 \pm 0.4744	-0.0624 \pm 0.5433	0.43
131375.00 < <i>runNumber</i> < 131945.00	-1.3740 \pm 0.2654	-1.2156 \pm 0.4759	-0.1584 \pm 0.5449	0.25
133615.00 < <i>runNumber</i> < 133790.00	-0.4350 \pm 0.8877	-3.6778 \pm 1.5676	3.2428 \pm 1.8015	1.97
down TIS	-0.2274 \pm 0.0814	-0.4563 \pm 0.1456	0.2289 \pm 0.1669	-
111440.00 < <i>runNumber</i> < 113150.00	0.1467 \pm 0.3017	-0.4902 \pm 0.5374	0.6369 \pm 0.6163	0.69
114310.00 < <i>runNumber</i> < 115470.00	-0.0037 \pm 0.2699	-0.6888 \pm 0.4884	0.6851 \pm 0.5580	0.86
117185.00 < <i>runNumber</i> < 117570.00	-0.8091 \pm 0.3311	-0.2109 \pm 0.6033	-0.5982 \pm 0.6882	1.24
117620.00 < <i>runNumber</i> < 118295.00	-0.2049 \pm 0.3224	0.2226 \pm 0.5894	-0.4274 \pm 0.6718	1.01
123905.00 < <i>runNumber</i> < 124390.00	-0.1264 \pm 0.2577	-0.4637 \pm 0.4588	0.3373 \pm 0.5263	0.22
124400.00 < <i>runNumber</i> < 125120.00	-0.1844 \pm 0.2662	-1.0564 \pm 0.4742	0.8721 \pm 0.5438	1.24
126820.00 < <i>runNumber</i> < 127165.00	0.0045 \pm 0.2943	-1.1914 \pm 0.5224	1.1959 \pm 0.5996	1.68
127185.00 < <i>runNumber</i> < 128115.00	-0.7457 \pm 0.2992	-0.0136 \pm 0.5293	-0.7322 \pm 0.6080	1.64
130310.00 < <i>runNumber</i> < 130645.00	-0.0419 \pm 0.2990	-0.2921 \pm 0.5321	0.2502 \pm 0.6104	0.04
130650.00 < <i>runNumber</i> < 130870.00	-0.3348 \pm 0.3142	-0.7894 \pm 0.5556	0.4546 \pm 0.6383	0.37
131965.00 < <i>runNumber</i> < 132640.00	-0.5058 \pm 0.2285	0.0837 \pm 0.4090	-0.5895 \pm 0.4685	1.87
132845.00 < <i>runNumber</i> < 133595.00	-0.0522 \pm 0.2527	-0.5775 \pm 0.4506	0.5253 \pm 0.5166	0.61
up TOS	-1.2968 \pm 0.1031	-1.1535 \pm 0.1847	-0.1432 \pm 0.2115	-
114200.00 < <i>runNumber</i> < 114290.00	-0.9875 \pm 1.7897	-1.8874 \pm 3.1136	0.8999 \pm 3.5913	0.29
115510.00 < <i>runNumber</i> < 116195.00	-1.5760 \pm 0.3708	-2.2325 \pm 0.6669	0.6565 \pm 0.7631	1.09
116210.00 < <i>runNumber</i> < 117110.00	-0.7384 \pm 0.4151	-0.8455 \pm 0.7384	0.1071 \pm 0.8471	0.31
118320.00 < <i>runNumber</i> < 118885.00	-1.2205 \pm 0.3251	-1.2299 \pm 0.5804	0.0094 \pm 0.6653	0.24
119950.00 < <i>runNumber</i> < 120800.00	-1.5421 \pm 0.4431	-0.2234 \pm 0.7886	-1.3187 \pm 0.9045	1.34
121705.00 < <i>runNumber</i> < 123803.00	-1.1800 \pm 0.2758	-1.6385 \pm 0.4903	0.4585 \pm 0.5626	1.15
125560.00 < <i>runNumber</i> < 126215.00	-1.7542 \pm 0.3168	-1.8564 \pm 0.5638	0.1021 \pm 0.6467	0.40
126230.00 < <i>runNumber</i> < 126685.00	-1.5721 \pm 0.3401	0.3229 \pm 0.5990	-1.8949 \pm 0.6888	2.67
128405.00 < <i>runNumber</i> < 128500.00	-1.1242 \pm 0.5756	-1.3273 \pm 1.0300	0.2031 \pm 1.1799	0.30
129530.00 < <i>runNumber</i> < 129985.00	-1.5728 \pm 0.2944	-1.2648 \pm 0.5232	-0.3080 \pm 0.6003	0.29
130905.00 < <i>runNumber</i> < 131374.00	-0.8753 \pm 0.3303	-0.3061 \pm 0.5901	-0.5691 \pm 0.6763	0.66
131375.00 < <i>runNumber</i> < 131945.00	-1.0542 \pm 0.3330	-1.3237 \pm 0.5976	0.2696 \pm 0.6841	0.63
133615.00 < <i>runNumber</i> < 133790.00	-0.1214 \pm 1.1268	-3.8541 \pm 2.0082	3.7328 \pm 2.3027	1.69
down TOS	-0.4554 \pm 0.1028	-0.1838 \pm 0.1812	-0.2716 \pm 0.2083	-
111440.00 < <i>runNumber</i> < 113150.00	-0.5139 \pm 0.3747	0.9186 \pm 0.6605	-1.4325 \pm 0.7594	1.59
114310.00 < <i>runNumber</i> < 115470.00	-0.1437 \pm 0.3406	0.0764 \pm 0.6000	-0.2201 \pm 0.6900	0.08
117185.00 < <i>runNumber</i> < 117570.00	-1.0078 \pm 0.4171	-1.0743 \pm 0.7340	0.0666 \pm 0.8443	0.41
117620.00 < <i>runNumber</i> < 118295.00	-0.6479 \pm 0.4055	-0.5307 \pm 0.7110	-0.1171 \pm 0.8185	0.20
123905.00 < <i>runNumber</i> < 124390.00	-0.3536 \pm 0.3261	0.0794 \pm 0.5725	-0.4329 \pm 0.6589	0.26
124400.00 < <i>runNumber</i> < 125120.00	-0.1054 \pm 0.3339	1.1451 \pm 0.5936	-1.2505 \pm 0.6811	1.51
126820.00 < <i>runNumber</i> < 127165.00	-0.3891 \pm 0.3726	-0.6575 \pm 0.6574	0.2684 \pm 0.7557	0.74
127185.00 < <i>runNumber</i> < 128115.00	-0.9146 \pm 0.3797	-0.4211 \pm 0.6619	-0.4935 \pm 0.7631	0.30
130310.00 < <i>runNumber</i> < 130645.00	-0.0091 \pm 0.3769	-0.5429 \pm 0.6659	0.5338 \pm 0.7652	1.09
130650.00 < <i>runNumber</i> < 130870.00	-0.5960 \pm 0.3976	0.0957 \pm 0.6974	-0.6917 \pm 0.8028	0.54
131965.00 < <i>runNumber</i> < 132640.00	-0.6852 \pm 0.2915	-1.0039 \pm 0.5177	0.3187 \pm 0.5941	1.06
132845.00 < <i>runNumber</i> < 133595.00	-0.3690 \pm 0.3216	-0.3882 \pm 0.5675	0.0192 \pm 0.6523	0.47

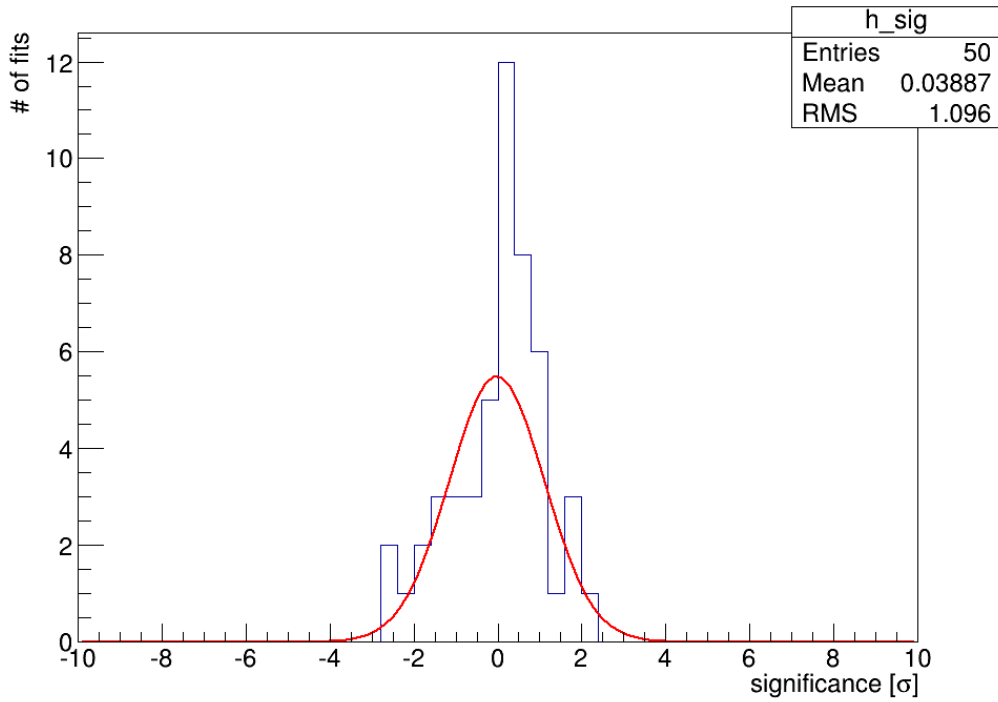
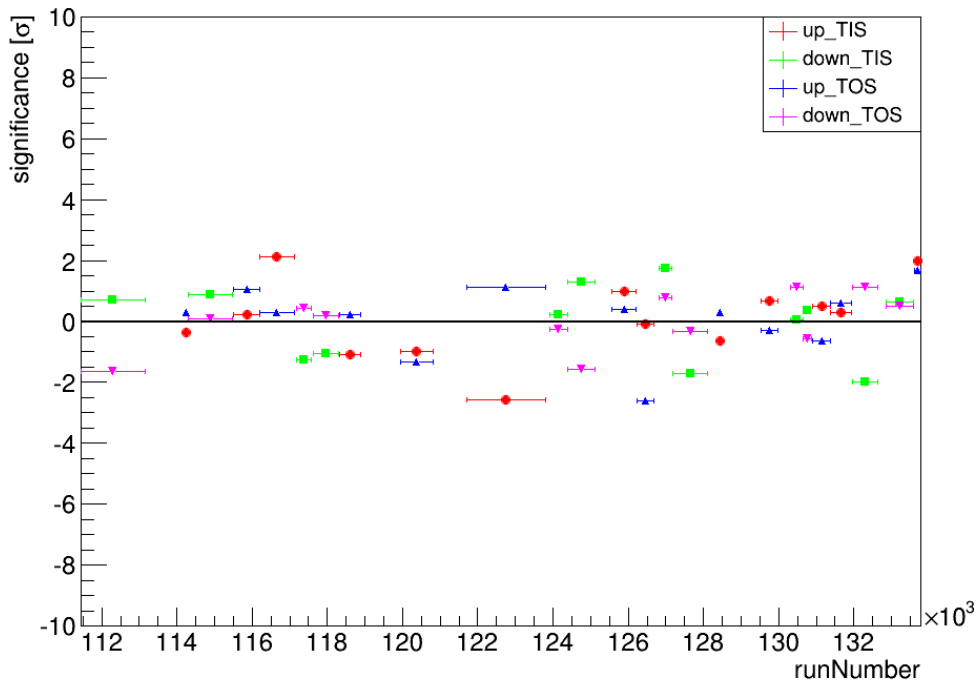


Figure A.12.: Significance vs. *runNumber* (top) and histogram of significances (bottom) for 2012 data.

A.3. Number of primary vertices

In Fig. A.13 and A.15 the individual asymmetries and ΔA_{CP} versus the number of primary vertices can be found for 2011 and 2012, respectively. The significances of the deviations of results from the baseline result in that class of magnetic polarity and trigger can be found in Fig. A.14 and A.16. In Tab. A.3 and A.4 the results are shown for 2011 and 2012, respectively.

Table A.3.: Results of the individual asymmetries in the different nPVs bins, separated by magnetic field polarity and trigger for 2011 data. Highest significance: 2.16

Sample	$A_{raw}(KK)[\%]$	$A_{raw}(\pi\pi)[\%]$	$\Delta A_{CP}[\%]$	significance
up TIS	-1.8660 ± 0.1368	-1.6779 ± 0.2505	-0.1881 ± 0.2854	-
$0.50 < \#PVs < 1.50$	-2.1678 ± 0.2580	-2.0083 ± 0.4582	-0.1596 ± 0.5258	0.06
$1.50 < \#PVs < 2.50$	-1.6565 ± 0.2198	-1.7923 ± 0.3966	0.1358 ± 0.4534	0.92
$2.50 < \#PVs < 3.50$	-1.9228 ± 0.2903	-0.8965 ± 0.5309	-1.0263 ± 0.6051	1.57
$3.50 < \#PVs < 4.50$	-2.4426 ± 0.5243	-2.2887 ± 0.9796	-0.1539 ± 1.1111	0.03
$4.50 < \#PVs < 5.50$	-2.1655 ± 1.2147	-2.0903 ± 2.2384	-0.0752 ± 2.5467	0.04
$5.50 < \#PVs < 6.50$	-4.4839 ± 3.5319	1.4689 ± 6.5583	-5.9528 ± 7.4489	0.77
down TIS	-0.0274 ± 0.1151	-0.0383 ± 0.2102	0.0109 ± 0.2397	-
$0.50 < \#PVs < 1.50$	-0.0823 ± 0.2162	0.1330 ± 0.3843	-0.2152 ± 0.4409	0.61
$1.50 < \#PVs < 2.50$	-0.2369 ± 0.1835	-0.1340 ± 0.3303	-0.1029 ± 0.3778	0.39
$2.50 < \#PVs < 3.50$	0.2363 ± 0.2446	-0.4469 ± 0.4486	0.6832 ± 0.5110	1.49
$3.50 < \#PVs < 4.50$	0.1202 ± 0.4490	0.9984 ± 0.8321	-0.8781 ± 0.9455	0.97
$4.50 < \#PVs < 5.50$	-0.4281 ± 1.0792	1.0027 ± 2.0225	-1.4308 ± 2.2924	0.63
$5.50 < \#PVs < 6.50$	-5.2620 ± 3.2319	-3.7995 ± 6.0151	-1.4625 ± 6.8284	0.22
up TOS	-1.3870 ± 0.1665	-1.0138 ± 0.3011	-0.3732 ± 0.3440	-
$0.50 < \#PVs < 1.50$	-1.1639 ± 0.2835	-1.4323 ± 0.4981	0.2684 ± 0.5731	1.40
$1.50 < \#PVs < 2.50$	-1.6874 ± 0.2703	-1.2662 ± 0.4795	-0.4212 ± 0.5505	0.11
$2.50 < \#PVs < 3.50$	-1.4401 ± 0.3867	0.4089 ± 0.7036	-1.8490 ± 0.8029	2.03
$3.50 < \#PVs < 4.50$	-0.8764 ± 0.7465	-1.1658 ± 1.3670	0.2894 ± 1.5575	0.44
$4.50 < \#PVs < 5.50$	2.4469 ± 1.8306	-5.1875 ± 3.3263	7.6344 ± 3.7968	2.12
$5.50 < \#PVs < 6.50$	-1.3201 ± 5.6017	22.8353 ± 9.4794	-24.1554 ± 11.0108	2.16
down TOS	-0.5525 ± 0.1383	-0.2554 ± 0.2507	-0.2971 ± 0.2863	-
$0.50 < \#PVs < 1.50$	-0.9226 ± 0.2346	-0.3621 ± 0.4122	-0.5605 ± 0.4743	0.70
$1.50 < \#PVs < 2.50$	-0.5082 ± 0.2227	-0.1219 ± 0.3994	-0.3863 ± 0.4573	0.25
$2.50 < \#PVs < 3.50$	-0.3142 ± 0.3233	0.2049 ± 0.5868	-0.5191 ± 0.6700	0.37
$3.50 < \#PVs < 4.50$	-0.7048 ± 0.6335	-1.7884 ± 1.1655	1.0836 ± 1.3265	1.07
$4.50 < \#PVs < 5.50$	-0.4763 ± 1.6238	-5.3453 ± 2.9832	4.8691 ± 3.3965	1.53
$5.50 < \#PVs < 6.50$	-4.7239 ± 4.9529	13.6381 ± 9.9663	-18.3619 ± 11.1291	1.62

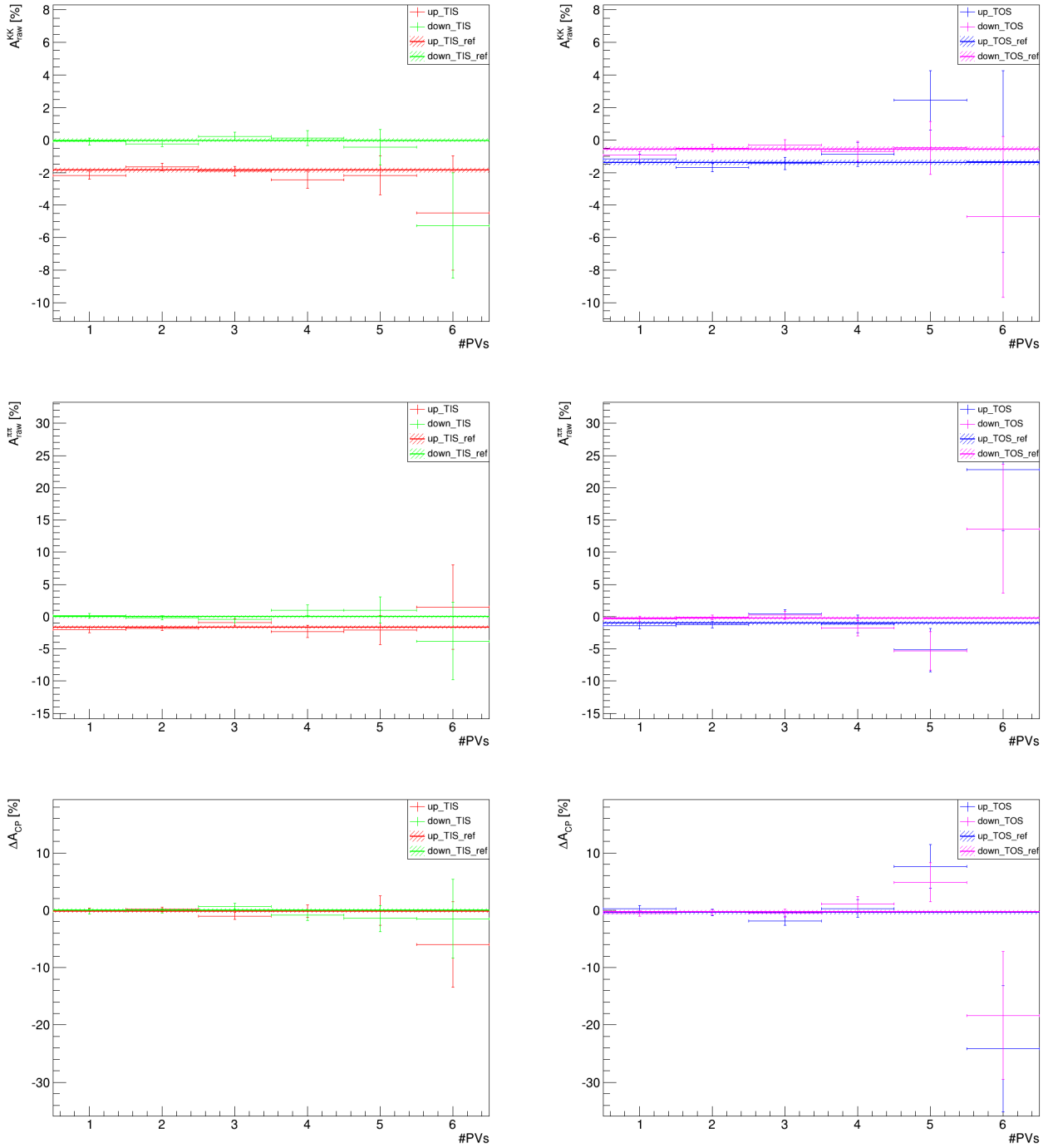


Figure A.13.: A_{raw} vs. $nPVs$, separated by magnetic field polarity and trigger setting for 2011 data.

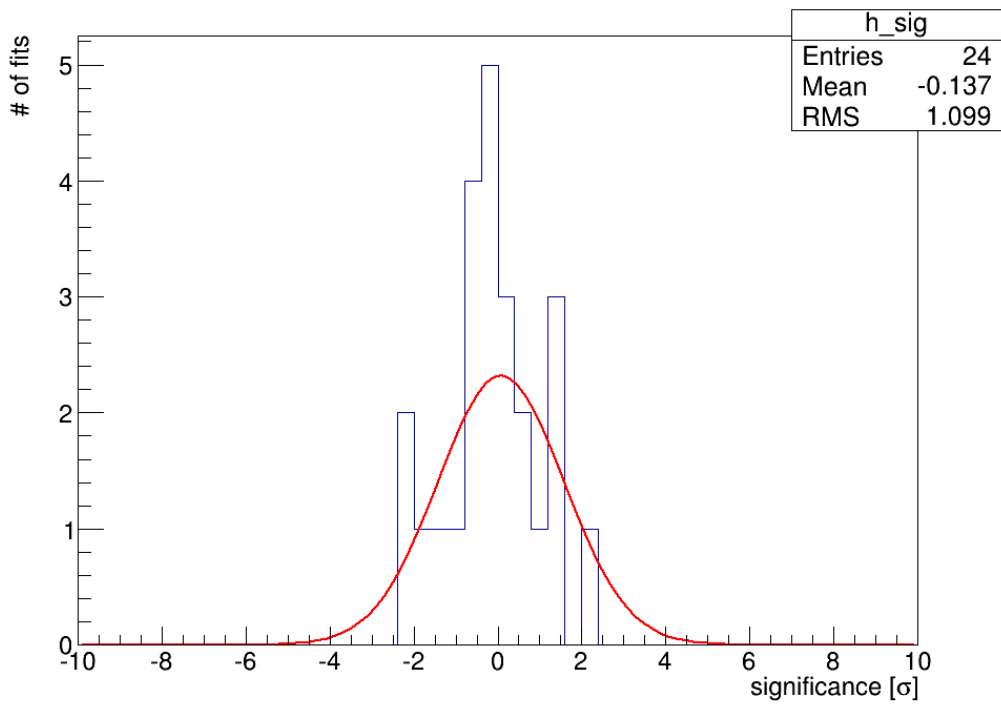
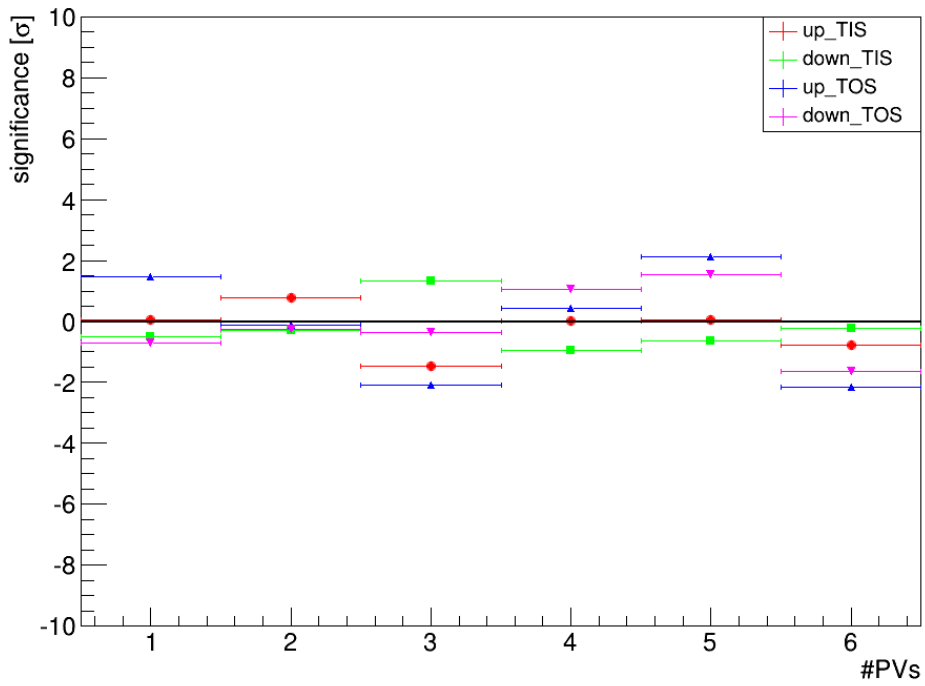


Figure A.14.: Significance vs. $nPVs$ (top) and histogram of significances (bottom) for 2011 data.

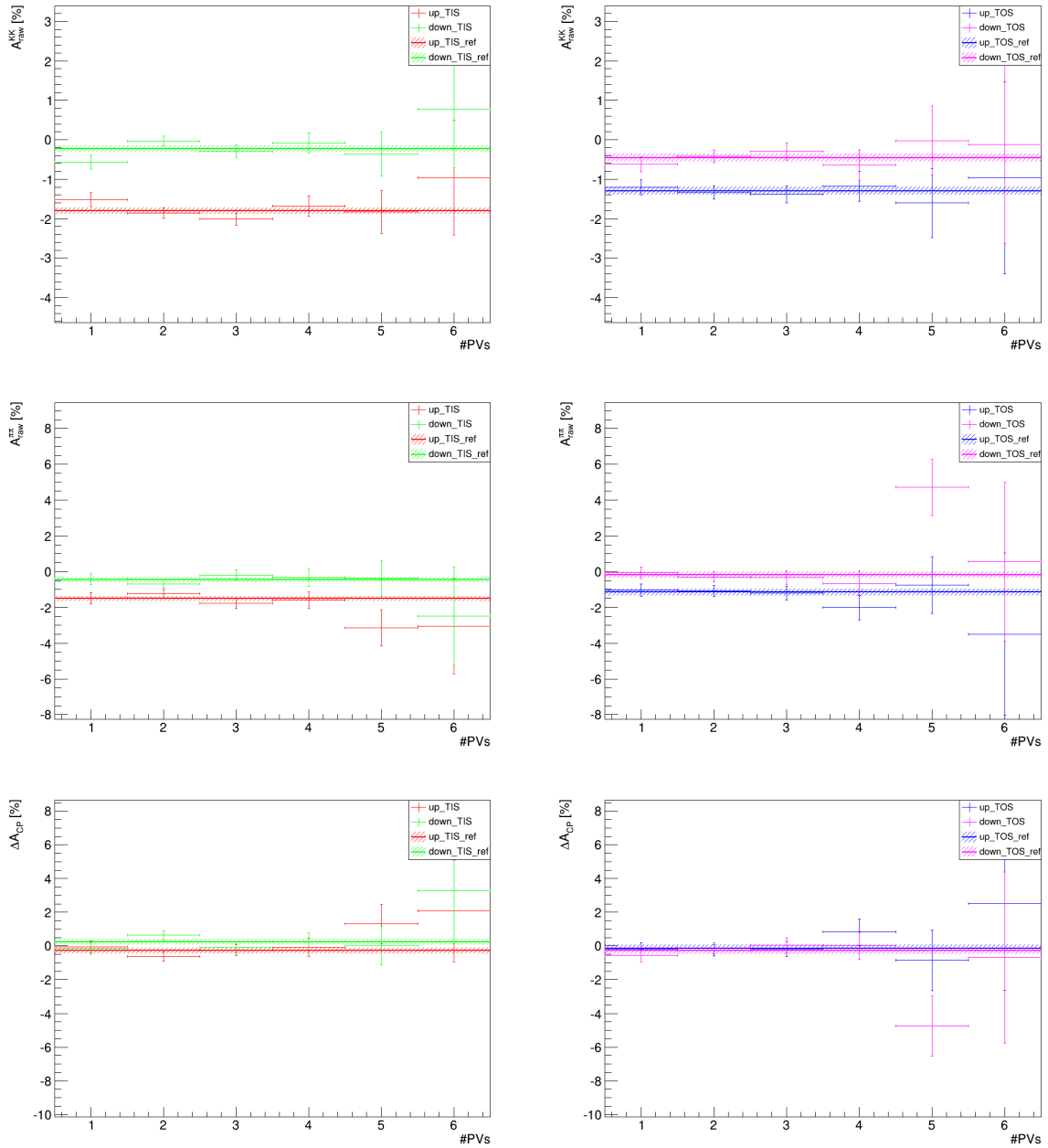


Figure A.15.: A_{raw} vs. $nPVs$, separated by magnetic field polarity and trigger setting for 2012 data.

Table A.4.: Results of the individual asymmetries in the different nPVs bins, separated by magnetic field polarity and trigger for 2012 data. Highest significance: 2.51

Sample	$A_{raw}(KK)$ [%]	$A_{raw}(\pi\pi)$ [%]	ΔA_{CP} [%]	significance
up TIS	-1.7988 ± 0.0825	-1.5120 ± 0.1487	-0.2868 ± 0.1700	-
0.50 < #PVs < 1.50	-1.5183 ± 0.1766	-1.4689 ± 0.3128	-0.0493 ± 0.3592	0.75
1.50 < #PVs < 2.50	-1.8516 ± 0.1332	-1.2343 ± 0.2388	-0.6173 ± 0.2734	1.54
2.50 < #PVs < 3.50	-2.0066 ± 0.1574	-1.7697 ± 0.2869	-0.2369 ± 0.3272	0.18
3.50 < #PVs < 4.50	-1.6796 ± 0.2576	-1.5993 ± 0.4721	-0.0803 ± 0.5378	0.40
4.50 < #PVs < 5.50	-1.8234 ± 0.5438	-3.1321 ± 1.0198	1.3088 ± 1.1557	1.40
5.50 < #PVs < 6.50	-0.9652 ± 1.4496	-3.0440 ± 2.6559	2.0787 ± 3.0257	0.78
down TIS	-0.2274 ± 0.0814	-0.4563 ± 0.1456	0.2289 ± 0.1669	-
0.50 < #PVs < 1.50	-0.5680 ± 0.1711	-0.4240 ± 0.3018	-0.1440 ± 0.3470	1.23
1.50 < #PVs < 2.50	-0.0341 ± 0.1312	-0.6787 ± 0.2337	0.6445 ± 0.2680	1.98
2.50 < #PVs < 3.50	-0.2920 ± 0.1570	-0.2020 ± 0.2833	-0.0899 ± 0.3238	1.15
3.50 < #PVs < 4.50	-0.0817 ± 0.2592	-0.3354 ± 0.4713	0.2538 ± 0.5379	0.05
4.50 < #PVs < 5.50	-0.3610 ± 0.5532	-0.3704 ± 1.0028	0.0093 ± 1.1452	0.19
5.50 < #PVs < 6.50	0.7761 ± 1.4806	-2.4907 ± 2.7584	3.2668 ± 3.1307	0.97
up TOS	-1.2968 ± 0.1031	-1.1535 ± 0.1847	-0.1432 ± 0.2115	-
0.50 < #PVs < 1.50	-1.2049 ± 0.1935	-1.0285 ± 0.3388	-0.1764 ± 0.3902	0.10
1.50 < #PVs < 2.50	-1.3345 ± 0.1655	-1.0761 ± 0.2949	-0.2584 ± 0.3382	0.44
2.50 < #PVs < 3.50	-1.3785 ± 0.2155	-1.1952 ± 0.3895	-0.1833 ± 0.4451	0.10
3.50 < #PVs < 4.50	-1.1772 ± 0.3786	-2.0036 ± 0.6880	0.8264 ± 0.7853	1.28
4.50 < #PVs < 5.50	-1.6046 ± 0.8700	-0.7465 ± 1.5832	-0.8581 ± 1.8065	0.40
5.50 < #PVs < 6.50	-0.9665 ± 2.4337	-3.4890 ± 4.5244	2.5226 ± 5.1374	0.52
down TOS	-0.4554 ± 0.1028	-0.1838 ± 0.1812	-0.2716 ± 0.2083	-
0.50 < #PVs < 1.50	-0.6272 ± 0.1892	-0.0558 ± 0.3285	-0.5715 ± 0.3791	0.95
1.50 < #PVs < 2.50	-0.4164 ± 0.1641	-0.2939 ± 0.2891	-0.1225 ± 0.3324	0.58
2.50 < #PVs < 3.50	-0.2959 ± 0.2155	-0.3307 ± 0.3846	0.0348 ± 0.4409	0.79
3.50 < #PVs < 4.50	-0.6414 ± 0.3831	-0.6499 ± 0.6925	0.0085 ± 0.7914	0.37
4.50 < #PVs < 5.50	-0.0200 ± 0.8699	4.7096 ± 1.5657	-4.7296 ± 1.7912	2.51
5.50 < #PVs < 6.50	-0.1256 ± 2.4962	0.5559 ± 4.4315	-0.6815 ± 5.0862	0.08

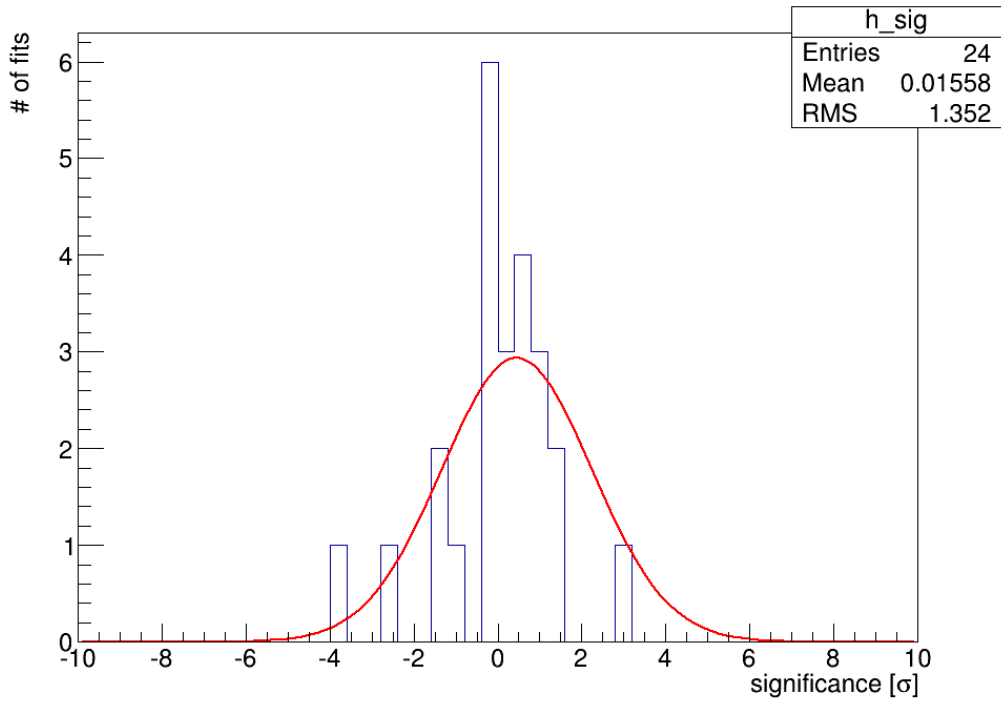
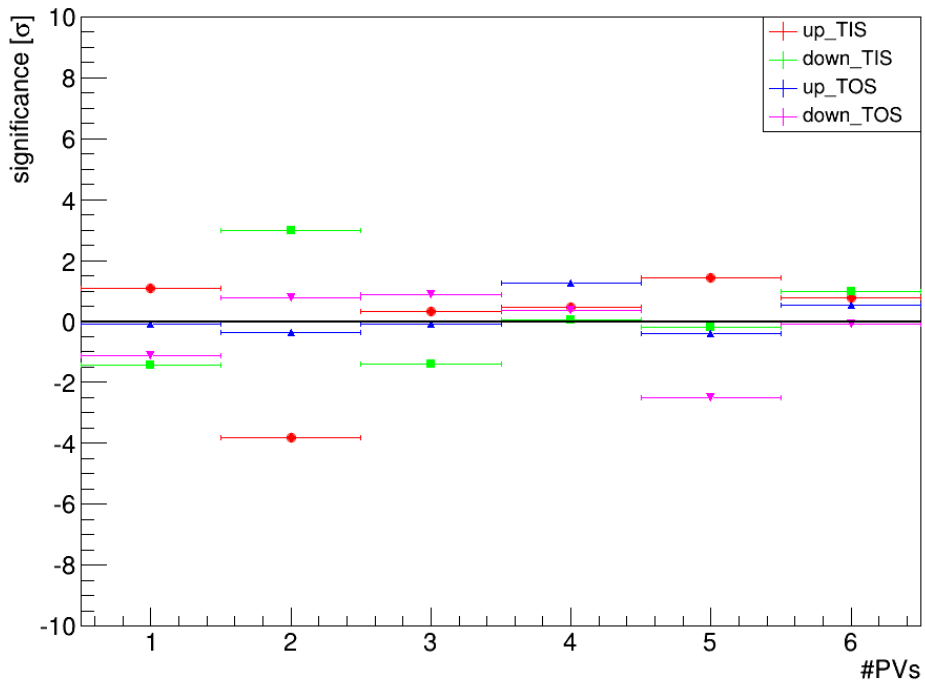


Figure A.16.: Significance vs. $nPVs$ (top) and histogram of significances (bottom) for 2012 data.

A.4. The quality of the fitted $\pi_s D^0$ vertex

In Fig. A.17 and A.19 the individual asymmetries and ΔA_{CP} versus the χ_{DTF}^2 can be found for 2011 and 2012, respectively. The significances of the deviations of results from the baseline result in that class of magnetic polarity and trigger can be found in Fig. A.18 and A.20. In Tab. A.5 and A.6 the results are shown for 2011 and 2012, respectively.

Table A.5.: Results of the individual asymmetries in the different χ_{DTF}^2 bins, separated by magnetic field polarity and trigger for 2011 data. Highest significance: 1.91

Sample	$A_{raw}(KK)[\%]$	$A_{raw}(\pi\pi)[\%]$	$\Delta A_{CP}[\%]$	significance
up TIS	-1.8660 ± 0.1368	-1.6779 ± 0.2505	-0.1881 ± 0.2854	-
$0.05 < \chi_{DTF}^2 < 2.15$	-2.0366 ± 0.4149	-1.5583 ± 0.7400	-0.4783 ± 0.8484	0.36
$2.15 < \chi_{DTF}^2 < 3.25$	-1.0863 ± 0.4054	-0.5295 ± 0.7245	-0.5568 ± 0.8302	0.47
$3.25 < \chi_{DTF}^2 < 4.35$	-1.6297 ± 0.3949	-1.7633 ± 0.7128	0.1336 ± 0.8149	0.42
$4.35 < \chi_{DTF}^2 < 5.45$	-2.3451 ± 0.4095	-1.6337 ± 0.7367	-0.7115 ± 0.8429	0.66
$5.45 < \chi_{DTF}^2 < 6.65$	-2.0859 ± 0.4151	-2.2150 ± 0.7486	0.1290 ± 0.8560	0.39
$6.65 < \chi_{DTF}^2 < 8.05$	-2.6320 ± 0.4209	-1.7590 ± 0.7593	-0.8730 ± 0.8682	0.84
$8.05 < \chi_{DTF}^2 < 9.75$	-1.1584 ± 0.4374	-1.3672 ± 0.7950	0.2088 ± 0.9074	0.46
$9.75 < \chi_{DTF}^2 < 12.35$	-2.0260 ± 0.4459	-3.1852 ± 0.8076	1.1593 ± 0.9225	1.54
$12.35 < \chi_{DTF}^2 < 19.05$	-3.3301 ± 0.4708	-2.7578 ± 0.8707	-0.5723 ± 0.9899	0.41
$19.05 < \chi_{DTF}^2 < 750.00$	-14.0856 ± 0.8603	-12.6999 ± 1.5549	-1.3856 ± 1.7770	0.68
down TIS	-0.0274 ± 0.1151	-0.0383 ± 0.2102	0.0109 ± 0.2397	-
$0.05 < \chi_{DTF}^2 < 2.15$	-0.5066 ± 0.3497	0.5918 ± 0.6268	-1.0983 ± 0.7177	1.64
$2.15 < \chi_{DTF}^2 < 3.25$	-0.0142 ± 0.3421	0.0270 ± 0.6105	-0.0412 ± 0.6998	0.08
$3.25 < \chi_{DTF}^2 < 4.35$	0.4092 ± 0.3324	0.2000 ± 0.5954	0.2092 ± 0.6819	0.31
$4.35 < \chi_{DTF}^2 < 5.45$	-0.3735 ± 0.3411	-1.0616 ± 0.6149	0.6881 ± 0.7031	1.02
$5.45 < \chi_{DTF}^2 < 6.65$	-0.3519 ± 0.3487	-0.4575 ± 0.6279	0.1057 ± 0.7182	0.14
$6.65 < \chi_{DTF}^2 < 8.05$	0.2439 ± 0.3549	-0.0672 ± 0.6404	0.3111 ± 0.7322	0.43
$8.05 < \chi_{DTF}^2 < 9.75$	0.2376 ± 0.3646	0.5056 ± 0.6635	-0.2680 ± 0.7571	0.39
$9.75 < \chi_{DTF}^2 < 12.35$	-0.7951 ± 0.3738	-0.1942 ± 0.6804	-0.6008 ± 0.7763	0.83
$12.35 < \chi_{DTF}^2 < 19.05$	-1.0020 ± 0.3953	-0.9363 ± 0.7221	-0.0658 ± 0.8232	0.10
$19.05 < \chi_{DTF}^2 < 750.00$	-8.8103 ± 0.7172	-10.8588 ± 1.4102	2.0485 ± 1.5821	1.30
up TOS	-1.3870 ± 0.1665	-1.0138 ± 0.3011	-0.3732 ± 0.3440	-
$0.05 < \chi_{DTF}^2 < 2.15$	-1.4257 ± 0.5032	-1.8678 ± 0.8902	0.4421 ± 1.0226	0.85
$2.15 < \chi_{DTF}^2 < 3.25$	-0.8966 ± 0.4996	-1.4595 ± 0.8815	0.5629 ± 1.0133	0.98
$3.25 < \chi_{DTF}^2 < 4.35$	-1.7081 ± 0.4879	-0.5778 ± 0.8646	-1.1303 ± 0.9927	0.81
$4.35 < \chi_{DTF}^2 < 5.45$	-1.4963 ± 0.5049	-1.1470 ± 0.8922	-0.3493 ± 1.0252	0.02
$5.45 < \chi_{DTF}^2 < 6.65$	-0.3853 ± 0.5150	-0.8190 ± 0.9156	0.4337 ± 1.0505	0.81
$6.65 < \chi_{DTF}^2 < 8.05$	-2.3704 ± 0.5178	-1.1869 ± 0.9191	-1.1835 ± 1.0549	0.81
$8.05 < \chi_{DTF}^2 < 9.75$	-1.4245 ± 0.5326	-1.0383 ± 0.9547	-0.3862 ± 1.0932	0.01
$9.75 < \chi_{DTF}^2 < 12.35$	-1.6454 ± 0.5403	-1.7861 ± 0.9673	0.1407 ± 1.1079	0.49
$12.35 < \chi_{DTF}^2 < 19.05$	-2.2652 ± 0.5631	-0.4244 ± 1.0142	-1.8409 ± 1.1600	1.32
$19.05 < \chi_{DTF}^2 < 750.00$	-8.8481 ± 0.9091	-7.6874 ± 1.6979	-1.1606 ± 1.9260	0.42
down TOS	-0.5525 ± 0.1383	-0.2554 ± 0.2507	-0.2971 ± 0.2863	-
$0.05 < \chi_{DTF}^2 < 2.15$	-0.0720 ± 0.4189	-0.5044 ± 0.7410	0.4324 ± 0.8513	0.91
$2.15 < \chi_{DTF}^2 < 3.25$	-0.9030 ± 0.4146	-0.0776 ± 0.7379	-0.8254 ± 0.8464	0.66
$3.25 < \chi_{DTF}^2 < 4.35$	-1.1348 ± 0.4052	-0.2225 ± 0.7172	-0.9123 ± 0.8238	0.80
$4.35 < \chi_{DTF}^2 < 5.45$	-1.4540 ± 0.4190	-0.0348 ± 0.7387	-1.4192 ± 0.8492	1.40
$5.45 < \chi_{DTF}^2 < 6.65$	0.0958 ± 0.4245	-1.1686 ± 0.7538	1.2644 ± 0.8651	1.91
$6.65 < \chi_{DTF}^2 < 8.05$	-0.8556 ± 0.4302	-0.1621 ± 0.7716	-0.6935 ± 0.8834	0.47
$8.05 < \chi_{DTF}^2 < 9.75$	-0.8489 ± 0.4405	0.4592 ± 0.7917	-1.3081 ± 0.9060	1.18
$9.75 < \chi_{DTF}^2 < 12.35$	-1.0925 ± 0.4459	-1.5812 ± 0.8089	0.4887 ± 0.9237	0.89
$12.35 < \chi_{DTF}^2 < 19.05$	-0.1025 ± 0.4679	-0.1278 ± 0.8488	0.0253 ± 0.9692	0.35
$19.05 < \chi_{DTF}^2 < 750.00$	-8.2504 ± 0.7592	-7.3982 ± 1.3994	-0.8523 ± 1.5921	0.35

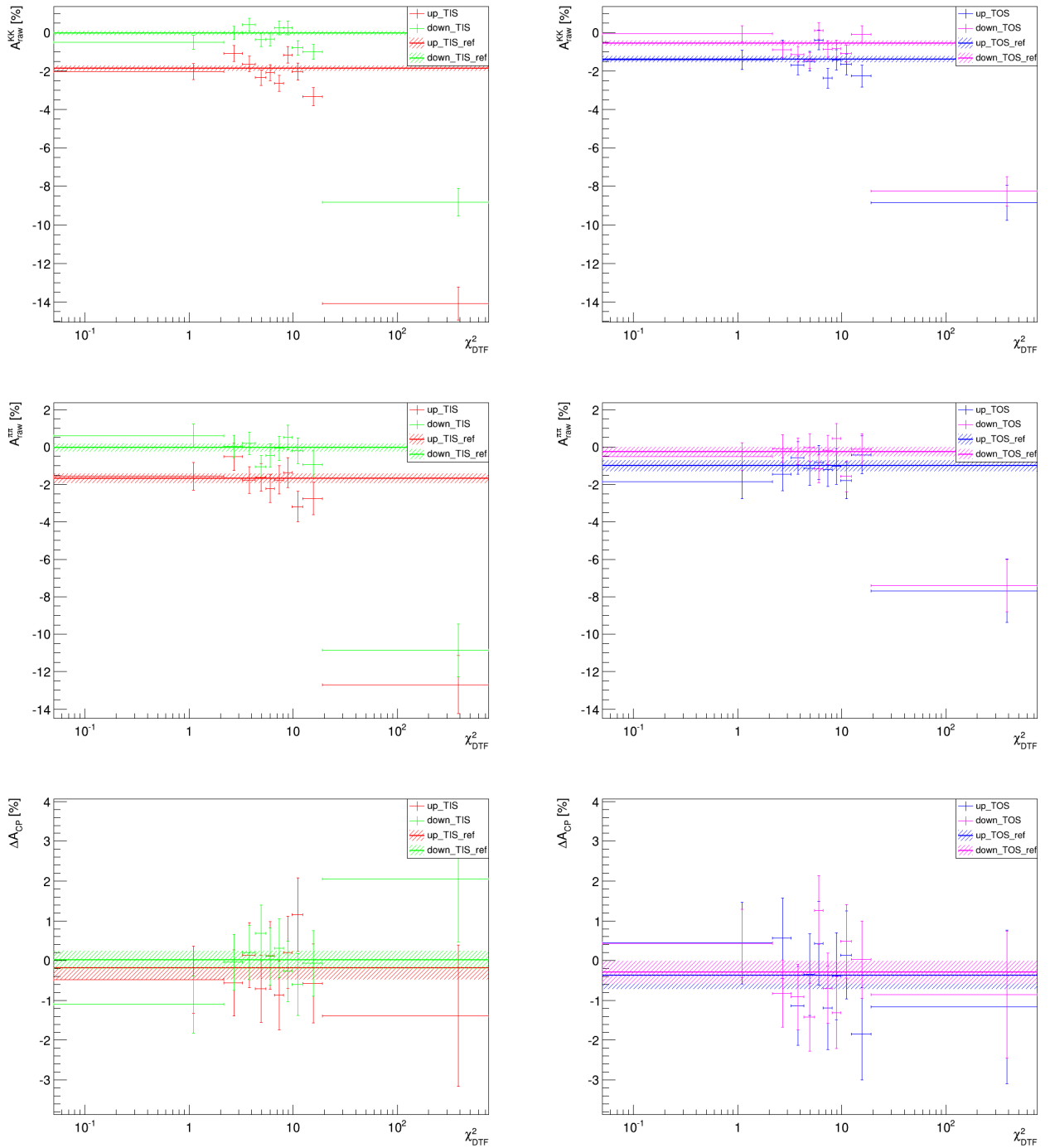


Figure A.17.: A_{raw} vs. χ^2_{DTF} , separated by magnetic field polarity and trigger setting for 2011 data.

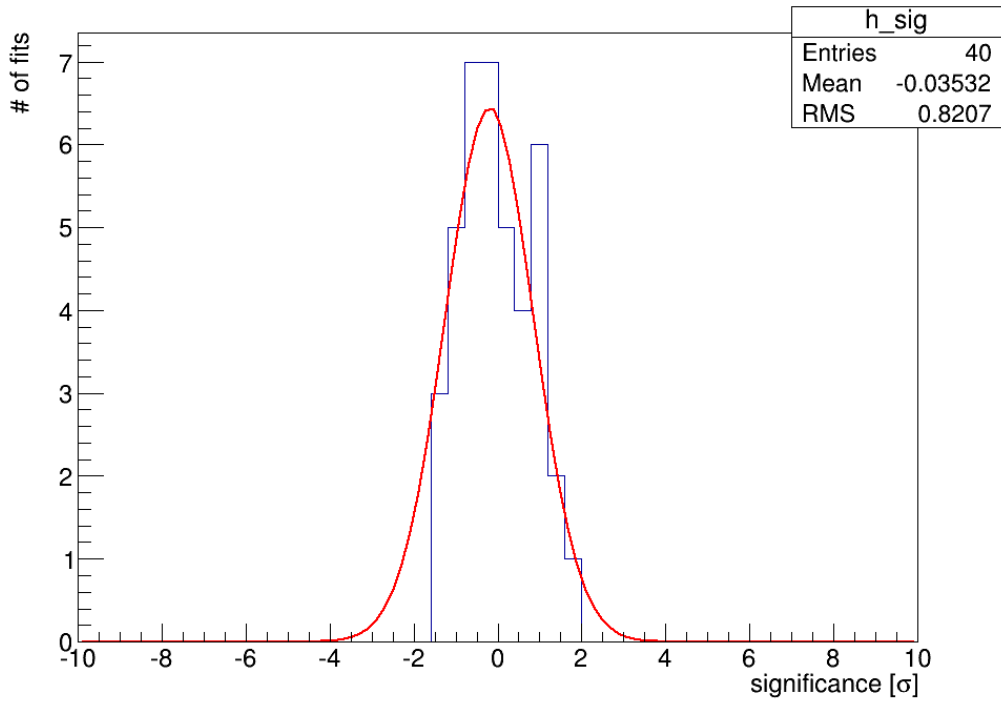
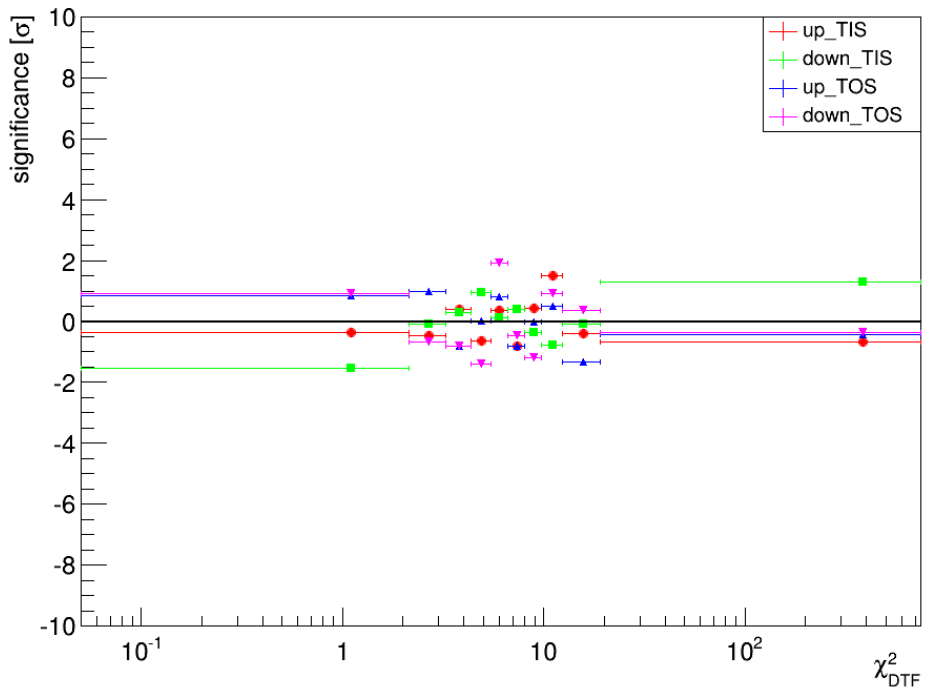


Figure A.18.: Significance vs. χ^2_{DTF} (top) and histogram of significances (bottom) for 2011 data.

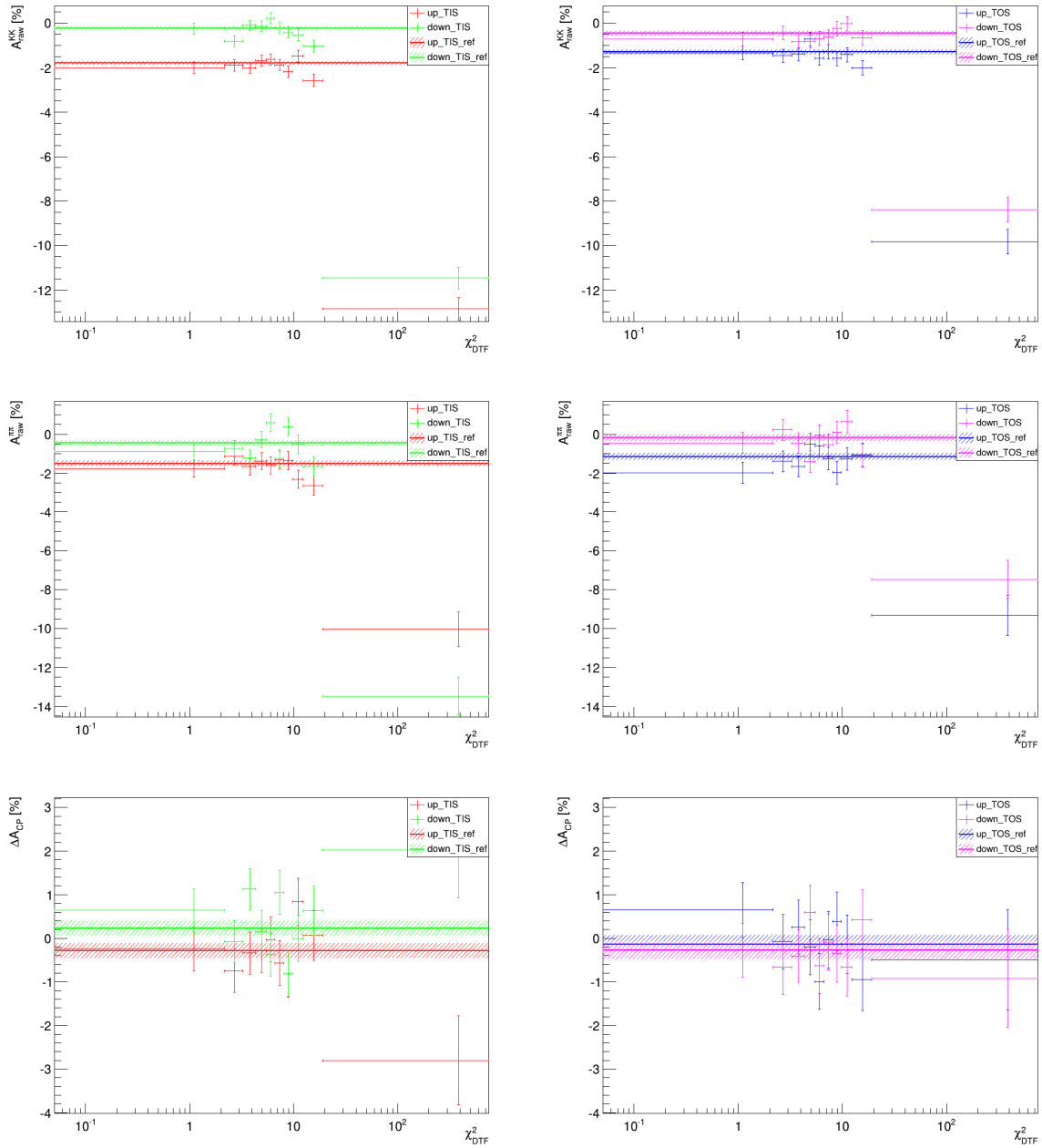


Figure A.19.: A_{raw} vs. χ_{DTF}^2 , separated by magnetic field polarity and trigger setting for 2012 data.

Table A.6.: Results of the individual asymmetries in the different χ_{DTF}^2 bins, separated by magnetic field polarity and trigger for 2012 data. Highest significance: 2.49

Sample	$A_{raw}(KK)[\%]$	$A_{raw}(\pi\pi)[\%]$	$\Delta_{ACP}[\%]$	significance
up TIS	-1.7988 \pm 0.0825	-1.5120 \pm 0.1487	-0.2868 \pm 0.1700	-
0.05 < χ_{DTF}^2 < 2.15	-1.9980 \pm 0.2467	-1.7557 \pm 0.4376	-0.2424 \pm 0.5023	0.09
2.15 < χ_{DTF}^2 < 3.25	-1.8961 \pm 0.2424	-1.1467 \pm 0.4327	-0.7495 \pm 0.4960	0.99
3.25 < χ_{DTF}^2 < 4.35	-2.0037 \pm 0.2362	-1.6656 \pm 0.4218	-0.3382 \pm 0.4834	0.11
4.35 < χ_{DTF}^2 < 5.45	-1.6825 \pm 0.2428	-1.3913 \pm 0.4356	-0.2911 \pm 0.4987	0.01
5.45 < χ_{DTF}^2 < 6.65	-1.6289 \pm 0.2471	-1.6005 \pm 0.4446	-0.0284 \pm 0.5086	0.54
6.65 < χ_{DTF}^2 < 8.05	-1.8804 \pm 0.2503	-1.3117 \pm 0.4506	-0.5687 \pm 0.5155	0.58
8.05 < χ_{DTF}^2 < 9.75	-2.1809 \pm 0.2577	-1.3633 \pm 0.4685	-0.8176 \pm 0.5347	1.05
9.75 < χ_{DTF}^2 < 12.35	-1.4778 \pm 0.2626	-2.3146 \pm 0.4771	0.8368 \pm 0.5446	2.17
12.35 < χ_{DTF}^2 < 19.05	-2.5801 \pm 0.2749	-2.6433 \pm 0.5041	0.0632 \pm 0.5742	0.64
19.05 < χ_{DTF}^2 < 750.00	-12.8386 \pm 0.5054	-10.0400 \pm 0.8909	-2.7986 \pm 1.0243	2.49
down TIS	-0.2274 \pm 0.0814	-0.4563 \pm 0.1456	0.2289 \pm 0.1669	-
0.05 < χ_{DTF}^2 < 2.15	-0.2406 \pm 0.2440	-0.8830 \pm 0.4313	0.6424 \pm 0.4956	0.89
2.15 < χ_{DTF}^2 < 3.25	-0.8103 \pm 0.2396	-0.7336 \pm 0.4245	-0.0766 \pm 0.4874	0.67
3.25 < χ_{DTF}^2 < 4.35	-0.1002 \pm 0.2325	-1.2290 \pm 0.4111	1.1288 \pm 0.4723	2.04
4.35 < χ_{DTF}^2 < 5.45	-0.1250 \pm 0.2397	-0.2769 \pm 0.4268	0.1519 \pm 0.4895	0.17
5.45 < χ_{DTF}^2 < 6.65	0.2177 \pm 0.2439	0.5935 \pm 0.4353	-0.3757 \pm 0.4990	1.29
6.65 < χ_{DTF}^2 < 8.05	-0.1973 \pm 0.2475	-1.2490 \pm 0.4420	1.0517 \pm 0.5066	1.72
8.05 < χ_{DTF}^2 < 9.75	-0.4209 \pm 0.2542	0.3856 \pm 0.4576	-0.8065 \pm 0.5234	2.09
9.75 < χ_{DTF}^2 < 12.35	-0.5156 \pm 0.2592	-0.5159 \pm 0.4679	0.0003 \pm 0.5349	0.45
12.35 < χ_{DTF}^2 < 19.05	-1.0253 \pm 0.2725	-1.6562 \pm 0.4949	0.6309 \pm 0.5649	0.74
19.05 < χ_{DTF}^2 < 750.00	-11.4599 \pm 0.4925	-13.4788 \pm 0.9827	2.0189 \pm 1.0992	1.65
up TOS	-1.2968 \pm 0.1031	-1.1535 \pm 0.1847	-0.1432 \pm 0.2115	-
0.05 < χ_{DTF}^2 < 2.15	-1.3304 \pm 0.3100	-1.9836 \pm 0.5463	0.6532 \pm 0.6281	1.35
2.15 < χ_{DTF}^2 < 3.25	-1.4645 \pm 0.3077	-1.3894 \pm 0.5426	-0.0751 \pm 0.6238	0.12
3.25 < χ_{DTF}^2 < 4.35	-1.3877 \pm 0.3016	-1.6455 \pm 0.5342	0.2578 \pm 0.6135	0.70
4.35 < χ_{DTF}^2 < 5.45	-0.7164 \pm 0.3108	-0.5104 \pm 0.5527	-0.2060 \pm 0.6341	0.11
5.45 < χ_{DTF}^2 < 6.65	-1.5699 \pm 0.3158	-0.5806 \pm 0.5574	-0.9893 \pm 0.6407	1.40
6.65 < χ_{DTF}^2 < 8.05	-1.2677 \pm 0.3191	-1.2368 \pm 0.5706	-0.0310 \pm 0.6538	0.18
8.05 < χ_{DTF}^2 < 9.75	-1.5822 \pm 0.3253	-1.9691 \pm 0.5847	0.3869 \pm 0.6691	0.84
9.75 < χ_{DTF}^2 < 12.35	-1.4140 \pm 0.3274	-1.2725 \pm 0.5850	-0.1415 \pm 0.6704	0.00
12.35 < χ_{DTF}^2 < 19.05	-2.0008 \pm 0.3379	-1.0490 \pm 0.6101	-0.9518 \pm 0.6974	1.22
19.05 < χ_{DTF}^2 < 750.00	-9.8239 \pm 0.5422	-9.3292 \pm 1.0167	-0.4946 \pm 1.1522	0.31
down TOS	-0.4554 \pm 0.1028	-0.1838 \pm 0.1812	-0.2716 \pm 0.2083	-
0.05 < χ_{DTF}^2 < 2.15	-0.7134 \pm 0.3075	-0.4382 \pm 0.5370	-0.2752 \pm 0.6188	0.01
2.15 < χ_{DTF}^2 < 3.25	-0.4362 \pm 0.3047	0.2306 \pm 0.5348	-0.6667 \pm 0.6155	0.68
3.25 < χ_{DTF}^2 < 4.35	-0.8417 \pm 0.2993	-0.4360 \pm 0.5231	-0.4057 \pm 0.6027	0.24
4.35 < χ_{DTF}^2 < 5.45	-0.8192 \pm 0.3075	-1.4120 \pm 0.5410	0.5928 \pm 0.6223	1.47
5.45 < χ_{DTF}^2 < 6.65	-0.6888 \pm 0.3133	-0.0592 \pm 0.5466	-0.6296 \pm 0.6300	0.60
6.65 < χ_{DTF}^2 < 8.05	-0.6259 \pm 0.3154	-0.5363 \pm 0.5583	-0.0896 \pm 0.6412	0.30
8.05 < χ_{DTF}^2 < 9.75	-0.2383 \pm 0.3221	0.1143 \pm 0.5714	-0.3526 \pm 0.6559	0.13
9.75 < χ_{DTF}^2 < 12.35	-0.0251 \pm 0.3254	0.6398 \pm 0.5760	-0.6649 \pm 0.6616	0.63
12.35 < χ_{DTF}^2 < 19.05	-0.6612 \pm 0.3346	-1.0902 \pm 0.5983	0.4290 \pm 0.6855	1.07
19.05 < χ_{DTF}^2 < 750.00	-8.3839 \pm 0.5418	-7.4638 \pm 0.9828	-0.9200 \pm 1.1222	0.59

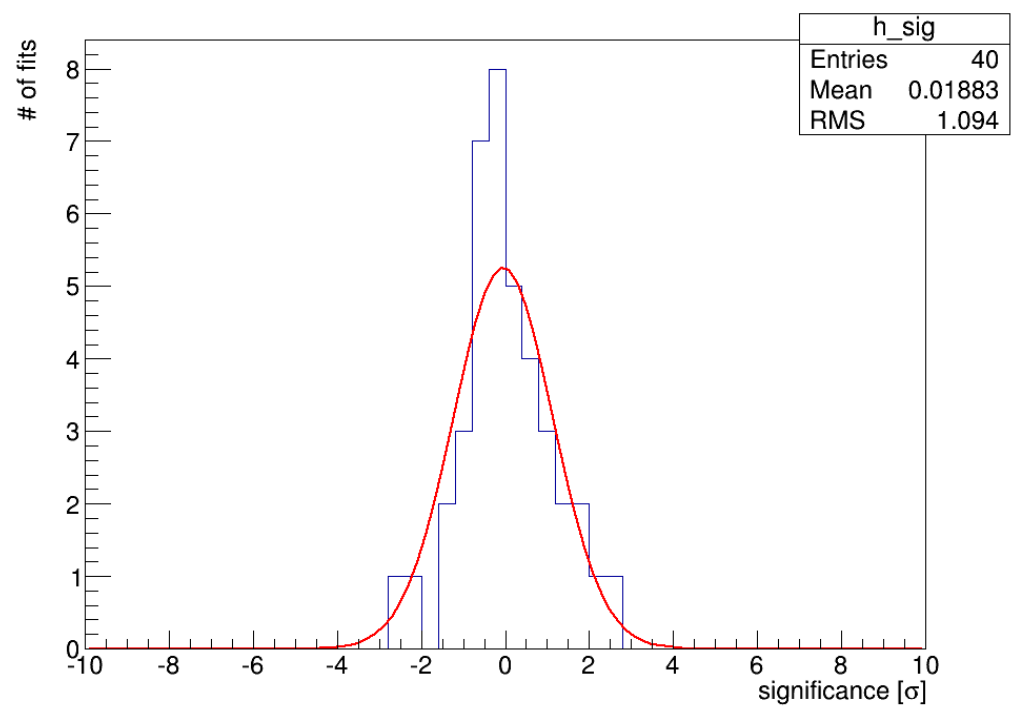
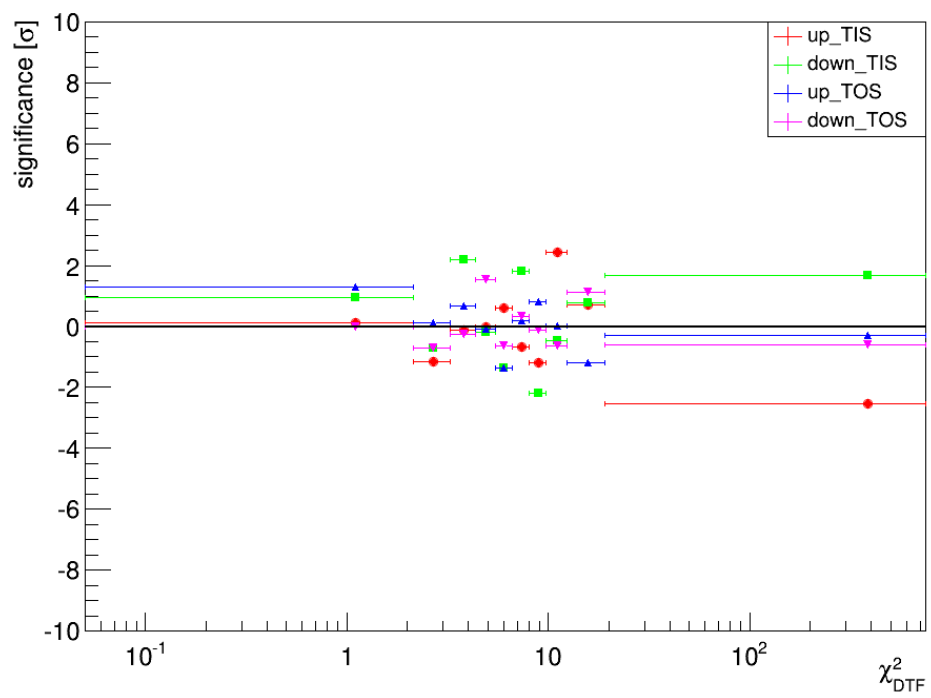


Figure A.20.: Significance vs. χ^2_{DTF} (top) and histogram of significances (bottom) for 2012 data.

A.5. The quality of the slow pion impact parameter

In Fig. A.21 and A.23 the individual asymmetries and ΔA_{CP} versus the $\pi_s IP\chi^2$ can be found for 2011 and 2012, respectively. The significances of the deviations of results from the baseline result in that class of magnetic polarity and trigger can be found in Fig. A.22 and A.24. In Tab. A.7 and A.8 the results are shown for 2011 and 2012, respectively.

Table A.7.: Highest significance: 2.34

Sample	$A_{raw}(KK)[\%]$	$A_{raw}(\pi\pi)[\%]$	$\Delta A_{CP}[\%]$	significance
up TIS	-1.8660 ± 0.1368	-1.6779 ± 0.2505	-0.1881 ± 0.2854	-
$0.05 < \pi_s IP\chi^2 < 0.25$	-1.1902 ± 0.4916	-1.7956 ± 0.8799	0.6054 ± 1.0079	0.82
$0.25 < \pi_s IP\chi^2 < 0.55$	-1.7592 ± 0.4310	-1.2850 ± 0.7725	-0.4742 ± 0.8846	0.34
$0.55 < \pi_s IP\chi^2 < 0.95$	-1.6076 ± 0.4086	-1.3301 ± 0.7331	-0.2775 ± 0.8392	0.11
$0.95 < \pi_s IP\chi^2 < 1.35$	-1.7186 ± 0.4547	-0.6224 ± 0.8195	-1.0962 ± 0.9372	1.02
$1.35 < \pi_s IP\chi^2 < 1.95$	-1.9111 ± 0.4168	-2.9868 ± 0.7567	1.0756 ± 0.8639	1.55
$1.95 < \pi_s IP\chi^2 < 2.85$	-1.8912 ± 0.4037	-2.6264 ± 0.7326	0.7352 ± 0.8365	1.17
$2.85 < \pi_s IP\chi^2 < 4.05$	-2.8803 ± 0.4286	-1.4004 ± 0.7789	-1.4799 ± 0.8891	1.53
$4.05 < \pi_s IP\chi^2 < 6.25$	-1.7329 ± 0.4233	-2.7900 ± 0.7598	1.0571 ± 0.8698	1.52
$6.25 < \pi_s IP\chi^2 < 11.35$	-2.6590 ± 0.4504	-2.0812 ± 0.8161	-0.5778 ± 0.9321	0.44
$11.35 < \pi_s IP\chi^2 < 3000.00$	-9.3438 ± 0.6185	-7.2279 ± 1.1383	-2.1158 ± 1.2955	1.53
down TIS	-0.0274 ± 0.1151	-0.0383 ± 0.2102	0.0109 ± 0.2397	-
$0.05 < \pi_s IP\chi^2 < 0.25$	0.2633 ± 0.4141	1.0352 ± 0.7404	-0.7719 ± 0.8484	0.96
$0.25 < \pi_s IP\chi^2 < 0.55$	0.1137 ± 0.3621	0.0614 ± 0.6588	0.0523 ± 0.7517	0.06
$0.55 < \pi_s IP\chi^2 < 0.95$	-0.3053 ± 0.3436	-0.3649 ± 0.6204	0.0596 ± 0.7092	0.07
$0.95 < \pi_s IP\chi^2 < 1.35$	-0.0923 ± 0.3810	0.0679 ± 0.6866	-0.1602 ± 0.7852	0.23
$1.35 < \pi_s IP\chi^2 < 1.95$	-0.1642 ± 0.3512	-0.4808 ± 0.6329	0.3167 ± 0.7238	0.45
$1.95 < \pi_s IP\chi^2 < 2.85$	-0.5121 ± 0.3363	0.7949 ± 0.6054	-1.3070 ± 0.6925	2.03
$2.85 < \pi_s IP\chi^2 < 4.05$	0.2369 ± 0.3602	0.1466 ± 0.6513	0.0903 ± 0.7443	0.11
$4.05 < \pi_s IP\chi^2 < 6.25$	0.1406 ± 0.3553	-1.4750 ± 0.6409	1.6156 ± 0.7328	2.32
$6.25 < \pi_s IP\chi^2 < 11.35$	-0.8073 ± 0.3782	-0.8050 ± 0.6867	-0.0023 ± 0.7839	0.02
$11.35 < \pi_s IP\chi^2 < 3000.00$	-6.1513 ± 0.5243	-5.1501 ± 0.9643	-1.0011 ± 1.0976	0.94
up TOS	-1.3870 ± 0.1665	-1.0138 ± 0.3011	-0.3732 ± 0.3440	-
$0.05 < \pi_s IP\chi^2 < 0.25$	-1.3327 ± 0.5639	-0.6066 ± 1.0076	-0.7260 ± 1.1546	0.32
$0.25 < \pi_s IP\chi^2 < 0.55$	-1.2239 ± 0.5065	-1.6525 ± 0.9021	0.4286 ± 1.0346	0.82
$0.55 < \pi_s IP\chi^2 < 0.95$	-1.7077 ± 0.4944	-1.7570 ± 0.8649	0.0493 ± 0.9962	0.45
$0.95 < \pi_s IP\chi^2 < 1.35$	-1.2689 ± 0.5533	-1.7241 ± 0.9792	0.4552 ± 1.1247	0.77
$1.35 < \pi_s IP\chi^2 < 1.95$	-1.4581 ± 0.5195	-2.4257 ± 0.9249	0.9676 ± 1.0608	1.34
$1.95 < \pi_s IP\chi^2 < 2.85$	-1.7665 ± 0.5053	-2.1402 ± 0.8992	0.3738 ± 1.0314	0.77
$2.85 < \pi_s IP\chi^2 < 4.05$	-1.1162 ± 0.5444	0.7477 ± 0.9705	-1.8639 ± 1.1128	1.41
$4.05 < \pi_s IP\chi^2 < 6.25$	-1.3537 ± 0.5363	0.8578 ± 0.9577	-2.2115 ± 1.0977	1.76
$6.25 < \pi_s IP\chi^2 < 11.35$	-1.9330 ± 0.5502	-1.5120 ± 0.9857	-0.4211 ± 1.1289	0.04
$11.35 < \pi_s IP\chi^2 < 3000.00$	-5.9497 ± 0.7309	-4.6968 ± 1.3405	-1.2529 ± 1.5268	0.59
down TOS	-0.5525 ± 0.1383	-0.2554 ± 0.2507	-0.2971 ± 0.2863	-
$0.05 < \pi_s IP\chi^2 < 0.25$	-0.7983 ± 0.4724	-0.2818 ± 0.8398	-0.5165 ± 0.9636	0.24
$0.25 < \pi_s IP\chi^2 < 0.55$	-0.1295 ± 0.4184	-1.6141 ± 0.7479	1.4846 ± 0.8570	2.21
$0.55 < \pi_s IP\chi^2 < 0.95$	-0.9647 ± 0.4077	-0.2647 ± 0.7287	-0.7000 ± 0.8350	0.51
$0.95 < \pi_s IP\chi^2 < 1.35$	-1.2565 ± 0.4610	1.1380 ± 0.8207	-2.3945 ± 0.9413	2.34
$1.35 < \pi_s IP\chi^2 < 1.95$	-0.1045 ± 0.4293	0.0099 ± 0.7677	-0.1144 ± 0.8796	0.22
$1.95 < \pi_s IP\chi^2 < 2.85$	-0.6481 ± 0.4199	-0.5741 ± 0.7441	-0.0740 ± 0.8544	0.28
$2.85 < \pi_s IP\chi^2 < 4.05$	-0.8720 ± 0.4519	0.3098 ± 0.7979	-1.1819 ± 0.9169	1.02
$4.05 < \pi_s IP\chi^2 < 6.25$	-1.0505 ± 0.4431	-0.5676 ± 0.7936	-0.4829 ± 0.9089	0.22
$6.25 < \pi_s IP\chi^2 < 11.35$	-1.0269 ± 0.4571	-0.8848 ± 0.8262	-0.1420 ± 0.9442	0.17
$11.35 < \pi_s IP\chi^2 < 3000.00$	-4.7918 ± 0.6086	-4.7671 ± 1.1140	-0.0247 ± 1.2694	0.22

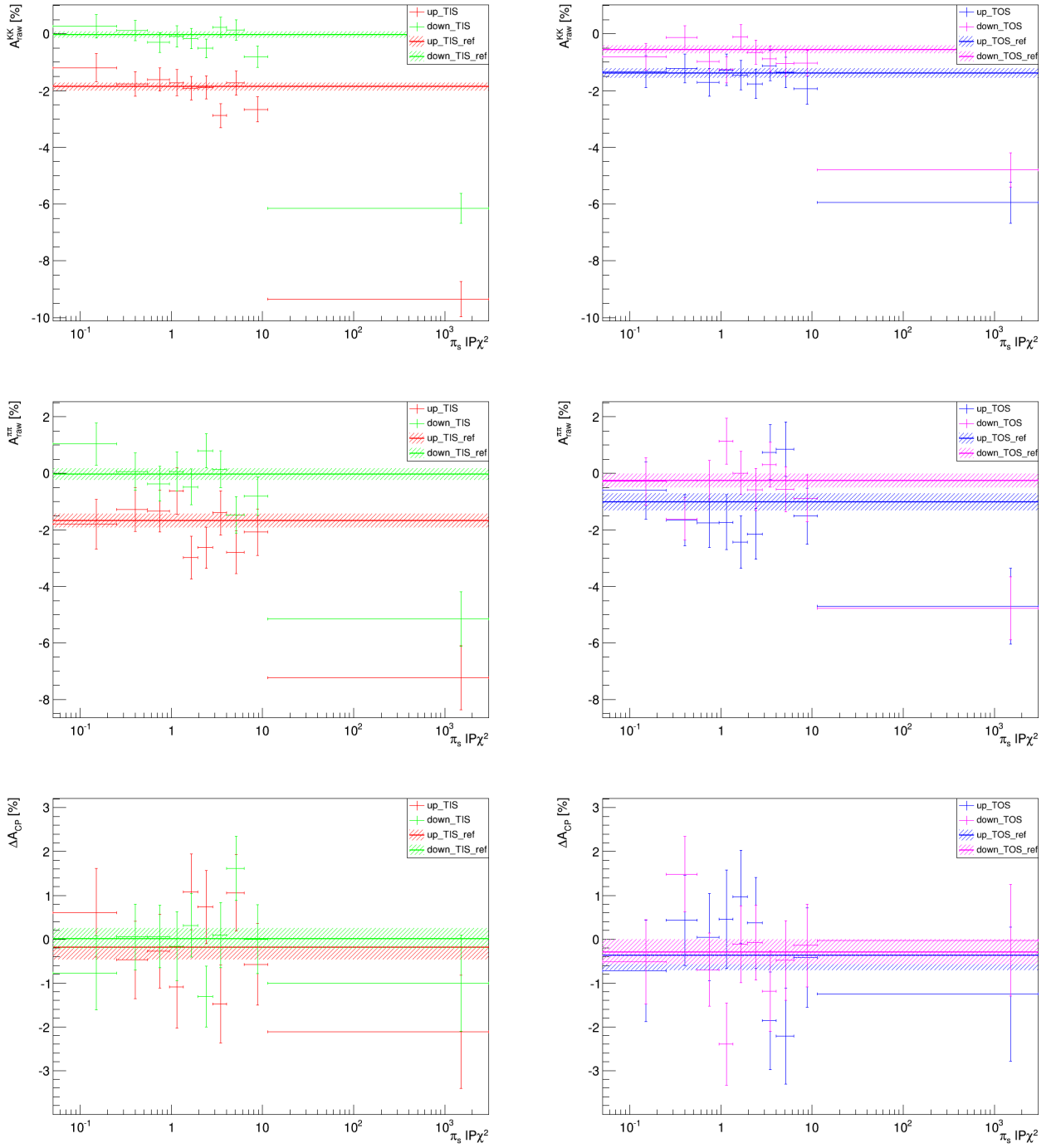


Figure A.21.: A_{raw} vs. $\pi_s IP\chi^2$, separated by magnetic field polarity and trigger setting for 2011 data.

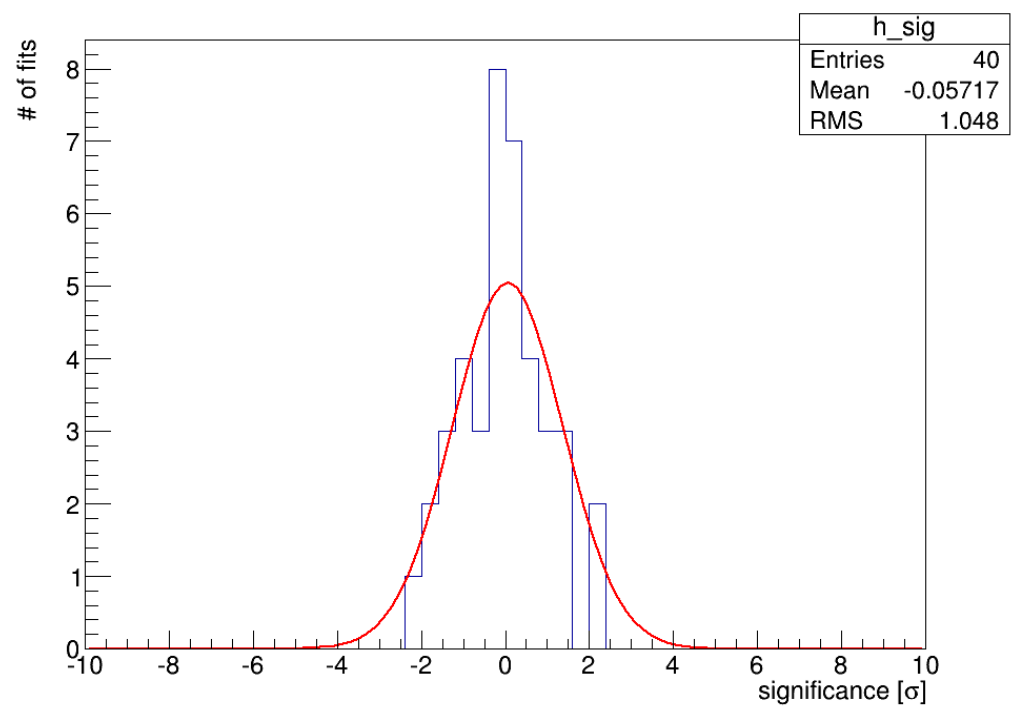
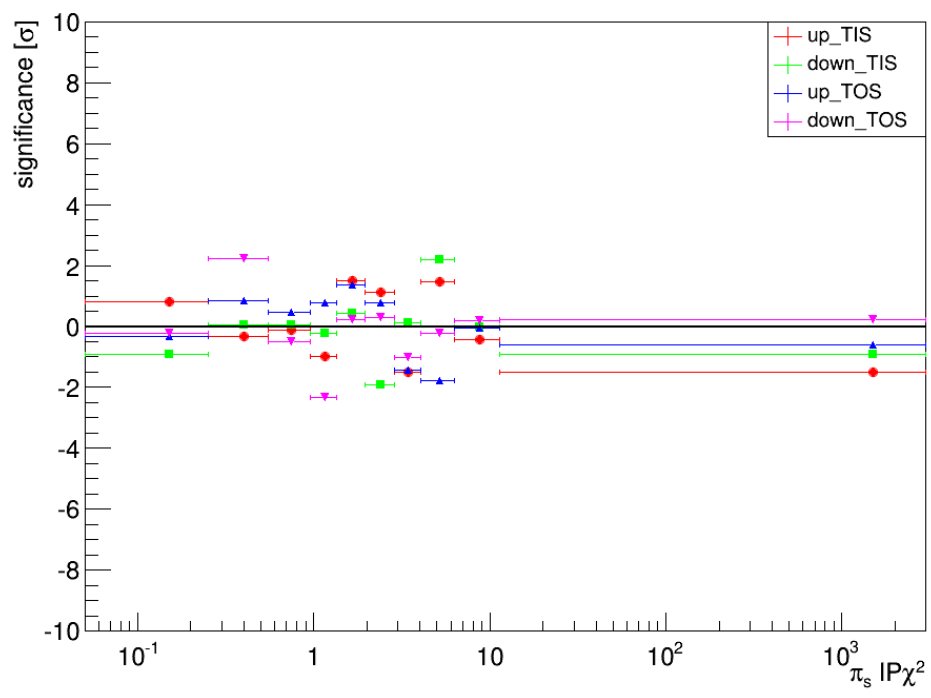


Figure A.22.: Significance vs. $\pi_s IP\chi^2$ (top) and histogram of significances (bottom) for 2011 data.

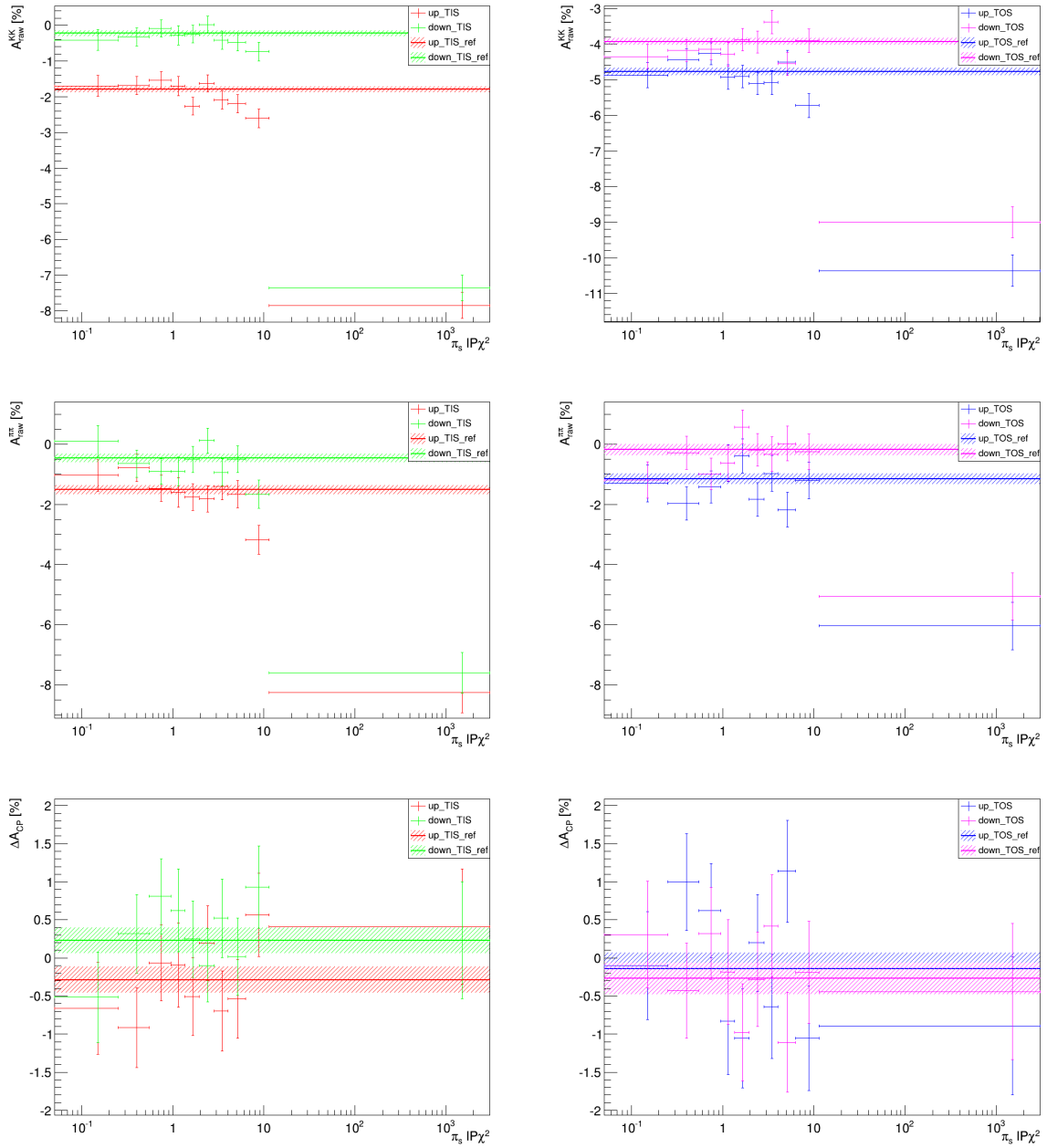


Figure A.23.: A_{raw} vs. $\pi_s IP\chi^2$, separated by magnetic field polarity and trigger setting for 2012 data.

Table A.8.: Results of the individual asymmetries in the different $\pi_s IP\chi^2$ bins, separated by magnetic field polarity and trigger for 2012 data. Highest significance: 2.02

Sample	$A_{raw}(KK)[\%]$	$A_{raw}(\pi\pi)[\%]$	$\Delta A_{CP}[\%]$	significance
up TIS	-1.7988 \pm 0.0825	-1.5120 \pm 0.1487	-0.2868 \pm 0.1700	-
0.05 < $\pi_s IP\chi^2$ < 0.25	-1.6953 \pm 0.2920	-1.0348 \pm 0.5276	-0.6605 \pm 0.6030	0.65
0.25 < $\pi_s IP\chi^2$ < 0.55	-1.6928 \pm 0.2558	-0.7800 \pm 0.4603	-0.9128 \pm 0.5266	1.26
0.55 < $\pi_s IP\chi^2$ < 0.95	-1.5353 \pm 0.2431	-1.4699 \pm 0.4363	-0.0655 \pm 0.4995	0.47
0.95 < $\pi_s IP\chi^2$ < 1.35	-1.6965 \pm 0.2698	-1.6007 \pm 0.4849	-0.0958 \pm 0.5549	0.36
1.35 < $\pi_s IP\chi^2$ < 1.95	-2.2675 \pm 0.2485	-1.7574 \pm 0.4470	-0.5102 \pm 0.5114	0.46
1.95 < $\pi_s IP\chi^2$ < 2.85	-1.6211 \pm 0.2390	-1.8140 \pm 0.4303	0.1929 \pm 0.4922	1.04
2.85 < $\pi_s IP\chi^2$ < 4.05	-2.0881 \pm 0.2559	-1.3922 \pm 0.4576	-0.6959 \pm 0.5243	0.82
4.05 < $\pi_s IP\chi^2$ < 6.25	-2.1955 \pm 0.2503	-1.6597 \pm 0.4507	-0.5358 \pm 0.5156	0.51
6.25 < $\pi_s IP\chi^2$ < 11.35	-2.6055 \pm 0.2654	-3.1703 \pm 0.4810	0.5649 \pm 0.5493	1.63
11.35 < $\pi_s IP\chi^2$ < 3000.00	-7.8471 \pm 0.3639	-8.2572 \pm 0.6616	0.4101 \pm 0.7550	0.95
down TIS	-0.2274 \pm 0.0814	-0.4563 \pm 0.1456	0.2289 \pm 0.1669	-
0.05 < $\pi_s IP\chi^2$ < 0.25	-0.4099 \pm 0.2890	0.1062 \pm 0.5162	-0.5160 \pm 0.5916	1.31
0.25 < $\pi_s IP\chi^2$ < 0.55	-0.3222 \pm 0.2524	-0.6399 \pm 0.4518	0.3177 \pm 0.5176	0.18
0.55 < $\pi_s IP\chi^2$ < 0.95	-0.0928 \pm 0.2402	-0.9013 \pm 0.4317	0.8085 \pm 0.4940	1.25
0.95 < $\pi_s IP\chi^2$ < 1.35	-0.2799 \pm 0.2667	-0.9049 \pm 0.4744	0.6250 \pm 0.5442	0.76
1.35 < $\pi_s IP\chi^2$ < 1.95	-0.2496 \pm 0.2450	-0.4982 \pm 0.4358	0.2485 \pm 0.5000	0.04
1.95 < $\pi_s IP\chi^2$ < 2.85	0.0206 \pm 0.2356	0.1186 \pm 0.4190	-0.0980 \pm 0.4807	0.73
2.85 < $\pi_s IP\chi^2$ < 4.05	-0.4134 \pm 0.2517	-0.9359 \pm 0.4504	0.5224 \pm 0.5160	0.60
4.05 < $\pi_s IP\chi^2$ < 6.25	-0.4709 \pm 0.2480	-0.4900 \pm 0.4413	0.0190 \pm 0.5062	0.44
6.25 < $\pi_s IP\chi^2$ < 11.35	-0.7345 \pm 0.2624	-1.6643 \pm 0.4712	0.9299 \pm 0.5394	1.37
11.35 < $\pi_s IP\chi^2$ < 3000.00	-7.3622 \pm 0.3591	-7.5935 \pm 0.6765	0.2313 \pm 0.7658	0.00
up TOS	-1.2968 \pm 0.1031	-1.1535 \pm 0.1847	-0.1432 \pm 0.2115	-
0.05 < $\pi_s IP\chi^2$ < 0.25	-1.4001 \pm 0.3486	-1.3004 \pm 0.6160	-0.0997 \pm 0.7078	0.06
0.25 < $\pi_s IP\chi^2$ < 0.55	-0.9732 \pm 0.3112	-1.9704 \pm 0.5524	0.9971 \pm 0.6340	1.91
0.55 < $\pi_s IP\chi^2$ < 0.95	-0.7967 \pm 0.3031	-1.4206 \pm 0.5360	0.6239 \pm 0.6157	1.33
0.95 < $\pi_s IP\chi^2$ < 1.35	-1.4546 \pm 0.3408	-0.6229 \pm 0.6105	-0.8317 \pm 0.6992	1.03
1.35 < $\pi_s IP\chi^2$ < 1.95	-1.4381 \pm 0.3180	-0.3837 \pm 0.5661	-1.0544 \pm 0.6493	1.48
1.95 < $\pi_s IP\chi^2$ < 2.85	-1.6348 \pm 0.3113	-1.8339 \pm 0.5531	0.1991 \pm 0.6347	0.57
2.85 < $\pi_s IP\chi^2$ < 4.05	-1.6065 \pm 0.3337	-0.9685 \pm 0.5956	-0.6381 \pm 0.6827	0.76
4.05 < $\pi_s IP\chi^2$ < 6.25	-1.0351 \pm 0.3264	-2.1726 \pm 0.5819	1.1375 \pm 0.6671	2.02
6.25 < $\pi_s IP\chi^2$ < 11.35	-2.2593 \pm 0.3335	-1.2062 \pm 0.5984	-1.0531 \pm 0.6851	1.40
11.35 < $\pi_s IP\chi^2$ < 3000.00	-6.9282 \pm 0.4373	-6.0387 \pm 0.7952	-0.8895 \pm 0.9075	0.85
down TOS	-0.4554 \pm 0.1028	-0.1838 \pm 0.1812	-0.2716 \pm 0.2083	-
0.05 < $\pi_s IP\chi^2$ < 0.25	-0.8804 \pm 0.3460	-1.1871 \pm 0.6072	0.3067 \pm 0.6989	0.87
0.25 < $\pi_s IP\chi^2$ < 0.55	-0.7107 \pm 0.3090	-0.2820 \pm 0.5440	-0.4287 \pm 0.6256	0.27
0.55 < $\pi_s IP\chi^2$ < 0.95	-0.6703 \pm 0.2995	-0.9901 \pm 0.5250	0.3199 \pm 0.6044	1.04
0.95 < $\pi_s IP\chi^2$ < 1.35	-0.8130 \pm 0.3369	-0.6265 \pm 0.5986	-0.1866 \pm 0.6869	0.13
1.35 < $\pi_s IP\chi^2$ < 1.95	-0.4003 \pm 0.3149	0.5765 \pm 0.5518	-0.9768 \pm 0.6353	1.17
1.95 < $\pi_s IP\chi^2$ < 2.85	-0.4693 \pm 0.3085	-0.1901 \pm 0.5421	-0.2793 \pm 0.6237	0.01
2.85 < $\pi_s IP\chi^2$ < 4.05	0.0891 \pm 0.3316	-0.3296 \pm 0.5817	0.4187 \pm 0.6696	1.08
4.05 < $\pi_s IP\chi^2$ < 6.25	-1.0828 \pm 0.3239	0.0242 \pm 0.5731	-1.1070 \pm 0.6583	1.34
6.25 < $\pi_s IP\chi^2$ < 11.35	-0.4295 \pm 0.3298	-0.2411 \pm 0.5859	-0.1884 \pm 0.6724	0.13
11.35 < $\pi_s IP\chi^2$ < 3000.00	-5.5022 \pm 0.4359	-5.0585 \pm 0.7803	-0.4436 \pm 0.8938	0.20

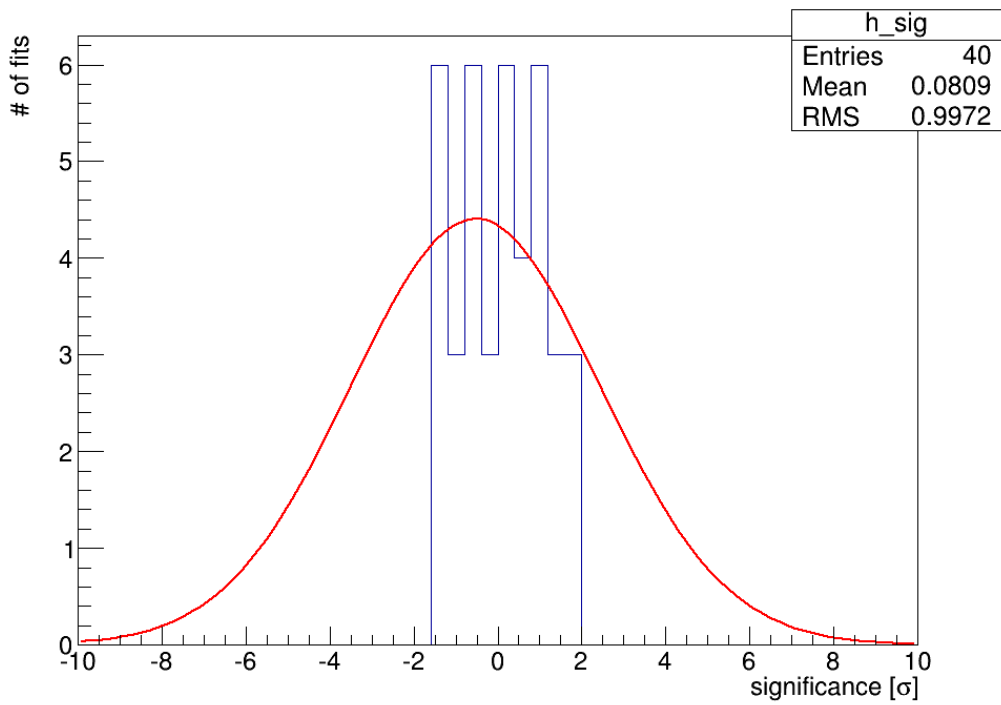
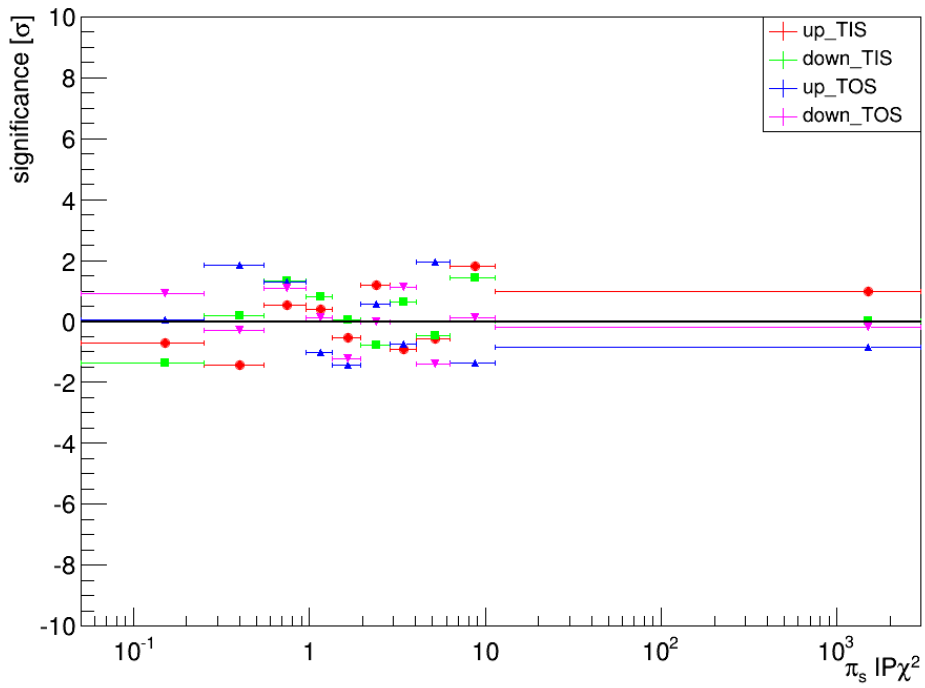


Figure A.24.: Significance vs. $\pi_s IP\chi^2$ (top) and histogram of significances (bottom) for 2012 data.

A.6. Slow pion transverse momentum

In Fig. A.25 and A.27 the individual asymmetries and ΔA_{CP} versus the $\pi_s p_T$ can be found for 2011 and 2012, respectively. The significances of the deviations of results from the baseline result in that class of magnetic polarity and trigger can be found in Fig. A.26 and A.28. In Tab. A.9 and A.10 the results are shown for 2011 and 2012, respectively.

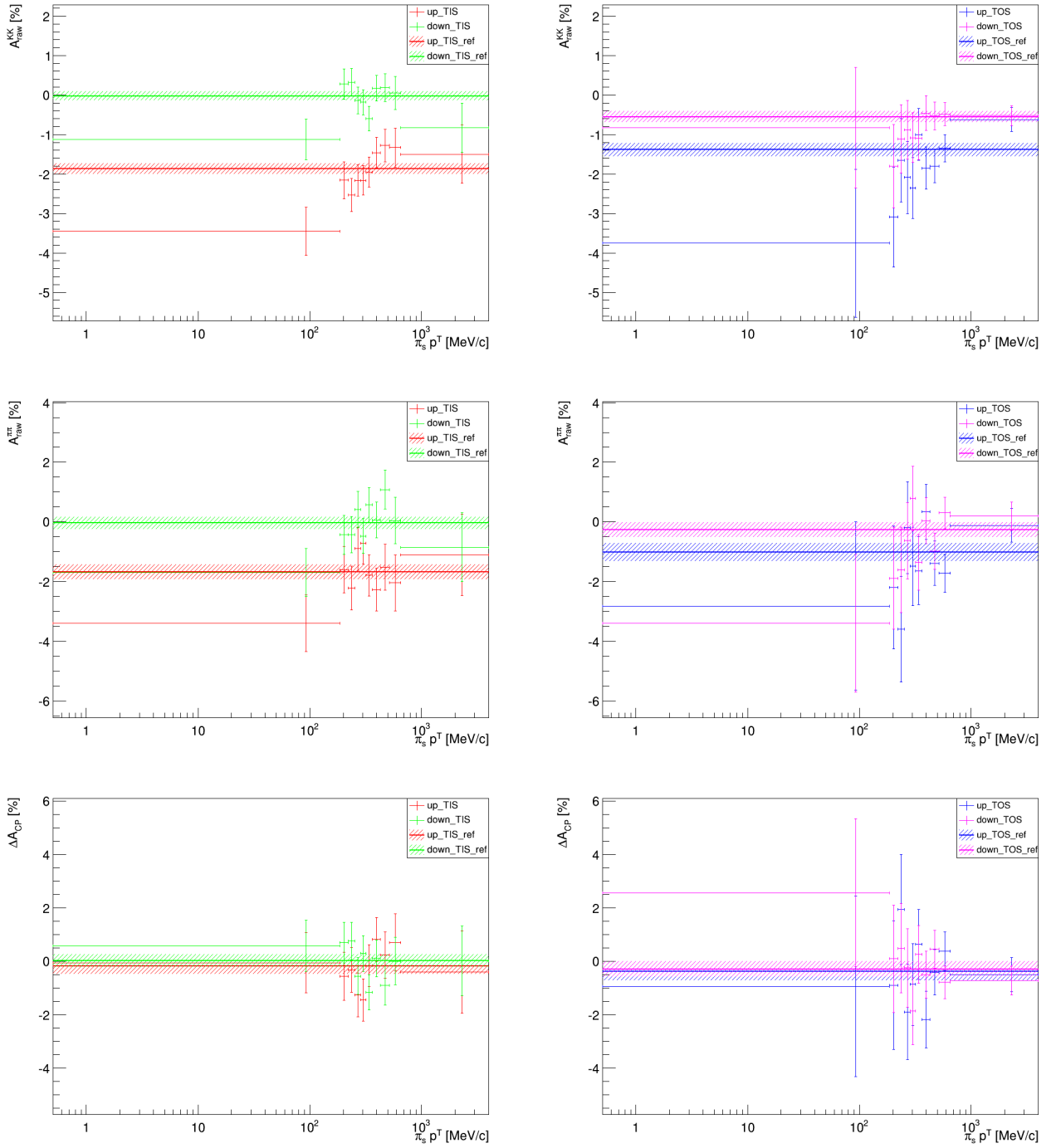


Figure A.25.: A_{raw} vs. $\pi_s p_T$, separated by magnetic field polarity and trigger setting for 2011 data.

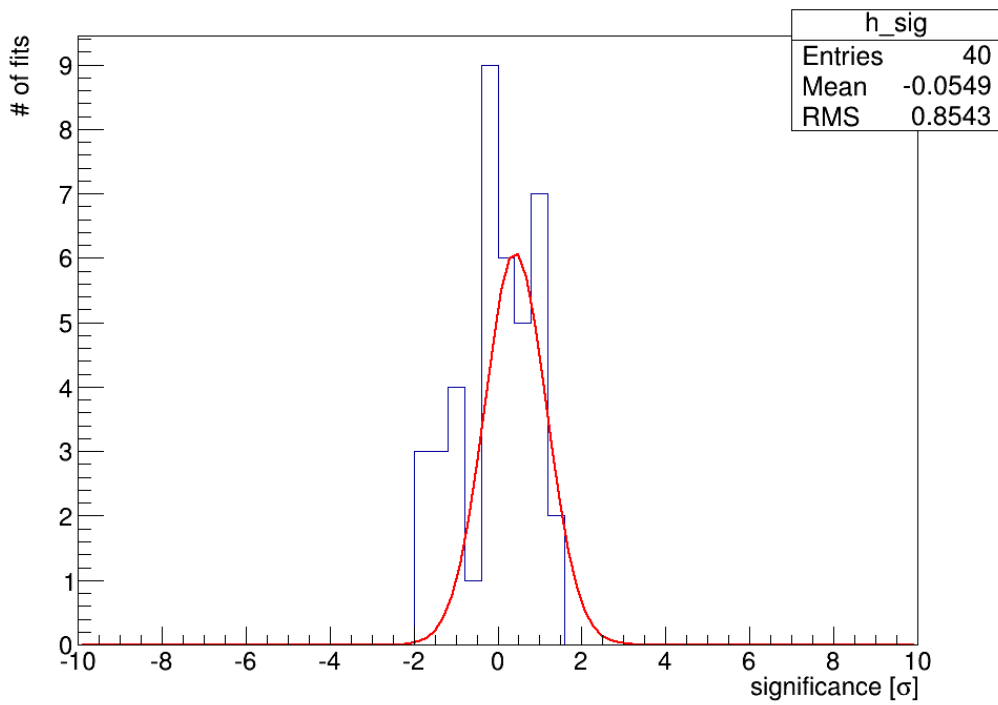
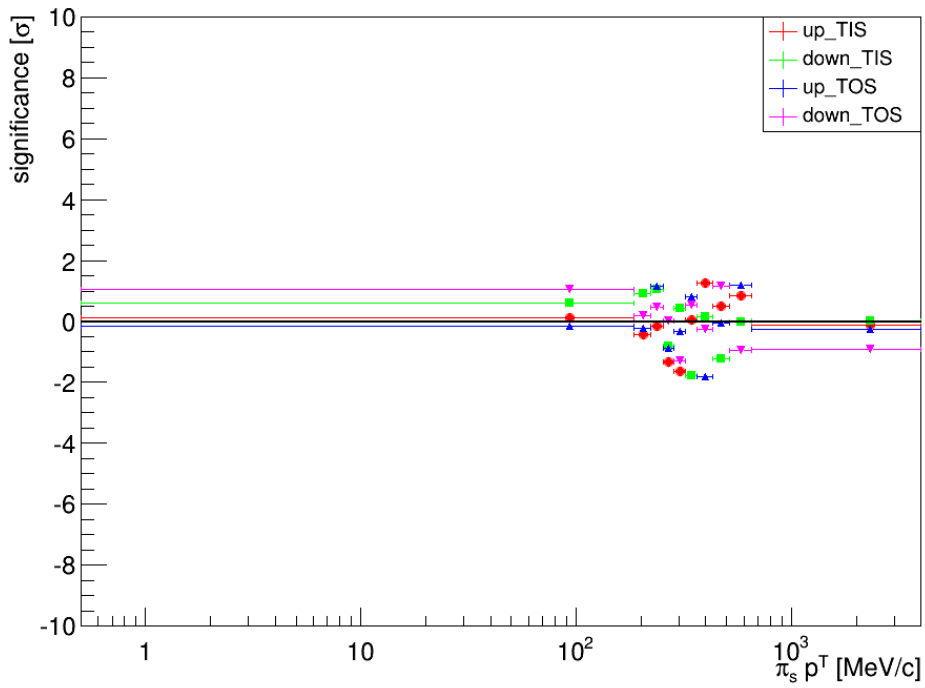


Figure A.26.: Significance vs. $\pi_s p_T$ (top) and histogram of significances (bottom) for 2011 data.

Table A.9.: Results of the individual asymmetries in the different $\pi_s p_T$ bins, separated by magnetic field polarity and trigger for 2011 data. Highest significance: 1.91

Sample	$A_{raw}(KK)[\%]$	$A_{raw}(\pi\pi)[\%]$	$\Delta A_{CP}[\%]$	significance
up TIS	-1.8660 \pm 0.1368	-1.6779 \pm 0.2505	-0.1881 \pm 0.2854	-
0.50 < $\pi_s p^T$ [MeV/c] < 185.50	-3.4479 \pm 0.6117	-3.3927 \pm 0.9504	-0.0553 \pm 1.1303	0.12
185.50 < $\pi_s p^T$ [MeV/c] < 222.50	-2.1586 \pm 0.4621	-1.5955 \pm 0.7813	-0.5631 \pm 0.9077	0.44
222.50 < $\pi_s p^T$ [MeV/c] < 254.50	-2.5304 \pm 0.4140	-2.2063 \pm 0.7324	-0.3241 \pm 0.8413	0.17
254.50 < $\pi_s p^T$ [MeV/c] < 285.50	-2.1601 \pm 0.3959	-0.8962 \pm 0.7202	-1.2639 \pm 0.8218	1.40
285.50 < $\pi_s p^T$ [MeV/c] < 320.50	-2.1594 \pm 0.3770	-0.7103 \pm 0.6981	-1.4490 \pm 0.7933	1.70
320.50 < $\pi_s p^T$ [MeV/c] < 365.50	-1.9465 \pm 0.3751	-1.7850 \pm 0.6907	-0.1615 \pm 0.7860	0.04
365.50 < $\pi_s p^T$ [MeV/c] < 428.50	-1.4559 \pm 0.3849	-2.2682 \pm 0.7186	0.8123 \pm 0.8152	1.31
428.50 < $\pi_s p^T$ [MeV/c] < 516.50	-1.2797 \pm 0.4149	-1.5094 \pm 0.7660	0.2297 \pm 0.8711	0.51
516.50 < $\pi_s p^T$ [MeV/c] < 654.50	-1.3334 \pm 0.4996	-2.0390 \pm 0.9387	0.7057 \pm 1.0634	0.87
654.50 < $\pi_s p^T$ [MeV/c] < 4000.00	-1.4965 \pm 0.7337	-1.0999 \pm 1.3564	-0.3966 \pm 1.5421	0.14
down TIS	-0.0274 \pm 0.1151	-0.0383 \pm 0.2102	0.0109 \pm 0.2397	-
0.50 < $\pi_s p^T$ [MeV/c] < 185.50	-1.1232 \pm 0.5174	-1.6964 \pm 0.8038	0.5733 \pm 0.9560	0.61
185.50 < $\pi_s p^T$ [MeV/c] < 222.50	0.2765 \pm 0.3882	-0.4288 \pm 0.6538	0.7053 \pm 0.7604	0.96
222.50 < $\pi_s p^T$ [MeV/c] < 254.50	0.3267 \pm 0.3469	-0.4287 \pm 0.6077	0.7554 \pm 0.6997	1.13
254.50 < $\pi_s p^T$ [MeV/c] < 285.50	-0.1366 \pm 0.3328	0.4186 \pm 0.6012	-0.5552 \pm 0.6872	0.88
285.50 < $\pi_s p^T$ [MeV/c] < 320.50	-0.1824 \pm 0.3175	-0.4702 \pm 0.5847	0.2878 \pm 0.6653	0.45
320.50 < $\pi_s p^T$ [MeV/c] < 365.50	-0.5949 \pm 0.3142	0.5705 \pm 0.5819	-1.1654 \pm 0.6613	1.91
365.50 < $\pi_s p^T$ [MeV/c] < 428.50	0.1758 \pm 0.3232	0.0645 \pm 0.6039	0.1113 \pm 0.6849	0.16
428.50 < $\pi_s p^T$ [MeV/c] < 516.50	0.1870 \pm 0.3483	1.0830 \pm 0.6520	-0.8959 \pm 0.7392	1.30
516.50 < $\pi_s p^T$ [MeV/c] < 654.50	0.0520 \pm 0.4175	0.0470 \pm 0.7827	0.0050 \pm 0.8871	0.01
654.50 < $\pi_s p^T$ [MeV/c] < 4000.00	-0.8271 \pm 0.6173	-0.8435 \pm 1.1502	0.0164 \pm 1.3054	0.00
up TOS	-1.3870 \pm 0.1665	-1.0138 \pm 0.3011	-0.3732 \pm 0.3440	-
0.50 < $\pi_s p^T$ [MeV/c] < 185.50	-3.7519 \pm 1.8700	-2.8137 \pm 2.8138	-0.9382 \pm 3.3785	0.17
185.50 < $\pi_s p^T$ [MeV/c] < 222.50	-3.0917 \pm 1.2641	-2.1968 \pm 2.0535	-0.8949 \pm 2.4114	0.22
222.50 < $\pi_s p^T$ [MeV/c] < 254.50	-1.6529 \pm 1.0566	-3.5924 \pm 1.7697	1.9395 \pm 2.0611	1.14
254.50 < $\pi_s p^T$ [MeV/c] < 285.50	-2.0889 \pm 0.9088	-0.1880 \pm 1.5426	-1.9008 \pm 1.7904	0.87
285.50 < $\pi_s p^T$ [MeV/c] < 320.50	-2.3549 \pm 0.7681	-1.4839 \pm 1.3187	-0.8710 \pm 1.5261	0.33
320.50 < $\pi_s p^T$ [MeV/c] < 365.50	-0.9986 \pm 0.6585	-1.6307 \pm 1.1296	0.6321 \pm 1.3075	0.80
365.50 < $\pi_s p^T$ [MeV/c] < 428.50	-1.8480 \pm 0.5288	0.3387 \pm 0.9248	-2.1867 \pm 1.0653	1.80
428.50 < $\pi_s p^T$ [MeV/c] < 516.50	-1.7990 \pm 0.4184	-1.3856 \pm 0.7447	-0.4133 \pm 0.8542	0.05
516.50 < $\pi_s p^T$ [MeV/c] < 654.50	-1.3465 \pm 0.3502	-1.7155 \pm 0.6299	0.3689 \pm 0.7207	1.17
654.50 < $\pi_s p^T$ [MeV/c] < 4000.00	-0.6193 \pm 0.3066	-0.1181 \pm 0.5642	-0.5011 \pm 0.6421	0.24
down TOS	-0.5525 \pm 0.1383	-0.2554 \pm 0.2507	-0.2971 \pm 0.2863	-
0.50 < $\pi_s p^T$ [MeV/c] < 185.50	-0.8287 \pm 1.5291	-3.3895 \pm 2.3117	2.5608 \pm 2.7717	1.04
185.50 < $\pi_s p^T$ [MeV/c] < 222.50	-1.8004 \pm 1.0523	-1.8878 \pm 1.7075	0.0874 \pm 2.0057	0.19
222.50 < $\pi_s p^T$ [MeV/c] < 254.50	-1.1126 \pm 0.8685	-1.5968 \pm 1.4305	0.4842 \pm 1.6735	0.47
254.50 < $\pi_s p^T$ [MeV/c] < 285.50	-0.8791 \pm 0.7430	-0.6278 \pm 1.2711	-0.2513 \pm 1.4724	0.03
285.50 < $\pi_s p^T$ [MeV/c] < 320.50	-1.0828 \pm 0.6284	0.7864 \pm 1.0807	-1.8691 \pm 1.2501	1.29
320.50 < $\pi_s p^T$ [MeV/c] < 365.50	-1.1023 \pm 0.5417	-1.3561 \pm 0.9329	0.2538 \pm 1.0787	0.53
365.50 < $\pi_s p^T$ [MeV/c] < 428.50	-0.4595 \pm 0.4394	0.0391 \pm 0.7630	-0.4986 \pm 0.8805	0.24
428.50 < $\pi_s p^T$ [MeV/c] < 516.50	-0.5306 \pm 0.3496	-0.9788 \pm 0.6155	0.4482 \pm 0.7078	1.15
516.50 < $\pi_s p^T$ [MeV/c] < 654.50	-0.4828 \pm 0.2906	0.3093 \pm 0.5274	-0.7922 \pm 0.6022	0.93
654.50 < $\pi_s p^T$ [MeV/c] < 4000.00	-0.5202 \pm 0.2544	0.1958 \pm 0.4760	-0.7160 \pm 0.5397	0.92

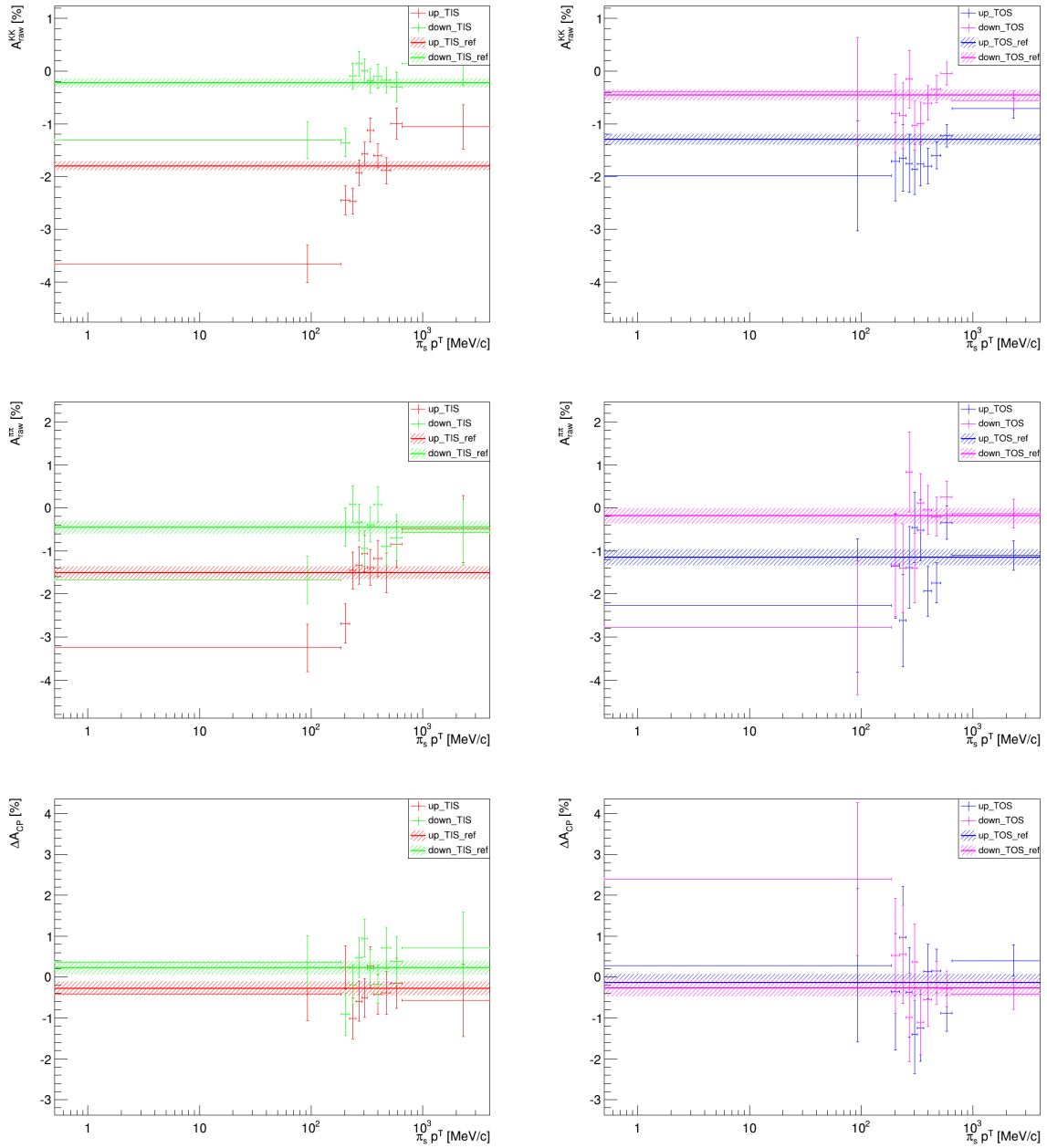


Figure A.27.: A_{raw} vs. $\pi_s p_T$, separated by magnetic field polarity and trigger setting for 2012 data.

Table A.10.: Results of the individual asymmetries in the different $\pi_s p_T$ bins, separated by magnetic field polarity and trigger for 2012 data. Highest significance: 2.29

Sample	$A_{raw}(KK)[\%]$	$A_{raw}(\pi\pi)[\%]$	$\Delta A_{CP}[\%]$	significance
up TIS	-1.7988 \pm 0.0825	-1.5120 \pm 0.1487	-0.2868 \pm 0.1700	-
0.50 < $\pi_s p^T$ [MeV/c] < 185.50	-3.6608 \pm 0.3524	-3.2502 \pm 0.5515	-0.4106 \pm 0.6545	0.20
185.50 < $\pi_s p^T$ [MeV/c] < 222.50	-2.4528 \pm 0.2722	-2.6846 \pm 0.4577	0.2318 \pm 0.5325	1.03
222.50 < $\pi_s p^T$ [MeV/c] < 254.50	-2.4676 \pm 0.2458	-1.4537 \pm 0.4317	-1.0139 \pm 0.4968	1.56
254.50 < $\pi_s p^T$ [MeV/c] < 285.50	-1.9279 \pm 0.2372	-1.3356 \pm 0.4296	-0.5923 \pm 0.4908	0.66
285.50 < $\pi_s p^T$ [MeV/c] < 320.50	-1.5743 \pm 0.2275	-1.0654 \pm 0.4181	-0.5089 \pm 0.4760	0.50
320.50 < $\pi_s p^T$ [MeV/c] < 365.50	-1.1208 \pm 0.2243	-1.3839 \pm 0.4144	0.2631 \pm 0.4712	1.25
365.50 < $\pi_s p^T$ [MeV/c] < 428.50	-1.6022 \pm 0.2291	-1.1756 \pm 0.4247	-0.4266 \pm 0.4825	0.31
428.50 < $\pi_s p^T$ [MeV/c] < 516.50	-1.8896 \pm 0.2452	-1.5067 \pm 0.4577	-0.3829 \pm 0.5192	0.20
516.50 < $\pi_s p^T$ [MeV/c] < 654.50	-0.9938 \pm 0.2910	-0.8447 \pm 0.5410	-0.1491 \pm 0.6143	0.23
654.50 < $\pi_s p^T$ [MeV/c] < 4000.00	-1.0570 \pm 0.4174	-0.4886 \pm 0.7829	-0.5684 \pm 0.8872	0.32
down TIS	-0.2274 \pm 0.0814	-0.4563 \pm 0.1456	0.2289 \pm 0.1669	-
0.50 < $\pi_s p^T$ [MeV/c] < 185.50	-1.3074 \pm 0.3489	-1.6681 \pm 0.5451	0.3607 \pm 0.6472	0.21
185.50 < $\pi_s p^T$ [MeV/c] < 222.50	-1.3540 \pm 0.2683	-0.4416 \pm 0.4512	-0.9124 \pm 0.5249	2.29
222.50 < $\pi_s p^T$ [MeV/c] < 254.50	-0.0950 \pm 0.2435	0.0909 \pm 0.4243	-0.1859 \pm 0.4892	0.90
254.50 < $\pi_s p^T$ [MeV/c] < 285.50	0.1448 \pm 0.2342	-0.3316 \pm 0.4216	0.4765 \pm 0.4823	0.55
285.50 < $\pi_s p^T$ [MeV/c] < 320.50	0.0080 \pm 0.2241	-0.9415 \pm 0.4077	0.9494 \pm 0.4653	1.66
320.50 < $\pi_s p^T$ [MeV/c] < 365.50	-0.1849 \pm 0.2217	-0.3918 \pm 0.4043	0.2070 \pm 0.4611	0.05
365.50 < $\pi_s p^T$ [MeV/c] < 428.50	-0.0988 \pm 0.2262	0.0798 \pm 0.4143	-0.1786 \pm 0.4720	0.92
428.50 < $\pi_s p^T$ [MeV/c] < 516.50	-0.1704 \pm 0.2414	-0.8859 \pm 0.4476	0.7155 \pm 0.5085	1.01
516.50 < $\pi_s p^T$ [MeV/c] < 654.50	-0.3029 \pm 0.2878	-0.6873 \pm 0.5330	0.3845 \pm 0.6058	0.27
654.50 < $\pi_s p^T$ [MeV/c] < 4000.00	0.1420 \pm 0.4152	-0.5680 \pm 0.7708	0.7101 \pm 0.8755	0.56
up TOS	-1.2968 \pm 0.1031	-1.1535 \pm 0.1847	-0.1432 \pm 0.2115	-
0.50 < $\pi_s p^T$ [MeV/c] < 185.50	-1.9867 \pm 1.0447	-2.2699 \pm 1.5532	0.2833 \pm 1.8718	0.23
185.50 < $\pi_s p^T$ [MeV/c] < 222.50	-1.7155 \pm 0.7455	-1.3539 \pm 1.2123	-0.3617 \pm 1.4231	0.16
222.50 < $\pi_s p^T$ [MeV/c] < 254.50	-1.6500 \pm 0.6330	-2.6216 \pm 1.0695	0.9717 \pm 1.2428	0.91
254.50 < $\pi_s p^T$ [MeV/c] < 285.50	-1.7518 \pm 0.5517	-1.3842 \pm 0.9495	-0.3675 \pm 1.0981	0.21
285.50 < $\pi_s p^T$ [MeV/c] < 320.50	-1.8616 \pm 0.4746	-0.4566 \pm 0.8201	-1.4050 \pm 0.9475	1.37
320.50 < $\pi_s p^T$ [MeV/c] < 365.50	-1.7651 \pm 0.4136	-0.5229 \pm 0.7072	-1.2421 \pm 0.8192	1.39
365.50 < $\pi_s p^T$ [MeV/c] < 428.50	-1.7992 \pm 0.3353	-1.9363 \pm 0.5801	0.1371 \pm 0.6701	0.44
428.50 < $\pi_s p^T$ [MeV/c] < 516.50	-1.5961 \pm 0.2628	-1.7449 \pm 0.4644	0.1489 \pm 0.5336	0.60
516.50 < $\pi_s p^T$ [MeV/c] < 654.50	-1.2254 \pm 0.2152	-0.3444 \pm 0.3889	-0.8810 \pm 0.4445	1.89
654.50 < $\pi_s p^T$ [MeV/c] < 4000.00	-0.7042 \pm 0.1826	-1.1055 \pm 0.3377	0.4013 \pm 0.3839	1.70
down TOS	-0.4554 \pm 0.1028	-0.1838 \pm 0.1812	-0.2716 \pm 0.2083	-
0.50 < $\pi_s p^T$ [MeV/c] < 185.50	-0.3858 \pm 1.0294	-2.7823 \pm 1.5531	2.3965 \pm 1.8633	1.44
185.50 < $\pi_s p^T$ [MeV/c] < 222.50	-0.7978 \pm 0.7388	-1.3201 \pm 1.1964	0.5224 \pm 1.4061	0.57
222.50 < $\pi_s p^T$ [MeV/c] < 254.50	-0.8419 \pm 0.6231	-1.3957 \pm 1.0321	0.5538 \pm 1.2056	0.70
254.50 < $\pi_s p^T$ [MeV/c] < 285.50	-0.1541 \pm 0.5487	0.8371 \pm 0.9354	-0.9912 \pm 1.0845	0.68
285.50 < $\pi_s p^T$ [MeV/c] < 320.50	-1.0333 \pm 0.4698	-1.4027 \pm 0.8051	0.3693 \pm 0.9321	0.71
320.50 < $\pi_s p^T$ [MeV/c] < 365.50	-0.9902 \pm 0.4078	0.1110 \pm 0.6854	-1.1011 \pm 0.7976	1.08
365.50 < $\pi_s p^T$ [MeV/c] < 428.50	-0.6027 \pm 0.3318	-0.0501 \pm 0.5692	-0.5527 \pm 0.6588	0.45
428.50 < $\pi_s p^T$ [MeV/c] < 516.50	-0.3417 \pm 0.2599	-0.2040 \pm 0.4564	-0.1377 \pm 0.5252	0.28
516.50 < $\pi_s p^T$ [MeV/c] < 654.50	-0.0451 \pm 0.2131	0.2470 \pm 0.3811	-0.2921 \pm 0.4366	0.05
654.50 < $\pi_s p^T$ [MeV/c] < 4000.00	-0.5527 \pm 0.1818	-0.1336 \pm 0.3314	-0.4191 \pm 0.3780	0.47

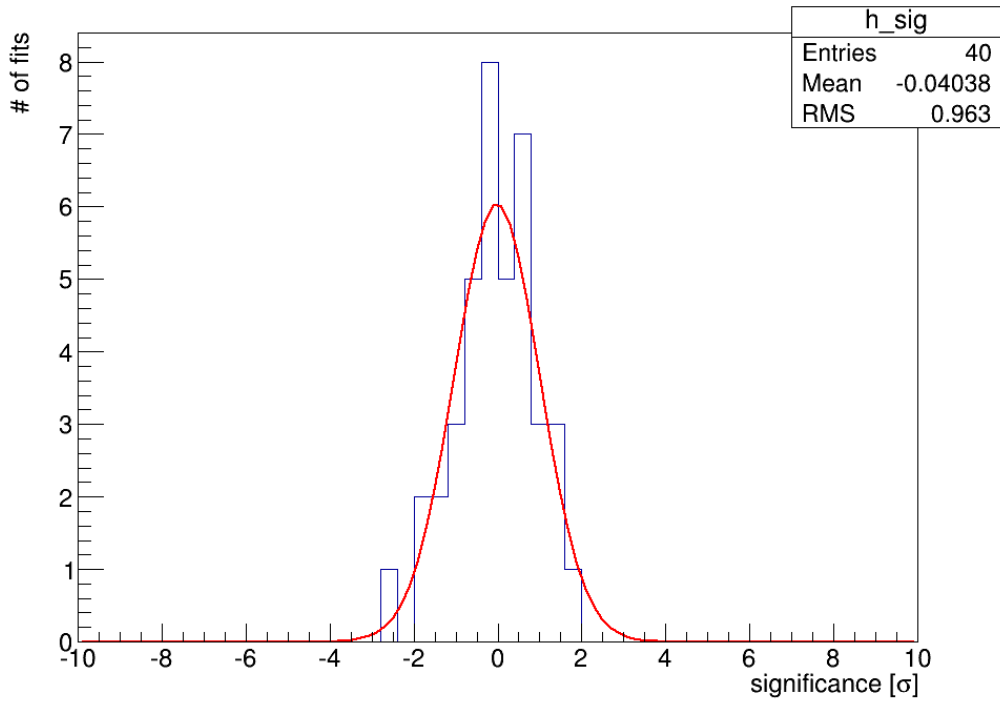
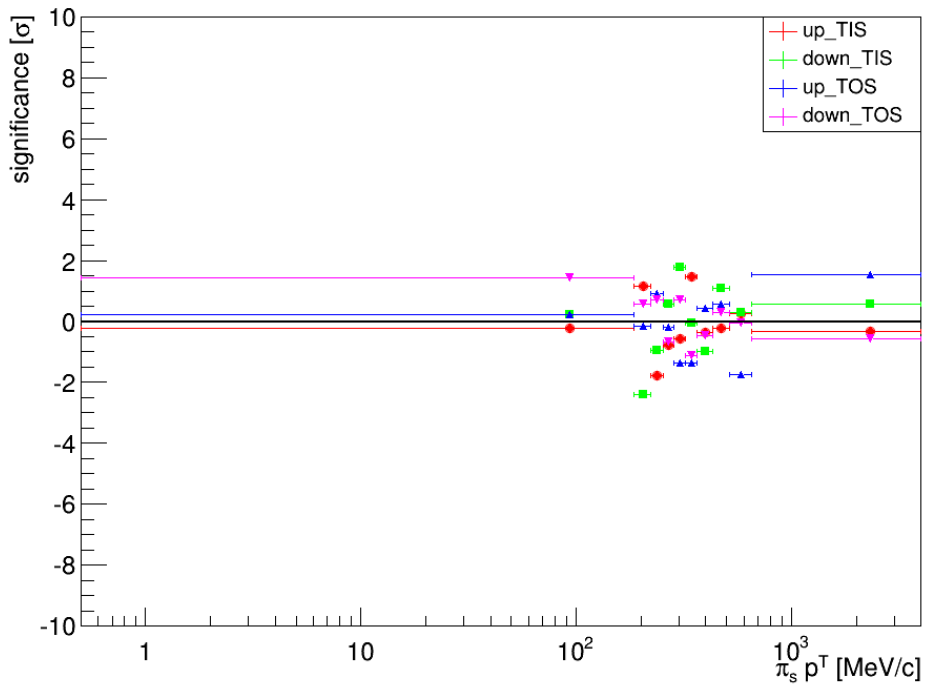


Figure A.28.: Significance vs. $\pi_s p_T$ (top) and histogram of significances (bottom) for 2012 data.

A.7. Separation in phase space

In Fig. A.29 and A.31 the individual asymmetries and ΔA_{CP} versus the ΔR can be found for 2011 and 2012, respectively. The significances of the deviations of results from the baseline result in that class of magnetic polarity and trigger can be found in Fig. A.30 and A.32. In Tab. A.11 and A.12 the results are shown for 2011 and 2012, respectively.

Table A.11.: Results of the individual asymmetries in the different ΔR bins, separated by magnetic field polarity and trigger for 2011 data. Highest significance: 2.63

Sample	$A_{raw}(KK)[\%]$	$A_{raw}(\pi\pi)[\%]$	$\Delta A_{CP}[\%]$	significance
up TIS	-1.8660 ± 0.1368	-1.6779 ± 0.2505	-0.1881 ± 0.2854	-
$0.00 < \Delta R < 0.01$	-1.5700 ± 2.4542	3.0633 ± 4.4302	-4.6333 ± 5.0646	0.88
$0.01 < \Delta R < 0.02$	-2.3384 ± 1.1394	-3.4690 ± 2.1059	1.1306 ± 2.3944	0.55
$0.02 < \Delta R < 0.04$	0.3140 ± 0.8230	-2.9887 ± 1.5328	3.3026 ± 1.7398	2.03
$0.04 < \Delta R < 0.05$	-0.5826 ± 0.6721	0.1892 ± 1.2260	-0.7718 ± 1.3981	0.43
$0.05 < \Delta R < 0.06$	-1.6450 ± 0.5479	-2.0333 ± 1.0174	0.3883 ± 1.1556	0.51
$0.06 < \Delta R < 0.08$	-2.1882 ± 0.4462	-0.9962 ± 0.8298	-1.1920 ± 0.9421	1.12
$0.08 < \Delta R < 0.09$	-1.9889 ± 0.3637	-2.5176 ± 0.6712	0.5288 ± 0.7634	1.01
$0.09 < \Delta R < 0.12$	-1.7871 ± 0.3069	-2.2479 ± 0.5642	0.4608 ± 0.6423	1.13
$0.12 < \Delta R < 0.16$	-2.3226 ± 0.2776	-0.8186 ± 0.5047	-1.5040 ± 0.5760	2.63
$0.16 < \Delta R < 1.00$	-2.5099 ± 0.3611	-2.2571 ± 0.5971	-0.2528 ± 0.6978	0.10
down TIS	-0.0274 ± 0.1151	-0.0383 ± 0.2102	0.0109 ± 0.2397	-
$0.00 < \Delta R < 0.01$	2.6990 ± 2.0105	-6.5569 ± 3.8222	9.2558 ± 4.3187	2.14
$0.01 < \Delta R < 0.02$	0.1623 ± 0.9607	0.7179 ± 1.7815	-0.5556 ± 2.0240	0.28
$0.02 < \Delta R < 0.04$	-1.1590 ± 0.6891	-1.0808 ± 1.2833	-0.0783 ± 1.4566	0.06
$0.04 < \Delta R < 0.05$	0.1957 ± 0.5651	0.5860 ± 1.0342	-0.3903 ± 1.1785	0.35
$0.05 < \Delta R < 0.06$	-0.3096 ± 0.4587	-0.6207 ± 0.8572	0.3111 ± 0.9722	0.32
$0.06 < \Delta R < 0.08$	-0.0784 ± 0.3735	0.2926 ± 0.6887	-0.3710 ± 0.7835	0.51
$0.08 < \Delta R < 0.09$	-0.1961 ± 0.3051	-0.0494 ± 0.5694	-0.1467 ± 0.6460	0.26
$0.09 < \Delta R < 0.12$	-0.0620 ± 0.2580	0.8869 ± 0.4732	-0.9489 ± 0.5390	1.99
$0.12 < \Delta R < 0.16$	-0.0404 ± 0.2333	-0.3013 ± 0.4225	0.2609 ± 0.4826	0.60
$0.16 < \Delta R < 1.00$	0.1314 ± 0.3035	-0.6330 ± 0.5004	0.7644 ± 0.5853	1.41
up TOS	-1.3870 ± 0.1665	-1.0138 ± 0.3011	-0.3732 ± 0.3440	-
$0.00 < \Delta R < 0.01$	1.1436 ± 1.6890	-1.2138 ± 3.0479	2.3574 ± 3.4846	0.79
$0.01 < \Delta R < 0.02$	-1.0414 ± 0.8088	1.6369 ± 1.4716	-2.6783 ± 1.6792	1.40
$0.02 < \Delta R < 0.04$	-1.4683 ± 0.5807	-1.3477 ± 1.0550	-0.1207 ± 1.2043	0.22
$0.04 < \Delta R < 0.05$	-0.4320 ± 0.4643	-0.7873 ± 0.8534	0.3554 ± 0.9715	0.80
$0.05 < \Delta R < 0.06$	-0.8648 ± 0.4011	-0.8031 ± 0.7290	-0.0616 ± 0.8321	0.41
$0.06 < \Delta R < 0.08$	-1.5865 ± 0.3897	-1.9718 ± 0.6985	0.3853 ± 0.7999	1.05
$0.08 < \Delta R < 0.09$	-1.4781 ± 0.4219	-1.7378 ± 0.7432	0.2597 ± 0.8546	0.81
$0.09 < \Delta R < 0.12$	-2.1281 ± 0.5095	0.1650 ± 0.8819	-2.2931 ± 1.0185	2.00
$0.12 < \Delta R < 0.16$	-2.3482 ± 0.6520	-0.1325 ± 1.0940	-2.2157 ± 1.2736	1.50
$0.16 < \Delta R < 1.00$	-3.0937 ± 1.0859	-2.9550 ± 1.7065	-0.1387 ± 2.0227	0.12
down TOS	-0.5525 ± 0.1383	-0.2554 ± 0.2507	-0.2971 ± 0.2863	-
$0.00 < \Delta R < 0.01$	2.5292 ± 1.3757	-0.8406 ± 2.5479	3.3699 ± 2.8956	1.27
$0.01 < \Delta R < 0.02$	0.9599 ± 0.6687	0.8718 ± 1.2342	0.0881 ± 1.4037	0.28
$0.02 < \Delta R < 0.04$	-0.9513 ± 0.4822	0.7860 ± 0.8801	-1.7373 ± 1.0036	1.50
$0.04 < \Delta R < 0.05$	-0.3671 ± 0.3856	-1.2438 ± 0.7135	0.8767 ± 0.8110	1.55
$0.05 < \Delta R < 0.06$	-1.1689 ± 0.3330	-0.2042 ± 0.6121	-0.9648 ± 0.6968	1.05
$0.06 < \Delta R < 0.08$	-0.1662 ± 0.3243	0.1901 ± 0.5857	-0.3563 ± 0.6695	0.10
$0.08 < \Delta R < 0.09$	-1.0842 ± 0.3508	0.3510 ± 0.6191	-1.4352 ± 0.7116	1.75
$0.09 < \Delta R < 0.12$	-0.9700 ± 0.4213	-1.3175 ± 0.7196	0.3474 ± 0.8338	0.82
$0.12 < \Delta R < 0.16$	-0.2959 ± 0.5317	-0.8225 ± 0.9026	0.5267 ± 1.0476	0.82
$0.16 < \Delta R < 1.00$	-1.8280 ± 0.9042	-1.4599 ± 1.3832	-0.3682 ± 1.6525	0.04

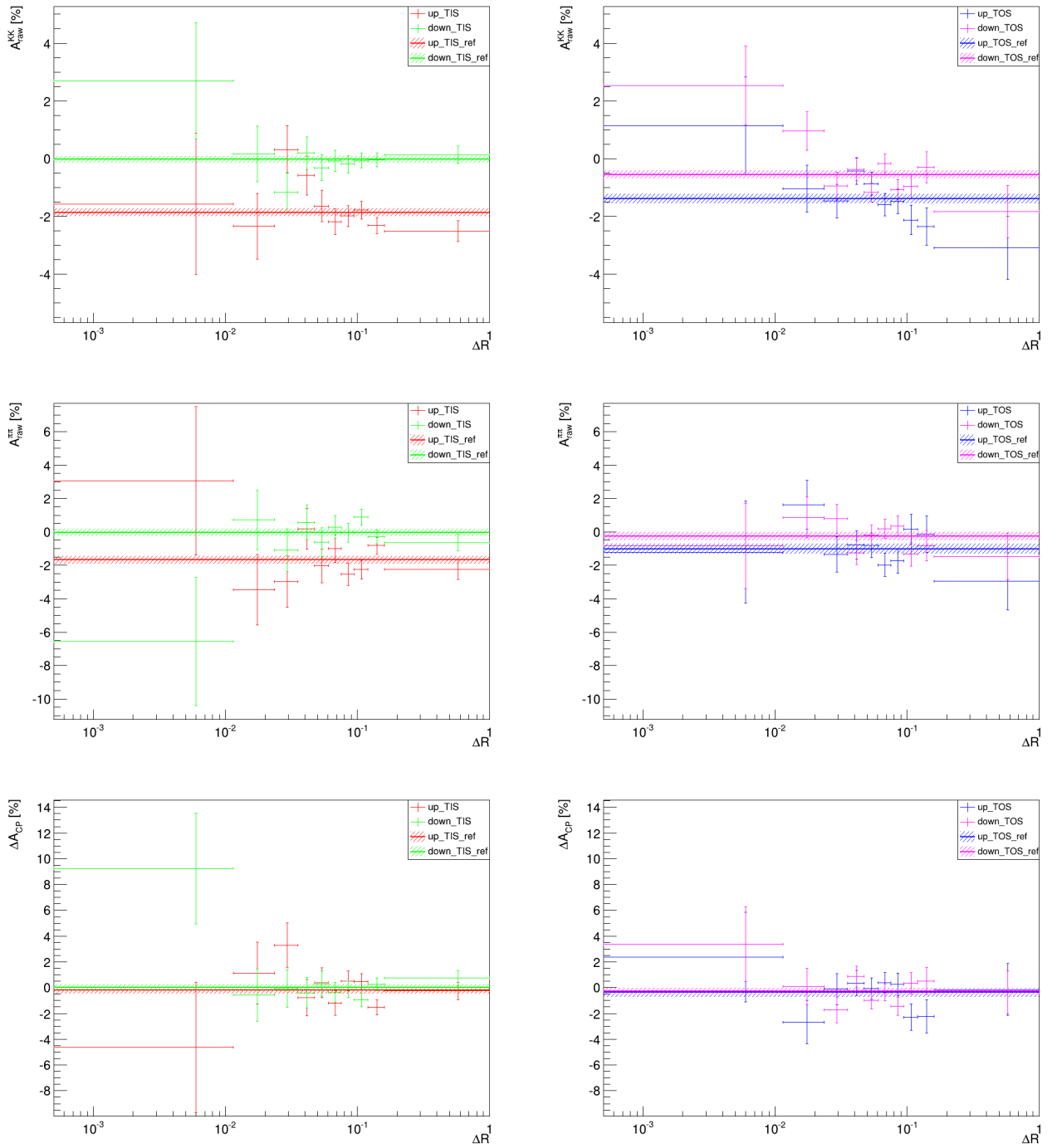


Figure A.29.: A_{raw} vs. ΔR , separated by magnetic field polarity and trigger setting for 2011 data.

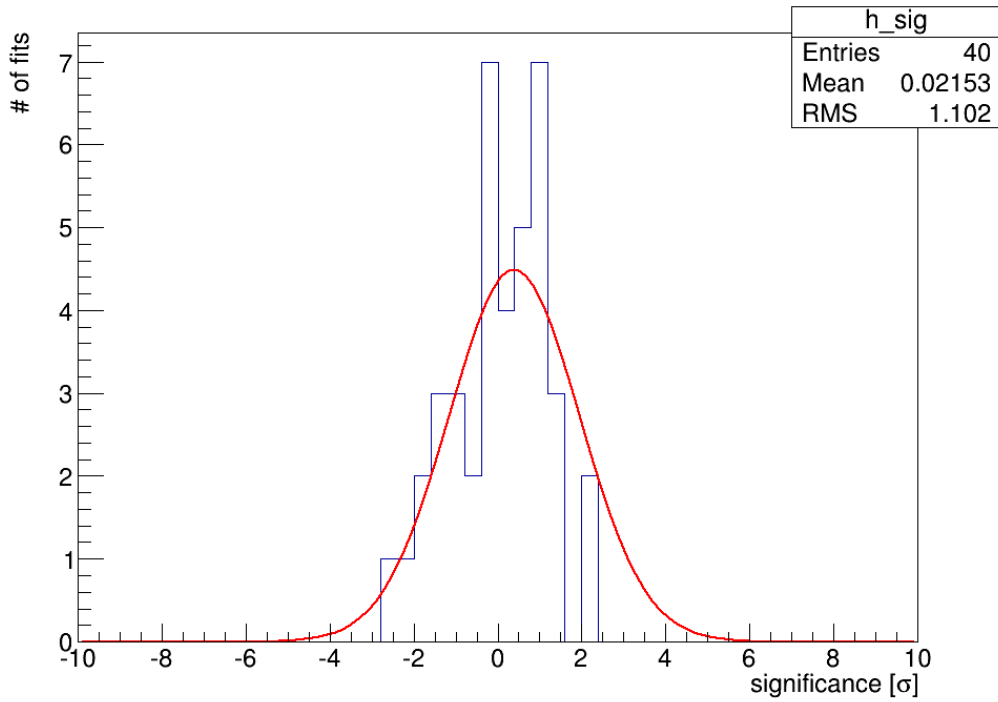
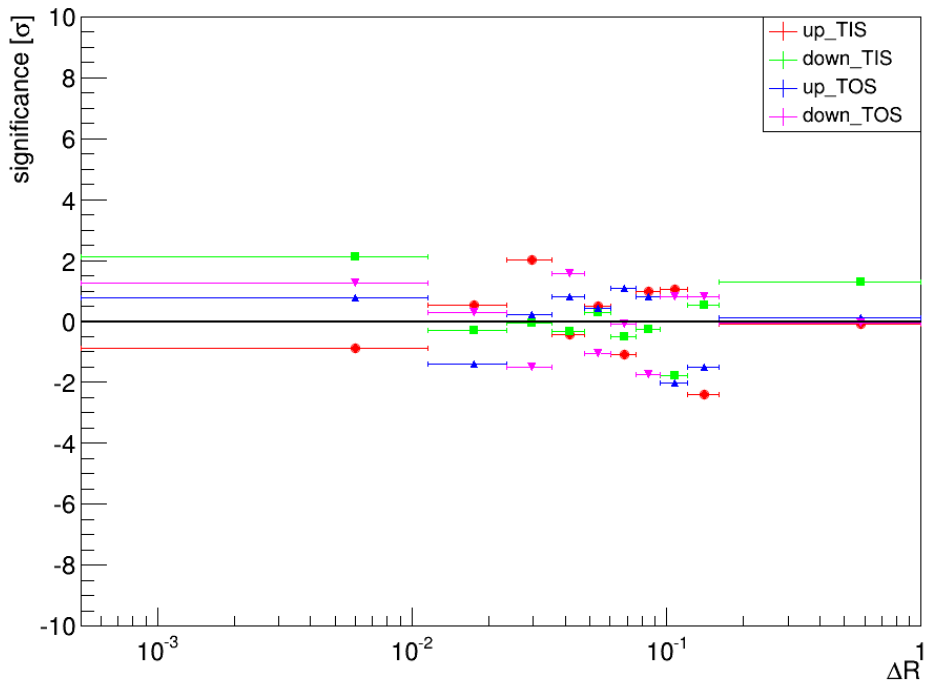


Figure A.30.: Significance vs. ΔR (top) and histogram of significances (bottom) for 2011 data.

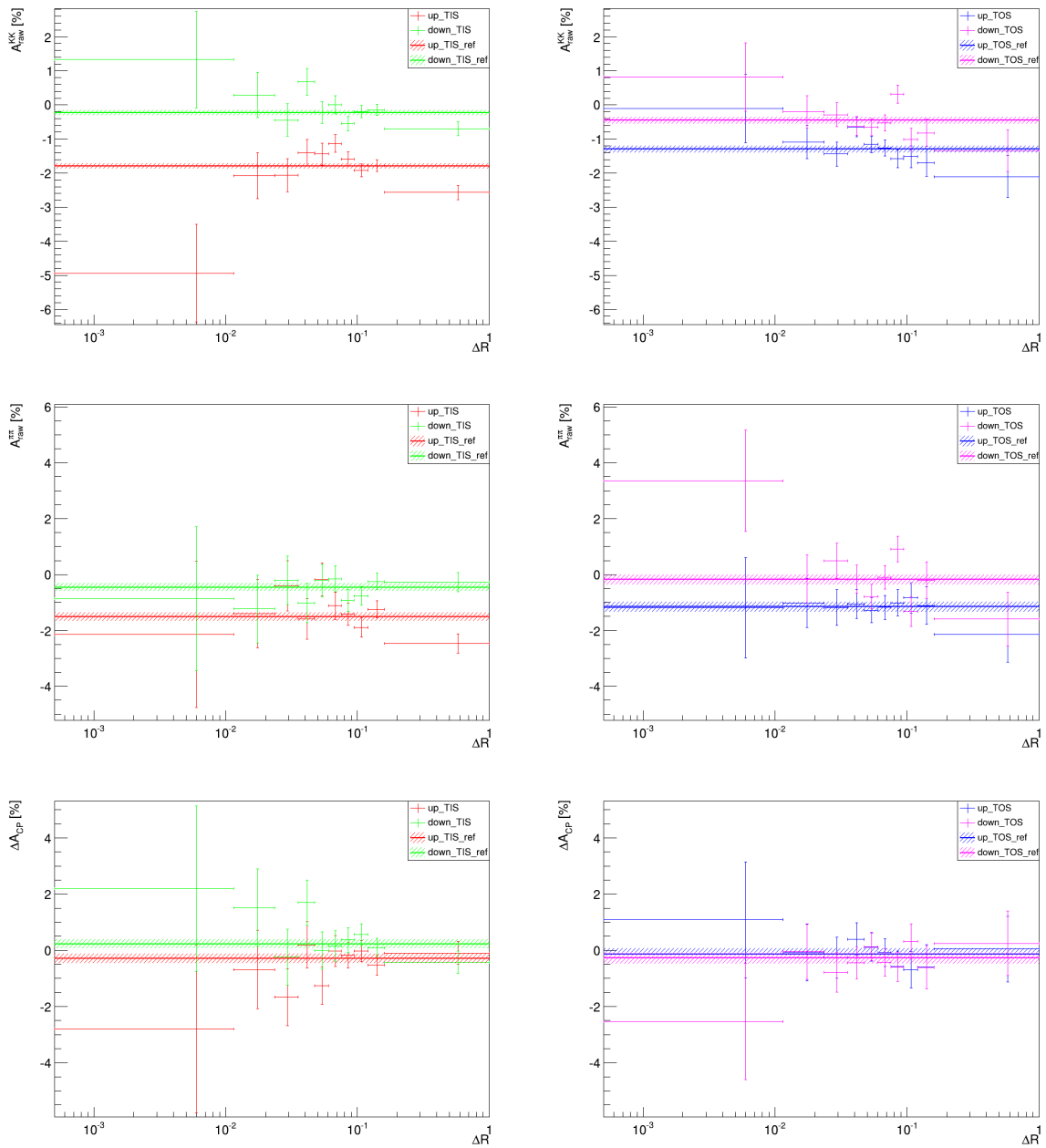


Figure A.31.: A_{raw} vs. ΔR , separated by magnetic field polarity and trigger setting for 2012 data.

Table A.12.: Results of the individual asymmetries in the different ΔR bins, separated by magnetic field polarity and trigger for 2012 data. Highest significance: 1.85

Sample	$A_{raw}(KK)[\%]$	$A_{raw}(\pi\pi)[\%]$	$\Delta A_{CP}[\%]$	significance
up TIS	-1.7988 ± 0.0825	-1.5120 ± 0.1487	-0.2868 ± 0.1700	-
$0.00 < \Delta R < 0.01$	-4.9352 ± 1.4311	-2.1410 ± 2.6110	-2.7942 ± 2.9775	0.84
$0.01 < \Delta R < 0.02$	-2.0803 ± 0.6746	-1.3987 ± 1.2274	-0.6816 ± 1.4005	0.28
$0.02 < \Delta R < 0.04$	-2.0610 ± 0.4805	-0.4018 ± 0.8955	-1.6592 ± 1.0163	1.37
$0.04 < \Delta R < 0.05$	-1.4011 ± 0.3927	-1.5908 ± 0.7299	0.1897 ± 0.8288	0.59
$0.05 < \Delta R < 0.06$	-1.4383 ± 0.3197	-0.1803 ± 0.5913	-1.2580 ± 0.6722	1.49
$0.06 < \Delta R < 0.08$	-1.1330 ± 0.2624	-1.1160 ± 0.4849	-0.0171 ± 0.5513	0.51
$0.08 < \Delta R < 0.09$	-1.5867 ± 0.2162	-1.4126 ± 0.3981	-0.1740 ± 0.4531	0.27
$0.09 < \Delta R < 0.12$	-1.9223 ± 0.1835	-1.8933 ± 0.3366	-0.0289 ± 0.3833	0.75
$0.12 < \Delta R < 0.16$	-1.7773 ± 0.1672	-1.2516 ± 0.3026	-0.5257 ± 0.3457	0.79
$0.16 < \Delta R < 1.00$	-2.5639 ± 0.2104	-2.4658 ± 0.3486	-0.0982 ± 0.4072	0.51
down TIS	-0.2274 ± 0.0814	-0.4563 ± 0.1456	0.2289 ± 0.1669	-
$0.00 < \Delta R < 0.01$	1.3283 ± 1.4129	-0.8665 ± 2.5827	2.1949 ± 2.9439	0.67
$0.01 < \Delta R < 0.02$	0.2876 ± 0.6650	-1.2326 ± 1.2126	1.5203 ± 1.3830	0.94
$0.02 < \Delta R < 0.04$	-0.4434 ± 0.4750	-0.2082 ± 0.8746	-0.2351 ± 0.9952	0.47
$0.04 < \Delta R < 0.05$	0.6825 ± 0.3890	-1.0142 ± 0.7123	1.6967 ± 0.8116	1.85
$0.05 < \Delta R < 0.06$	-0.2198 ± 0.3169	-0.2160 ± 0.5837	-0.0039 ± 0.6642	0.36
$0.06 < \Delta R < 0.08$	0.0043 ± 0.2594	-0.1501 ± 0.4744	0.1543 ± 0.5407	0.15
$0.08 < \Delta R < 0.09$	-0.5498 ± 0.2132	-0.9226 ± 0.3908	0.3728 ± 0.4452	0.35
$0.09 < \Delta R < 0.12$	-0.1930 ± 0.1810	-0.7589 ± 0.3281	0.5659 ± 0.3747	1.00
$0.12 < \Delta R < 0.16$	-0.1487 ± 0.1648	-0.2448 ± 0.2959	0.0962 ± 0.3388	0.45
$0.16 < \Delta R < 1.00$	-0.6974 ± 0.2083	-0.2694 ± 0.3436	-0.4280 ± 0.4018	1.80
up TOS	-1.2968 ± 0.1031	-1.1535 ± 0.1847	-0.1432 ± 0.2115	-
$0.00 < \Delta R < 0.01$	-0.1052 ± 1.0031	-1.1952 ± 1.7974	1.0900 ± 2.0583	0.60
$0.01 < \Delta R < 0.02$	-1.0865 ± 0.4855	-1.0106 ± 0.8816	-0.0759 ± 1.0065	0.07
$0.02 < \Delta R < 0.04$	-1.4408 ± 0.3482	-1.1820 ± 0.6422	-0.2589 ± 0.7306	0.17
$0.04 < \Delta R < 0.05$	-0.6552 ± 0.2799	-1.0563 ± 0.5138	0.4011 ± 0.5851	1.00
$0.05 < \Delta R < 0.06$	-1.1576 ± 0.2438	-1.2754 ± 0.4433	0.1179 ± 0.5059	0.57
$0.06 < \Delta R < 0.08$	-1.2634 ± 0.2395	-1.1754 ± 0.4313	-0.0881 ± 0.4933	0.12
$0.08 < \Delta R < 0.09$	-1.5777 ± 0.2647	-1.0100 ± 0.4661	-0.5677 ± 0.5361	0.86
$0.09 < \Delta R < 0.12$	-1.5216 ± 0.3214	-0.8330 ± 0.5514	-0.6886 ± 0.6382	0.91
$0.12 < \Delta R < 0.16$	-1.6971 ± 0.3997	-1.1106 ± 0.6728	-0.5865 ± 0.7825	0.59
$0.16 < \Delta R < 1.00$	-2.1013 ± 0.6218	-2.1462 ± 0.9887	0.0448 ± 1.1680	0.16
down TOS	-0.4554 ± 0.1028	-0.1838 ± 0.1812	-0.2716 ± 0.2083	-
$0.00 < \Delta R < 0.01$	0.8210 ± 1.0005	3.3539 ± 1.8194	-2.5329 ± 2.0764	1.09
$0.01 < \Delta R < 0.02$	-0.2057 ± 0.4805	-0.1592 ± 0.8668	-0.0464 ± 0.9910	0.23
$0.02 < \Delta R < 0.04$	-0.2849 ± 0.3460	0.4944 ± 0.6242	-0.7793 ± 0.7137	0.74
$0.04 < \Delta R < 0.05$	-0.6161 ± 0.2788	-0.1716 ± 0.5044	-0.4446 ± 0.5763	0.32
$0.05 < \Delta R < 0.06$	-0.6488 ± 0.2412	-0.7856 ± 0.4353	0.1367 ± 0.4976	0.90
$0.06 < \Delta R < 0.08$	-0.5279 ± 0.2380	-0.0957 ± 0.4235	-0.4322 ± 0.4858	0.37
$0.08 < \Delta R < 0.09$	0.3150 ± 0.2614	0.9046 ± 0.4568	-0.5895 ± 0.5263	0.66
$0.09 < \Delta R < 0.12$	-1.0051 ± 0.3184	-1.3210 ± 0.5388	0.3158 ± 0.6259	1.00
$0.12 < \Delta R < 0.16$	-0.8191 ± 0.3937	-0.2076 ± 0.6603	-0.6115 ± 0.7687	0.46
$0.16 < \Delta R < 1.00$	-1.3420 ± 0.6167	-1.5917 ± 0.9648	0.2497 ± 1.1451	0.46

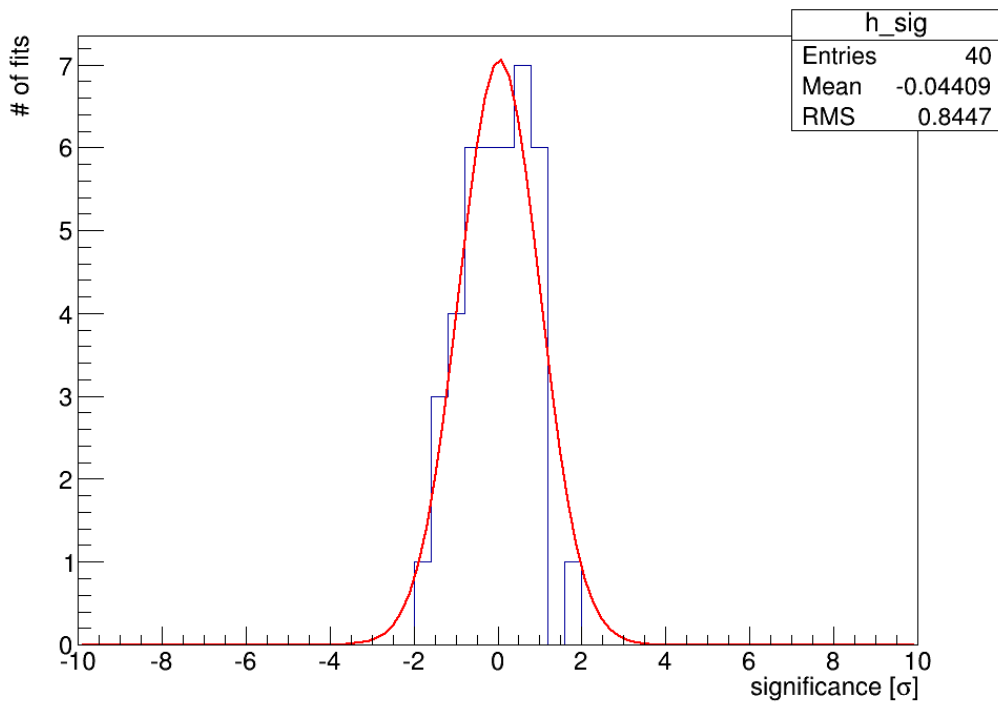
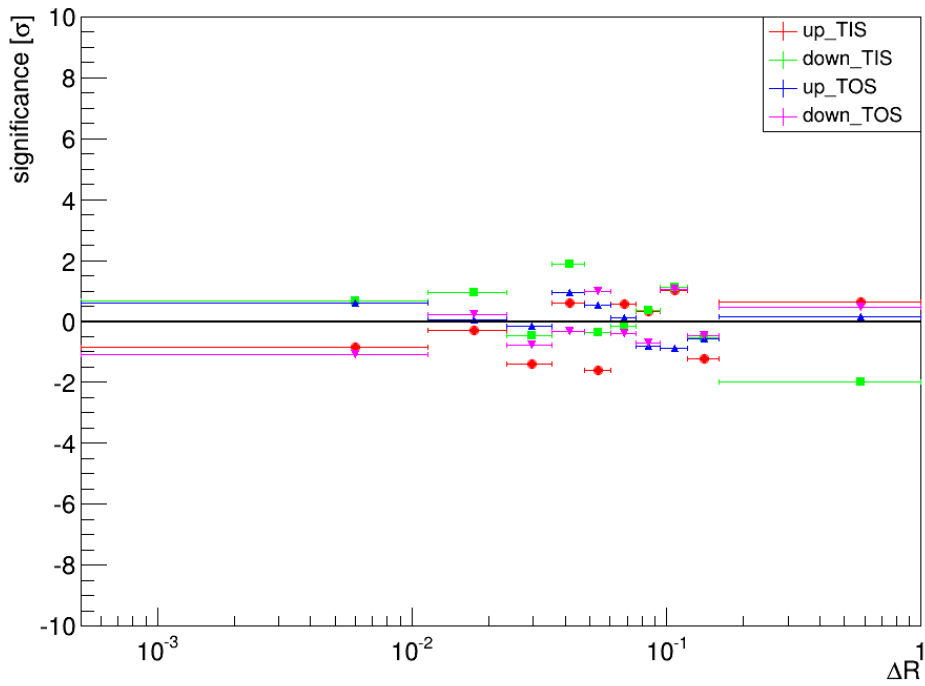


Figure A.32.: Significance vs. ΔR (top) and histogram of significances (bottom) for 2012 data.

A.8. D^0 flight distance

In Fig. A.33 and A.35 the individual asymmetries and ΔA_{CP} versus the D^0 flight distance can be found for 2011 and 2012, respectively. The significances of the deviations of results from the baseline result in that class of magnetic polarity and trigger can be found in Fig. A.34 and A.36. In Tab. A.13 and A.14 the results are shown for 2011 and 2012, respectively.

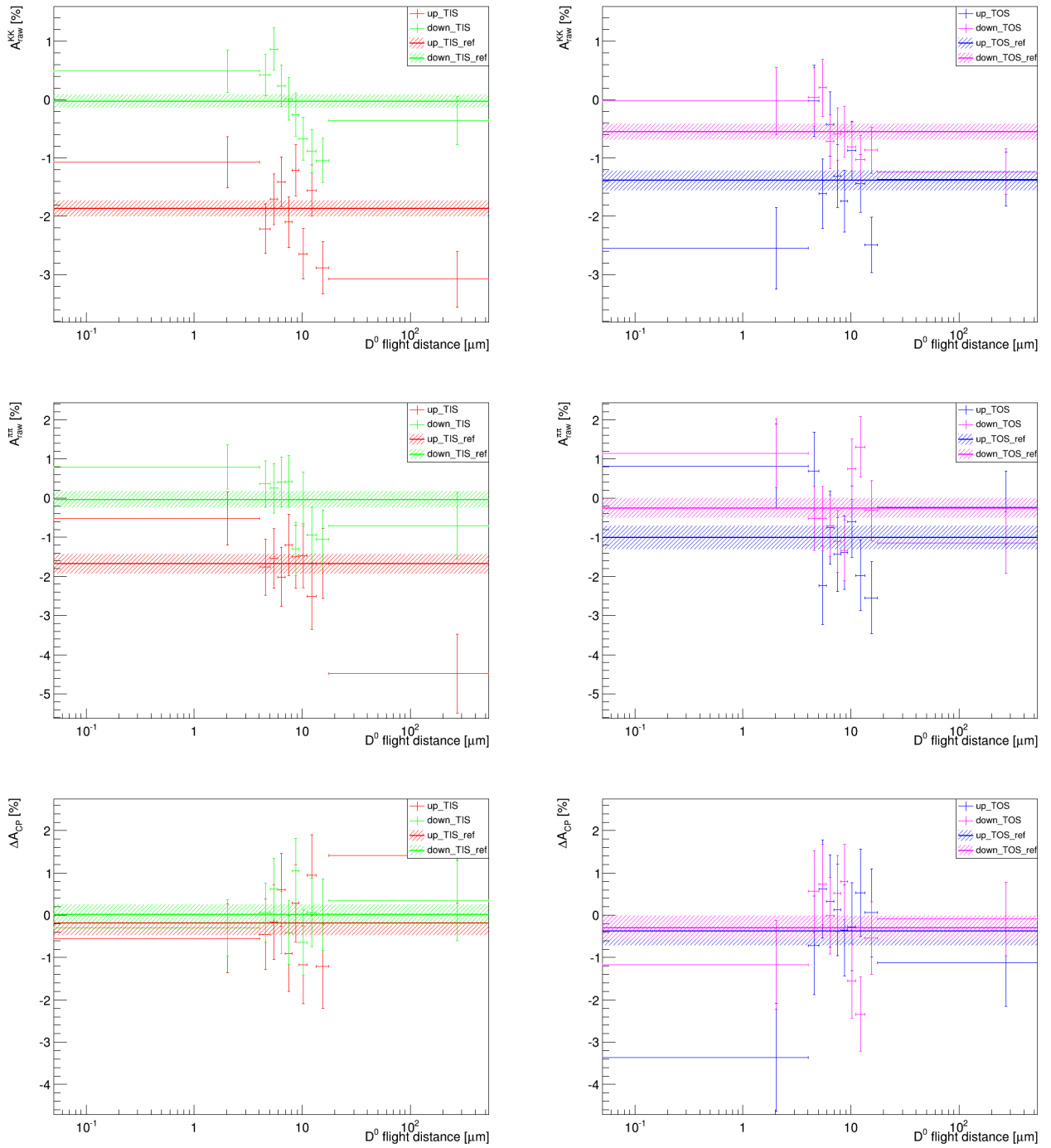


Figure A.33.: A_{raw} vs. D^0 flight distance, separated by magnetic field polarity and trigger setting for 2011 data.

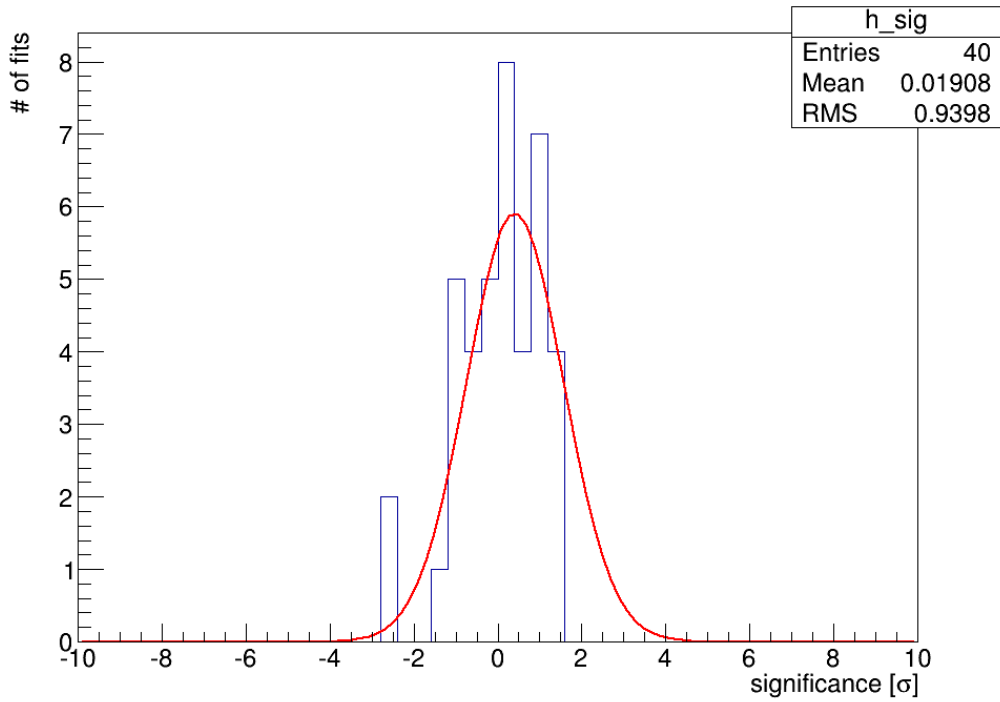
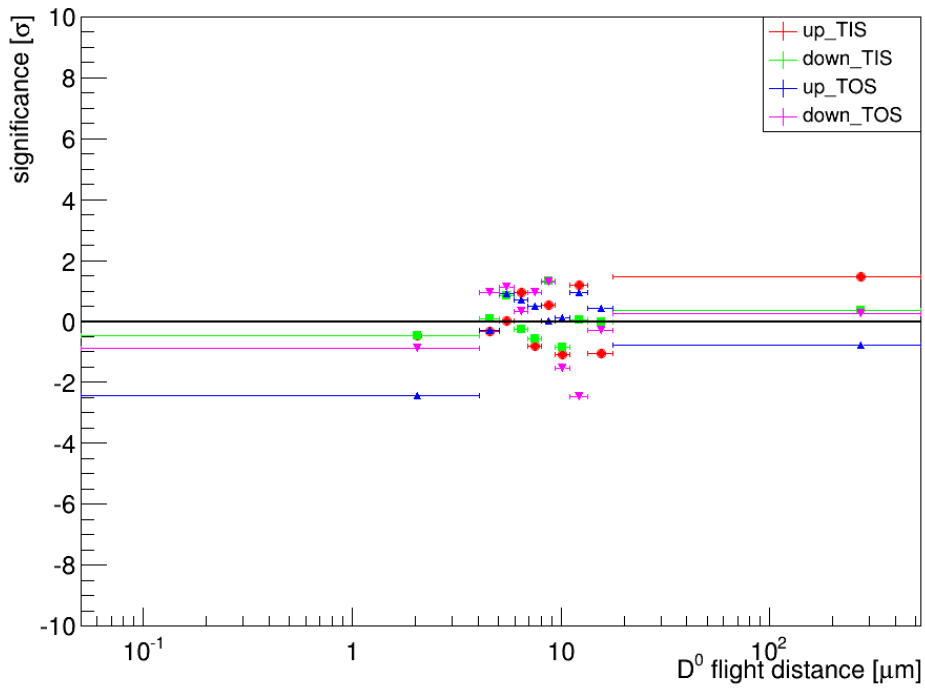


Figure A.34.: Significance vs. D^0 flight distance (top) and histogram of significances (bottom) for 2011 data.

Table A.13.: Results of the individual asymmetries in the different D^0 flight distance bins, separated by magnetic field polarity and trigger for 2011 data. Highest significance: 2.47.

Sample	$A_{raw}(KK)$ [%]	$A_{raw}(\pi\pi)$ [%]	ΔA_{CP} [%]	significance
up TIS				-
0.05 < D^0 flightdistance[#mum] < 4.05	-1.8660 ± 0.1368	-1.6779 ± 0.2505	-0.1881 ± 0.2854	0.48
4.05 < D^0 flightdistance[#mum] < 5.05	-2.2106 ± 0.4242	-1.7618 ± 0.7128	-0.4489 ± 0.8294	0.33
5.05 < D^0 flightdistance[#mum] < 5.95	-1.7060 ± 0.4363	-1.5439 ± 0.7603	-0.1621 ± 0.8766	0.03
5.95 < D^0 flightdistance[#mum] < 6.95	-1.4085 ± 0.4248	-2.0103 ± 0.7527	0.6019 ± 0.8643	0.97
6.95 < D^0 flightdistance[#mum] < 8.05	-2.1004 ± 0.4319	-1.1950 ± 0.7842	-0.9054 ± 0.8953	0.85
8.05 < D^0 flightdistance[#mum] < 9.35	-1.2120 ± 0.4365	-1.4973 ± 0.8006	0.2854 ± 0.9118	0.55
9.35 < D^0 flightdistance[#mum] < 11.05	-2.6421 ± 0.4320	-1.4688 ± 0.8133	-1.1733 ± 0.9209	1.13
11.05 < D^0 flightdistance[#mum] < 13.45	-1.5579 ± 0.4396	-2.5036 ± 0.8518	0.9457 ± 0.9585	1.24
13.45 < D^0 flightdistance[#mum] < 17.75	-2.8800 ± 0.4475	-1.6707 ± 0.8896	-1.2093 ± 0.9958	1.07
17.75 < D^0 flightdistance[#mum] < 530.00	-3.0772 ± 0.4802	-4.4854 ± 1.0068	1.4081 ± 1.1155	1.48
down TIS				-
0.05 < D^0 flightdistance[#mum] < 4.05	0.4864 ± 0.3597	0.7920 ± 0.5620	-0.3056 ± 0.6673	0.51
4.05 < D^0 flightdistance[#mum] < 5.05	0.4236 ± 0.3528	0.3591 ± 0.5902	0.0645 ± 0.6876	0.08
5.05 < D^0 flightdistance[#mum] < 5.95	0.8682 ± 0.3634	0.2514 ± 0.6309	0.6168 ± 0.7281	0.88
5.95 < D^0 flightdistance[#mum] < 6.95	0.2377 ± 0.3546	0.4117 ± 0.6353	-0.1741 ± 0.7276	0.27
6.95 < D^0 flightdistance[#mum] < 8.05	0.0153 ± 0.3632	0.4247 ± 0.6615	-0.4093 ± 0.7547	0.59
8.05 < D^0 flightdistance[#mum] < 9.35	-0.2551 ± 0.3679	-1.2967 ± 0.6822	1.0415 ± 0.7750	1.40
9.35 < D^0 flightdistance[#mum] < 11.05	-0.6692 ± 0.3665	-0.0238 ± 0.6883	-0.6453 ± 0.7798	0.88
11.05 < D^0 flightdistance[#mum] < 13.45	-0.8843 ± 0.3730	-0.9480 ± 0.7208	0.0636 ± 0.8116	0.07
13.45 < D^0 flightdistance[#mum] < 17.75	-1.0431 ± 0.3807	-1.0536 ± 0.7544	0.0106 ± 0.8450	0.00
17.75 < D^0 flightdistance[#mum] < 530.00	-0.3628 ± 0.4108	-0.7067 ± 0.8518	0.3439 ± 0.9457	0.36
up TOS				-
0.05 < D^0 flightdistance[#mum] < 4.05	-1.3870 ± 0.1665	-1.0138 ± 0.3011	-0.3732 ± 0.3440	2.41
4.05 < D^0 flightdistance[#mum] < 5.05	-2.5470 ± 0.6978	0.8122 ± 1.0772	-3.3591 ± 1.2835	0.30
5.05 < D^0 flightdistance[#mum] < 5.95	-0.0208 ± 0.6105	0.6904 ± 0.9947	-0.7112 ± 1.1671	0.89
5.95 < D^0 flightdistance[#mum] < 6.95	-1.6110 ± 0.5936	-2.2289 ± 0.9969	0.6179 ± 1.1603	0.69
6.95 < D^0 flightdistance[#mum] < 8.05	-0.4197 ± 0.5538	-0.7545 ± 0.9333	0.3348 ± 1.0852	0.48
8.05 < D^0 flightdistance[#mum] < 9.35	-1.3110 ± 0.5416	-1.4380 ± 0.9435	0.1270 ± 1.0879	0.02
9.35 < D^0 flightdistance[#mum] < 11.05	-1.7412 ± 0.5281	-1.3874 ± 0.9380	-0.3538 ± 1.0765	0.10
11.05 < D^0 flightdistance[#mum] < 13.45	-0.8739 ± 0.5065	-0.6034 ± 0.9132	-0.2704 ± 1.0443	0.93
13.45 < D^0 flightdistance[#mum] < 17.75	-1.4344 ± 0.4941	-1.9690 ± 0.9100	0.5346 ± 1.0355	0.44
17.75 < D^0 flightdistance[#mum] < 530.00	-2.4868 ± 0.4764	-2.5459 ± 0.9199	0.0591 ± 1.0359	0.77
down TOS				-
0.05 < D^0 flightdistance[#mum] < 4.05	-0.5525 ± 0.1383	-0.2554 ± 0.2507	-0.2971 ± 0.2863	0.86
4.05 < D^0 flightdistance[#mum] < 5.05	-0.0195 ± 0.5747	1.1466 ± 0.8751	-1.1661 ± 1.0470	0.94
5.05 < D^0 flightdistance[#mum] < 5.95	0.0429 ± 0.5032	-0.5196 ± 0.8159	0.5626 ± 0.9586	1.13
5.95 < D^0 flightdistance[#mum] < 6.95	0.2033 ± 0.4866	-0.5254 ± 0.8193	0.7287 ± 0.9529	0.33
6.95 < D^0 flightdistance[#mum] < 8.05	-0.7205 ± 0.4574	-0.7075 ± 0.7807	-0.0131 ± 0.9048	0.94
8.05 < D^0 flightdistance[#mum] < 9.35	-0.5878 ± 0.4441	-1.1000 ± 0.7909	0.5122 ± 0.9070	1.29
9.35 < D^0 flightdistance[#mum] < 11.05	-0.5455 ± 0.4368	-1.3376 ± 0.7774	0.7921 ± 0.8917	1.51
11.05 < D^0 flightdistance[#mum] < 13.45	-0.8096 ± 0.4218	0.7406 ± 0.7679	-1.5502 ± 0.8761	2.47
13.45 < D^0 flightdistance[#mum] < 17.75	-1.0291 ± 0.4125	1.3098 ± 0.7732	-2.3388 ± 0.8763	0.30
17.75 < D^0 flightdistance[#mum] < 530.00	-0.8643 ± 0.3987	-0.3212 ± 0.7630	-0.5431 ± 0.8609	0.25

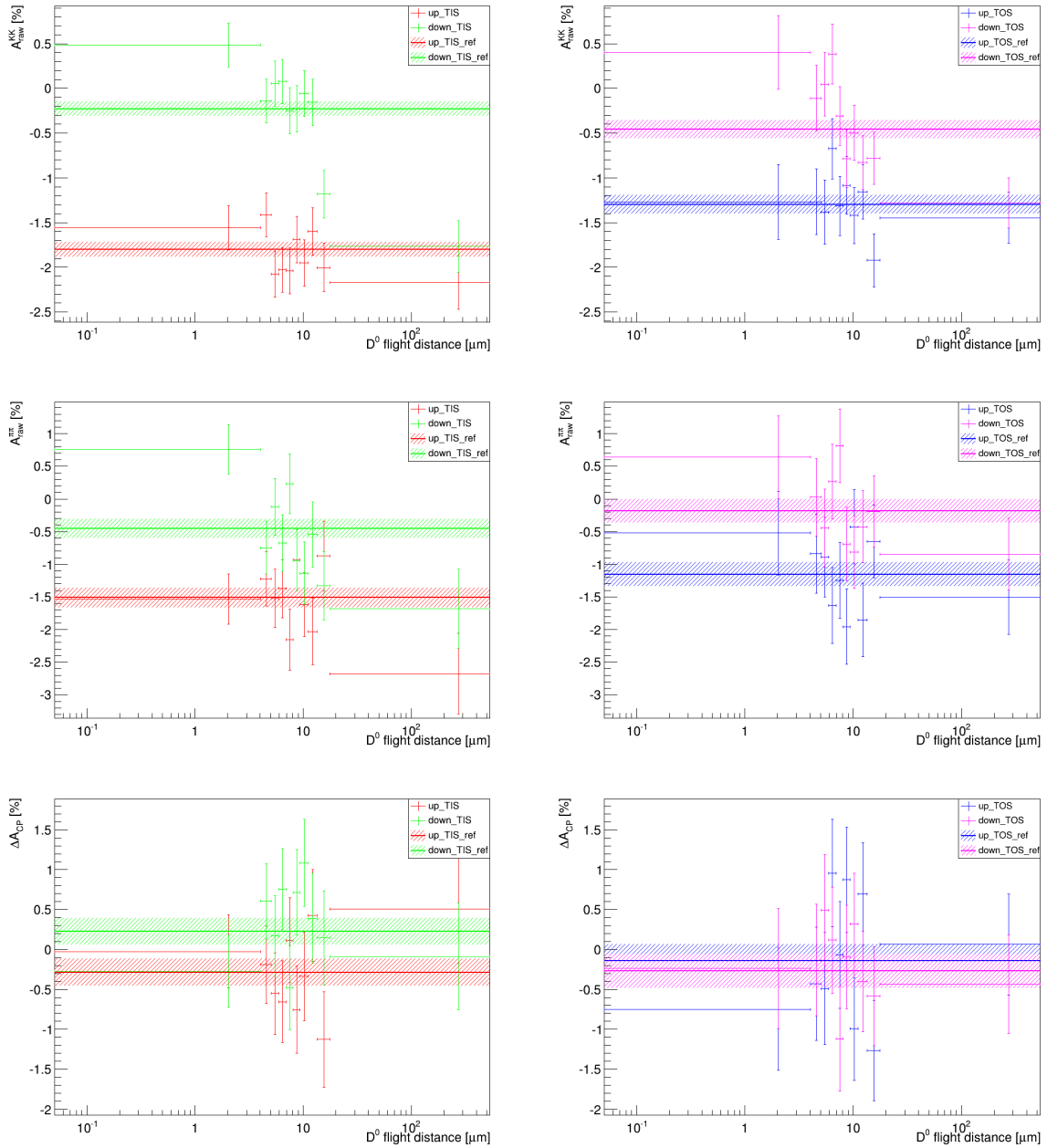


Figure A.35.: A_{raw} vs. D^0 flight distance, separated by magnetic field polarity and trigger setting for 2012 data.

Table A.14.: Results of the individual asymmetries in the different D^0 flight distance bins, separated by magnetic field polarity and trigger for 2012 data. Highest significance: 1.90

Sample	$A_{raw}(KK)$ [%]	$A_{raw}(\pi\pi)$ [%]	ΔA_{CP} [%]	significance
up TIS	-1.7988 ± 0.0825	-1.5120 ± 0.1487	-0.2868 ± 0.1700	-
0.05 < D^0 flightdistance[#mum] < 4.05	-1.5578 ± 0.2492	-1.5333 ± 0.3866	-0.0245 ± 0.4600	0.61
4.05 < D^0 flightdistance[#mum] < 5.05	-1.4104 ± 0.2457	-1.2205 ± 0.4167	-0.1900 ± 0.4838	0.21
5.05 < D^0 flightdistance[#mum] < 5.95	-2.0735 ± 0.2550	-1.5220 ± 0.4455	-0.5515 ± 0.5133	0.55
5.95 < D^0 flightdistance[#mum] < 6.95	-2.0254 ± 0.2506	-1.3708 ± 0.4461	-0.6546 ± 0.5117	0.76
6.95 < D^0 flightdistance[#mum] < 8.05	-2.0407 ± 0.2562	-2.1563 ± 0.4667	0.1155 ± 0.5324	0.80
8.05 < D^0 flightdistance[#mum] < 9.35	-1.6875 ± 0.2601	-0.9319 ± 0.4811	-0.7556 ± 0.5469	0.90
9.35 < D^0 flightdistance[#mum] < 11.05	-1.9505 ± 0.2605	-1.6152 ± 0.4920	-0.3354 ± 0.5567	0.09
11.05 < D^0 flightdistance[#mum] < 13.45	-1.5991 ± 0.2648	-2.0285 ± 0.5101	0.4294 ± 0.5747	1.30
13.45 < D^0 flightdistance[#mum] < 17.75	-2.0006 ± 0.2727	-0.8737 ± 0.5339	-1.1269 ± 0.5995	1.46
17.75 < D^0 flightdistance[#mum] < 530.00	-2.1705 ± 0.2973	-2.6780 ± 0.6179	0.5076 ± 0.6857	1.20
down TIS	-0.2274 ± 0.0814	-0.4563 ± 0.1456	0.2289 ± 0.1669	-
0.05 < D^0 flightdistance[#mum] < 4.05	0.4866 ± 0.2464	0.7600 ± 0.3807	-0.2734 ± 0.4535	1.19
4.05 < D^0 flightdistance[#mum] < 5.05	-0.1400 ± 0.2430	-0.7452 ± 0.4079	0.6053 ± 0.4748	0.85
5.05 < D^0 flightdistance[#mum] < 5.95	0.0542 ± 0.2520	-0.1161 ± 0.4348	0.1703 ± 0.5026	0.12
5.95 < D^0 flightdistance[#mum] < 6.95	0.0801 ± 0.2481	-0.6782 ± 0.4390	0.7583 ± 0.5042	1.11
6.95 < D^0 flightdistance[#mum] < 8.05	-0.2479 ± 0.2539	0.2312 ± 0.4571	-0.4791 ± 0.5229	1.43
8.05 < D^0 flightdistance[#mum] < 9.35	-0.2263 ± 0.2575	-0.9424 ± 0.4689	0.7161 ± 0.5350	0.96
9.35 < D^0 flightdistance[#mum] < 11.05	-0.0551 ± 0.2570	-1.1399 ± 0.4798	1.0848 ± 0.5443	1.65
11.05 < D^0 flightdistance[#mum] < 13.45	-0.1553 ± 0.2618	-0.5441 ± 0.5023	0.3888 ± 0.5665	0.30
13.45 < D^0 flightdistance[#mum] < 17.75	-1.1815 ± 0.2678	-1.3294 ± 0.5259	0.1479 ± 0.5902	0.14
17.75 < D^0 flightdistance[#mum] < 530.00	-1.7666 ± 0.2907	-1.6809 ± 0.6035	-0.0857 ± 0.6699	0.48
up TOS	-1.2968 ± 0.1031	-1.1535 ± 0.1847	-0.1432 ± 0.2115	-
0.05 < D^0 flightdistance[#mum] < 4.05	-1.2704 ± 0.4177	-0.5217 ± 0.6431	-0.7487 ± 0.7669	0.82
4.05 < D^0 flightdistance[#mum] < 5.05	-1.2663 ± 0.3694	-0.8361 ± 0.6055	-0.4302 ± 0.7094	0.42
5.05 < D^0 flightdistance[#mum] < 5.95	-1.3812 ± 0.3601	-0.8914 ± 0.6064	-0.4898 ± 0.7053	0.52
5.95 < D^0 flightdistance[#mum] < 6.95	-0.6727 ± 0.3368	-1.6308 ± 0.5821	0.9580 ± 0.6725	1.73
6.95 < D^0 flightdistance[#mum] < 8.05	-1.3125 ± 0.3312	-1.2458 ± 0.5800	-0.0667 ± 0.6679	0.12
8.05 < D^0 flightdistance[#mum] < 9.35	-1.0826 ± 0.3234	-1.9562 ± 0.5748	0.8736 ± 0.6595	1.63
9.35 < D^0 flightdistance[#mum] < 11.05	-1.4204 ± 0.3117	-0.4257 ± 0.5686	-0.9947 ± 0.6484	1.39
11.05 < D^0 flightdistance[#mum] < 13.45	-1.1548 ± 0.3043	-1.8526 ± 0.5653	0.6978 ± 0.6420	1.39
13.45 < D^0 flightdistance[#mum] < 17.75	-1.9213 ± 0.2941	-0.6542 ± 0.5562	-1.2671 ± 0.6292	1.90
17.75 < D^0 flightdistance[#mum] < 530.00	-1.4455 ± 0.2851	-1.5084 ± 0.5679	0.0629 ± 0.6355	0.34
down TOS	-0.4554 ± 0.1028	-0.1838 ± 0.1812	-0.2716 ± 0.2083	-
0.05 < D^0 flightdistance[#mum] < 4.05	0.4014 ± 0.4124	0.6385 ± 0.6310	-0.2371 ± 0.7538	0.05
4.05 < D^0 flightdistance[#mum] < 5.05	-0.1080 ± 0.3673	0.0253 ± 0.5951	-0.1333 ± 0.6993	0.21
5.05 < D^0 flightdistance[#mum] < 5.95	0.0463 ± 0.3568	-0.4483 ± 0.5972	0.4946 ± 0.6956	1.15
5.95 < D^0 flightdistance[#mum] < 6.95	0.3833 ± 0.3352	0.2666 ± 0.5732	0.1168 ± 0.6640	0.62
6.95 < D^0 flightdistance[#mum] < 8.05	-0.3066 ± 0.3288	0.8133 ± 0.5671	-1.1199 ± 0.6555	1.36
8.05 < D^0 flightdistance[#mum] < 9.35	-0.7851 ± 0.3204	-0.6904 ± 0.5653	-0.0947 ± 0.6497	0.29
9.35 < D^0 flightdistance[#mum] < 11.05	-0.4962 ± 0.3096	-0.8150 ± 0.5552	0.3188 ± 0.6357	0.98
11.05 < D^0 flightdistance[#mum] < 13.45	-0.8295 ± 0.3017	-0.4259 ± 0.5521	-0.4037 ± 0.6292	0.22
13.45 < D^0 flightdistance[#mum] < 17.75	-0.7796 ± 0.2917	-0.1939 ± 0.5489	-0.5857 ± 0.6216	0.54
17.75 < D^0 flightdistance[#mum] < 530.00	-1.2787 ± 0.2809	-0.8445 ± 0.5529	-0.4343 ± 0.6202	0.28

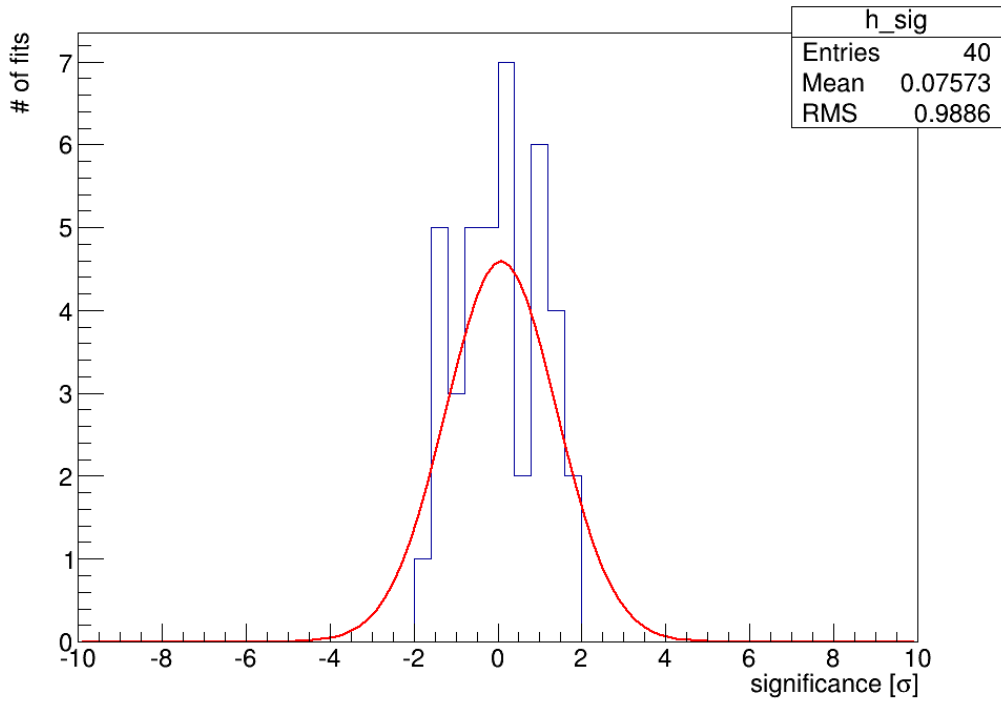
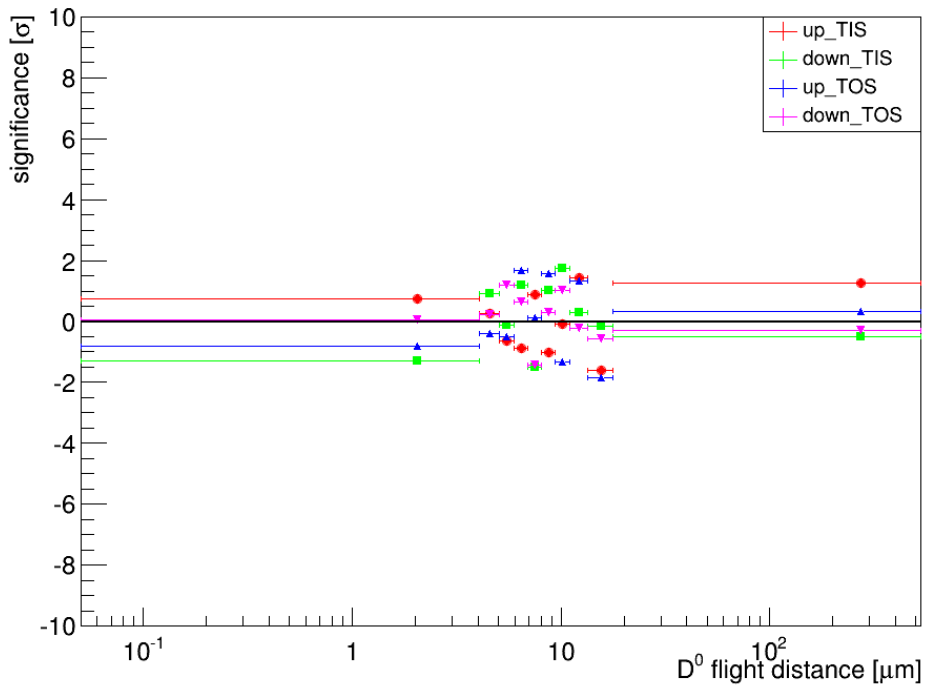


Figure A.36.: Significance vs. D^0 flight distance (top) and histogram of significances (bottom) for 2012 data.

A.9. D^0 transverse momentum

In Fig. A.37 and A.39 the individual asymmetries and ΔA_{CP} versus the $D^0 p_T$ can be found for 2011 and 2012, respectively. The significances of the deviations of results from the baseline result in that class of magnetic polarity and trigger can be found in Fig. A.38 and A.40. In Tab. A.15 and A.16 the results are shown for 2011 and 2012, respectively.

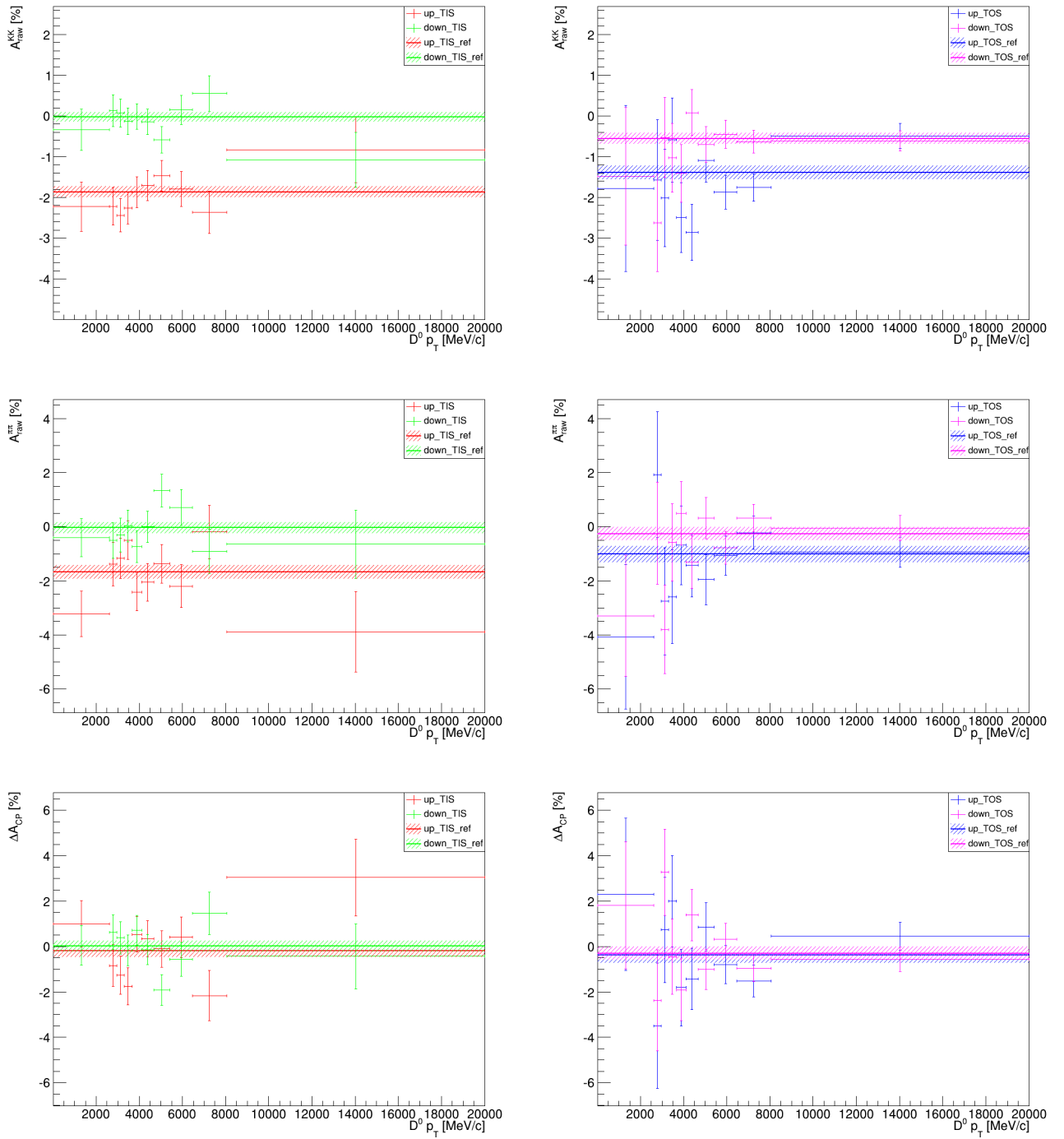


Figure A.37.: A_{raw} vs. $D^0 p_T$, separated by magnetic field polarity and trigger setting for 2011 data.

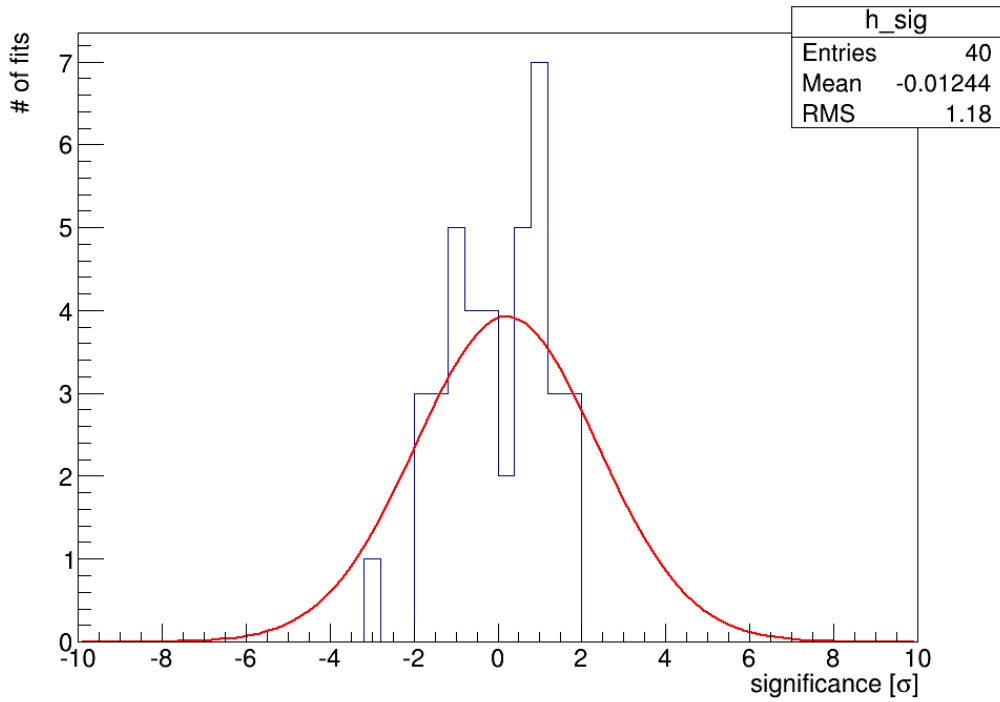
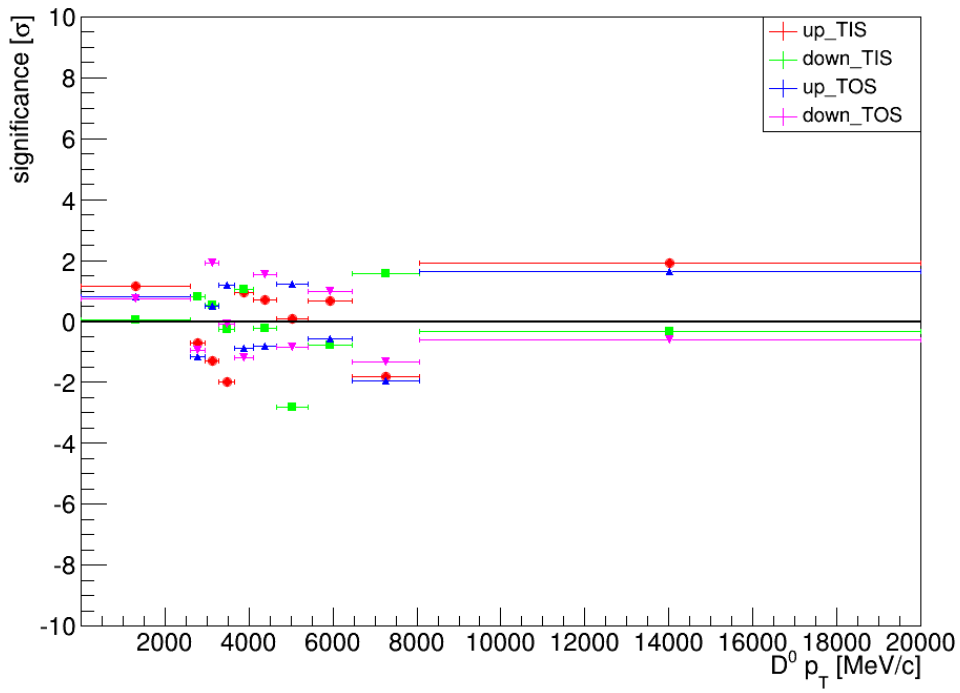


Figure A.38.: Significance vs. $D^0 p_T$ (top) and histogram of significances (bottom) for 2011 data.

Table A.15.: Results of the individual asymmetries in the different $D^0 p_T$ bins, separated by magnetic field polarity and trigger for 2011 data. Highest significance: 3.01

Sample	$A_{raw}(KK)[\%]$	$A_{raw}(\pi\pi)[\%]$	$\Delta_{ACP}[\%]$	significance
up TIS				-
0.50 < $D^0 p_T [MeV/c]$ < 2606.50	-1.8660 ± 0.1368	-1.6779 ± 0.2505	-0.1881 ± 0.2854	
2606.50 < $D^0 p_T [MeV/c]$ < 2957.50	-2.2249 ± 0.6002	-3.2205 ± 0.8365	0.9956 ± 1.0295	1.20
2957.50 < $D^0 p_T [MeV/c]$ < 3292.50	-2.2199 ± 0.4609	-1.3780 ± 0.7975	-0.8419 ± 0.9211	0.75
3292.50 < $D^0 p_T [MeV/c]$ < 3662.50	-2.4361 ± 0.4116	-1.1685 ± 0.7401	-1.2675 ± 0.8468	1.35
3662.50 < $D^0 p_T [MeV/c]$ < 4106.50	-2.2575 ± 0.3866	-0.4975 ± 0.7128	-1.7600 ± 0.8109	2.07
4106.50 < $D^0 p_T [MeV/c]$ < 4667.50	-1.8658 ± 0.3740	-2.4083 ± 0.6945	0.5425 ± 0.7889	0.99
4667.50 < $D^0 p_T [MeV/c]$ < 5412.50	-1.7053 ± 0.3713	-2.0477 ± 0.6930	0.3424 ± 0.7862	0.72
5412.50 < $D^0 p_T [MeV/c]$ < 6453.50	-1.4682 ± 0.3817	-1.3616 ± 0.7150	-0.1066 ± 0.8105	0.11
6453.50 < $D^0 p_T [MeV/c]$ < 8052.50	-1.7915 ± 0.4245	-2.1982 ± 0.7908	0.4067 ± 0.8975	0.70
8052.50 < $D^0 p_T [MeV/c]$ < 20000.00	-2.3604 ± 0.5201	-0.1948 ± 0.9833	-2.1656 ± 1.1123	1.84
	-0.8313 ± 0.8080	-3.8780 ± 1.4854	3.0467 ± 1.6909	1.94
down TIS				-
0.50 < $D^0 p_T [MeV/c]$ < 2606.50	-0.0274 ± 0.1151	-0.0383 ± 0.2102	0.0109 ± 0.2397	
2606.50 < $D^0 p_T [MeV/c]$ < 2957.50	-0.3428 ± 0.5062	-0.3956 ± 0.7027	0.0528 ± 0.8660	0.05
2957.50 < $D^0 p_T [MeV/c]$ < 3292.50	0.1266 ± 0.3872	-0.5058 ± 0.6599	0.6324 ± 0.7651	0.86
3292.50 < $D^0 p_T [MeV/c]$ < 3662.50	0.0723 ± 0.3446	-0.3121 ± 0.6265	0.3844 ± 0.7150	0.55
3662.50 < $D^0 p_T [MeV/c]$ < 4106.50	-0.1319 ± 0.3242	0.0276 ± 0.5949	-0.1595 ± 0.6774	0.27
4106.50 < $D^0 p_T [MeV/c]$ < 4667.50	-0.0112 ± 0.3142	-0.7301 ± 0.5824	0.7190 ± 0.6618	1.15
4667.50 < $D^0 p_T [MeV/c]$ < 5412.50	-0.1374 ± 0.3116	0.0016 ± 0.5824	-0.1390 ± 0.6606	0.24
5412.50 < $D^0 p_T [MeV/c]$ < 6453.50	-0.5818 ± 0.3218	1.3338 ± 0.6037	-1.9156 ± 0.6841	3.01
6453.50 < $D^0 p_T [MeV/c]$ < 8052.50	0.1501 ± 0.3552	0.7171 ± 0.6646	-0.5670 ± 0.7536	0.81
8052.50 < $D^0 p_T [MeV/c]$ < 20000.00	0.5533 ± 0.4375	-0.9101 ± 0.8238	1.4634 ± 0.9328	1.61
	-1.0816 ± 0.6776	-0.6452 ± 1.2576	-0.4363 ± 1.4285	0.32
up TOS				-
0.50 < $D^0 p_T [MeV/c]$ < 2606.50	-1.3870 ± 0.1665	-1.0138 ± 0.3011	-0.3732 ± 0.3440	
2606.50 < $D^0 p_T [MeV/c]$ < 2957.50	-1.7755 ± 2.0371	-4.0720 ± 2.6631	2.2964 ± 3.3529	0.80
2957.50 < $D^0 p_T [MeV/c]$ < 3292.50	-1.5731 ± 1.4812	1.9181 ± 2.3297	-3.4911 ± 2.7608	1.14
3292.50 < $D^0 p_T [MeV/c]$ < 3662.50	-2.0162 ± 1.1916	-2.7518 ± 1.9876	0.7356 ± 2.3174	0.48
3662.50 < $D^0 p_T [MeV/c]$ < 4106.50	-0.5893 ± 1.0277	-2.5872 ± 1.7361	1.9979 ± 2.0175	1.19
4106.50 < $D^0 p_T [MeV/c]$ < 4667.50	-2.4889 ± 0.8592	-0.6792 ± 1.4597	-1.8097 ± 1.6937	0.87
4667.50 < $D^0 p_T [MeV/c]$ < 5412.50	-2.8519 ± 0.6869	-1.4209 ± 1.1740	-1.4310 ± 1.3602	0.80
5412.50 < $D^0 p_T [MeV/c]$ < 6453.50	-1.0921 ± 0.5320	-1.9547 ± 0.9229	0.8626 ± 1.0653	1.23
6453.50 < $D^0 p_T [MeV/c]$ < 8052.50	-1.8650 ± 0.4137	-1.0656 ± 0.7320	-0.7993 ± 0.8408	0.56
8052.50 < $D^0 p_T [MeV/c]$ < 20000.00	-1.7485 ± 0.3376	-0.2210 ± 0.6124	-1.5275 ± 0.6993	1.90
	-0.4875 ± 0.3001	-0.9373 ± 0.5530	0.4498 ± 0.6292	1.56
down TOS				-
0.50 < $D^0 p_T [MeV/c]$ < 2606.50	-0.5525 ± 0.1383	-0.2554 ± 0.2507	-0.2971 ± 0.2863	
2606.50 < $D^0 p_T [MeV/c]$ < 2957.50	-1.4795 ± 1.6833	-3.2940 ± 2.2414	1.8145 ± 2.8031	0.76
2957.50 < $D^0 p_T [MeV/c]$ < 3292.50	-2.6189 ± 1.1956	-0.2427 ± 1.8854	-2.3762 ± 2.2325	0.94
3292.50 < $D^0 p_T [MeV/c]$ < 3662.50	-0.5273 ± 0.9810	-3.7984 ± 1.6288	3.2711 ± 1.9014	1.90
3662.50 < $D^0 p_T [MeV/c]$ < 4106.50	-1.0286 ± 0.8452	-0.5721 ± 1.4269	-0.4565 ± 1.6584	0.10
4106.50 < $D^0 p_T [MeV/c]$ < 4667.50	-1.4070 ± 0.7073	0.4984 ± 1.1722	-1.9054 ± 1.3690	1.20
4667.50 < $D^0 p_T [MeV/c]$ < 5412.50	0.0820 ± 0.5681	-1.3018 ± 0.9711	1.3838 ± 1.1250	1.54
5412.50 < $D^0 p_T [MeV/c]$ < 6453.50	-0.6965 ± 0.4403	0.3144 ± 0.7652	-1.0109 ± 0.8828	0.85
6453.50 < $D^0 p_T [MeV/c]$ < 8052.50	-0.4538 ± 0.3432	-0.7714 ± 0.6060	0.3175 ± 0.6964	0.97
8052.50 < $D^0 p_T [MeV/c]$ < 20000.00	-0.6325 ± 0.2814	0.3250 ± 0.5097	-0.9575 ± 0.5822	1.30
	-0.6122 ± 0.2488	-0.0508 ± 0.4675	-0.5614 ± 0.5296	0.59

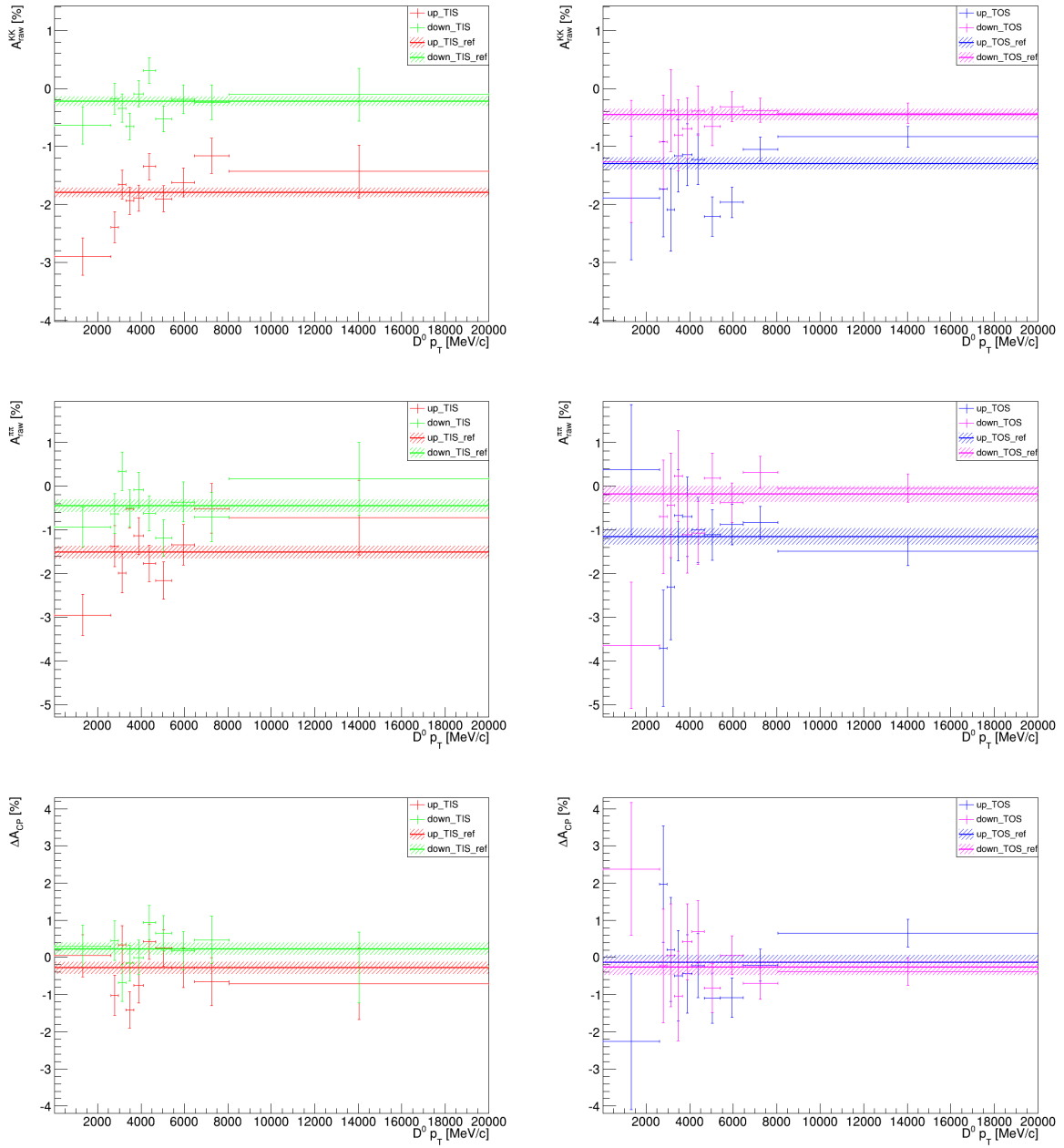


Figure A.39.: A_{raw} vs. $D^0 p_T$, separated by magnetic field polarity and trigger setting for 2012 data.

Table A.16.: Results of the individual asymmetries in the different $D^0 p_T$ bins, separated by magnetic field polarity and trigger for 2012 data. Highest significance: 2.56

Sample	$A_{raw}(KK)[\%]$	$A_{raw}(\pi\pi)[\%]$	$\Delta A_{CP}[\%]$	significance
up TIS	-1.7988 ± 0.0825	-1.5120 ± 0.1487	-0.2868 ± 0.1700	-
0.50 < $D^0 p_T$ [MeV/c] < 2606.50	-2.8971 ± 0.3229	-2.9454 ± 0.4661	0.0483 ± 0.5671	0.62
2606.50 < $D^0 p_T$ [MeV/c] < 2957.50	-2.3935 ± 0.2689	-1.3728 ± 0.4645	-1.0207 ± 0.5367	1.44
2957.50 < $D^0 p_T$ [MeV/c] < 3292.50	-1.6550 ± 0.2478	-1.9909 ± 0.4474	0.3359 ± 0.5114	1.29
3292.50 < $D^0 p_T$ [MeV/c] < 3662.50	-1.9363 ± 0.2348	-0.5238 ± 0.4311	-1.4125 ± 0.4909	2.44
3662.50 < $D^0 p_T$ [MeV/c] < 4106.50	-1.8918 ± 0.2271	-1.1390 ± 0.4201	-0.7529 ± 0.4775	1.04
4106.50 < $D^0 p_T$ [MeV/c] < 4667.50	-1.3474 ± 0.2234	-1.7728 ± 0.4134	0.4254 ± 0.4699	1.63
4667.50 < $D^0 p_T$ [MeV/c] < 5412.50	-1.9020 ± 0.2282	-2.1537 ± 0.4257	0.2517 ± 0.4830	1.19
5412.50 < $D^0 p_T$ [MeV/c] < 6453.50	-1.6234 ± 0.2493	-1.3410 ± 0.4654	-0.2824 ± 0.5280	0.01
6453.50 < $D^0 p_T$ [MeV/c] < 8052.50	-1.1609 ± 0.3038	-0.5085 ± 0.5705	-0.6524 ± 0.6464	0.59
8052.50 < $D^0 p_T$ [MeV/c] < 20000.00	-1.4287 ± 0.4546	-0.7213 ± 0.8507	-0.7074 ± 0.9646	0.44
down TIS	-0.2274 ± 0.0814	-0.4563 ± 0.1456	0.2289 ± 0.1669	-
0.50 < $D^0 p_T$ [MeV/c] < 2606.50	-0.6374 ± 0.3208	-0.9374 ± 0.4590	0.2999 ± 0.5600	0.13
2606.50 < $D^0 p_T$ [MeV/c] < 2957.50	-0.1806 ± 0.2658	-0.6319 ± 0.4586	0.4513 ± 0.5300	0.44
2957.50 < $D^0 p_T$ [MeV/c] < 3292.50	-0.3408 ± 0.2448	0.3430 ± 0.4401	-0.6838 ± 0.5036	1.92
3292.50 < $D^0 p_T$ [MeV/c] < 3662.50	-0.6563 ± 0.2319	-0.5033 ± 0.4226	-0.1530 ± 0.4820	0.84
3662.50 < $D^0 p_T$ [MeV/c] < 4106.50	-0.0926 ± 0.2234	-0.0909 ± 0.4093	-0.0017 ± 0.4663	0.53
4106.50 < $D^0 p_T$ [MeV/c] < 4667.50	0.3074 ± 0.2206	-0.6264 ± 0.4043	0.9338 ± 0.4606	1.64
4667.50 < $D^0 p_T$ [MeV/c] < 5412.50	-0.5270 ± 0.2246	-1.1800 ± 0.4150	0.6530 ± 0.4719	0.96
5412.50 < $D^0 p_T$ [MeV/c] < 6453.50	-0.1861 ± 0.2463	-0.3645 ± 0.4575	0.1784 ± 0.5196	0.10
6453.50 < $D^0 p_T$ [MeV/c] < 8052.50	-0.2387 ± 0.3005	-0.7094 ± 0.5581	0.4707 ± 0.6338	0.40
8052.50 < $D^0 p_T$ [MeV/c] < 20000.00	-0.1085 ± 0.4530	0.1640 ± 0.8332	-0.2726 ± 0.9484	0.54
up TOS	-1.2968 ± 0.1031	-1.1535 ± 0.1847	-0.1432 ± 0.2115	-
0.50 < $D^0 p_T$ [MeV/c] < 2606.50	-1.8862 ± 1.0646	0.3788 ± 1.4894	-2.2650 ± 1.8307	1.17
2606.50 < $D^0 p_T$ [MeV/c] < 2957.50	-1.7357 ± 0.8264	-3.7092 ± 1.3253	1.9735 ± 1.5618	1.37
2957.50 < $D^0 p_T$ [MeV/c] < 3292.50	-2.0935 ± 0.7117	-2.3055 ± 1.2061	0.2120 ± 1.4004	0.26
3292.50 < $D^0 p_T$ [MeV/c] < 3662.50	-1.1616 ± 0.6222	-0.6674 ± 1.0465	-0.4942 ± 1.2175	0.29
3662.50 < $D^0 p_T$ [MeV/c] < 4106.50	-1.1448 ± 0.5356	-0.7000 ± 0.9094	-0.4448 ± 1.0554	0.29
4106.50 < $D^0 p_T$ [MeV/c] < 4667.50	-1.2222 ± 0.4332	-1.0030 ± 0.7406	-0.2192 ± 0.8580	0.09
4667.50 < $D^0 p_T$ [MeV/c] < 5412.50	-2.2107 ± 0.3385	-1.1141 ± 0.5808	-1.0966 ± 0.6723	1.49
5412.50 < $D^0 p_T$ [MeV/c] < 6453.50	-1.9639 ± 0.2608	-0.8803 ± 0.4588	-1.0836 ± 0.5278	1.94
6453.50 < $D^0 p_T$ [MeV/c] < 8052.50	-1.0491 ± 0.2082	-0.8358 ± 0.3768	-0.2133 ± 0.4305	0.19
8052.50 < $D^0 p_T$ [MeV/c] < 20000.00	-0.8329 ± 0.1784	-1.4871 ± 0.3315	0.6543 ± 0.3764	2.56
down TOS	-0.4554 ± 0.1028	-0.1838 ± 0.1812	-0.2716 ± 0.2083	-
0.50 < $D^0 p_T$ [MeV/c] < 2606.50	-1.2610 ± 1.0524	-3.6398 ± 1.4461	2.3788 ± 1.7885	1.49
2606.50 < $D^0 p_T$ [MeV/c] < 2957.50	-0.9269 ± 0.8138	-0.6988 ± 1.2965	-0.2281 ± 1.5307	0.03
2957.50 < $D^0 p_T$ [MeV/c] < 3292.50	-0.3840 ± 0.7067	-0.4400 ± 1.1902	0.0560 ± 1.3842	0.24
3292.50 < $D^0 p_T$ [MeV/c] < 3662.50	-0.8050 ± 0.6118	0.2306 ± 1.0398	-1.0357 ± 1.2064	0.64
3662.50 < $D^0 p_T$ [MeV/c] < 4106.50	-0.6908 ± 0.5277	-1.1077 ± 0.8791	0.4170 ± 1.0253	0.69
4106.50 < $D^0 p_T$ [MeV/c] < 4667.50	-0.3863 ± 0.4296	-1.0785 ± 0.7200	0.6922 ± 0.8385	1.19
4667.50 < $D^0 p_T$ [MeV/c] < 5412.50	-0.6523 ± 0.3339	0.1786 ± 0.5700	-0.8309 ± 0.6607	0.89
5412.50 < $D^0 p_T$ [MeV/c] < 6453.50	-0.3203 ± 0.2572	-0.3763 ± 0.4507	0.0560 ± 0.5190	0.69
6453.50 < $D^0 p_T$ [MeV/c] < 8052.50	-0.3800 ± 0.2069	0.3175 ± 0.3694	-0.6975 ± 0.4234	1.16
8052.50 < $D^0 p_T$ [MeV/c] < 20000.00	-0.4258 ± 0.1774	-0.0455 ± 0.3253	-0.3803 ± 0.3705	0.35

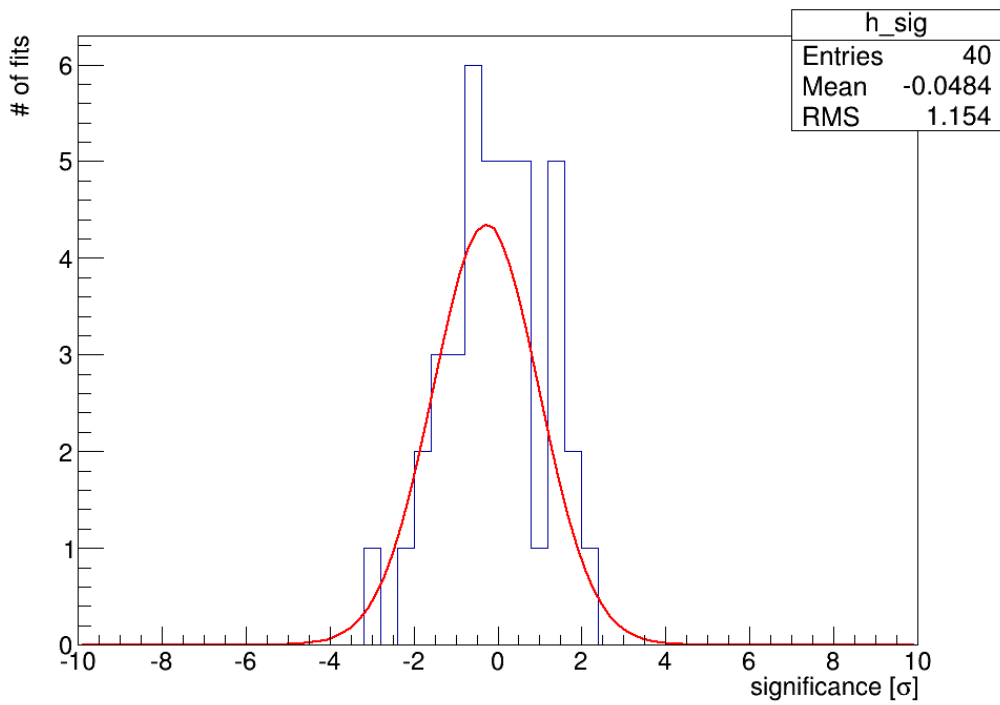
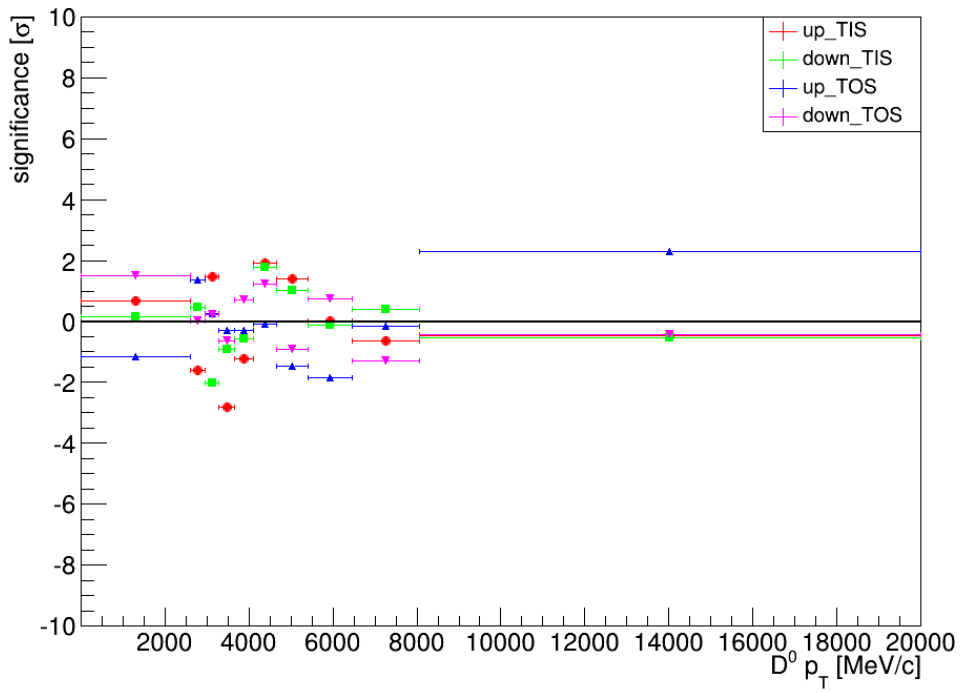


Figure A.40.: Significance vs. $D^0 p_T$ (top) and histogram of significances (bottom) for 2012 data.

A.10. The quality of the D^0 impact parameter

In Fig. A.41 and A.43 the individual asymmetries and ΔA_{CP} versus the $D^0 IP \chi^2$ can be found for 2011 and 2012, respectively. The significances of the deviations of results from the baseline result in that class of magnetic polarity and trigger can be found in Fig. A.42 and A.44. In Tab. A.17 and A.18 the results are shown for 2011 and 2012, respectively.

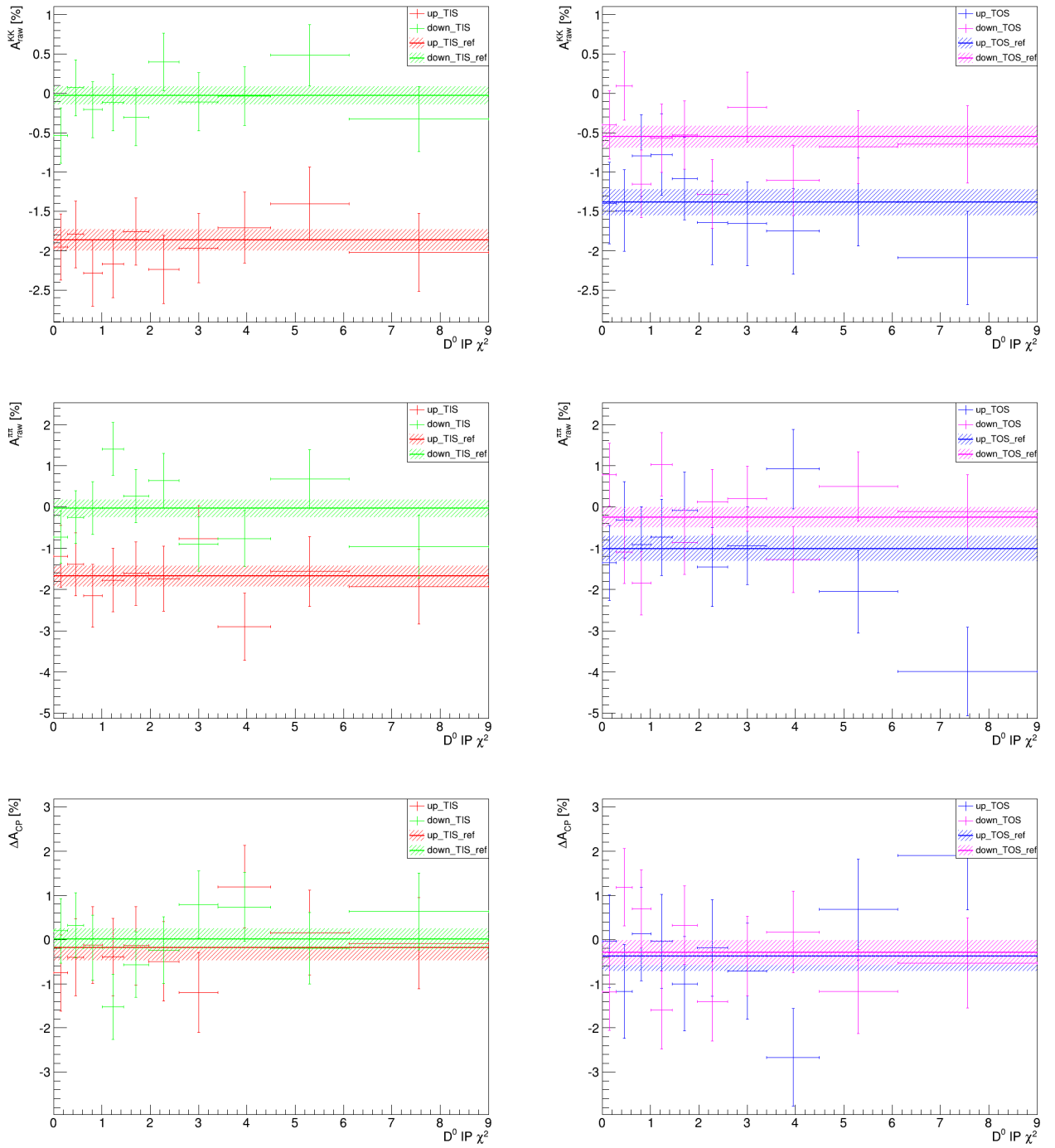


Figure A.41.: A_{raw} vs. $D^0 IP \chi^2$, separated by magnetic field polarity and trigger setting for 2011 data.

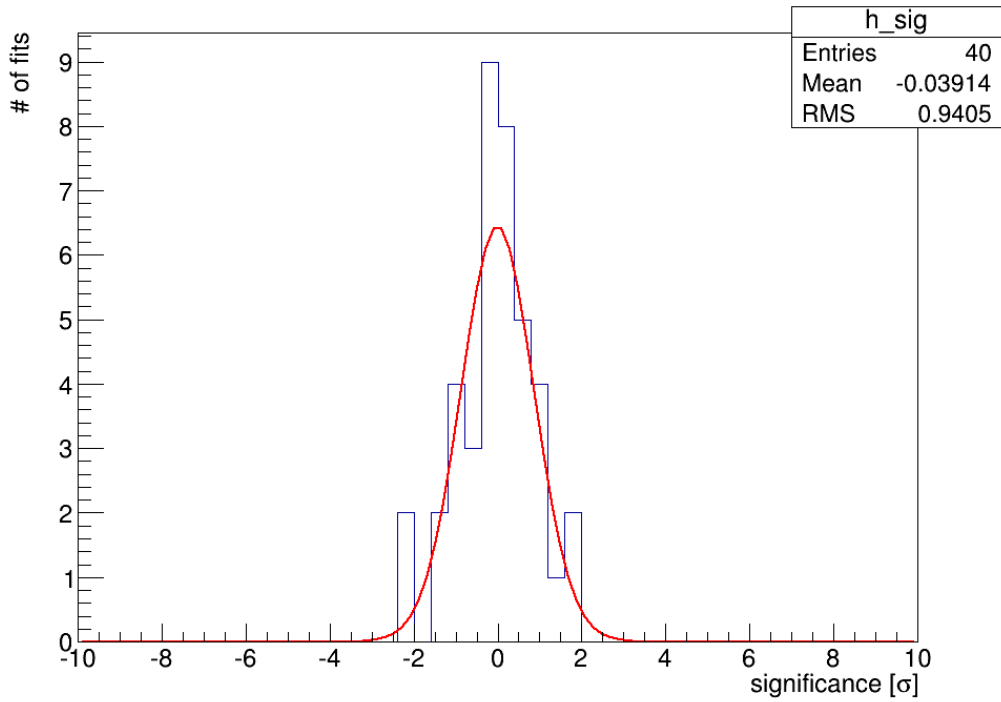
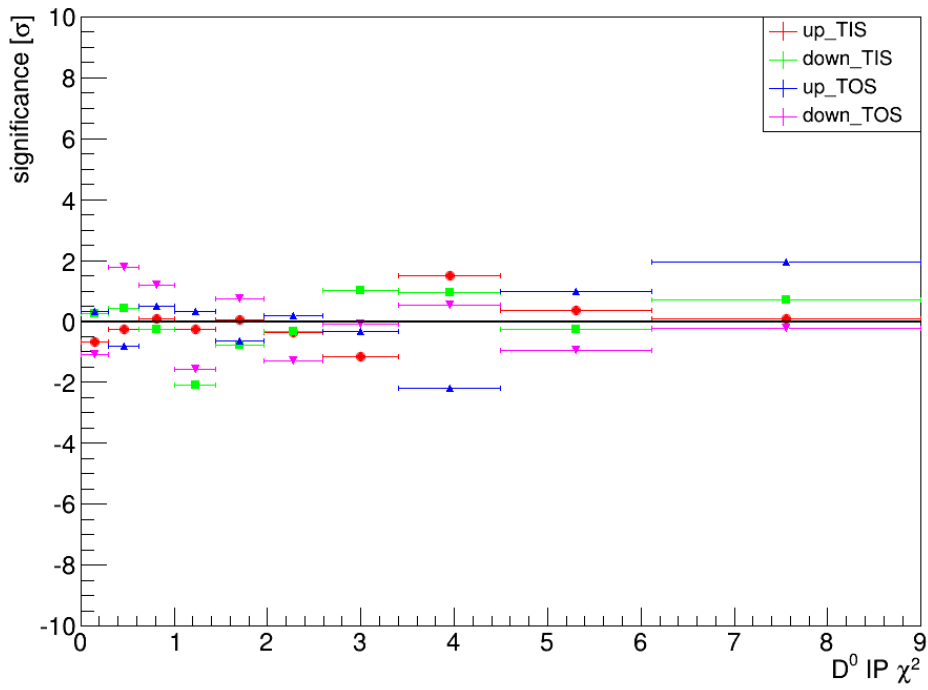


Figure A.42.: Significance vs. $D^0 IP \chi^2$ (top) and histogram of significances (bottom) for 2011 data.

Table A.17.: Results of the individual asymmetries in the different $D^0IP\chi^2$ bins, separated by magnetic field polarity and trigger for 2011 data. Highest significance: 2.20

Sample	$A_{raw}(KK)[\%]$	$A_{raw}(\pi\pi)[\%]$	$\Delta A_{CP}[\%]$	significance
up TIS	-1.8660 ± 0.1368	-1.6779 ± 0.2505	-0.1881 ± 0.2854	-
0.00 < $D^0IP\chi^2$ < 0.29	-1.9552 ± 0.4204	-1.1980 ± 0.7520	-0.7572 ± 0.8615	0.70
0.29 < $D^0IP\chi^2$ < 0.62	-1.7911 ± 0.4237	-1.3881 ± 0.7612	-0.4030 ± 0.8712	0.26
0.62 < $D^0IP\chi^2$ < 1.00	-2.2828 ± 0.4219	-2.1582 ± 0.7624	-0.1247 ± 0.8714	0.08
1.00 < $D^0IP\chi^2$ < 1.45	-2.1688 ± 0.4259	-1.7731 ± 0.7660	-0.3957 ± 0.8765	0.25
1.45 < $D^0IP\chi^2$ < 1.97	-1.7573 ± 0.4295	-1.6160 ± 0.7710	-0.1413 ± 0.8826	0.06
1.97 < $D^0IP\chi^2$ < 2.60	-2.2350 ± 0.4344	-1.7425 ± 0.7851	-0.4925 ± 0.8972	0.36
2.60 < $D^0IP\chi^2$ < 3.40	-1.9675 ± 0.4388	-0.7667 ± 0.7926	-1.2008 ± 0.9060	1.18
3.40 < $D^0IP\chi^2$ < 4.50	-1.7064 ± 0.4495	-2.9024 ± 0.8163	1.1960 ± 0.9319	1.56
4.50 < $D^0IP\chi^2$ < 6.12	-1.4025 ± 0.4630	-1.5611 ± 0.8456	0.1585 ± 0.9640	0.38
6.12 < $D^0IP\chi^2$ < 9.00	-2.0217 ± 0.4942	-1.9355 ± 0.9043	-0.0862 ± 1.0305	0.10
down TIS	-0.0274 ± 0.1151	-0.0383 ± 0.2102	0.0109 ± 0.2397	-
0.00 < $D^0IP\chi^2$ < 0.29	-0.5375 ± 0.3539	-0.7337 ± 0.6356	0.1963 ± 0.7275	0.27
0.29 < $D^0IP\chi^2$ < 0.62	0.0711 ± 0.3565	-0.2511 ± 0.6418	0.3222 ± 0.7342	0.45
0.62 < $D^0IP\chi^2$ < 1.00	-0.2070 ± 0.3564	-0.0231 ± 0.6388	-0.1839 ± 0.7315	0.28
1.00 < $D^0IP\chi^2$ < 1.45	-0.1192 ± 0.3584	1.4043 ± 0.6433	-1.5235 ± 0.7364	2.20
1.45 < $D^0IP\chi^2$ < 1.97	-0.3051 ± 0.3614	0.2643 ± 0.6471	-0.5693 ± 0.7412	0.83
1.97 < $D^0IP\chi^2$ < 2.60	0.3989 ± 0.3650	0.6397 ± 0.6592	-0.2408 ± 0.7535	0.35
2.60 < $D^0IP\chi^2$ < 3.40	-0.1070 ± 0.3674	-0.9003 ± 0.6609	0.7933 ± 0.7561	1.09
3.40 < $D^0IP\chi^2$ < 4.50	-0.0342 ± 0.3749	-0.7704 ± 0.6785	0.7363 ± 0.7752	0.98
4.50 < $D^0IP\chi^2$ < 6.12	0.4843 ± 0.3878	0.6803 ± 0.7071	-0.1960 ± 0.8065	0.27
6.12 < $D^0IP\chi^2$ < 9.00	-0.3269 ± 0.4129	-0.9628 ± 0.7644	0.6359 ± 0.8688	0.75
up TOS	-1.3870 ± 0.1665	-1.0138 ± 0.3011	-0.3732 ± 0.3440	-
0.00 < $D^0IP\chi^2$ < 0.29	-1.3961 ± 0.5175	-1.3586 ± 0.9169	-0.0374 ± 1.0528	0.34
0.29 < $D^0IP\chi^2$ < 0.62	-1.4908 ± 0.5192	-0.3139 ± 0.9252	-1.1769 ± 1.0609	0.80
0.62 < $D^0IP\chi^2$ < 1.00	-0.7930 ± 0.5192	-0.9166 ± 0.9212	0.1236 ± 1.0574	0.50
1.00 < $D^0IP\chi^2$ < 1.45	-0.7773 ± 0.5209	-0.7382 ± 0.9283	-0.0392 ± 1.0645	0.33
1.45 < $D^0IP\chi^2$ < 1.97	-1.0823 ± 0.5250	-0.0827 ± 0.9305	-0.9996 ± 1.0684	0.62
1.97 < $D^0IP\chi^2$ < 2.60	-1.6444 ± 0.5319	-1.4553 ± 0.9523	-0.1891 ± 1.0908	0.18
2.60 < $D^0IP\chi^2$ < 3.40	-1.6570 ± 0.5328	-0.9373 ± 0.9446	-0.7197 ± 1.0844	0.34
3.40 < $D^0IP\chi^2$ < 4.50	-1.7510 ± 0.5452	0.9186 ± 0.9612	-2.6696 ± 1.1050	2.19
4.50 < $D^0IP\chi^2$ < 6.12	-1.3773 ± 0.5589	-2.0564 ± 0.9961	0.6792 ± 1.1422	0.97
6.12 < $D^0IP\chi^2$ < 9.00	-2.0911 ± 0.5926	-3.9929 ± 1.0721	1.9018 ± 1.2250	1.93
down TOS	-0.5525 ± 0.1383	-0.2554 ± 0.2507	-0.2971 ± 0.2863	-
0.00 < $D^0IP\chi^2$ < 0.29	-0.4014 ± 0.4307	0.7815 ± 0.7650	-1.1829 ± 0.8779	1.07
0.29 < $D^0IP\chi^2$ < 0.62	0.0945 ± 0.4326	-1.0891 ± 0.7655	1.1835 ± 0.8793	1.78
0.62 < $D^0IP\chi^2$ < 1.00	-1.1503 ± 0.4327	-1.8493 ± 0.7705	0.6990 ± 0.8837	1.19
1.00 < $D^0IP\chi^2$ < 1.45	-0.5690 ± 0.4328	1.0275 ± 0.7666	-1.5966 ± 0.8803	1.56
1.45 < $D^0IP\chi^2$ < 1.97	-0.5323 ± 0.4343	-0.8604 ± 0.7765	0.3280 ± 0.8897	0.74
1.97 < $D^0IP\chi^2$ < 2.60	-1.2793 ± 0.4399	0.1214 ± 0.7851	-1.4007 ± 0.8999	1.29
2.60 < $D^0IP\chi^2$ < 3.40	-0.1749 ± 0.4417	0.1952 ± 0.7874	-0.3701 ± 0.9028	0.09
3.40 < $D^0IP\chi^2$ < 4.50	-1.1048 ± 0.4488	-1.2758 ± 0.8056	0.1709 ± 0.9222	0.53
4.50 < $D^0IP\chi^2$ < 6.12	-0.6819 ± 0.4619	0.4907 ± 0.8382	-1.1726 ± 0.9571	0.96
6.12 < $D^0IP\chi^2$ < 9.00	-0.6478 ± 0.4911	-0.1157 ± 0.8919	-0.5321 ± 1.0181	0.24

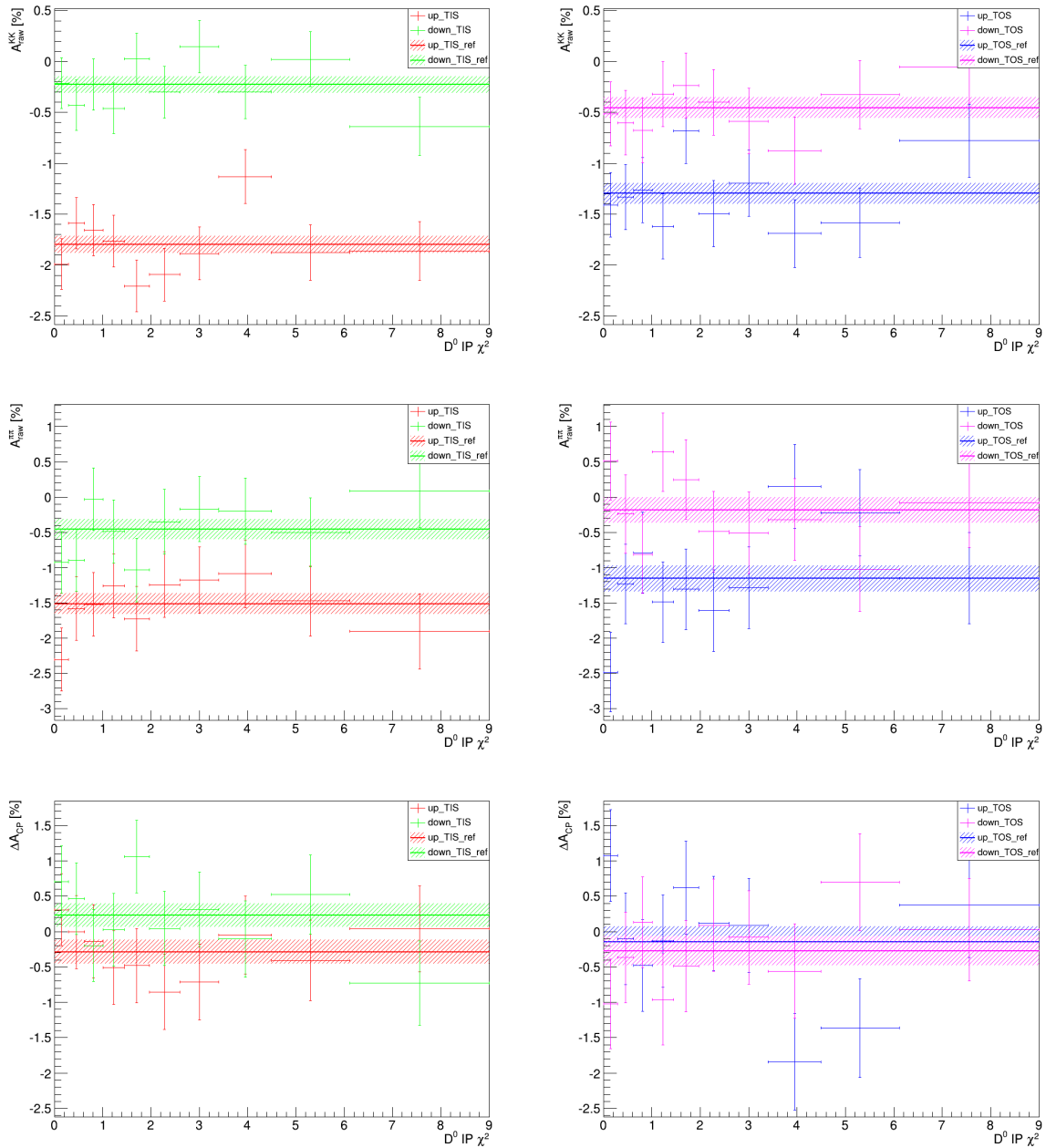


Figure A.43.: A_{raw} vs. $D^0 IP \chi^2$, separated by magnetic field polarity and trigger setting for 2012 data.

Table A.18.: Results of the individual asymmetries in the different $D^0IP\chi^2$ bins, separated by magnetic field polarity and trigger for 2012 data. Highest significance: 2.62

Sample	$A_{raw}(KK)[\%]$	$A_{raw}(\pi\pi)[\%]$	$\Delta A_{CP}[\%]$	significance
up TIS	-1.7988 ± 0.0825	-1.5120 ± 0.1487	-0.2868 ± 0.1700	-
0.00 < $D^0IP\chi^2$ < 0.29	-1.9898 ± 0.2504	-2.2986 ± 0.4451	0.3088 ± 0.5107	1.24
0.29 < $D^0IP\chi^2$ < 0.62	-1.5884 ± 0.2518	-1.5818 ± 0.4497	-0.0066 ± 0.5154	0.58
0.62 < $D^0IP\chi^2$ < 1.00	-1.6557 ± 0.2521	-1.5191 ± 0.4520	-0.1366 ± 0.5175	0.31
1.00 < $D^0IP\chi^2$ < 1.45	-1.7657 ± 0.2542	-1.2568 ± 0.4541	-0.5089 ± 0.5203	0.45
1.45 < $D^0IP\chi^2$ < 1.97	-2.2054 ± 0.2550	-1.7232 ± 0.4601	-0.4821 ± 0.5260	0.39
1.97 < $D^0IP\chi^2$ < 2.60	-2.0929 ± 0.2587	-1.2391 ± 0.4632	-0.8538 ± 0.5306	1.13
2.60 < $D^0IP\chi^2$ < 3.40	-1.8855 ± 0.2600	-1.1761 ± 0.4688	-0.7095 ± 0.5361	0.83
3.40 < $D^0IP\chi^2$ < 4.50	-1.1322 ± 0.2653	-1.0872 ± 0.4823	-0.0450 ± 0.5504	0.46
4.50 < $D^0IP\chi^2$ < 6.12	-1.8795 ± 0.2727	-1.4725 ± 0.4967	-0.4070 ± 0.5667	0.22
6.12 < $D^0IP\chi^2$ < 9.00	-1.8627 ± 0.2883	-1.9031 ± 0.5349	0.0404 ± 0.6076	0.56
down TIS	-0.2274 ± 0.0814	-0.4563 ± 0.1456	0.2289 ± 0.1669	-
0.00 < $D^0IP\chi^2$ < 0.29	-0.2135 ± 0.2478	-0.9222 ± 0.4385	0.7087 ± 0.5036	1.01
0.29 < $D^0IP\chi^2$ < 0.62	-0.4293 ± 0.2486	-0.8922 ± 0.4409	0.4629 ± 0.5062	0.49
0.62 < $D^0IP\chi^2$ < 1.00	-0.2261 ± 0.2493	-0.0293 ± 0.4415	-0.1968 ± 0.5070	0.89
1.00 < $D^0IP\chi^2$ < 1.45	-0.4599 ± 0.2505	-0.4872 ± 0.4454	0.0272 ± 0.5110	0.42
1.45 < $D^0IP\chi^2$ < 1.97	0.0256 ± 0.2519	-1.0343 ± 0.4494	1.0599 ± 0.5151	1.71
1.97 < $D^0IP\chi^2$ < 2.60	-0.3021 ± 0.2553	-0.3467 ± 0.4573	0.0446 ± 0.5237	0.37
2.60 < $D^0IP\chi^2$ < 3.40	0.1440 ± 0.2566	-0.1674 ± 0.4597	0.3114 ± 0.5265	0.17
3.40 < $D^0IP\chi^2$ < 4.50	-0.3009 ± 0.2616	-0.1965 ± 0.4692	-0.1044 ± 0.5372	0.65
4.50 < $D^0IP\chi^2$ < 6.12	0.0212 ± 0.2696	-0.5007 ± 0.4877	0.5219 ± 0.5573	0.55
6.12 < $D^0IP\chi^2$ < 9.00	-0.6388 ± 0.2851	0.0867 ± 0.5228	-0.7255 ± 0.5955	1.67
up TOS	-1.2968 ± 0.1031	-1.1535 ± 0.1847	-0.1432 ± 0.2115	-
0.00 < $D^0IP\chi^2$ < 0.29	-1.4085 ± 0.3180	-2.4800 ± 0.5653	1.0716 ± 0.6486	1.98
0.29 < $D^0IP\chi^2$ < 0.62	-1.3315 ± 0.3192	-1.2304 ± 0.5628	-0.1011 ± 0.6470	0.07
0.62 < $D^0IP\chi^2$ < 1.00	-1.2647 ± 0.3191	-0.7858 ± 0.5681	-0.4789 ± 0.6516	0.54
1.00 < $D^0IP\chi^2$ < 1.45	-1.6209 ± 0.3208	-1.4861 ± 0.5705	-0.1348 ± 0.6545	0.01
1.45 < $D^0IP\chi^2$ < 1.97	-0.6807 ± 0.3215	-1.3054 ± 0.5730	0.6247 ± 0.6570	1.23
1.97 < $D^0IP\chi^2$ < 2.60	-1.4937 ± 0.3254	-1.6085 ± 0.5801	0.1148 ± 0.6651	0.41
2.60 < $D^0IP\chi^2$ < 3.40	-1.1961 ± 0.3262	-1.2820 ± 0.5788	0.0859 ± 0.6644	0.36
3.40 < $D^0IP\chi^2$ < 4.50	-1.6898 ± 0.3328	0.1503 ± 0.5936	-1.8400 ± 0.6805	2.62
4.50 < $D^0IP\chi^2$ < 6.12	-1.5839 ± 0.3399	-0.2194 ± 0.6110	-1.3645 ± 0.6992	1.83
6.12 < $D^0IP\chi^2$ < 9.00	-0.7772 ± 0.3587	-1.1492 ± 0.6465	0.3720 ± 0.7393	0.73
down TOS	-0.4554 ± 0.1028	-0.1838 ± 0.1812	-0.2716 ± 0.2083	-
0.00 < $D^0IP\chi^2$ < 0.29	-0.5123 ± 0.3148	0.5097 ± 0.5531	-1.0220 ± 0.6364	1.25
0.29 < $D^0IP\chi^2$ < 0.62	-0.6024 ± 0.3175	-0.2385 ± 0.5555	-0.3639 ± 0.6398	0.15
0.62 < $D^0IP\chi^2$ < 1.00	-0.6787 ± 0.3158	-0.8094 ± 0.5559	0.1307 ± 0.6394	0.67
1.00 < $D^0IP\chi^2$ < 1.45	-0.3198 ± 0.3183	0.6379 ± 0.5574	-0.9577 ± 0.6419	1.13
1.45 < $D^0IP\chi^2$ < 1.97	-0.2390 ± 0.3197	0.2494 ± 0.5614	-0.4884 ± 0.6460	0.35
1.97 < $D^0IP\chi^2$ < 2.60	-0.3998 ± 0.3224	-0.4894 ± 0.5687	0.0896 ± 0.6537	0.58
2.60 < $D^0IP\chi^2$ < 3.40	-0.5867 ± 0.3232	-0.5055 ± 0.5753	-0.0811 ± 0.6599	0.30
3.40 < $D^0IP\chi^2$ < 4.50	-0.8762 ± 0.3288	-0.3163 ± 0.5800	-0.5598 ± 0.6667	0.46
4.50 < $D^0IP\chi^2$ < 6.12	-0.3244 ± 0.3363	-1.0196 ± 0.5977	0.6952 ± 0.6858	1.48
6.12 < $D^0IP\chi^2$ < 9.00	-0.0537 ± 0.3557	-0.0789 ± 0.6306	0.0251 ± 0.7240	0.43

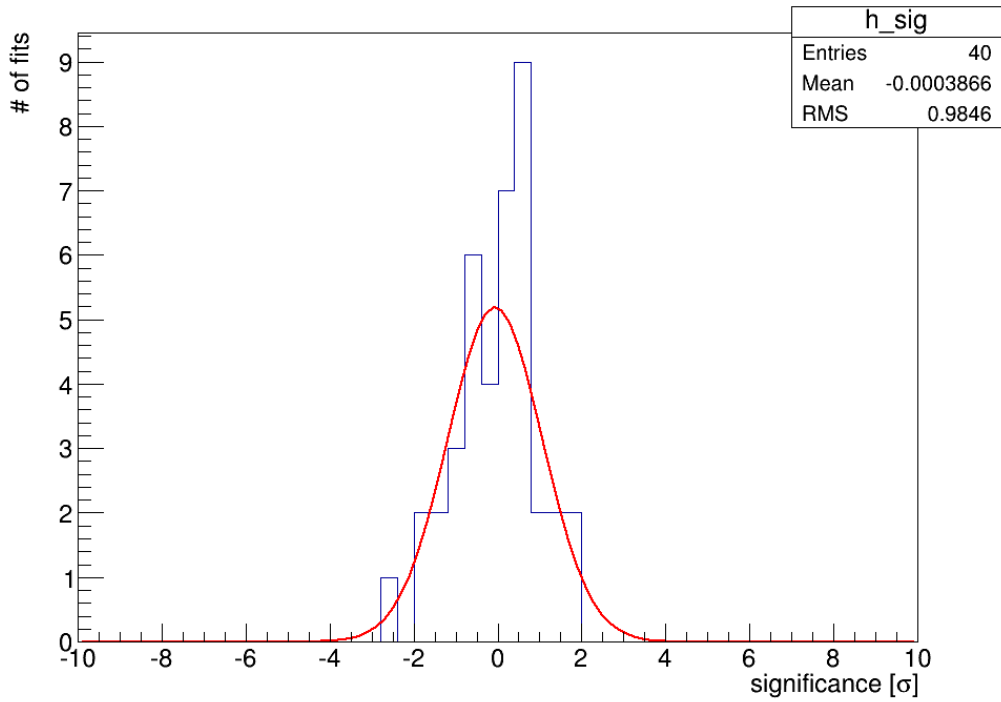
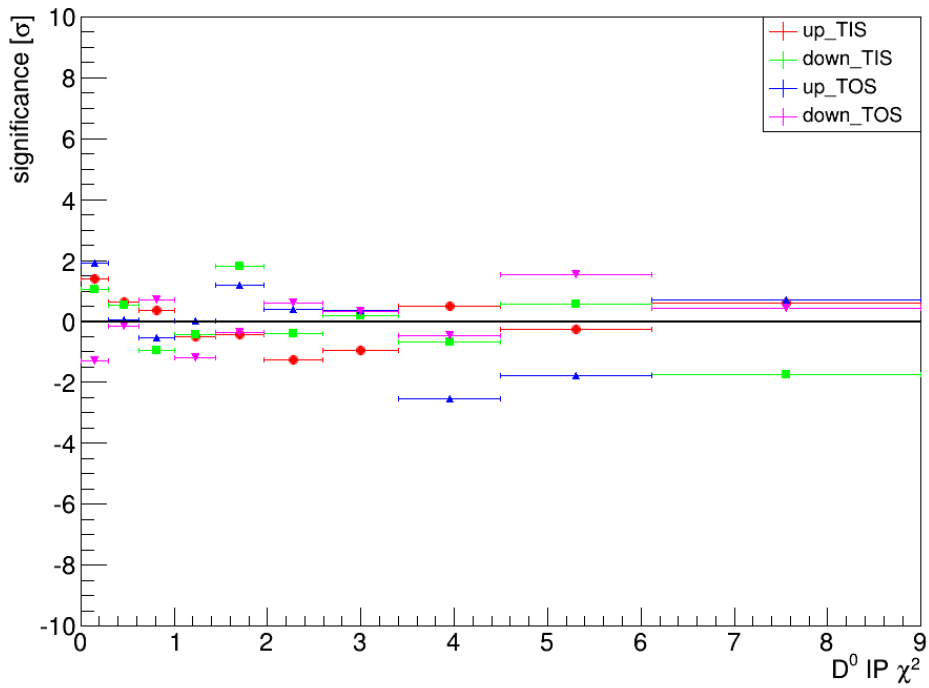


Figure A.44.: Significance vs. $D^0 IP \chi^2$ (top) and histogram of significances (bottom) for 2012 data.

A.11. The azimuthal angle of D^0

In Fig. A.45 and A.47 the individual asymmetries and ΔA_{CP} versus the $D^0\phi$ can be found for 2011 and 2012, respectively. The significances of the deviations of results from the baseline result in that class of magnetic polarity and trigger can be found in Fig. A.46 and A.48. In Tab. A.19 and A.20 the results are shown for 2011 and 2012, respectively.

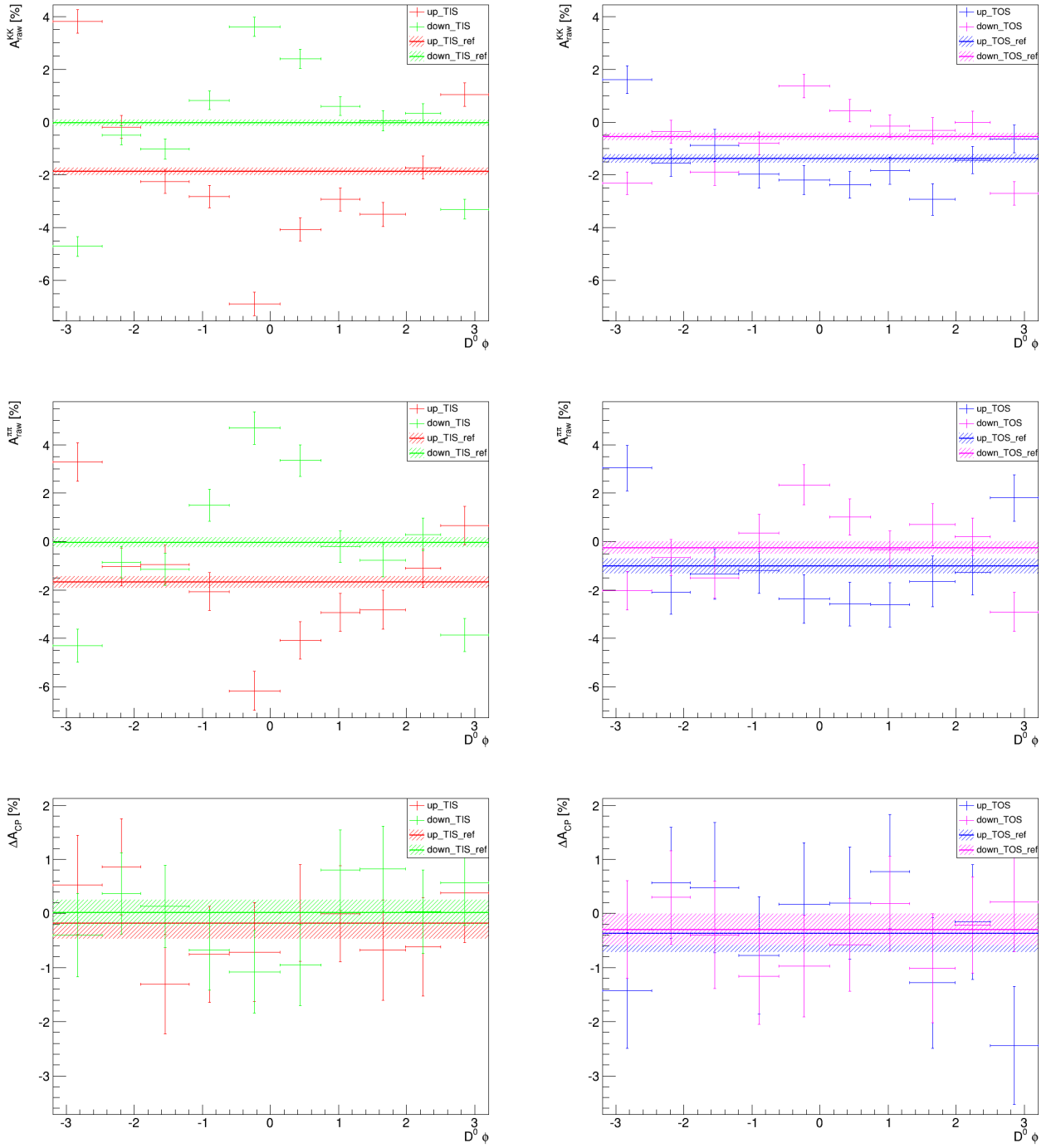


Figure A.45.: A_{raw} vs. $D^0 \phi$, separated by magnetic field polarity and trigger setting for 2011 data.

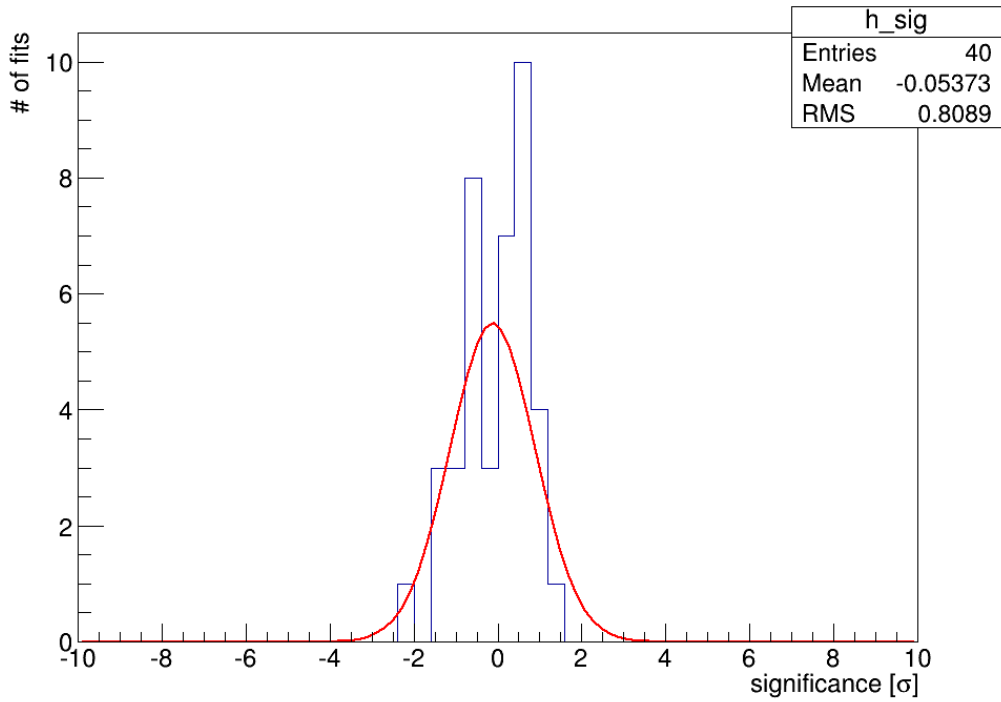
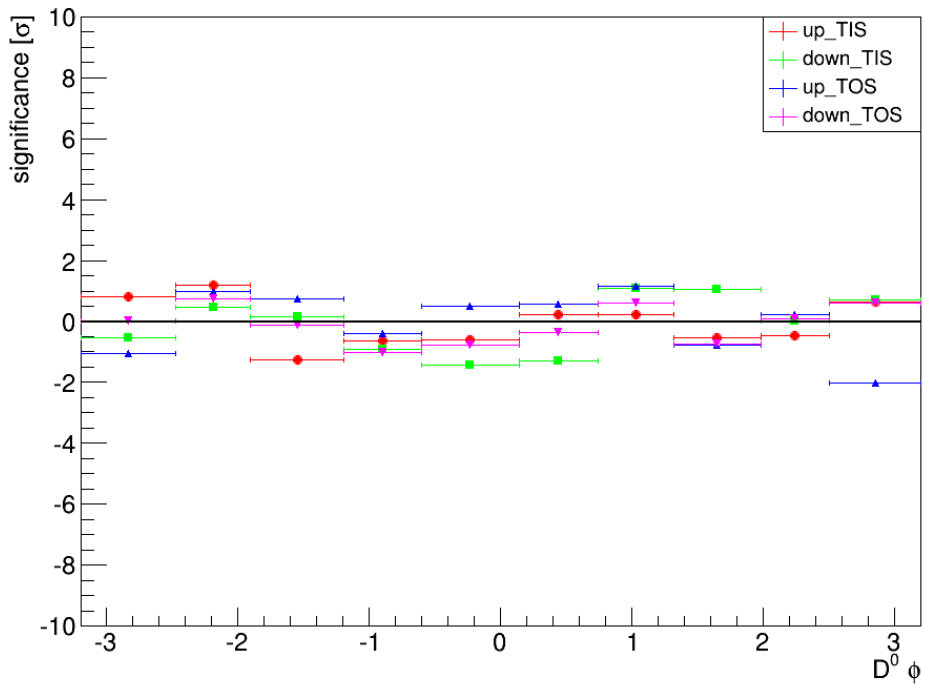


Figure A.46.: Significance vs. $D^0 \phi$ (top) and histogram of significances (bottom) for 2011 data.

Table A.19.: Results of the individual asymmetries in the different $D^0 \phi$ bins, separated by magnetic field polarity and trigger for 2011 data. Highest significance: 2.00

Sample	$A_{raw}(KK)[\%]$	$A_{raw}(\pi\pi)[\%]$	$\Delta A_{CP}[\%]$	significance
up TIS	-1.8660 ± 0.1368	-1.6779 ± 0.2505	-0.1881 ± 0.2854	-
-3.20 < $D^0 \phi$ < -2.47	3.8093 ± 0.4451	3.2830 ± 0.7973	0.5264 ± 0.9131	0.82
-2.47 < $D^0 \phi$ < -1.90	-0.1837 ± 0.4308	-1.0438 ± 0.7775	0.8601 ± 0.8889	1.25
-1.90 < $D^0 \phi$ < -1.19	-2.2456 ± 0.4529	-0.9396 ± 0.7976	-1.3060 ± 0.9172	1.28
-1.19 < $D^0 \phi$ < -0.60	-2.8232 ± 0.4197	-2.0683 ± 0.7821	-0.7548 ± 0.8876	0.67
-0.60 < $D^0 \phi$ < 0.14	-6.8811 ± 0.4385	-6.1675 ± 0.8010	-0.7136 ± 0.9132	0.61
0.14 < $D^0 \phi$ < 0.74	-4.0671 ± 0.4355	-4.0788 ± 0.7789	0.0117 ± 0.8924	0.24
0.74 < $D^0 \phi$ < 1.32	-2.9302 ± 0.4285	-2.9274 ± 0.7783	-0.0028 ± 0.8885	0.22
1.32 < $D^0 \phi$ < 1.98	-3.4960 ± 0.4616	-2.8194 ± 0.8092	-0.6766 ± 0.9316	0.55
1.98 < $D^0 \phi$ < 2.50	-1.7203 ± 0.4307	-1.1055 ± 0.7995	-0.6148 ± 0.9081	0.49
2.50 < $D^0 \phi$ < 3.20	1.0422 ± 0.4472	0.6587 ± 0.8021	0.3834 ± 0.9184	0.65
down TIS	-0.0274 ± 0.1151	-0.0383 ± 0.2102	0.0109 ± 0.2397	-
-3.20 < $D^0 \phi$ < -2.47	-4.7024 ± 0.3762	-4.3019 ± 0.6742	-0.4005 ± 0.7720	0.56
-2.47 < $D^0 \phi$ < -1.90	-0.4880 ± 0.3625	-0.8574 ± 0.6530	0.3695 ± 0.7469	0.51
-1.90 < $D^0 \phi$ < -1.19	-1.0200 ± 0.3789	-1.1481 ± 0.6573	0.1281 ± 0.7586	0.16
-1.19 < $D^0 \phi$ < -0.60	0.8236 ± 0.3503	1.5019 ± 0.6555	-0.6783 ± 0.7432	0.98
-0.60 < $D^0 \phi$ < 0.14	3.6071 ± 0.3692	4.6870 ± 0.6691	-1.0800 ± 0.7642	1.50
0.14 < $D^0 \phi$ < 0.74	2.3917 ± 0.3649	3.3450 ± 0.6541	-0.9534 ± 0.7490	1.36
0.74 < $D^0 \phi$ < 1.32	0.5988 ± 0.3553	-0.2072 ± 0.6490	0.8059 ± 0.7399	1.14
1.32 < $D^0 \phi$ < 1.98	0.0500 ± 0.3877	-0.7753 ± 0.6811	0.8254 ± 0.7837	1.09
1.98 < $D^0 \phi$ < 2.50	0.3258 ± 0.3657	0.2955 ± 0.6761	0.0302 ± 0.7687	0.03
2.50 < $D^0 \phi$ < 3.20	-3.2966 ± 0.3769	-3.8601 ± 0.6807	0.5635 ± 0.7781	0.75
up TOS	-1.3870 ± 0.1665	-1.0138 ± 0.3011	-0.3732 ± 0.3440	-
-3.20 < $D^0 \phi$ < -2.47	1.6094 ± 0.5197	3.0325 ± 0.9373	-1.4231 ± 1.0717	1.03
-2.47 < $D^0 \phi$ < -1.90	-1.5382 ± 0.5173	-2.1040 ± 0.8868	0.5658 ± 1.0267	0.97
-1.90 < $D^0 \phi$ < -1.19	-0.8715 ± 0.6081	-1.3495 ± 1.0356	0.4780 ± 1.2009	0.74
-1.19 < $D^0 \phi$ < -0.60	-1.9716 ± 0.5196	-1.1942 ± 0.9502	-0.7774 ± 1.0830	0.39
-0.60 < $D^0 \phi$ < 0.14	-2.2007 ± 0.5446	-2.3678 ± 0.9977	0.1670 ± 1.1367	0.50
0.14 < $D^0 \phi$ < 0.74	-2.3829 ± 0.5072	-2.5725 ± 0.9043	0.1897 ± 1.0368	0.58
0.74 < $D^0 \phi$ < 1.32	-1.8385 ± 0.5219	-2.6095 ± 0.9160	0.7709 ± 1.0542	1.15
1.32 < $D^0 \phi$ < 1.98	-2.9265 ± 0.6022	-1.6451 ± 1.0483	-1.2814 ± 1.2090	0.78
1.98 < $D^0 \phi$ < 2.50	-1.4357 ± 0.5124	-1.2785 ± 0.9281	-0.1572 ± 1.0601	0.22
2.50 < $D^0 \phi$ < 3.20	-0.6424 ± 0.5272	1.7982 ± 0.9544	-2.4406 ± 1.0903	2.00
down TOS	-0.5525 ± 0.1383	-0.2554 ± 0.2507	-0.2971 ± 0.2863	-
-3.20 < $D^0 \phi$ < -2.47	-2.3168 ± 0.4319	-2.0232 ± 0.7919	-0.2935 ± 0.9020	0.00
-2.47 < $D^0 \phi$ < -1.90	-0.3615 ± 0.4336	-0.6598 ± 0.7478	0.2984 ± 0.8644	0.73
-1.90 < $D^0 \phi$ < -1.19	-1.8878 ± 0.5012	-1.4914 ± 0.8558	-0.3964 ± 0.9917	0.10
-1.19 < $D^0 \phi$ < -0.60	-0.8078 ± 0.4310	0.3520 ± 0.7811	-1.1597 ± 0.8921	1.02
-0.60 < $D^0 \phi$ < 0.14	1.3720 ± 0.4460	2.3465 ± 0.8213	-0.9744 ± 0.9346	0.76
0.14 < $D^0 \phi$ < 0.74	0.4322 ± 0.4174	1.0132 ± 0.7486	-0.5810 ± 0.8571	0.35
0.74 < $D^0 \phi$ < 1.32	-0.1443 ± 0.4258	-0.3304 ± 0.7614	0.1860 ± 0.8723	0.59
1.32 < $D^0 \phi$ < 1.98	-0.3155 ± 0.4943	0.6960 ± 0.8747	-1.0115 ± 1.0047	0.74
1.98 < $D^0 \phi$ < 2.50	-0.0138 ± 0.4364	0.2020 ± 0.7712	-0.2157 ± 0.8861	0.10
2.50 < $D^0 \phi$ < 3.20	-2.6946 ± 0.4406	-2.9066 ± 0.8024	0.2119 ± 0.9154	0.59

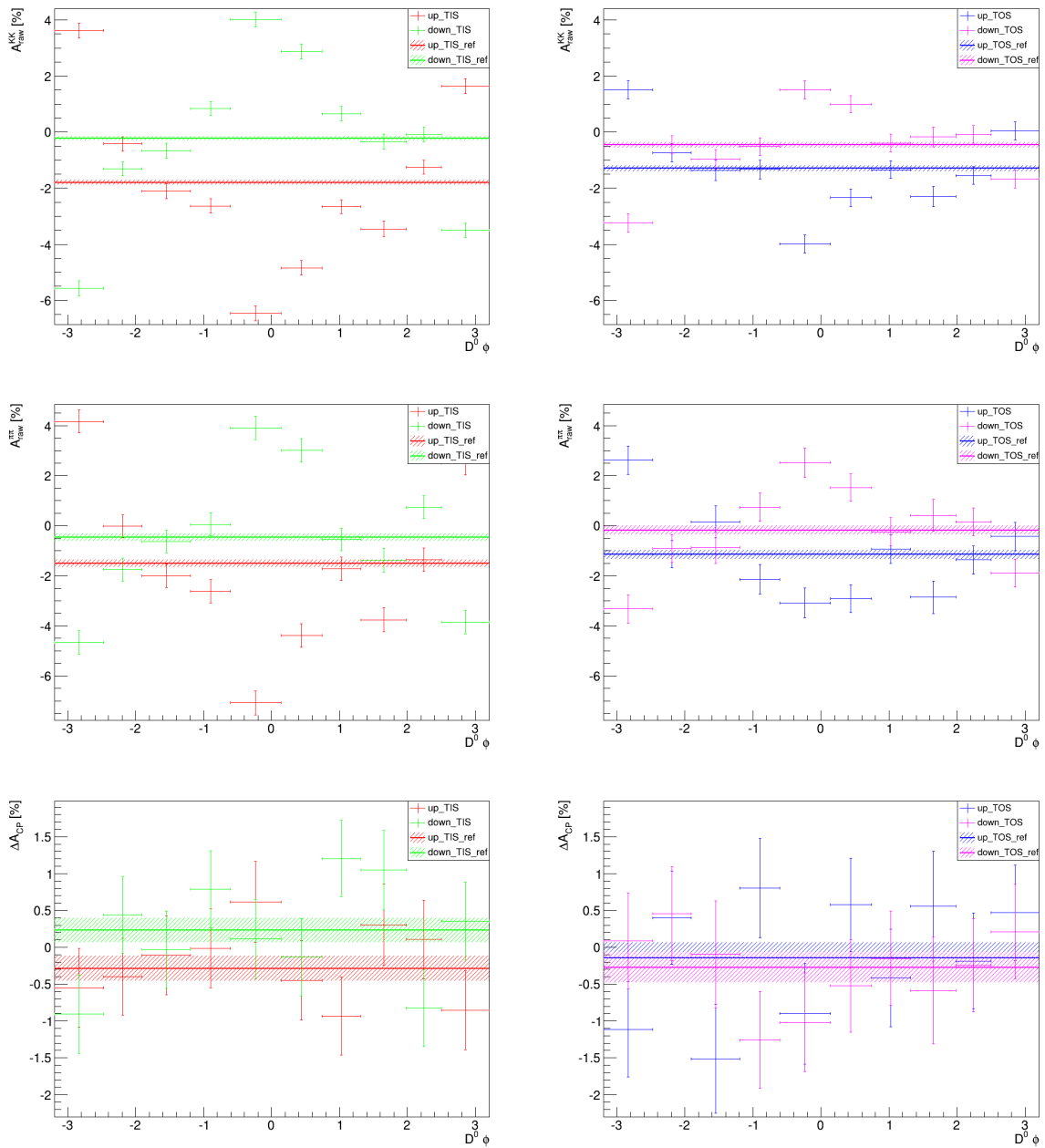


Figure A.47.: A_{raw} vs. $D^0 \phi$, separated by magnetic field polarity and trigger setting for 2012 data.

Table A.20.: Results of the individual asymmetries in the different $D^0 \phi$ bins, separated by magnetic field polarity and trigger for 2012 data. Highest significance: 2.25

Sample	$A_{raw}(KK)[\%]$	$A_{raw}(\pi\pi)[\%]$	$\Delta A_{CP}[\%]$	significance
up TIS	-1.7988 ± 0.0825	-1.5120 ± 0.1487	-0.2868 ± 0.1700	-
-3.20 < $D^0 \phi$ < -2.47	3.6217 ± 0.2630	4.1714 ± 0.4661	-0.5498 ± 0.5352	0.52
-2.47 < $D^0 \phi$ < -1.90	-0.4183 ± 0.2543	-0.0217 ± 0.4535	-0.3966 ± 0.5199	0.22
-1.90 < $D^0 \phi$ < -1.19	-2.1039 ± 0.2660	-1.9959 ± 0.4618	-0.1080 ± 0.5329	0.35
-1.19 < $D^0 \phi$ < -0.60	-2.6305 ± 0.2521	-2.6140 ± 0.4716	-0.0165 ± 0.5347	0.53
-0.60 < $D^0 \phi$ < 0.14	-6.4660 ± 0.2626	-7.0802 ± 0.4838	0.6141 ± 0.5505	1.72
0.14 < $D^0 \phi$ < 0.74	-4.8364 ± 0.2608	-4.3913 ± 0.4705	-0.4451 ± 0.5379	0.31
0.74 < $D^0 \phi$ < 1.32	-2.6569 ± 0.2547	-1.7238 ± 0.4639	-0.9330 ± 0.5292	1.29
1.32 < $D^0 \phi$ < 1.98	-3.4524 ± 0.2723	-3.7599 ± 0.4800	0.3075 ± 0.5519	1.13
1.98 < $D^0 \phi$ < 2.50	-1.2496 ± 0.2547	-1.3552 ± 0.4687	0.1056 ± 0.5334	0.78
2.50 < $D^0 \phi$ < 3.20	1.6363 ± 0.2629	2.4917 ± 0.4690	-0.8554 ± 0.5377	1.11
down TIS	-0.2274 ± 0.0814	-0.4563 ± 0.1456	0.2289 ± 0.1669	-
-3.20 < $D^0 \phi$ < -2.47	-5.5682 ± 0.2618	-4.6601 ± 0.4644	-0.9080 ± 0.5331	2.25
-2.47 < $D^0 \phi$ < -1.90	-1.3041 ± 0.2512	-1.7469 ± 0.4543	0.4428 ± 0.5191	0.44
-1.90 < $D^0 \phi$ < -1.19	-0.6612 ± 0.2615	-0.6293 ± 0.4542	-0.0319 ± 0.5241	0.52
-1.19 < $D^0 \phi$ < -0.60	0.8478 ± 0.2499	0.0592 ± 0.4566	0.7886 ± 0.5205	1.14
-0.60 < $D^0 \phi$ < 0.14	4.0215 ± 0.2619	3.9081 ± 0.4701	0.1133 ± 0.5382	0.23
0.14 < $D^0 \phi$ < 0.74	2.8777 ± 0.2584	3.0110 ± 0.4605	-0.1333 ± 0.5280	0.72
0.74 < $D^0 \phi$ < 1.32	0.6595 ± 0.2495	-0.5446 ± 0.4516	1.2041 ± 0.5160	2.00
1.32 < $D^0 \phi$ < 1.98	-0.3357 ± 0.2661	-1.3826 ± 0.4656	1.0469 ± 0.5363	1.61
1.98 < $D^0 \phi$ < 2.50	-0.0824 ± 0.2504	0.7401 ± 0.4571	-0.8225 ± 0.5212	2.13
2.50 < $D^0 \phi$ < 3.20	-3.4989 ± 0.2602	-3.8534 ± 0.4602	0.3545 ± 0.5287	0.25
up TOS	-1.2968 ± 0.1031	-1.1535 ± 0.1847	-0.1432 ± 0.2115	-
-3.20 < $D^0 \phi$ < -2.47	1.5085 ± 0.3197	2.6196 ± 0.5668	-1.1111 ± 0.6508	1.57
-2.47 < $D^0 \phi$ < -1.90	-0.7364 ± 0.3207	-1.1375 ± 0.5468	0.4011 ± 0.6339	0.91
-1.90 < $D^0 \phi$ < -1.19	-1.3669 ± 0.3679	0.1480 ± 0.6409	-1.5149 ± 0.7390	1.94
-1.19 < $D^0 \phi$ < -0.60	-1.3328 ± 0.3273	-2.1387 ± 0.5875	0.8059 ± 0.6725	1.49
-0.60 < $D^0 \phi$ < 0.14	-3.9880 ± 0.3260	-3.0885 ± 0.6031	-0.8994 ± 0.6856	1.16
0.14 < $D^0 \phi$ < 0.74	-2.3409 ± 0.3119	-2.9174 ± 0.5542	0.5764 ± 0.6359	1.20
0.74 < $D^0 \phi$ < 1.32	-1.3395 ± 0.3189	-0.9242 ± 0.5775	-0.4153 ± 0.6597	0.44
1.32 < $D^0 \phi$ < 1.98	-2.2966 ± 0.3621	-2.8533 ± 0.6525	0.5567 ± 0.7463	0.98
1.98 < $D^0 \phi$ < 2.50	-1.5534 ± 0.3140	-1.3684 ± 0.5686	-0.1850 ± 0.6495	0.07
2.50 < $D^0 \phi$ < 3.20	0.0461 ± 0.3207	-0.4216 ± 0.5643	0.4677 ± 0.6491	1.00
down TOS	-0.4554 ± 0.1028	-0.1838 ± 0.1812	-0.2716 ± 0.2083	-
-3.20 < $D^0 \phi$ < -2.47	-3.2362 ± 0.3261	-3.3241 ± 0.5609	0.0879 ± 0.6488	0.59
-2.47 < $D^0 \phi$ < -1.90	-0.4540 ± 0.3192	-0.9100 ± 0.5525	0.4560 ± 0.6380	1.21
-1.90 < $D^0 \phi$ < -1.19	-0.9709 ± 0.3566	-0.8738 ± 0.6312	-0.0971 ± 0.7250	0.25
-1.19 < $D^0 \phi$ < -0.60	-0.5179 ± 0.3214	0.7389 ± 0.5711	-1.2568 ± 0.6553	1.59
-0.60 < $D^0 \phi$ < 0.14	1.5009 ± 0.3209	2.5194 ± 0.5868	-1.0186 ± 0.6688	1.18
0.14 < $D^0 \phi$ < 0.74	0.9962 ± 0.3093	1.5201 ± 0.5435	-0.5240 ± 0.6254	0.43
0.74 < $D^0 \phi$ < 1.32	-0.3903 ± 0.3147	-0.2407 ± 0.5596	-0.1496 ± 0.6420	0.20
1.32 < $D^0 \phi$ < 1.98	-0.1751 ± 0.3573	0.4134 ± 0.6283	-0.5885 ± 0.7228	0.46
1.98 < $D^0 \phi$ < 2.50	-0.0862 ± 0.3125	0.1561 ± 0.5519	-0.2423 ± 0.6342	0.05
2.50 < $D^0 \phi$ < 3.20	-1.6723 ± 0.3194	-1.8846 ± 0.5575	0.2123 ± 0.6425	0.80

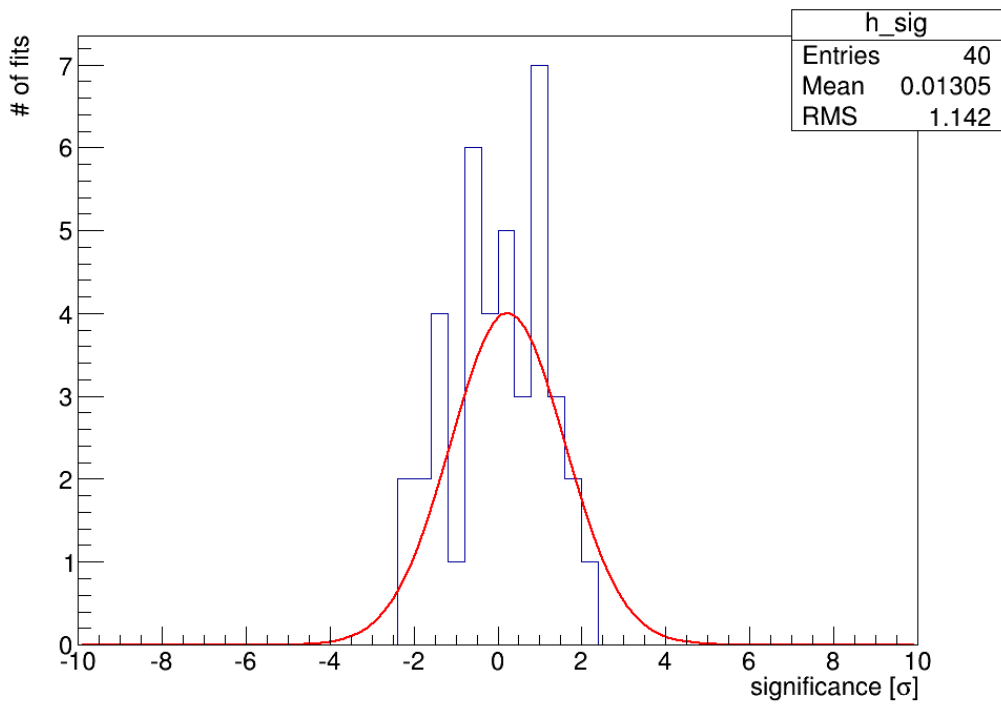
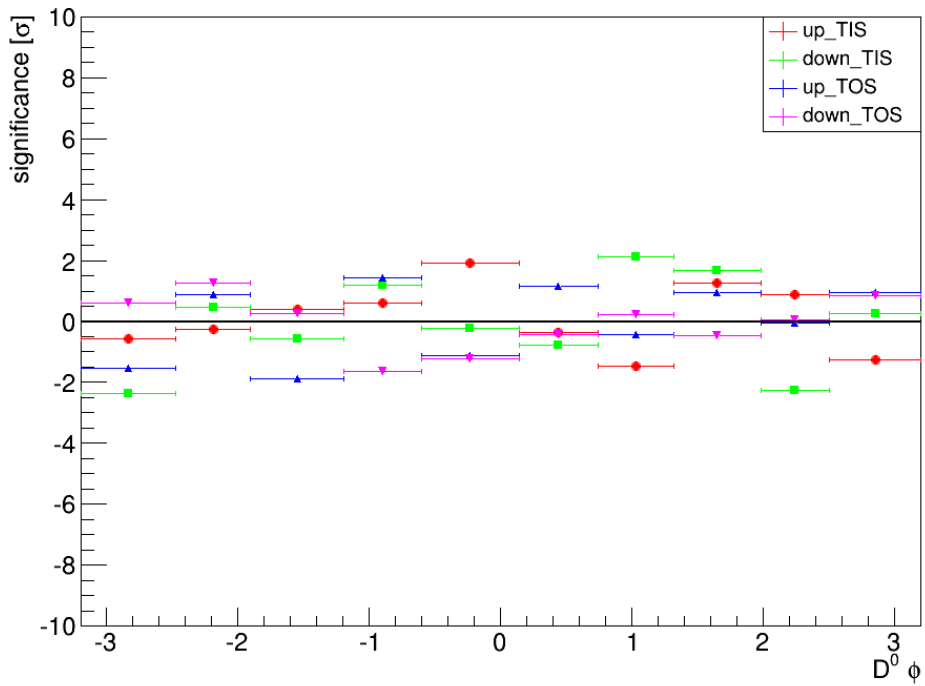


Figure A.48.: Significance vs. $D^0 \phi$ (top) and histogram of significances (bottom) for 2012 data.

A.12. The D^0 mass

In Fig. A.49 and A.51 the individual asymmetries and ΔA_{CP} versus $m(D^0)$ can be found for 2011 and 2012, respectively. The significances of the deviations of results from the baseline result in that class of magnetic polarity and trigger can be found in Fig. A.50 and A.52. In Tab. A.21 and A.22 the results are shown for 2011 and 2012, respectively.

Table A.21.: Results of the individual asymmetries in the different $m(D^0)$ bins, separated by magnetic field polarity and trigger for 2011 data. Highest significance: 2.20

Sample	$A_{raw}(KK)[\%]$	$A_{raw}(\pi\pi)[\%]$	$\Delta A_{CP}[\%]$	significance
up TIS	-1.8660 ± 0.1368	-1.6779 ± 0.2505	-0.1881 ± 0.2854	-
$1845.00 < m(D^0)[MeV/c^2] < 1856.70$	-1.8468 ± 0.5396	-2.7549 ± 0.7340	0.9081 ± 0.9109	1.27
$1856.70 < m(D^0)[MeV/c^2] < 1860.33$	-1.7188 ± 0.4373	-0.4706 ± 0.7939	-1.2482 ± 0.9064	1.23
$1860.33 < m(D^0)[MeV/c^2] < 1862.80$	-1.2182 ± 0.4233	-2.3366 ± 0.8221	1.1183 ± 0.9246	1.49
$1862.80 < m(D^0)[MeV/c^2] < 1864.86$	-1.9035 ± 0.4167	-1.3741 ± 0.8425	-0.5294 ± 0.9399	0.38
$1864.86 < m(D^0)[MeV/c^2] < 1866.76$	-2.2079 ± 0.4156	-0.8425 ± 0.8513	-1.3654 ± 0.9474	1.30
$1866.76 < m(D^0)[MeV/c^2] < 1868.66$	-2.2939 ± 0.4129	-1.1845 ± 0.8404	-1.1093 ± 0.9364	1.03
$1868.66 < m(D^0)[MeV/c^2] < 1870.73$	-2.6000 ± 0.4151	-2.4421 ± 0.8253	-0.1579 ± 0.9238	0.03
$1870.73 < m(D^0)[MeV/c^2] < 1873.20$	-1.5287 ± 0.4218	-1.0047 ± 0.8044	-0.5240 ± 0.9083	0.39
$1873.20 < m(D^0)[MeV/c^2] < 1876.80$	-1.8196 ± 0.4355	-1.2799 ± 0.7584	-0.5398 ± 0.8746	0.43
$1876.80 < m(D^0)[MeV/c^2] < 1889.00$	-2.2984 ± 0.5252	-2.7114 ± 0.6972	0.4130 ± 0.8729	0.73
down TIS	-0.0274 ± 0.1151	-0.0383 ± 0.2102	0.0109 ± 0.2397	-
$1845.00 < m(D^0)[MeV/c^2] < 1856.70$	-1.3009 ± 0.4475	-0.2396 ± 0.6031	-1.0613 ± 0.7510	1.51
$1856.70 < m(D^0)[MeV/c^2] < 1860.33$	-0.2949 ± 0.3623	-0.7190 ± 0.6584	0.4241 ± 0.7515	0.58
$1860.33 < m(D^0)[MeV/c^2] < 1862.80$	-0.0099 ± 0.3517	0.0849 ± 0.6875	-0.0948 ± 0.7723	0.14
$1862.80 < m(D^0)[MeV/c^2] < 1864.86$	0.3137 ± 0.3465	0.5558 ± 0.7053	-0.2421 ± 0.7858	0.34
$1864.86 < m(D^0)[MeV/c^2] < 1866.76$	-0.2918 ± 0.3470	1.3546 ± 0.7121	-1.6464 ± 0.7921	2.20
$1866.76 < m(D^0)[MeV/c^2] < 1868.66$	0.1023 ± 0.3486	1.2376 ± 0.7086	-1.1353 ± 0.7897	1.52
$1868.66 < m(D^0)[MeV/c^2] < 1870.73$	0.3483 ± 0.3504	-0.0975 ± 0.6951	0.4458 ± 0.7784	0.59
$1870.73 < m(D^0)[MeV/c^2] < 1873.20$	0.5347 ± 0.3571	-0.6696 ± 0.6780	1.2043 ± 0.7663	1.64
$1873.20 < m(D^0)[MeV/c^2] < 1876.80$	-0.1871 ± 0.3711	-0.3198 ± 0.6452	0.1328 ± 0.7444	0.17
$1876.80 < m(D^0)[MeV/c^2] < 1889.00$	-0.6974 ± 0.4516	-1.0336 ± 0.5940	0.3362 ± 0.7462	0.46
up TOS	-1.3870 ± 0.1665	-1.0138 ± 0.3011	-0.3732 ± 0.3440	-
$1845.00 < m(D^0)[MeV/c^2] < 1856.70$	-2.0454 ± 0.6190	-1.5817 ± 0.8320	-0.4637 ± 1.0370	0.09
$1856.70 < m(D^0)[MeV/c^2] < 1860.33$	-1.0951 ± 0.5195	-0.8076 ± 0.9422	-0.2875 ± 1.0759	0.08
$1860.33 < m(D^0)[MeV/c^2] < 1862.80$	-1.3859 ± 0.5127	-0.5268 ± 0.9905	-0.8591 ± 1.1154	0.46
$1862.80 < m(D^0)[MeV/c^2] < 1864.86$	-0.9526 ± 0.5078	-1.4522 ± 1.0311	0.4995 ± 1.1493	0.80
$1864.86 < m(D^0)[MeV/c^2] < 1866.76$	-0.9436 ± 0.5112	-0.7383 ± 1.0367	-0.2054 ± 1.1559	0.15
$1866.76 < m(D^0)[MeV/c^2] < 1868.66$	-1.8582 ± 0.5116	-1.3163 ± 1.0350	-0.5419 ± 1.1545	0.15
$1868.66 < m(D^0)[MeV/c^2] < 1870.73$	-1.3729 ± 0.5162	0.2539 ± 1.0138	-1.6268 ± 1.1377	1.16
$1870.73 < m(D^0)[MeV/c^2] < 1873.20$	-1.7408 ± 0.5256	-0.6472 ± 0.9822	-1.0936 ± 1.1140	0.68
$1873.20 < m(D^0)[MeV/c^2] < 1876.80$	-1.3643 ± 0.5373	-1.1327 ± 0.9299	-0.2316 ± 1.0739	0.14
$1876.80 < m(D^0)[MeV/c^2] < 1889.00$	-1.2790 ± 0.6376	-1.7359 ± 0.8238	0.4570 ± 1.0417	0.84
down TOS	-0.5525 ± 0.1383	-0.2554 ± 0.2507	-0.2971 ± 0.2863	-
$1845.00 < m(D^0)[MeV/c^2] < 1856.70$	-0.0011 ± 0.5065	-1.0099 ± 0.6855	1.0088 ± 0.8523	1.63
$1856.70 < m(D^0)[MeV/c^2] < 1860.33$	-0.7645 ± 0.4251	0.7267 ± 0.7793	-1.4913 ± 0.8877	1.42
$1860.33 < m(D^0)[MeV/c^2] < 1862.80$	-0.7973 ± 0.4215	-1.1629 ± 0.8237	0.3656 ± 0.9253	0.75
$1862.80 < m(D^0)[MeV/c^2] < 1864.86$	-0.6648 ± 0.4203	-1.2248 ± 0.8467	0.5600 ± 0.9453	0.95
$1864.86 < m(D^0)[MeV/c^2] < 1866.76$	-0.2154 ± 0.4221	0.4984 ± 0.8558	-0.7138 ± 0.9542	0.46
$1866.76 < m(D^0)[MeV/c^2] < 1868.66$	-0.7903 ± 0.4265	-0.7861 ± 0.8618	-0.0042 ± 0.9615	0.32
$1868.66 < m(D^0)[MeV/c^2] < 1870.73$	-0.1992 ± 0.4291	0.1210 ± 0.8445	-0.3202 ± 0.9473	0.03
$1870.73 < m(D^0)[MeV/c^2] < 1873.20$	-0.7089 ± 0.4381	0.7859 ± 0.8256	-1.4948 ± 0.9346	1.35
$1873.20 < m(D^0)[MeV/c^2] < 1876.80$	-1.6437 ± 0.4517	-0.6961 ± 0.7794	-0.9476 ± 0.9009	0.76
$1876.80 < m(D^0)[MeV/c^2] < 1889.00$	-0.4925 ± 0.5394	0.1623 ± 0.6992	-0.6548 ± 0.8831	0.43

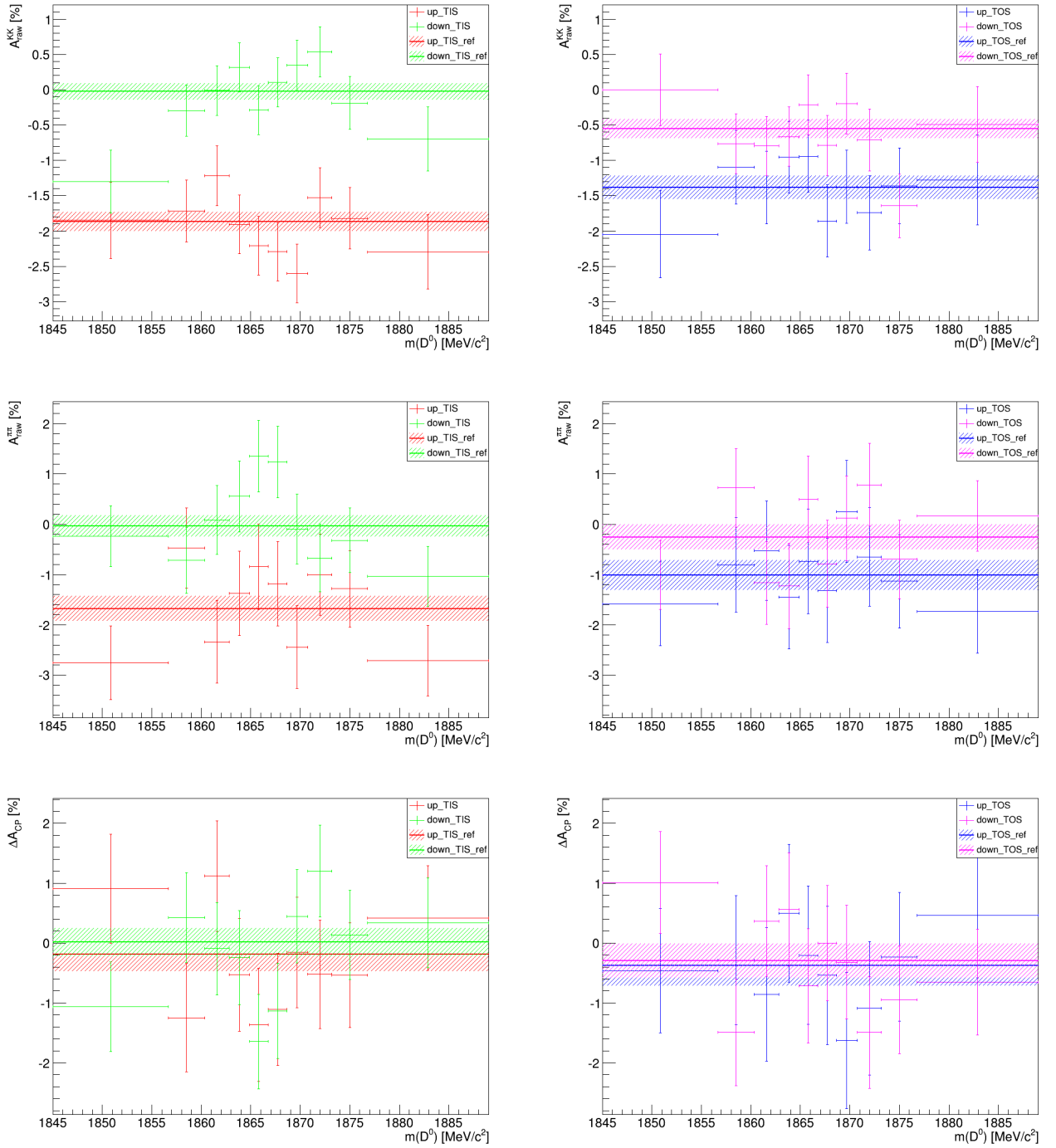


Figure A.49.: A_{raw} vs. $m(D^0)$, separated by magnetic field polarity and trigger setting for 2011 data.

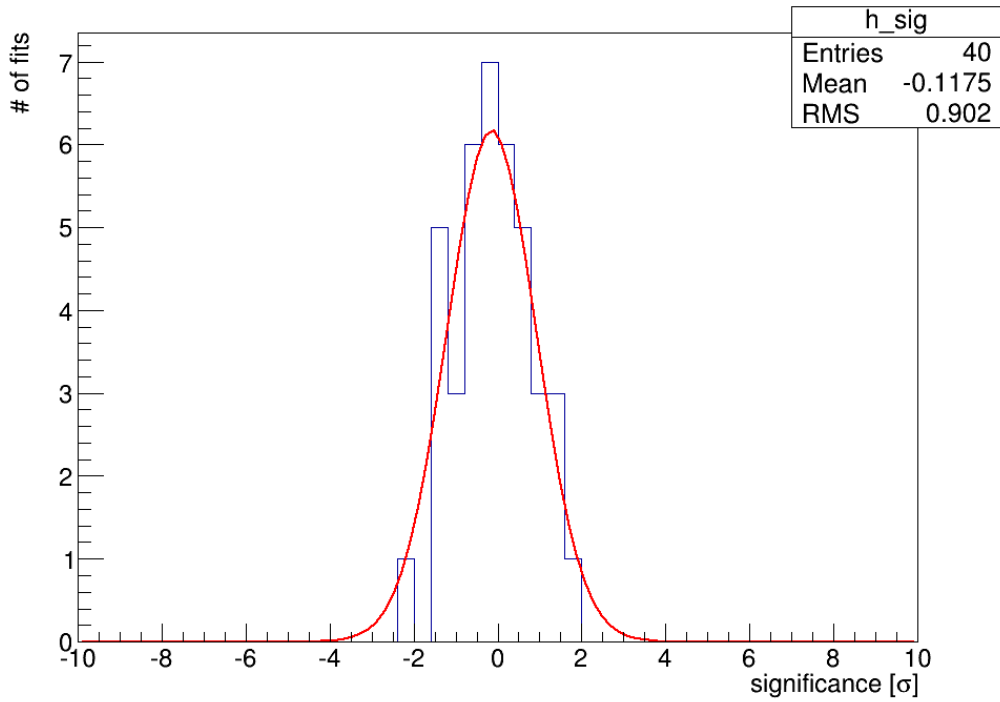
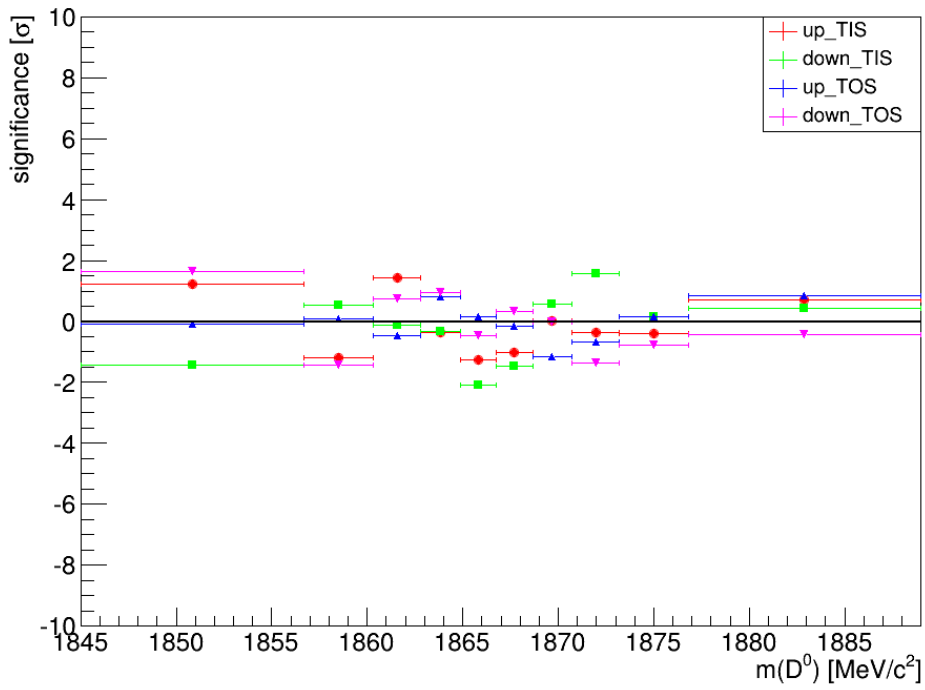


Figure A.50.: Significance vs. $m(D^0)$ (top) and histogram of significances (bottom) for 2011 data.

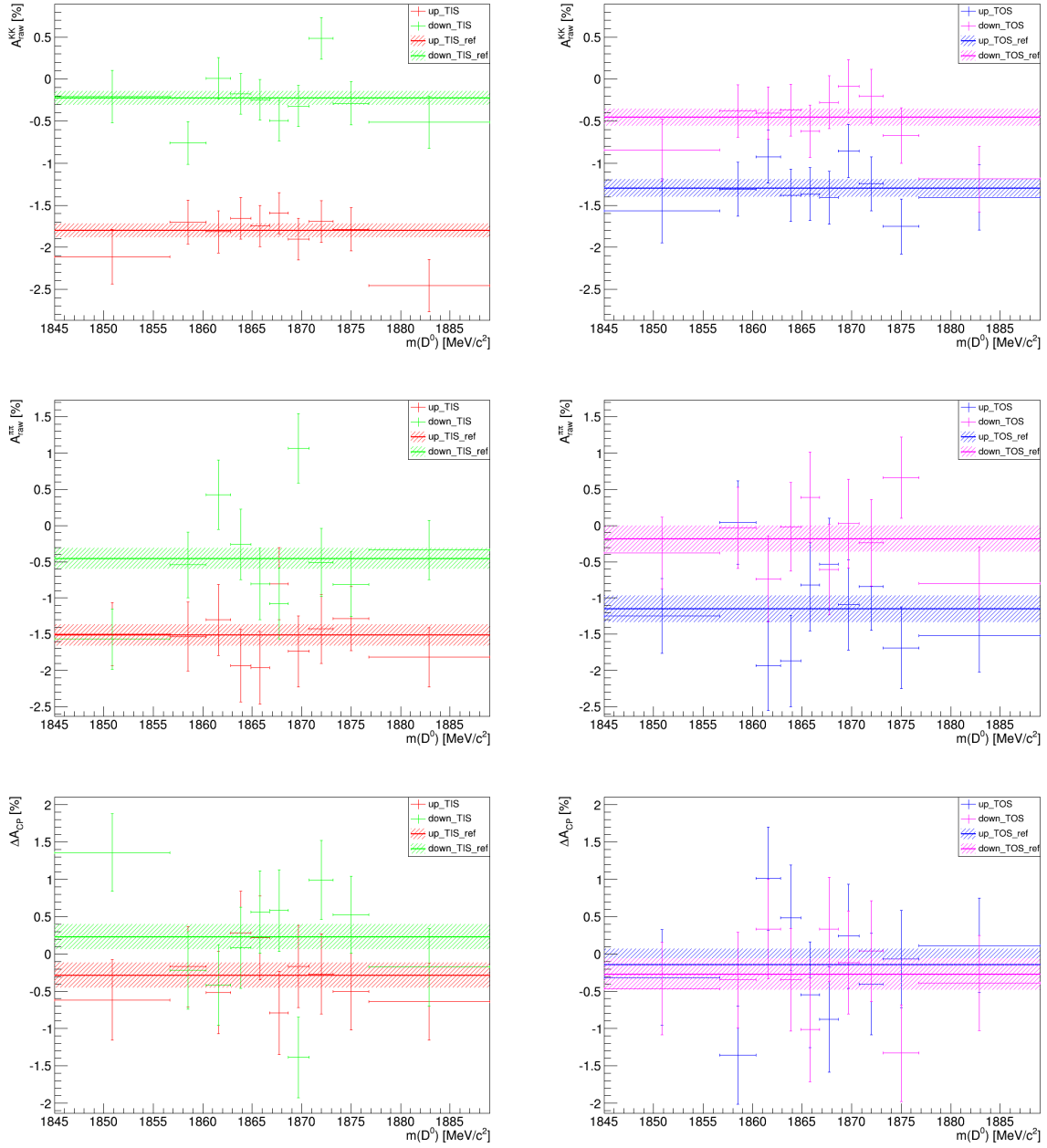


Figure A.51.: A_{raw} vs. $m(D^0)$, separated by magnetic field polarity and trigger setting for 2012 data.

Table A.22.: Results of the individual asymmetries in the different $m(D^0)$ bins, separated by magnetic field polarity and trigger for 2012 data. Highest significance: 3.15

Sample	$A_{raw}(KK)[\%]$	$A_{raw}(\pi\pi)[\%]$	$\Delta_{ACP}[\%]$	significance
up TIS	-1.7988 \pm 0.0825	-1.5120 \pm 0.1487	-0.2868 \pm 0.1700	-
1845.00 < $m(D^0)[MeV/c^2]$ < 1856.70	-2.1136 \pm 0.3225	-1.4974 \pm 0.4334	-0.6162 \pm 0.5402	0.64
1856.70 < $m(D^0)[MeV/c^2]$ < 1860.33	-1.7013 \pm 0.2605	-1.5309 \pm 0.4729	-0.1704 \pm 0.5399	0.23
1860.33 < $m(D^0)[MeV/c^2]$ < 1862.80	-1.8172 \pm 0.2518	-1.2999 \pm 0.4899	-0.5172 \pm 0.5508	0.44
1862.80 < $m(D^0)[MeV/c^2]$ < 1864.86	-1.6539 \pm 0.2475	-1.9335 \pm 0.5003	0.2796 \pm 0.5582	1.07
1864.86 < $m(D^0)[MeV/c^2]$ < 1866.76	-1.7461 \pm 0.2453	-1.9619 \pm 0.5031	0.2158 \pm 0.5597	0.94
1866.76 < $m(D^0)[MeV/c^2]$ < 1868.66	-1.5940 \pm 0.2450	-0.8025 \pm 0.4999	-0.7916 \pm 0.5567	0.95
1868.66 < $m(D^0)[MeV/c^2]$ < 1870.73	-1.9037 \pm 0.2464	-1.7352 \pm 0.4904	-0.1684 \pm 0.5488	0.23
1870.73 < $m(D^0)[MeV/c^2]$ < 1873.20	-1.6949 \pm 0.2493	-1.4245 \pm 0.4750	-0.2705 \pm 0.5364	0.03
1873.20 < $m(D^0)[MeV/c^2]$ < 1876.80	-1.7867 \pm 0.2570	-1.2832 \pm 0.4449	-0.5036 \pm 0.5139	0.45
1876.80 < $m(D^0)[MeV/c^2]$ < 1889.00	-2.4567 \pm 0.3115	-1.8167 \pm 0.4096	-0.6399 \pm 0.5146	0.73
down TIS	-0.2274 \pm 0.0814	-0.4563 \pm 0.1456	0.2289 \pm 0.1669	-
1845.00 < $m(D^0)[MeV/c^2]$ < 1856.70	-0.2077 \pm 0.3114	-1.5667 \pm 0.4154	1.3590 \pm 0.5191	2.30
1856.70 < $m(D^0)[MeV/c^2]$ < 1860.33	-0.7609 \pm 0.2526	-0.5415 \pm 0.4537	-0.2194 \pm 0.5193	0.91
1860.33 < $m(D^0)[MeV/c^2]$ < 1862.80	0.0101 \pm 0.2457	0.4253 \pm 0.4768	-0.4152 \pm 0.5364	1.26
1862.80 < $m(D^0)[MeV/c^2]$ < 1864.86	-0.1744 \pm 0.2427	-0.2588 \pm 0.4885	0.0843 \pm 0.5455	0.28
1864.86 < $m(D^0)[MeV/c^2]$ < 1866.76	-0.2453 \pm 0.2421	-0.8057 \pm 0.4931	0.5603 \pm 0.5493	0.63
1866.76 < $m(D^0)[MeV/c^2]$ < 1868.66	-0.4932 \pm 0.2429	-1.0740 \pm 0.4910	0.5808 \pm 0.5477	0.67
1868.66 < $m(D^0)[MeV/c^2]$ < 1870.73	-0.3189 \pm 0.2444	1.0674 \pm 0.4811	-1.3863 \pm 0.5396	3.15
1870.73 < $m(D^0)[MeV/c^2]$ < 1873.20	0.4865 \pm 0.2498	-0.5063 \pm 0.4683	0.9928 \pm 0.5308	1.52
1873.20 < $m(D^0)[MeV/c^2]$ < 1876.80	-0.2867 \pm 0.2584	-0.8115 \pm 0.4458	0.5248 \pm 0.5153	0.61
1876.80 < $m(D^0)[MeV/c^2]$ < 1889.00	-0.5121 \pm 0.3134	-0.3341 \pm 0.4094	-0.1780 \pm 0.5156	0.83
up TOS	-1.2968 \pm 0.1031	-1.1535 \pm 0.1847	-0.1432 \pm 0.2115	-
1845.00 < $m(D^0)[MeV/c^2]$ < 1856.70	-1.5648 \pm 0.3809	-1.2485 \pm 0.5158	-0.3163 \pm 0.6412	0.29
1856.70 < $m(D^0)[MeV/c^2]$ < 1860.33	-1.3104 \pm 0.3189	0.0429 \pm 0.5753	-1.3533 \pm 0.6578	1.94
1860.33 < $m(D^0)[MeV/c^2]$ < 1862.80	-0.9245 \pm 0.3146	-1.9347 \pm 0.6145	1.0102 \pm 0.6903	1.76
1862.80 < $m(D^0)[MeV/c^2]$ < 1864.86	-1.3824 \pm 0.3138	-1.8684 \pm 0.6320	0.4860 \pm 0.7056	0.93
1864.86 < $m(D^0)[MeV/c^2]$ < 1866.76	-1.3674 \pm 0.3137	-0.8214 \pm 0.6355	-0.5460 \pm 0.7087	0.60
1866.76 < $m(D^0)[MeV/c^2]$ < 1868.66	-1.4088 \pm 0.3137	-0.5301 \pm 0.6335	-0.8787 \pm 0.7069	1.09
1868.66 < $m(D^0)[MeV/c^2]$ < 1870.73	-0.8548 \pm 0.3149	-1.0940 \pm 0.6217	0.2393 \pm 0.6969	0.58
1870.73 < $m(D^0)[MeV/c^2]$ < 1873.20	-1.2439 \pm 0.3206	-0.8409 \pm 0.6023	-0.4030 \pm 0.6823	0.40
1873.20 < $m(D^0)[MeV/c^2]$ < 1876.80	-1.7530 \pm 0.3264	-1.6865 \pm 0.5625	-0.0665 \pm 0.6504	0.12
1876.80 < $m(D^0)[MeV/c^2]$ < 1889.00	-1.4064 \pm 0.3859	-1.5200 \pm 0.5023	0.1135 \pm 0.6334	0.43
down TOS	-0.4554 \pm 0.1028	-0.1838 \pm 0.1812	-0.2716 \pm 0.2083	-
1845.00 < $m(D^0)[MeV/c^2]$ < 1856.70	-0.8403 \pm 0.3693	-0.3753 \pm 0.4947	-0.4650 \pm 0.6174	0.33
1856.70 < $m(D^0)[MeV/c^2]$ < 1860.33	-0.3785 \pm 0.3104	-0.0306 \pm 0.5595	-0.3479 \pm 0.6399	0.13
1860.33 < $m(D^0)[MeV/c^2]$ < 1862.80	-0.4034 \pm 0.3087	-0.7356 \pm 0.5917	0.3322 \pm 0.6673	0.95
1862.80 < $m(D^0)[MeV/c^2]$ < 1864.86	-0.3660 \pm 0.3084	-0.0194 \pm 0.6119	-0.3466 \pm 0.6852	0.11
1864.86 < $m(D^0)[MeV/c^2]$ < 1866.76	-0.6202 \pm 0.3101	0.3920 \pm 0.6244	-1.0122 \pm 0.6971	1.11
1866.76 < $m(D^0)[MeV/c^2]$ < 1868.66	-0.2747 \pm 0.3135	-0.6048 \pm 0.6254	0.3301 \pm 0.6996	0.90
1868.66 < $m(D^0)[MeV/c^2]$ < 1870.73	-0.0856 \pm 0.3150	0.0297 \pm 0.6118	-0.1153 \pm 0.6881	0.24
1870.73 < $m(D^0)[MeV/c^2]$ < 1873.20	-0.2012 \pm 0.3208	-0.2383 \pm 0.5960	0.0371 \pm 0.6768	0.48
1873.20 < $m(D^0)[MeV/c^2]$ < 1876.80	-0.6688 \pm 0.3295	0.6599 \pm 0.5598	-1.3287 \pm 0.6496	1.72
1876.80 < $m(D^0)[MeV/c^2]$ < 1889.00	-1.1876 \pm 0.3897	-0.7996 \pm 0.5046	-0.3880 \pm 0.6376	0.19

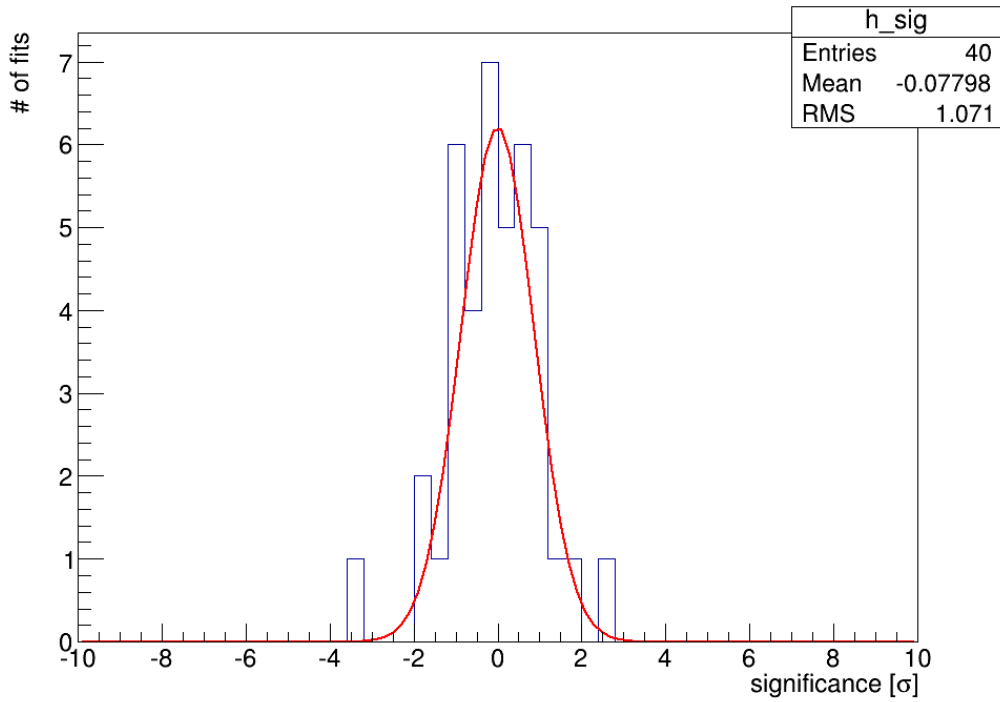
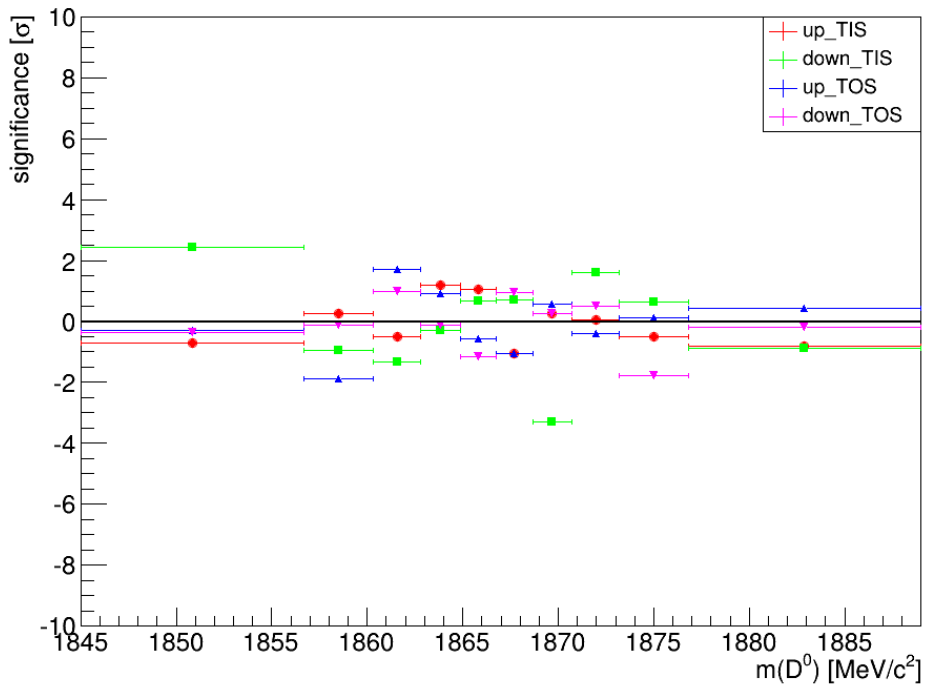


Figure A.52.: Significance vs. $m(D^0)$ (top) and histogram of significances (bottom) for 2012 data.

A.13. Particle identification

In Fig. A.53 the individual asymmetries and ΔA_{CP} versus the PIDK can be found for 2012 data. The significances of the deviations of results from the baseline result in that class of magnetic polarity and trigger can be found in Fig. A.54. In Tab. A.23 the results are shown for 2012 data.

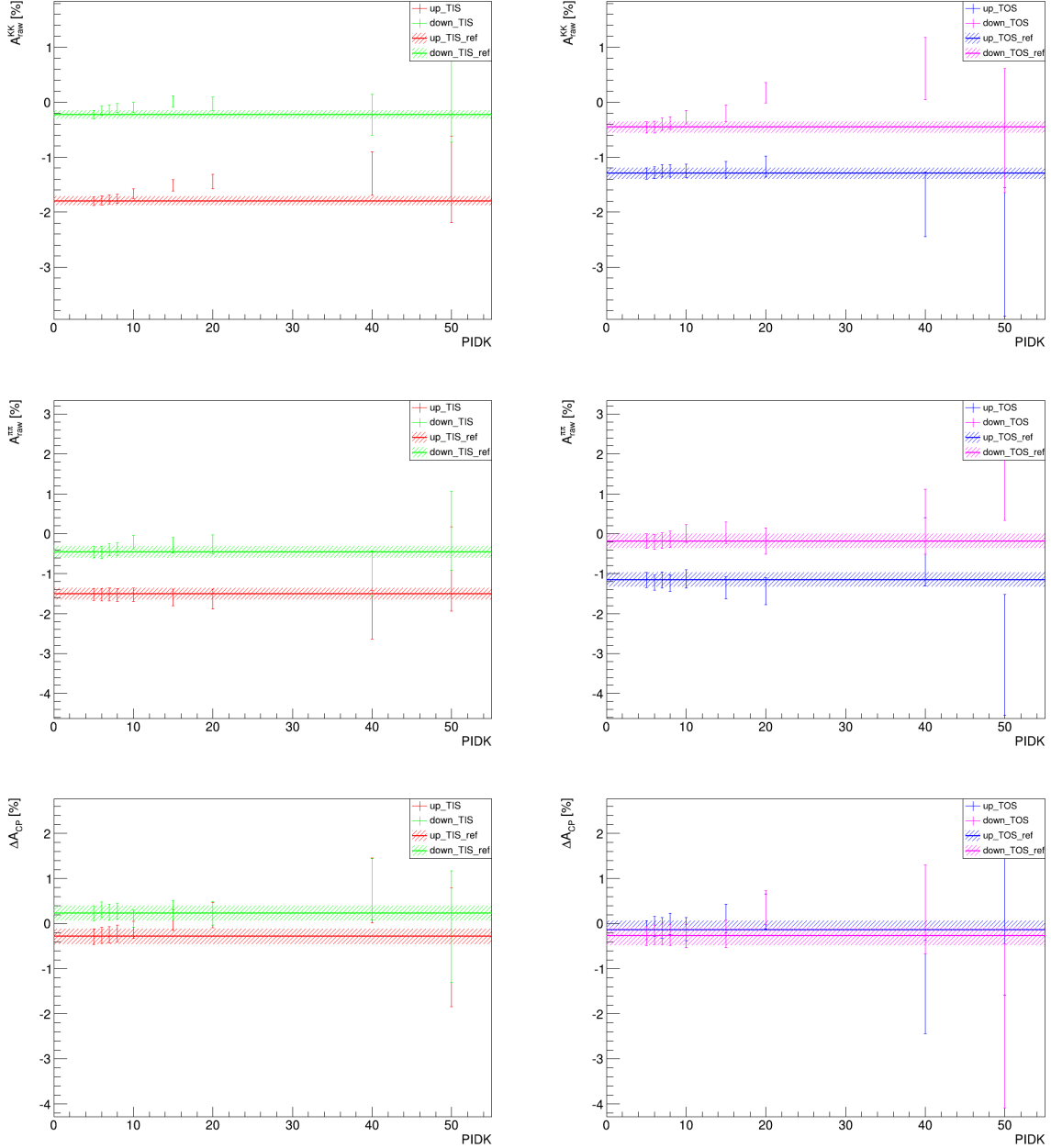


Figure A.53.: A_{raw} vs. $PIDK$, separated by magnetic field polarity and trigger setting for 2012 data.

Table A.23.: Results of the individual asymmetries in the different PIDK bins, separated by magnetic field polarity and trigger for 2012 data. Highest significance: 2.41

Sample	$A_{raw}(KK)[\%]$	$A_{raw}(\pi\pi)[\%]$	$\Delta A_{CP}[\%]$	significance
up TIS	-1.7988 ± 0.0825	-1.5120 ± 0.1487	-0.2868 ± 0.1700	-
5> (<)PIDK	-1.8024 ± 0.0823	-1.5160 ± 0.1482	-0.2864 ± 0.1695	0.03
6> (<)PIDK	-1.7883 ± 0.0838	-1.5293 ± 0.1523	-0.2590 ± 0.1738	0.77
7> (<)PIDK	-1.7699 ± 0.0854	-1.5194 ± 0.1567	-0.2506 ± 0.1785	0.67
8> (<)PIDK	-1.7574 ± 0.0872	-1.5374 ± 0.1614	-0.2199 ± 0.1835	0.97
10> (<)PIDK	-1.6642 ± 0.0913	-1.5255 ± 0.1718	-0.1387 ± 0.1946	1.57
15> (<)PIDK	-1.5119 ± 0.1054	-1.5950 ± 0.2031	0.0831 ± 0.2289	2.41
20> (<)PIDK	-1.4448 ± 0.1276	-1.6330 ± 0.2439	0.1883 ± 0.2753	2.19
40> (<)PIDK	-1.2957 ± 0.3942	-2.0295 ± 0.6020	0.7338 ± 0.7196	1.46
50> (<)PIDK	-1.4059 ± 0.7826	-0.8769 ± 1.0545	-0.5290 ± 1.3132	0.19
down TIS	-0.2274 ± 0.0814	-0.4563 ± 0.1456	0.2289 ± 0.1669	-
5> (<)PIDK	-0.2295 ± 0.0813	-0.4589 ± 0.1453	0.2293 ± 0.1665	0.04
6> (<)PIDK	-0.1533 ± 0.0827	-0.4639 ± 0.1491	0.3106 ± 0.1705	2.33
7> (<)PIDK	-0.1375 ± 0.0842	-0.3935 ± 0.1532	0.2559 ± 0.1748	0.52
8> (<)PIDK	-0.1056 ± 0.0859	-0.3860 ± 0.1576	0.2803 ± 0.1795	0.78
10> (<)PIDK	-0.0955 ± 0.0898	-0.2038 ± 0.1671	0.1083 ± 0.1897	1.34
15> (<)PIDK	0.0134 ± 0.1032	-0.2854 ± 0.1961	0.2988 ± 0.2216	0.48
20> (<)PIDK	-0.0278 ± 0.1241	-0.2582 ± 0.2337	0.2305 ± 0.2647	0.01
40> (<)PIDK	-0.2268 ± 0.3746	-0.9943 ± 0.5673	0.7675 ± 0.6798	0.82
50> (<)PIDK	0.0098 ± 0.7373	0.0761 ± 0.9890	-0.0664 ± 1.2336	0.24
up TOS	-1.2968 ± 0.1031	-1.1535 ± 0.1847	-0.1432 ± 0.2115	-
5> (<)PIDK	-1.2988 ± 0.1036	-1.1556 ± 0.1845	-0.1432 ± 0.2116	0.00
6> (<)PIDK	-1.2834 ± 0.1074	-1.2218 ± 0.1922	-0.0616 ± 0.2202	1.33
7> (<)PIDK	-1.2519 ± 0.1113	-1.1572 ± 0.2001	-0.0947 ± 0.2290	0.55
8> (<)PIDK	-1.2488 ± 0.1153	-1.2355 ± 0.2083	-0.0133 ± 0.2381	1.19
10> (<)PIDK	-1.2502 ± 0.1240	-1.1306 ± 0.2258	-0.1196 ± 0.2576	0.16
15> (<)PIDK	-1.2325 ± 0.1506	-1.3493 ± 0.2761	0.1168 ± 0.3145	1.12
20> (<)PIDK	-1.1718 ± 0.1875	-1.4412 ± 0.3381	0.2694 ± 0.3866	1.28
40> (<)PIDK	-1.8587 ± 0.5873	-0.4560 ± 0.8553	-1.4027 ± 1.0376	1.24
50> (<)PIDK	-2.7231 ± 1.1662	-3.0347 ± 1.5106	0.3117 ± 1.9084	0.24
down TOS	-0.4554 ± 0.1028	-0.1838 ± 0.1812	-0.2716 ± 0.2083	-
5> (<)PIDK	-0.4577 ± 0.1027	-0.1843 ± 0.1810	-0.2734 ± 0.2081	0.17
6> (<)PIDK	-0.4504 ± 0.1064	-0.2028 ± 0.1882	-0.2475 ± 0.2162	0.42
7> (<)PIDK	-0.3978 ± 0.1102	-0.1675 ± 0.1957	-0.2303 ± 0.2246	0.49
8> (<)PIDK	-0.3816 ± 0.1142	-0.1339 ± 0.2035	-0.2477 ± 0.2333	0.23
10> (<)PIDK	-0.2682 ± 0.1226	0.0077 ± 0.2200	-0.2759 ± 0.2519	0.03
15> (<)PIDK	-0.2047 ± 0.1483	0.0216 ± 0.2675	-0.2262 ± 0.3059	0.20
20> (<)PIDK	0.1721 ± 0.1840	-0.1785 ± 0.3270	0.3506 ± 0.3752	1.99
40> (<)PIDK	0.6147 ± 0.5665	0.3026 ± 0.8124	0.3121 ± 0.9904	0.60
50> (<)PIDK	-0.5149 ± 1.1280	1.7561 ± 1.4252	-2.2710 ± 1.8176	1.11

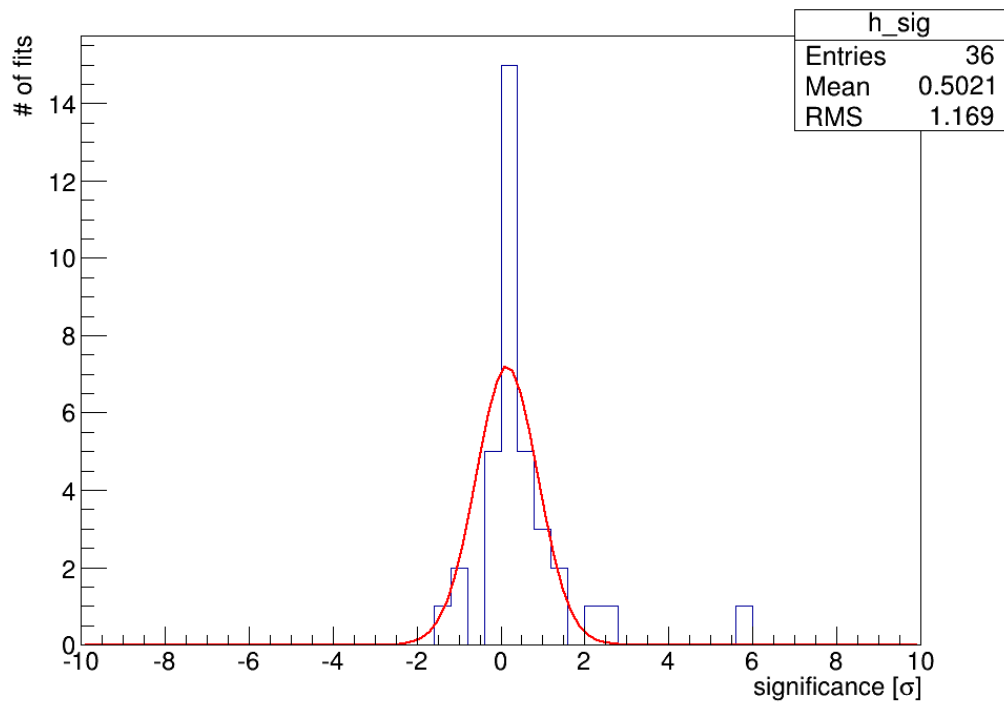
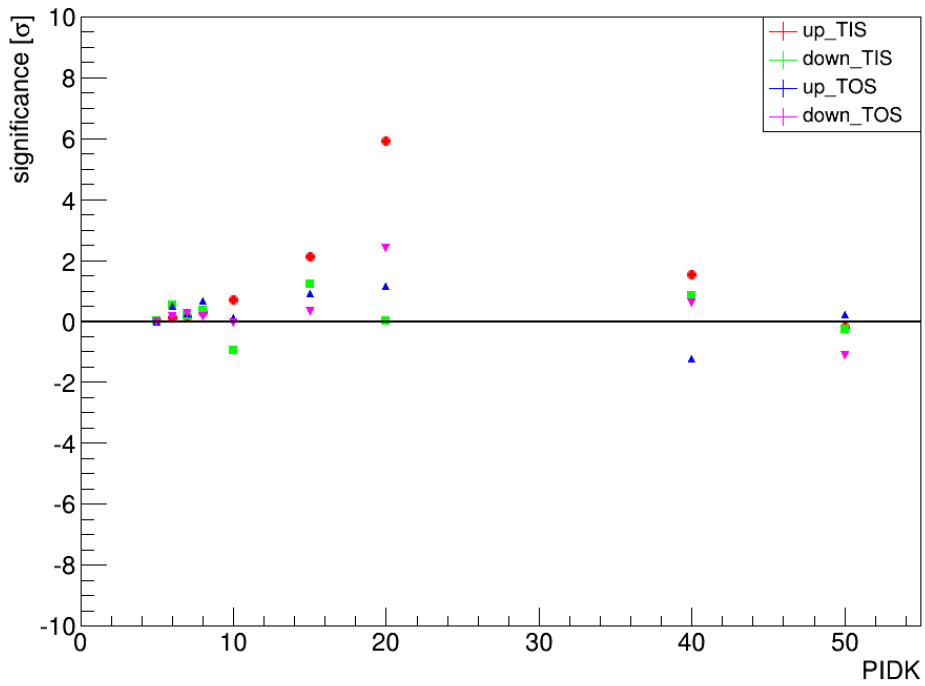


Figure A.54.: Significance vs. *PIDK* (top) and histogram of significances (bottom) for 2012 data.

References

- [1] A. Einstein, “Ist die Trägheit eines Körpers von seinem Energieinhalt abhängig?,” *Annalen der Physik* **323** no. 13, (1905) 639–641.
<http://dx.doi.org/10.1002/andp.19053231314>.
- [2] A. D. Sakharov, “Violation of cp in variance, c asymmetry, and baryon asymmetry of the universe,” *Soviet Physics Uspekhi* **34** no. 5, (1991) 392.
<http://stacks.iop.org/0038-5670/34/i=5/a=A08>.
- [3] **NOvA Collaboration**, D. Ayres *et al.*, “NOvA: Proposal to build a 30 kiloton off-axis detector to study $\nu_\mu \rightarrow \nu_e$ oscillations in the NuMI beamline,” [arXiv:hep-ex/0503053](https://arxiv.org/abs/hep-ex/0503053) [hep-ex].
- [4] **LHCb Collaboration**, A. Carbone, V. Vagnoni, M. Charles, and G. Wilkinson, “Search for time-integrated CP violation in $D^0 \rightarrow K^- K^+, \pi^- \pi^+$,” LHCb-ANA-2011-010.
- [5] **LHCb Collaboration**, R. Aaij *et al.*, “Evidence for CP violation in time-integrated $D^0 \rightarrow h^- h^+$ decay rates,” *Phys. Rev. Lett.* **108** (2012) 111602, [arXiv:1112.0938](https://arxiv.org/abs/1112.0938) [hep-ex].
- [6] **LHCb Collaboration**, A. Carbone *et al.*, “Search for time-integrated CP violation in $D^0 \rightarrow K^- K^+; \pi^- \pi^+$ in the 2011 data,” LHCb-ANA-2012-034.
- [7] **LHCb Collaboration**, R. Aaij *et al.*, “Search for direct CP violation in $D^0 \rightarrow h^- h^+$ modes using semileptonic B decays,” *Phys. Lett.* **B723** (2013) 33, [arXiv:1303.2614](https://arxiv.org/abs/1303.2614) [hep-ex].
- [8] **LHCb Collaboration**, R. Aaij *et al.*, “Measurement of CP asymmetry in $D^0 \rightarrow K^- K^+$ and $D^0 \rightarrow \pi^- \pi^+$ decays,” *JHEP* **07** (2014) 041, [arXiv:1405.2797](https://arxiv.org/abs/1405.2797) [hep-ex].
- [9] **CDF Collaboration**, T. Aaltonen *et al.*, “Measurement of the difference of CP-violating asymmetries in $D^0 \rightarrow K^+ K^-$ and $D^0 \rightarrow \pi^+ \pi^-$ decays at CDF,” *Phys.Rev.Lett.* **109** (2012) 111801, [arXiv:1207.2158](https://arxiv.org/abs/1207.2158) [hep-ex].
- [10] **Belle Collaboration**, B. R. Ko, “CP violation and mixing in the charm sector at Belle, and current HFAG averages,” [arXiv:1212.5320](https://arxiv.org/abs/1212.5320) [hep-ex].
- [11] **BaBar Collaboration**, B. Aubert *et al.*, “Search for CP violation in the decays

- $D^0 \rightarrow K^- K^+$ and $D^0 \rightarrow \pi^- \pi^+$,” *Phys.Rev.Lett.* **100** (2008) 061803, arXiv:0709.2715 [hep-ex].
- [12] **LHCb Collaboration**, A. Carbone *et al.*, “Search for time-integrated CP violation in $D^0 \rightarrow K^- K^+, \pi^- \pi^+$ in the 2011 data,”. LHCb-ANA-2011-059.
- [13] **LHCb Collaboration**, A. Carbone *et al.*, “Search for time-integrated CP violation in $D^0 \rightarrow K K^+, \pi^- \pi^+$ decays with 3 fb¹,”. LHCb-ANA-2014-075.
- [14] N. M. A. . Nobelprize.org, “The nobel prize in physics 2013,”. Retrieved on 22 Oct 2014, http://www.nobelprize.org/nobel_prizes/physics/laureates/2013/.
- [15] Dave Fehling, “The Standard Model of Particle Physics: A Lunchbox’s Guide. The Johns Hopkins University. Retrieved on 2008-12-03.,”. <http://www.pha.jhu.edu/dfehling>.
- [16] F. Englert and R. Brout, “Broken Symmetry and the Mass of Gauge Vector Mesons,” *Phys.Rev.Lett.* **13** (1964) 321–323.
- [17] P. W. Higgs, “Broken symmetries, massless particles and gauge fields,” *Phys.Lett.* **12** (1964) 132–133.
- [18] **Particle Data Group**, K. Olive *et al.*, “Review of Particle Physics,” *Chin.Phys.* **C38** (2014) 090001.
- [19] M. Kobayashi and T. Maskawa, “CP Violation in the Renormalizable Theory of Weak Interaction,” *Prog.Theor.Phys.* **49** (1973) 652–657.
- [20] L. Wolfenstein, “Parametrization of the kobayashi-maskawa matrix,” *Phys. Rev. Lett.* **51** (Nov, 1983) 1945–1947. <http://link.aps.org/doi/10.1103/PhysRevLett.51.1945>.
- [21] N. Cabibbo, “Unitary symmetry and leptonic decays,” *Phys. Rev. Lett.* **10** (Jun, 1963) 531–533. <http://link.aps.org/doi/10.1103/PhysRevLett.10.531>.
- [22] C. Jarlskog, “Commutator of the quark mass matrices in the standard electroweak model and a measure of maximal CP nonconservation,” *Phys. Rev. Lett.* **55** (Sep, 1985) 1039–1042. <http://link.aps.org/doi/10.1103/PhysRevLett.55.1039>.
- [23] S. Davidson, E. Nardi, and Y. Nir, “Leptogenesis,” *Phys.Rept.* **466** (2008) 105–177, arXiv:0802.2962 [hep-ph].
- [24] **WMAP**, E. Komatsu *et al.*, “Five-Year Wilkinson Microwave Anisotropy Probe (WMAP) Observations: Cosmological Interpretation,” *Astrophys.J.Suppl.* **180** (2009) 330–376, arXiv:0803.0547 [astro-ph].
- [25] A. Weiden, “Zeitintegriertes Verhältnis der $D^0 \rightarrow K^+ \pi^-$ und $D^0 \rightarrow K^- \pi^+$ Zerfälle bei LHCb,” Bachelor’s thesis, Heidelberg University, 2012.

<http://www.physi.uni-heidelberg.de/Publications/BachelorAndreas.pdf>
(in German).

- [26] **LHCb Collaboration** , R. Aaij *et al.*, “Measurement of $D^0-\bar{D}^0$ mixing parameters and search for CP violation using $D^0 \rightarrow K^+\pi^-$ decays,” *Phys. Rev. Lett.* **111** (2013) 251801, [arXiv:1309.6534 \[hep-ex\]](#).
- [27] **CLEO Collaboration** , D. Asner *et al.*, “Updated Measurement of the Strong Phase in $D^0 \rightarrow K^+\pi^-$ Decay Using Quantum Correlations in $e^+e^- \rightarrow D^0\bar{D}^0$ at CLEO,” *Phys.Rev.* **D86** (2012) 112001, [arXiv:1210.0939 \[hep-ex\]](#).
- [28] **LHCb Collaboration** , R. Aaij *et al.*, “Measurements of indirect CP asymmetries in $D^0 \rightarrow K^-K^+$ and $D^0 \rightarrow \pi^-\pi^+$ decays,” *Phys. Rev. Lett.* **112** (2014) 041801, [arXiv:1310.7201 \[hep-ex\]](#).
- [29] M. Gersabeck, M. Alexander, S. Borghi, V. Gligorov, and C. Parkes, “On the interplay of direct and indirect CP violation in the charm sector,” *J.Phys.* **G39** (2012) 045005, [arXiv:1111.6515 \[hep-ex\]](#).
- [30] Y. Grossman, A. L. Kagan, and Y. Nir, “New physics and CP violation in singly Cabibbo suppressed D decays,” *Phys.Rev.* **D75** (2007) 036008, [arXiv:hep-ph/0609178 \[hep-ph\]](#).
- [31] A. L. Kagan and M. D. Sokoloff, “On Indirect CP Violation and Implications for D^0 - anti- D^0 and $B(s)$ - anti- $B(s)$ mixing,” *Phys.Rev.* **D80** (2009) 076008, [arXiv:0907.3917 \[hep-ph\]](#).
- [32] **Heavy Flavor Averaging Group** , Y. Amhis *et al.*, “Averages of B-Hadron, C-Hadron, and tau-lepton properties as of early 2012,” [arXiv:1207.1158 \[hep-ex\]](#). and online update at <http://www.slac.stanford.edu/xorg/hfag>.
- [33] J. Brod, Y. Grossman, A. L. Kagan, and J. Zupan, “A Consistent Picture for Large Penguins in $D \rightarrow \pi^+\pi^-, K^+K^-$,” *JHEP* **1210** (2012) 161, [arXiv:1203.6659 \[hep-ph\]](#).
- [34] J. Charles, O. Deschamps, S. Descotes-Genon, R. Itoh, H. Lacker, *et al.*, “Predictions of selected flavour observables within the Standard Model,” *Phys.Rev.* **D84** (2011) 033005, [arXiv:1106.4041 \[hep-ph\]](#).
- [35] **CKMfitter Group** , J. Charles *et al.*, “ CP Violation and the CKM Matrix: Assessing the Impact of the Asymmetric B Factories,” *Eur. Phys. J.* **C41** (2005) 1–131, [arXiv:0406184 \[hep-ph\]](#). updated results and plots available at: <http://ckmfitter.in2p3.fr/>.
- [36] M. Gersabeck, “Brief Review of Charm Physics,” *Mod. Phys. Lett. A* **27** (Jul, 2012) 1230026, [arXiv:1207.2195 \[hep-ex\]](#).

- [37] Y. Nir and N. Seiberg, “Should squarks be degenerate?,” *Phys.Lett.* **B309** (1993) 337–343, [arXiv:hep-ph/9304307](#) [hep-ph].
- [38] M. Leurer, Y. Nir, and N. Seiberg, “Mass matrix models: The Sequel,” *Nucl.Phys.* **B420** (1994) 468–504, [arXiv:hep-ph/9310320](#) [hep-ph].
- [39] O. S. Brning, P. Collier, P. Lebrun, S. Myers, R. Ostojic, J. Poole, and P. Proudlock, *LHC Design Report*. CERN, Geneva, 2004.
- [40] **LHCb Collaboration**, A. A. Alves Jr. *et al.*, “The LHCb detector at the LHC,” *JINST* **3** (2008) S08005.
- [41] **LHCb Collaboration**, “Prompt charm production in pp collisions at $\sqrt{s} = 7\text{TeV}$,”.
- [42] **LHCb Collaboration**, R. Aaij *et al.*, “Measurement of $\sigma(pp \rightarrow b\bar{b}X)$ at $\sqrt{s} = 7\text{ TeV}$ in the forward region,” *Phys.Lett.* **B694** (2010) 209–216, [arXiv:1009.2731](#) [hep-ex].
- [43] J. Wenninger and A. Gorzawski, “Implementation of luminosity leveling by betatron function adjustment at the LHC interaction points,” Tech. Rep. CERN-ACC-2014-0081, CERN, Geneva, Jun, 2014.
- [44] W. D. Hulsbergen, “Decay chain fitting with a Kalman filter,” *Nucl.Instrum.Meth.* **A552** (2005) 566–575, [arXiv:physics/0503191](#) [physics].
- [45] **Belle Collaboration**, M. Staric *et al.*, “Measurement of CP asymmetry in Cabibbo suppressed D^0 decays,” *Phys.Lett.* **B670** (2008) 190–195, [arXiv:0807.0148](#) [hep-ex].
- [46] M. T. Schiller, “Standalone track reconstruction for the outer tracker of the lhcb experiment using a cellular automaton,” Diploma thesis, Heidelberg University, 2007. <http://www.physi.uni-heidelberg.de/Publications/Schiller07.pdf>.
- [47] W. Verkerke and D. P. Kirkby, “The RooFit toolkit for data modeling,” *eConf* **C0303241** (2003) MOLT007, [arXiv:physics/0306116](#) [physics].
- [48] R. Brun and F. Rademakers, “Root - an object oriented data analysis framework,” in *AIHENP’96 Workshop, Lausanne*, vol. 389. 1996.
- [49] M. Pivk and F. R. Le Diberder, “sPlot: a statistical tool to unfold data distributions,” *Nucl.Instrum.Meth.* **A555** (2005) 356–369, [arXiv:physics/0402083](#) [physics.data-an].

Erklärung

Ich versichere, dass ich diese Arbeit selbständig verfasst und keine anderen als die angegebenen Quellen und Hilfsmittel benutzt habe.

Heidelberg, den 31. Oktober 2014
